Structural and functional characterisation of the 5' untranslated regions of β-catenin and HIF-1α mRNAs and their translational role in cancer cells under hypoxia

Javier Rol Moreno

Université de Strasbourg

UNIVERSITÉ DE STRASBOURG

École doctorale Sciences de la vie et de la santé | ED 414 Université de Strasbourg

ÉCOLE DOCTORALE DES SCIENCES DE LA VIE ET DE LA SANTÉ

Institut de Biologie Moléculaire et Cellulaire

Architecture et Réactivité de l'ARN – UPR 9002 (CNRS)

THÈSE présentée par :

Javier ROL MORENO

soutenue le : 11 mars 2022

Pour obtenir le grade de : **Docteur de l'Université de Strasbourg**

Discipline / Spécialité : Aspects moléculaires et cellulaires de la Biologie

Structural and functional characterization of the 5' untranslated regions of β-catenin and HIF-1α mRNAs and their translational role in cancer cells under hypoxia

THÈSE dirigée par :

Dr. Eric ENNIFAR Directeur de Recherche, IBMC, Université de Strasbourg

RAPPORTEURS :

Dr. Stéphan VAGNER Directeur de Recherche, Institut Curie, Université Paris-Saclay

Dr. Celia PLISSON-CHASTANG Directrice de Recherche, CBI, Université Toulouse-III-Paul-Sabatier

EXAMINATRICE :

Dr. Christine ALLMANG-CURA Directrice de Recherche, IBMC, Université de Strasbourg

INVITÉ :

Dr. Angelita SIMONETTI Chercheuse à l'INSERM, IBMC, Université de Strasbourg

Ahora que sabemos que el mérito no existe,
que al principio el esfuerzo es un sueño vacío,
podemos empezar desde un lugar diferente.

Belén Gopegui en su novela
«Quédate este día y esta noche conmigo»
(página 143)

Funding

I gratefully acknowledge the funding received from the *Association Nationale de la Recherche et de la Technologie* (ANRT) towards my doctoral project. This funding consisted in a PhD fellowship named *Conventions industrielles de formation par la recherche* (CIFRE) 2018/0898 that allowed me to have an hybrid position between my academic lab of reference at the IBMC and Sanofi-Aventis R&D (company) in Strasbourg. I would also like to thank the three additional months that were given to compensate the general lockdown due to COVID-19 pandemic during spring 2020. Finally, I acknowledge Instruct ERIC (European Research Infrastructure Consortium) for funding data acquisitions with Titan Krios electron microscope at IGBMC, Strasbourg.

Acknowledgments

I would like to thank Dr Pascale Romby and Dr Stefano Marzi, the two researchers that first gave me a place in IBMC, for believing in me. Thanks for introducing me the passionate field of mRNA translation and for the beautiful discussions about science.

Many thanks to my team members at the Sanofi site in Strasbourg: Oliver Broom, Eamonn Rooney, Walter Englaro, Renaud Morales and many others. It was a great opportunity to get an insight of the different dynamics when doing research in a company and I have appreciated a lot our meetings to launch the project. I acknowledge Dr Eric Ennifar, my thesis director, for the great chance of working in his lab, where I met biophysics and structural biology for the first time. I really appreciate your enthusiasm for research and your capacity of easily creating professional networks with scientists from public institutions but also on the private sector.

I do not know how to thank my supervisor Dr Angelita Simonetti enough, for being a boss, a friend and a second mother at the same time for these three years. Thank you for your mentoring, for the infinite hours you have spent next to me to discuss experiments and for your personal advises. I keep thinking that I was very lucky to end up doing my thesis under your supervision because I have felt free to be entirely myself and free to explore in my research. You have also let me make mistakes so that I could learn from them. With you, I have enormously expanded my knowledge in translation initiation and we have discovered together new insights of the translation mechanisms in cancer cells. I hope we will keep in touch for many years after my departure.

I would like to continue by remembering the rest of my fantastic team, Phillipe W., Isabelle L., Karl B., Pascal A. and, especially, Guillaume B. for bearing me every time I had something to ask or to order and Dominique for his vast knowledge beyond science and his great sense of humour – I will never forget you calling me Jaime all the time. I do not forget all my colleagues of the ARN research unit for creating a nice atmosphere to work, for being helpful and for all those giving a smile every day that we crossed in the corridors.

I thank Lauriane Kuhn and the mass spectrometry platform staff for their useful advises and their great job analysing the composition of initiation complexes. I acknowledge Tanja Seissler for introducing me the basics of cell culture and for her mentoring in cell extract preparation. I enormously thank Benoît Marteyn and his students for allowing me to utilize the

hypoxic workstation. Also, Alexandre Durand from the cryo-EM platform at IGBMC for his work during the data acquisition and the suggestions for the data processing.

Surprisingly, the four great friends I made in IBMC are girls whose names start with "E". With Elena I have enjoyed the best moments since I arrived in Strasbourg. You gave my life the sense of an exciting telenovela, full of emotions, trips and nights to remember. Thanks for being an open book and for making me a bit stronger. With Eva, I have spent my daily master, apartment and PhD life and we have lived lots of adventures together. In your case, my life often felt like a teenager high school series, sparkling, naïve, funny and far from mere scientific conversations. Thanks for making this PhD experience so pleasant. With Emma, I made a great connection since this first unexpected soirée chez Marion back in 2017. It was a pleasure to be in the same team, to travel together and made an unforgettable congress in Heidelberg. I will never forget these moments when you did not understand me and asked someone else "*Il a dit quoi?*". Elenia and I started being very close during the lockdown of spring 2020 – the perks of living in the same building. It has been fantastic to get to know you, discover your kind soul and make such a good *amicizia*. Also, it is fate that we share the same birthday, so we can blow out the candles and make "the party we deserve" once in a year. Please do not hate me because I googled facts you already know just to be sure... I do not forget the students I had the pleasure to meet at IBMC: Emma D., Lucas, Monika, Orian, Kevin, Martina, Mattia, Alexis, Lorine, Louise I. and others that I might have forgotten. I had also a very fulfilling experience with my stagiaire Louise B.

Je voulais aussi remercier à Sophie pour ces trois ans d'amitié et de m'avoir transmis cet enthousiasme pour la nature, la vraie politesse française, l'envie de rester jeune et de profiter des bons plaisirs comme une épicurienne. Aussi d'avoir supporté mes blagues et folies passagères. A David pour cette dernière année en colocation, merci d'avoir partagé des bons moments ensemble – notamment les soirées quand tout était fermé, les escape games et le karaoké box – et surtout ta passion pour les plantes.

Querría darles las gracias a mis mejores amigas, Laura y Miriam, por todo el apoyo personal recibido durante todos estos años y de haber mantenido un vínculo tan fuerte a pesar de haber vivido lejos desde que terminamos el bachillerato. Únicamente con vosotras he sido capaz de reír y haceros reír tanto, de sentirme querido y quereros con muchas ganas. Siento una inmensa gratitud de haber podido contar con vosotras, de sentirme comprendido y sobre todo por haber sido tan humildes. A Laura P. por el entusiasmo y la emoción que le causan las vivencias, como si muchos momentos de su vida ocurrieran por primera vez. De haber vivido tantos momentos juntos desde el colegio y poder disfrutar tanto de las conversaciones en retrospectiva. A Mario por ser un amigo comprensivo, pacífico y agradable. Sois muy importantes para mí.

Me gustaría agradecer enormemente a mis padres por su cariño, por la libertad de haberme dejado elegir mi camino y de haber apoyado siempre mis decisiones. En estas páginas quedan reflejadas la simplicidad, el esfuerzo incondicional y la memoria del mínimo detalle, que vienen a ser aspectos más allá de la ciencia que he aprendido de vosotros. Creo que estos años que he vivido fuera al contrario de alejarnos nos han servido para conocernos mejor, mejorar nuestra comunicación, querernos aún más, permitirnos ser naturales y entender de verdad cuales son las prioridades en la vida. A Carlos, por tu rol de hermano mayor, por valorarme siempre y por los mejores regalos heredados; el sentido del humor y el respeto. Gracias a todas las demás personas que no menciono y que han pasado por mi vida estos últimos años dejando bonitos recuerdos.

Résumé de la thèse

Introduction

La traduction de l'ARN messager eucaryote (ARNm) est un processus très complexe qui comprend quatre phases : initiation, élongation, terminaison et recyclage des ribosomes. Parmi elles, l'initiation de la traduction est l'étape limitante de la synthèse des protéines et un processus strictement régulé pour la recherche du codon initiateur. Dans l'initiation de la traduction canonique, 13 facteurs d'initiation (eIFs) garantissent la reconnaissance précise du codon de démarrage de l'ARNm grâce à une inspection base par base de l'ARNm depuis l'extrémité 5' – où se trouve généralement une coiffe modifiée, 7-méthyl guanosine. Cette recherche est opérée par le complexe ribosomique en cours d'inspection appelé complexe d'initiation 48S (48S IC). Le processus se termine lorsque l'interaction codon-anticodon stabilise le complexe d'initiation sur le codon de départ et culmine avec la formation d'un ribosome compétent en élongation 80S avec la libération concomitante des eIFs (Hinnebusch, 2011; Jackson et al., 2010). Au cours des dernières années, l'accumulation des évidences a rapporté des mécanismes non conventionnels d'initiation de la traduction échappant au modèle canonique, montrant le potentiel du ribosome à adapter sa machinerie en réponse aux différents stimuli en interprétant des signaux dans l'ARNm, souvent dans leur 5'UTR, pour le recrutement des ribosomes. Ces signaux sont tels que des éléments structuraux d'ARN (i.e. IRES, CITE, etc), des modifications d'ARN, des G-quadruplexes ou des uORF (Lacerda et al., 2017). De plus, ces mécanismes apparaitraient dans des conditions de stress que subissent souvent les cellules cancéreuses.

Le cancer est une maladie génétique qui se produit principalement due à l'accumulation d'altérations moléculaires dans le génome des cellules somatiques. Chez l'Homme, il devient actuellement la deuxième cause de décès dans le monde. Dans l'environnement tumoral, les cellules cancéreuses sont constamment confrontées à de nombreux stress tels que la carence en oxygène, la privation de nutriments et l'inflammation. Ces stress provoquent une inhibition de l'initiation de la traduction canonique et, par conséquent, la réduction globale de la synthèse des protéines. Néanmoins, la traduction de protéines spécifiques nécessaires à la réponse et à l'adaptation au stress est maintenue, ce qui peut conduire à la synthèse préférentielle de protéines oncogéniques qui favorisent la progression tumorale (Sriram, et al., 2018). La β-caténine et le facteur induit par hypoxie 1α (HIF-1α) sont deux protéines qui facilitent cette progression du cancer. Ces deux protéines sont induites pendant l'hypoxie, qui est un des stress les mieux caractérisés que subissent des nombreux types de tumeurs solides et aussi une condition qui peut induire des mécanismes de traduction alternatifs.

Le gène *CTNNB1* code pour la β-caténine, l'homologue vertébré de la protéine *armadillo* très connue chez la mouche *Drosophila melanogaster* (Peifer et al., 1992). Il s'agit d'une protéine multifonctionnelle avec deux rôles indépendants dans l'homéostasie cellulaire. L'une des fonctions est l'interaction intracellulaire avec les cadhérines qui stabilisent les jonctions adhérentes entre les cellules épithéliales. L'autre rôle est d'agir comme un facteur de transcription intégré dans la voie canonique Wnt/β-caténine. Quand cette voie de signalisation

s’active, elle permet à la β-caténine de s’accumuler dans le cytosol. Une fois déplacée au noyau, elle induit l'expression de gènes impliqués dans la prolifération et la migration cellulaire tels que c-myc et la cycline-D1 (Nusse et Clevers, 2017). La stabilité de la protéine est fortement régulée par un complexe de dégradation et son activité est également modulée par son état de phosphorylation – ainsi, la protéine phosphorylée est ensuite dégradée. Dans certains types de cancers, comme le cancer colorectal et hépatique, la β-caténine s'accumule de manière aberrante en raison de la dérégulation de la machinerie de dégradation. L'accumulation de β-caténine a également été rapportée dans des conditions hypoxiques dans des cellules cancéreuses, sans aucune variation du niveau d'ARNm (Hong et al., 2017). De plus, la présence d’un IRES a été rapportée dans le 5’UTR de la β-caténine, mais le mécanisme de traduction sous stress cellulaire est encore peu connu (Fu et al., 2015). De cette façon, le mécanisme d’accumulation est régulé soit traductionnellement, post-traductionnellement ou les deux, cependant nos connaissances sur le mécanisme de traduction de la β-caténine dans le cancer restent très limitées.

HIF-1 est un des facteurs qui interviennent dans la réponse transcriptionnelle adaptative à l'hypoxie. Il forme un hétérodimère comprenant une sous-unité α inductible agissant comme un capteur d'oxygène et une sous-unité β exprimée de manière constitutive (Semenza, 2012). La plupart des gènes cibles de HIF-1 sont impliqués dans l'angiogenèse, l'érythropoïèse, le métabolisme du glucose, la survie et la prolifération (Slemc et Kunej, 2016). La stabilité et l'activation de HIF-1 sont étroitement contrôlées par la régulation post-traductionnelle de la sous-unité α. HIF-1α est hydroxylé par les prolyl hydroxylases (PHD) lorsque les cellules sont dans des conditions normoxiques et est reconnu par la protéine von Hippel-Lindau (VHL) pour la dégradation protéasomale. Par conséquent, en l'absence de groupes hydroxyles dans l'hypoxie, la protéine est stabilisée et le niveau de protéine augmente, permettant son déplacement au noyau (Semenza, 2004). Dans les cellules tumorales émergentes présentant une vascularisation défectueuse, les changements transcriptionnels dérivés de l'activité HIF-1 favorisent la migration des cellules et l'invasion d'autres tissus pour échapper aux conditions hypoxiques défavorables du microenvironnement tumoral (Petrova et al., 2018). Compte tenu de l'impact de HIF-1α sur la progression du cancer, il existe un grand intérêt pour comprendre la dérégulation de la voie HIF-1α dans les cellules cancéreuses et le développement d'inhibiteurs de HIF-1. Cependant, la complexité de la voie HIF-1α a rendu le processus de conception de médicaments très difficile. De plus, le mécanisme de traduction de HIF-1α n'est pas assez connu et serait une stratégie innovante pour cibler directement la synthèse de la protéine.

Mon projet de doctorat vise à acquérir des connaissances sur le mécanisme d'initiation de la traduction induite par le stress de la β-caténine et HIF-1α dans les cellules cancéreuses, en utilisant une combinaison d'approches biochimiques, biophysiques et de biologie structurale. Pour atteindre cet objectif, j’ai d'abord identifié et caractérisé les éléments structuraux du 5’UTR de la β-caténine et de HIF-1α, ainsi qu’analysé leur rôle dans la traduction. Ensuite, j’ai isolé l'ARNm de la β-caténine lié au complexe d'initiation de la traduction 48S (48S IC) directement à partir de la lignée de cellules cancéreuses HeLa cultivée dans différentes conditions de stress dont la composition et la structure seront déterminées respectivement par spectrométrie de masse et cryo-microscopie électronique.

Cette approche permettra de révéler comment l'ARNm de la β-caténine est ancré sur la machinerie de traduction et d'identifier les facteurs d'initiation de la traduction et d'autres facteurs induits par le stress. Ce projet est un début pour la découverte de nouvelles thérapies contre différents types de cancers qui ciblent l'ARNm.

Modèle de structure secondaire du 5'UTR de la β-caténine et de HIF-1α.

Les premières sondes chimiques utilisées dans cette étude sont le cyanure de benzoyle (BzCN) et l'imidazolide d'acide 2-méthylnicotinique (NAI), qui modifient les hydroxiles en position 2' des riboses de nucléotides. Ensuite, pour obtenir un modèle structurel plus fiable, j'ai également utilisé comme sondes le sulfate de diméthyle (DMS) et le CMCT qui modifient respectivement les cytosines et les adénosines, ou les uraciles. Les nucléotides sont modifiés en fonction de leur flexibilité et leur exposition aux solvants.

Le 5'UTR de la β-caténine humaine a été synthétisé *in vitro* et la condition de repliement de l'ARN qui a conduit à un conformère unique a été établie. Ensuite, j'ai obtenu la structure secondaire du conformère principal du 5'UTR de la β-caténine par cartographie chimique en solution. Le modèle de structure secondaire du 5'UTR (Figure du résumé B) a montré deux principaux modules structurels: (I) un domaine riche en GC hautement structuré avec une jonction à trois voies et (II) un domaine riche en AU, qui est moins structuré et est situé plus en 3', en amont du codon d'initiation.

Le 5'UTR de HIF-1α humain comprend une jonction hautement compacte à quatre voies en forme d'arbre, suivi d'une région courte simple brin près du codon de départ. De plus, le profil d'ADN complémentaire du 5'UTR résultant de la transcription inverse a montré un très fort arrêt aux positions G_{86} et G_{87}. La production d'un mutant dans ces positions nous a permis de prédire la présence d'un G-quadruplex possible dans le 5'UTR de l'ARNm de HIF1A.

Analyse du rôle du 5'UTR de la β-caténine et son domaine riche en GC sur la traduction.

Pour définir les éléments d'ARN requis pour la traduction efficace de la β-caténine et sa dépendance vis-à-vis du niveau d'oxygène cellulaire, le système rapporteur luciférase a été utilisé. Le modèle 2D de la β-caténine 5′UTR a été utilisé pour concevoir des variants mutants à tester dans des tests de traduction *in vitro* (système acellulaire) et *in vivo* (transfection d'ARNm dans des cellules vivantes).

Pour ces études, j'ai utilisé des cellules HeLa ou SW480 (carcinome colorectal; où la β-caténine est fortement exprimée) cultivées dans différentes conditions d'O_2 (<0.1 ou 18 %). De plus, j'ai optimisé un précédent protocole de préparation d'extraits cellulaires actifs en traduction (Rakotondrafara et al., 2011). Étonnamment, dans les deux lignées cellulaires, j'ai observé une diminution significative du taux de traduction lorsque l'élément riche en GC du 5'UTR de la β-caténine est retiré. Ce résultat suggère que l'élément ARN riche en GC joue un

rôle crucial dans la traduction de la β-caténine dans des conditions d'oxygène standard en culture cellulaire.

Les mêmes transcrits d'ARN ont été transfectés dans des cellules cultivées dans des conditions hypoxiques et j'ai observé que la traduction du rapporteur était même augmentée lorsque le 5'UTR entier de la β-caténine était utilisée. Ce résultat valide davantage l'importance de l'élément riche en GC dans la régulation de la traduction induite par le stress O_2 de la β-caténine et peut expliquer l'accumulation de la protéine dans les cellules cancéreuses sous hypoxie, comme dans le cancer colorectal.

Analyse du rôle du 5'UTR de HIF-1α et son possible G-quadruplex sur la traduction.

Dans le cas du 5'UTR de HIF-1α, nous avons obtenue le modèle de structure secondaire (Figure du résumé B) et nous avons hypothétisé la présence possible d'un G-quadruplex. Nous nous sommes focalisés sur l'effet du possible G-quadruplex sur la traduction. Dans des essais de traduction *in vitro* en utilisant le compétiteur m7GpppG, nous avons observé que la traduction du transcrit *HIF1A* n'est pas affectée, ce qui suggère que eIF4E n'est pas nécessaire pour une traduction efficace du gène rapporteur contenant ce 5'UTR. De plus, le transcrit mutant dans les positions G86 et G87, qui empêcherai la formation du G-quadruplex, récupère la dépendance sur eIF4E. Ces résultats soutiennent l'hypothèse que le G-quadruplex est l'élément régulateur pour l'initiation de la traduction de l'ARNm de HIF1A d'une manière indépendante de la coiffe.

Dans de expériences de traduction sur de extraits cellulaires cultivés en hypoxie, la traduction de HIF-1α en hypoxie était deux fois plus élevée que son expression dans des cellules cultivées dans des conditions d'oxygène standard et cette augmentation de la traduction n'est pas observée dans le mutant. Pour cette raison, le G-quadruplex situé dans le 5'UTR serait l'élément régulateur responsable du basculement du mécanisme d'initiation de la traduction survenant en cas d'hypoxie. L'existence d'un mécanisme d'initiation indépendant de eIF4E représente pour l'ARNm de HIF1A un avantage de traduction en raison de l'indisponibilité décrite de ce facteur d'initiation pendant le stress hypoxique.

Isolement et caractérisation du complexe d'initiation 48S lié à l'ARNm de la β-caténine sous hypoxie.

La stratégie appelée approche Grad-Cryo-EM permet l'étude de la structure et de la composition de complexes intermédiaires de traduction par microscopie électronique cryogénique (cryo-EM) et par spectrométrie de masse (MS/MS). En utilisant cette méthode, j'ai pu isoler par fractionnement en gradient de saccharose l'ARNm de la bêta-globine lié au complexe d'initiation 48S IC directement à partir du lysat de réticulocytes de lapin (RRL), un extrait cellulaire disponible dans le commerce. Trois molécules ciblant différentes étapes du processus d'initiation de la traduction ont été utilisées : i) le GMPPNP (un nucléotide non hydrolysable) pour isoler le complexe d'initiation de la traduction 48S (48S IC) et ii) le cycloheximide et l'hygromycine pour isoler le 80S IC (Rol-Moreno et al., 2020).

J'ai ensuite adapté cette méthode pour purifier le 48S IC à partir de cellules HeLa cultivées dans des conditions standards ou hypoxiques. L'analyse par spectrométrie de masse de ces complexes a donné de légères différences dans la composition des protéines. Les complexes hypoxiques de l'ARNm de la β-caténine présentent une augmentation du facteur d'initiation eucaryote 4B (eIF4B), ainsi que l'absence de eIF4E et la présence de la kinase PKR qui phosphoryle eIF2α. Le changement d'abondance de ces deux derniers facteurs valide le fait que nous travaillons dans de conditions d'hypoxie. Les facteurs eIF4A et eIF4B sont impliqués dans le déroulement de l'ARNm qui permet au ribosome de scanner le 5'UTR et de trouver le codon initiateur. De plus, l'augmentation de eIF5B, nous fait hypothétiser la possibilité de son rôle dans la livraison d'ARNt initiateur par suite de l'inhibition de eIF2. Lorsque l'élément riche en GC est retiré, nous observons une réduction significative des trois sous-unités de eIF4G. Ce résultat nous suggère que les facteurs eIF4A, eIF4B, eIF4G et eIF5B maintiennent la traduction de l'ARNm de la β-caténine à travers la jonction à trois voies du 5'UTR dans les cellules cancéreuses soumis aux conditions hypoxiques.

Le complexe hypoxique 48S lié à l'ARNm de la β-caténine avec ou sans l'element riche en GC a été congelé sur des grilles pour une étude cryo-EM. Ces complexes ont été d'abord analysés sur le microscope électronique à transmission Glacios™ pour vérifier la qualité de l'échantillon – pureté, présence d'agrégation et épaisseur de la glace entre autres – et déterminer la concentration optimale de complexe pour une distribution et une orientation optimale, conditions préalables à l'obtention de cartes électroniques à haute résolution. Sur les meilleures grilles, en termes de distribution et d'orientation des particules, une collecte de données à haute résolution sur un microscope electronique Titan Krios équipé d'un détecteur direct Gatan K3 a été effectuée pour chaque complexe.

L'analyse structurale des deux complexes d'initiation obtenus par cryo-EM est encore en cours. Les densités électroniques montrent bien que tous les facteurs d'initiation attendus se trouvent dans le complexe comme confirme l'analyse par MS/MS du même complexe. En outre, des nouvelles densités non présentes dans des cartes électroniques précédentes restent à être identifiées. La résolution attendue de ces complexes est de 3-4 Å et de plus une modélisation moléculaire doit être faite.

<u>Interaction entre eIF4A et eIF4B avec le 5'UTR de la β-caténine.</u>

L'eIF4AI et eIF4B humains ont été récemment clonés et purifiés dans notre laboratoire. Nous avons émis l'hypothèse de l'existence d'un site d'interaction initiale pour eIF4A dans le 5'UTR qui comprend une région riche en purine et qui permettrait à la protéine d'augmenter son activité hélicase. En effet, les séquences de polypurine sont un substrat préférentiel pour eIF4A. Pour valider notre hypothèse, j'ai effectué des tests de retard sur gel (EMSA) sur différentes constructions du 5'UTR de la β-caténine. De cette façon, l'élément ARN riche en GC est responsable de l'interaction avec eIF4B. Cependant, nous n'avons pas pu démontrer l'interaction directe avec eIF4A. En revanche, nous avons délimité la zone d'interaction d'eIF4A et eIF4B sur l'élément riche en GC par *footprinting*, notamment dans les purines.

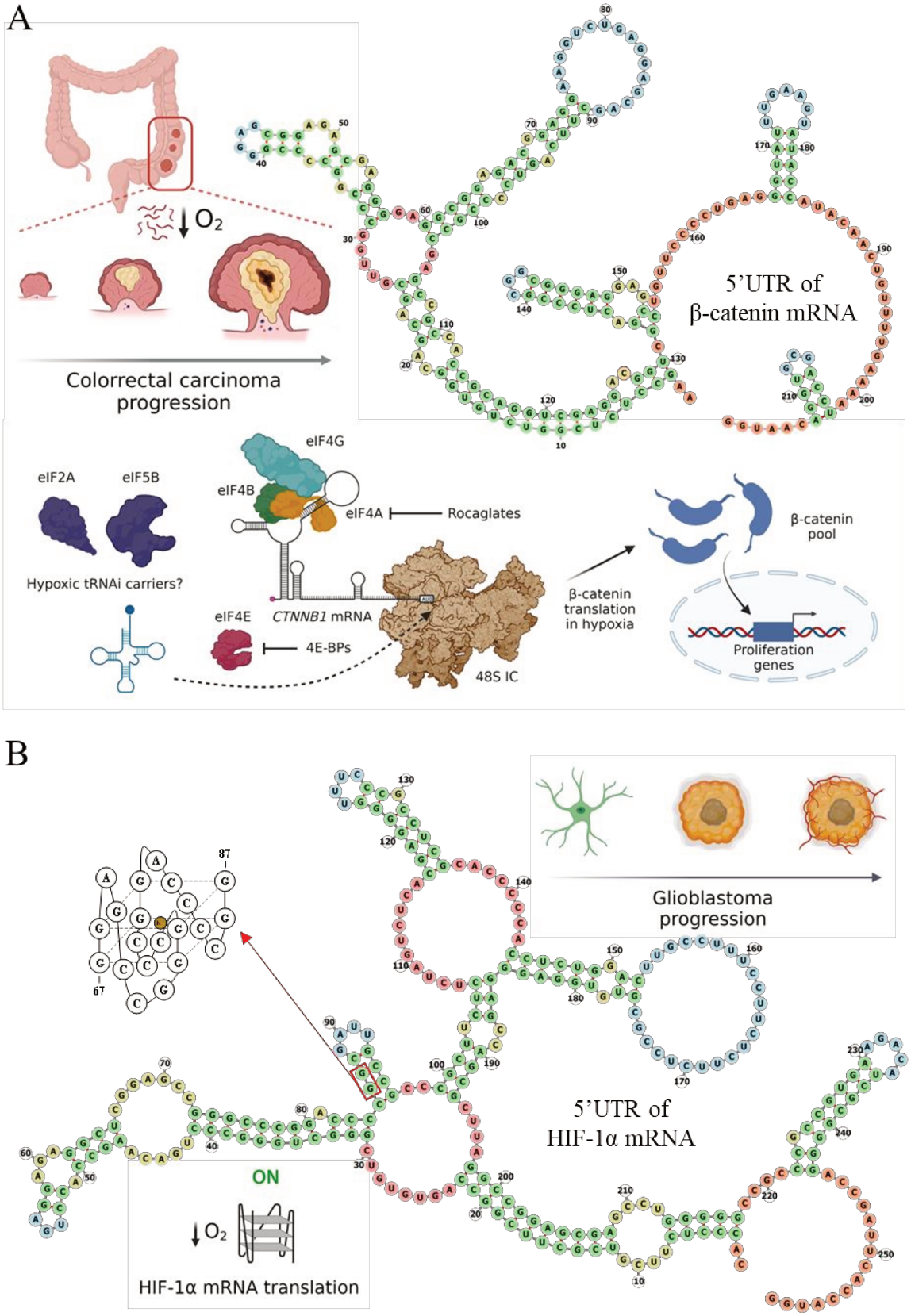

Figure du résumé de la thèse. (A) Représentation du modèle de structure secondaire du 5'UTR de la β-caténine (fait sur Forna, http://rna.tbi.univie.ac.at/forna/) ainsi qu'un schéma du cancer colorectal où la β-caténine est impliquée et une simplification du mécanisme proposé pour l'induction de la traduction de la β-caténine en hypoxie et son accumulation, qui permet à la protéine d'activer des gènes de prolifération dans la tumeur. (B) Représentation du modèle de structure secondaire du 5'UTR de HIF-1α, accompagné d'un modèle hypothétique

du G-quadruplex et son mécanisme d'activation, ainsi qu'un schéma du glioblastome, un cancer modèle de l'expression et implication de HIF-1α. Une partie de cette figure a été créé sur BioRender.com. Les couleurs des nucléotides indiquent leur position dans de motifs de structure secondaire : vert (appariement de bases), bleu (boucles), rouge (jonctions), orange (régions simple brin) et jaune (boucles internes ou renflements).

Cette étude a montré que les régions simple brin de la jonction à trois vois sont liée pars les deux facteurs d'initiation.

Inhibiteurs de la traduction de la β-caténine.

Nous avons réalisé des expériences de compétition *in vitro* avec un analogue de la coiffe pour estimer la dépendance de l'ARNm de β-caténine sur le facteur eIF4E et nous avons observé que sa traduction est relativement impactée lors de l'utilisation d'inhibiteur. Cependant, nous avons aussi constaté que la traduction de l'ARNm de β-caténine avec une coiffe inactive dans des extraits cellulaires hypoxiques est très important. Ces résultats donnent des indices sur la capacité de la β-caténine à se traduire en conditions d'hypoxie indépendamment de eIF4E.

Pour comprendre si eIF4A joue un rôle dans la traduction de la β-caténine, nous avons décidé de transfecter plusieurs constructions mutantes d'ARNm de β-caténine dans des cellules cultivées à différents niveaux d'oxygène et traitées avec du silvestrol. Cette molécule est un inhibiteur de l'activité hélicase de l'ARN eIF4A et appartient à la famille des flavaglines. Il est important de noter que l'inhibition de la traduction de la β-caténine a été observée exclusivement quand l'élément d'ARN riche en GC était présent dans des cellules cultivées en normoxie ou en hypoxie (à une concentration nanomolaire de silvestrol). Ce résultat est en accord avec notre hypothèse selon laquelle eIF4A et 4B sont impliqués dans le maintien de la traduction de la β-caténine pendant l'hypoxie dans les cellules cancéreuses. Nous avons aussi testé *in vitro*, l'effet du silvestrol et de la Rocaglamide A (une autre flavagline) sur la traduction de la β-caténine. Ainsi, d'autres composés comme le silvestrol et la Rocaglamide A devraient être criblés pour trouver les molécules les plus spécifiques pour inhiber la traduction de l'ARNm de la β-caténine dans le cancer. De plus, la sensibilité des cellules hypoxiques aux inhibiteurs d'eIF4A est un avantage supplémentaire pour réduire les possibles effets de résistance de ces médicaments dans les thérapies contre le cancer.

Conclusions et perspectives

Les études structurales et fonctionnelles du 5'UTR de la β-caténine et de HIF-1α ont permis de déterminer ces structures secondaires. Le 5'UTR de la β-caténine contient deux éléments, l'élément riche en AU et le domaine riche en GC, qui ont été validés comme modulateur de l'efficacité de la traduction dans les cellules en condition de culture standard et comme un inducteur dans la traduction l'ARNm de la β-caténine en hypoxie. Cet effet a été notamment démontré dans une lignée modèle du cancer colorectal, SW480, ainsi que dans les cellules HeLa. L'isolement du complexe d'initiation de la traduction 48S IC issue d'une lignée cellulaire HeLa cultivée en hypoxie a été obtenu avec l'ARNm de la β-caténine.

L’analyse de la composition de ce complexe suggère que les facteurs eIF4A, eIF4B et eIF4G pourraient être impliqués dans l’induction de la traduction de la β-caténine en hypoxie. En effet, l’interaction de eIF4B avec le domaine riche en GC a été validé par retard sur gel. De plus, l’inhibition de la traduction de la β-caténine pendant l’hypoxie en utilisant un inhibiteur de eIF4A, le silvestrol, démontre le rôle de cette protéine sur la traduction alternative de l’ARNm de la β-caténine en hypoxie.

Le 5’UTR de HIF-1α comprend une jonction à quatre voies en forme d'arbre avec un éventuel G-quadruplex, suivie d'une région simple brin près du codon d'initiation. Nous avons découvert certains aspects de la traduction de l’ARNm de HIF-1α comme son indépendance d’eIF4E pour être traduit de même que l’induction de la traduction en hypoxie régulée par le G-quadruplex. L'existence d'un mécanisme d'initiation indépendant de eIF4E représente un avantage translationnel pour l'ARNm de HIF1A en raison de l'indisponibilité rapportée de ce facteur d'initiation lors d'un stress hypoxique. L'objectif ultime de la caractérisation de ce 5'UTR sera de valider l’existence du G-quadruplex *in vivo* ainsi que d'obtenir le modèle atomique des complexes 48S normoxiques et hypoxiques liés à l'ARNm de HIF-1α et leur composition protéique par Grad-cryo-EM. L’obtention de la structure tridimensionnelle du G-quadruplex permettra d'effectuer un criblage à haut débit pour découvrir de petites molécules ciblant et inhibant la traduction de l'ARNm de HIF1A. Ces inhibiteurs contribueraient à établir une nouvelle stratégie anticancéreuse pour la thérapie combinée dans toutes les tumeurs où l'expression de HIF-1α est dérégulée ainsi qu'un nouvel espoir de trouver le remède à la maladie de von Hippel-Lindau.

Ce projet multidisciplinaire sur la caractérisation de la traduction de deux messagers impliqués dans la progression du cancer ajoute une nouvelle page dans l'analyse de la traduction dans des conditions de stress et soutient l'existence d'une diversité cachée de mécanismes d'initiation de la traduction qui réécriront sûrement les principes de la traduction dans l’avenir. De plus, cette étude pourra servir de point de départ pour le ciblage des ARNm avec des inhibiteurs de la traduction déjà connus et ouvre des nouvelles voies pour étudier d’autres stratégies pour bloquer la traduction des ARNm de manière spécifique.

Table of contents

List of Figures

Abbreviations

3'UTR: 3' untranslated region

^{32}P: Phosphorus-32

43S PIC: 43S pre-initiation complex

48S IC: 48S initiation complex

5'TOP: 5' terminal oligopyrimidine

5'UTR: 5' untranslated region

A: Adenine or adenosine

Å: angstrom

ABC: ATP-binding cassette

AMV: Avian Myeloblastosis Virus

APC: adenomatous polyposis coli

ARE: AU-rich element

ARNT: aryl hydrocarbon receptor nuclear translocator

ASO: antisense oligonucleotide

ATF4: Activating transcription factor 4

ATP: Adenosine triphosphate

bHLH: basic helix-loop-helix domain

bp: base pair

BSA: Bovin serum albumin

BzCN: benzoyl cyanide

ºC: Celsius degree

C: Cytosine or cytosine

cDNA: complementary DNA

CFTS: Cell-free translation system

CITE: cap-independent translation enhancer

CK-1: casein kinase 1

CLIP: crosslinking and immunoprecipitation

CMCT: 1-Cyclohexyl-(2-Morpholinoethyl) Carbodiimide metho-p-Toluene sulfonate

CNS: Central Nervous System

CPEB: cytoplasmic polyadenylation element binding protein

CP: Central Protuberance

CrPV: Cricket Paralysis Virus

cryo-EM: cryo electron microscopy

CTNNB1: Catenin Beta-1 or β-catenin

ddNTP: dideoxynucleoside triphosphate

DMEM: Dulbecco's Modified Eagle Medium

DMS: Dimethyl sulfate

DMSO: dimethyl sulfoxide

DNA: Deoxyribonucleic acid

dNTP: deoxynucleoside triphosphate

dsDNA: double-stranded DNA

DTT: dithiothreitol

EDTA: Ethylene-diamine-tetraacetic acid

eEF: eukaryotic Elongation Factor

EGTA: ethylene glycol bis (2-aminoethyl ether)-N,N,N',N'-tetraacetic acid

eIF: eukaryotic Initiation Factor

ER: Endoplasmic Reticulum

ES: Expansion segment

g: gram

G: Guanine or guanosine

GCN2: General control non-derepressible-2

GDPNP: Guanosine 5′-[β,γ-imido]triphosphate

GSK3: glycogen synthase kinase 3

GTP: Guanosine triphosphate

H or h: helix

HCV: Hepatitis C virus

HIF: Hypoxia-Inducible Factor

hnRNP: heterogeneous nuclear ribonucleoprotein

HRE: Hypoxia response element

HRI: Heme-regulated inhibitor kinase

i.e.: *id est* (latin)

IRES: Internal Ribosome Entry Site

ISR: Integrated Stress Response

KOAc: Potassium acetate

L: liter

LARP1: La Ribonucleoprotein 1

LiOAc: Lithium acetate

lncRNA: long non-coding RNA

LRP: low-density lipoprotein receptor–related protein

LS48S IC: late stage 48S initiation complex

M: molar

m5C: 5-methylcitosine

m6A: 6-methyladenosine

m7G: 7-methylguanosine

Met-tRNAi^{Met}: aminoacylated initiation tRNA

Mg(OAc)2: magnesium acetate

miRNA: micro-RNA

mmHg: millimeters of mercury

MNase: micrococcal nuclease

mRNA: Messenger RNA

mTOR: mammalian target of rapamycin

NAI: 2-methylnicotinic acid imidazolide

nano LC-MS/MS: Nanoscale liquid chromatography coupled to tandem mass spectrometry

NGS: Next Generation Sequencing

nm: nanometer

nt: nucleotide

NTP: nucleoside triphosphate

ORF: Open Reading Frame

PABP: Poly-A binding protein

PAGE: Polyacrylamide gel electrophoresis

PCR: Polymerase Chain Reaction

PDB: Protein Data Bank

PERK: PKR-like ER kinase

pH: potential of hydrogen

PHD: prolyl hydroxylases

pO_2: partial pressure of oxygen

PRK: Protein kinase R

QGRS: quadruplex forming G-rich sequences

RACK1: Receptor for activated C kinase 1

RBP: RNA-binding protein

rG4: RNA G-quadruplex

RNA: Ribonucleic acid

RNP: Ribonucleoparticle

rpm: revolutions per minute

RPMI: Roswell Park Memorial Institute

RRL: rabbit reticulocyte lysate

RRM: RNA Recognition Motif

rRNA: ribosomal RNA

RT: reverse transcriptase

RT-qPCR: Reverse transcriptase coupled to quantitative PCR

S: Svedberg unit

SC48S IC: scanning competent 48S initiation complex

SHAPE: Selective 2′-hydroxyl acylation analyzed by primer extension

siRNA: small interfering RNA

snoRNA: small nucleolar RNA

snRNA: small nuclear RNA

snRNA: small nuclear RNA

ssDNA: single-stranded DNA

TC: ternary complex

TCF: T-cell factor

TEV: Tobacco Etch Virus

TME: tumour microenvironment

TOP: Terminal Oligopyrimidine Tract

tRNA: transfer RNA

U: enzymatic unit

U: Uracil or uridine

uORF: upstream Open Reading Frame

UV: ultraviolet

v/v: volume/volume

VEGF: Vascular Endothelial Growth Factor

VHL: von Hippel-Lindau protein

Wnt or WNT: portmanteau word combining wingless and int

w/v: weight/volume

INTRODUCTION

RNA biochemistry

Ribonucleic acid (RNA) is a macromolecule formed by ribonucleotides, which are ribose sugars bound to four possible nitrogenous bases (adenine (A), cytosine (C), guanine (G) and uracil (U)) and phosphate groups, linked by 5' to 3' phosphodiester bonds. RNA is generated by an RNA polymerase from a DNA sequence containing a promoter in a process called transcription. Nevertheless, there are some exceptions where RNA is not originated from a DNA template, as for RNA-dependent RNA polymerases or DNA-independent RNA polymerases.

RNA is more prone to degradation than DNA; the 2' hydroxyl group in its ribose acts as a nucleophile that can react with neighbouring phosphates cleaving the backbone at the phosphodiester bond. Certain conditions can make RNA more vulnerable to non-enzymatic degradation, as hydrolysis mediated by magnesium or metal ions, and alkaline hydrolysis (AbouHaidar et al., 1999). Additionally, RNA-degradation systems formed by a plethora of ribonucleases are present in all species of the three domains of life (Houseley et al., 2009).

RNA structure

Even though RNA is usually found as a single macromolecule, it can intermolecularly form double-stranded structures with both a DNA and an RNA molecule. Triple helixes are also possible, including RNA-DNA triplex originated by long non-coding RNAs (Li et al., 2016).

Intramolecularly, one RNA molecule folds over and creates base pairs, that are stabilized by stacking, electrostatic interactions and solvation, together with hydrogen bonds between complementary bases. Watson and Crick canonical base pairing describes two possible interactions between a purine and a pyrimidine: A pairs U, and C interacts with G. In addition to the latter, G×U is a ubiquitous base pair that creates specific interaction sites for proteins, other RNAs and metal ions, and it confers unique conformational properties to RNA helixes (Varani *et al.*, 2000). Nonetheless, other non-Watson-Crick base pairs have been discovered through RNA structural biology. Three edges can be described around each nitrogenous base: the sugar edge, the Watson-Crick edge, the Hoogsteen edge in purines and the C-H edge in pyrimidines (Figure 1A). As a base pair is basically an edge-to-edge interaction, multiple possibilities are given when different edges of two or more nucleosides interact (Leontis & Westhof, 2001).

RNA generally folds into a canonical A-form helix, in contrast to the B-form adopted by DNA helixes (Figure 1B). A- or B-form helixes are folded both in an antiparallel right-handed helical conformation. Following classical criteria, A-form is characterized by a wide minor groove and a deep and narrow major groove. In contrast, B-form duplex is more compact, featuring limited core space, deep major and minor grooves and a wider major groove. Approximately 11 base pairs form one turn of an A-form helix and 10 base pairs in the case of a B-form duplex. Noteworthy, the 2' hydroxyl group of the ribose ring is responsible of locking RNA in an A-form helical structure, forcing a C3'-endo conformation,

while DNA B-form has riboses in C2' endo conformation. Furthermore, the 2' hydroxyl group builds a network of hydrogen bonds with water molecules in the minor groove. This particularity offers more stability to an RNA helix compared to a DNA duplex (Fohrer et al., 2006; Arias-Gonzalez, 2014; Anosova et al., 2016).

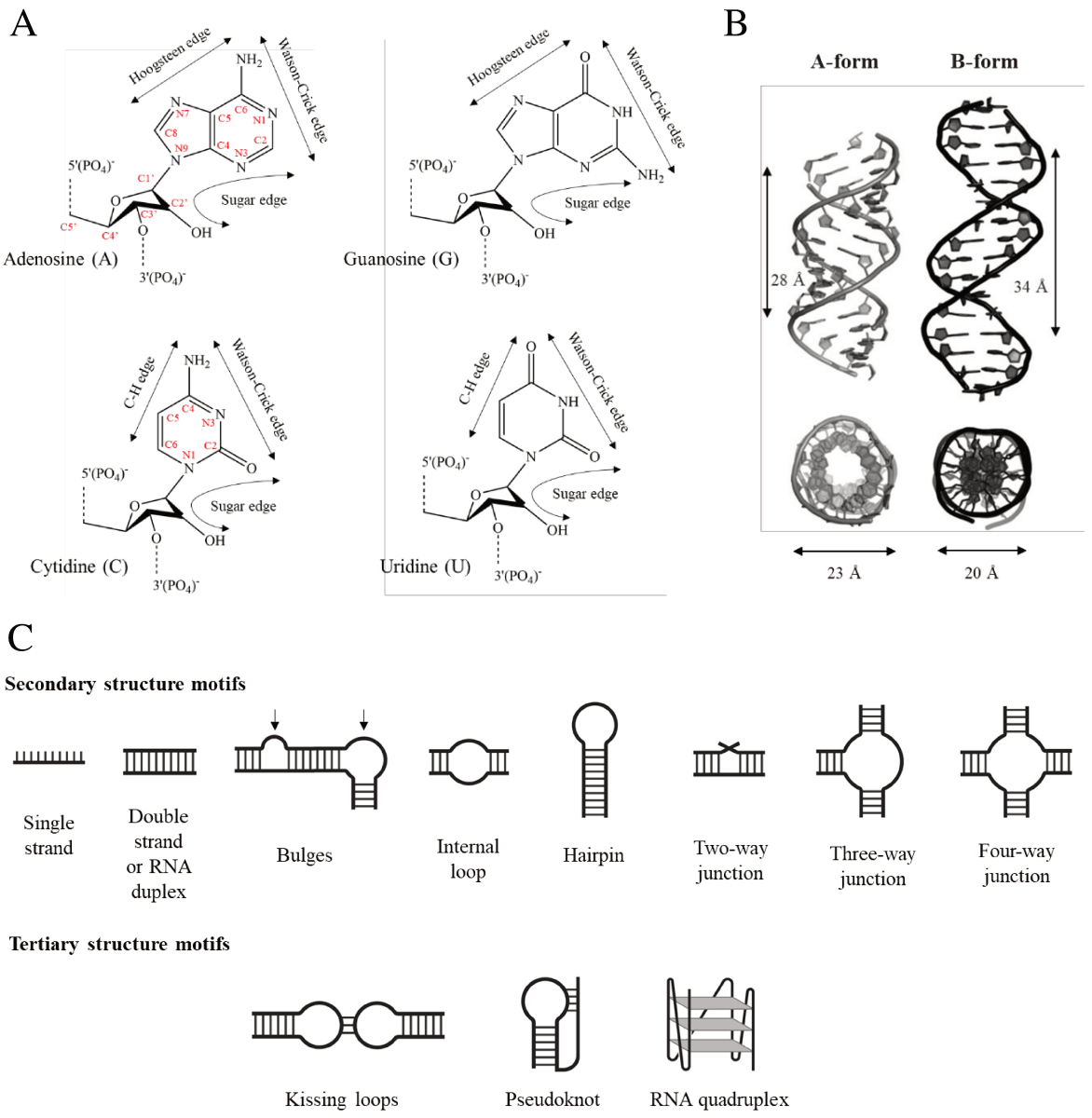

Figure 1. Ribonucleotides, nucleic acid helixes and RNA structure motifs. (A) RNA nucleoside (nitrogenous base + ribose) diphosphates are represented. Position of the edges around the nitrogenous bases are delimited by arrows. In red, atom positions in nitrogenous bases (N) are indicated in adenosine and uridine, as well as the atom number of riboses (N') in adenosine. (B) A- and B-form helixes are shown in frontal and transversal view. The helix width and helix turn size are indicated with arrows. Figure adapted from Anosova et al., 2016. (C) RNA secondary and tertiary structure motifs are schematized. This figure was created with BioRender.com.

RNA folding generates a variety of secondary structures. RNA base-pairing leads to double-stranded regions (helixes), and the unpaired regions between these helixes may be hairpin loops, bulges, internal loops and junctions (Figure 1C). Finally, RNA secondary structure elements are arranged into the space defining its tertiary structure. There are several possible long-range interactions within an RNA molecule; pseudoknots, kissing loops, triple-stranded RNAs, RNA quadruplexes and structures involving metal ions are considered as tertiary structure elements (Butcher et al., 2011).

RNA modifications

Nucleosides and phosphates of RNA can be subjected to chemical modifications. There are over a hundred different RNA modifications that can be found in all types of RNA, although researchers have been primarily focused on modifications in transfer RNA and ribosomal RNA. These modifications are introduced post-transcriptionally by enzymes called "writers", interpreted by protein "readers", and further removed or modified by "erasers" and "modifiers". RNA modifications possess context-dependent roles in many cellular processes, particularly in translation (Schaeffer et al., 2017).

Classification of RNA species by molecular function

RNA is present in all living organisms and some viruses. There are several types of RNAs attending to their structure, length, and function. In any case, RNAs can simply be divided into two different groups:

- RNAs directly related to the protein synthesis process: ribosomal RNA (rRNA), transfer RNA (tRNA) and messenger RNA (mRNA). These RNA will be briefly reviewed below.
- Regulatory RNAs: long non-coding RNA (lncRNA), micro-RNA (miRNA), small-interfering RNAs (siRNA), small nucleolar RNA (snoRNA), small nuclear (snRNA) and more.

Ribosomal RNA

This type of RNA is the principal component of ribosomes, and it is the most abundant RNA in cells. It is responsible of the peptide bond formation in protein synthesis. Ribosome can be considered as a ribozyme dependent on the structural support of ribosomal proteins (Cech, 2000). Ribosomal RNA is encoded in repeated gene clusters, and it is transcribed as a pre-ribosomal RNA.

In eukaryotes, there are four rRNAs; three are contained in a single pre-ribosomal RNA (18S, 5.8S and 25/28S rRNA) and separately, 5S rRNA is also transcribed as a precursor. Ribosome biogenesis starts in the nucleolus with the maturation and modification of rRNAs by snoRNAs, snRNA, pre-ribosomal factors, ribonucleases and the RNA exosome (Allmang et al., 2000; Henras et al., 2015). Ribosomal proteins are also involved in the rRNA maturation step, but more importantly in the assembly and the nuclear export of pre-

ribosomal particles. In the end, mature ribosomes can be located free in the cytosol or associated to the endoplasmic reticulum (ER).

Transfer RNA

The tRNA mainly participates in the elongation step of protein synthesis by carrying an amino acid that is associated to a specific codon sequence depending on the genetic code. Indeed, the universal genetic code defines 64 possible codons ((4 nucleotides)$^{3 \text{ positions}}$)) related to 20 amino acids and 3 stop signals. Several amino acids are coded by more than one codon, and this is known as codon degeneracy.

Apart from the genetic code, the secondary structure forming a cloverleaf and the tertiary structure folding into an L-shaped RNA, are also well-conserved features in most of the tRNAs (Westhof & Auffinger, 2012). In the ribosome, tRNAs can occupy three positions: the aminoacyl (A-site), peptidyl (P-site) or exit (E-site) position. The decoding step during translation elongation consists in the base pairing of the anticodon loop from the cognate tRNA with the codon of the messenger RNA in the A-site, therefore peptidyl-transfer reaction is catalyzed and the nascent chain is covalently bound to the A-site tRNA. Finally, a translocation step is produced, in this manner the peptidyl-tRNA in A-site and the tRNA in P-site are displaced into the P-site and E-site, respectively; hence, another elongation cycle starts (Frank et al., 2007).

Messenger RNA

This molecule functions as the intermediate transcript between the coding sequence of a gene and the protein sequence that is synthetised in the ribosome. As François Jacob and Jacques Monod once hypothesised sixty years ago: “messenger RNA is a short-lived intermediate, very heterogeneous in size, that reflects the DNA composition of a gene and becomes associated with ribosomes where the protein synthesis takes place” (Jacob and Monod, 1961).

In eukaryotes, the vast majority of mRNAs are monocystronic RNAs synthetised in the nucleus by RNA polymerase II. During transcription, two characteristic modifications are added into mRNAs: a 7-methylguanosine linked to the 5’ end by an atypical 5’-to-5’ phosphodiester bond and a poly-A tail at the 3’end of the mRNA. Still in the nucleus, the pre-mRNA is often spliced to remove intron sequences and join exons, forming the mature mRNA that is exported to the cytoplasm.

The protein-coding sequence into the mRNA, also known as open reading frame (ORF), is surrounded by the 5’ and 3’ untranslated regions (5’UTR and 3’UTR). The translation rate of an mRNA is influenced by the codon usage, RNA modifications and secondary structure – factors related to the primary nucleotide sequence of the transcript – as well as initiation factors and RBPs (Mauger et al., 2019).

UTRs present a great heterogeneity in length among individual genes, and they have expanded upon evolution in eukaryotes. In animals, the longest median length of 5’UTRs occurs in humans with 218 nucleotides. The evolution of 5’UTR length is dependent on genomic features as the presence of upstream ORF (uORF) or the 5’UTR size itself (Chen et

al., 2012). Almost half of the human 5'UTRs carry an uORF that can modulate the translation of the main ORF – often reducing its translation (Calvo et al., 2009). During the first step of eukaryotic protein synthesis, the translation machinery interacts with the cap and/or RNA elements of the 5'UTR (Leppek et al., 2018).

In general, 3'UTRs are notably longer than 5'UTR. Although they can directly affect protein synthesis, 3'UTRs rather modulate mRNA stability and localization. The regulatory roles of 3'UTR are given by *cis*-RNA elements (i.e., AU-rich elements, miRNA-targeting sequences and localization signals) and their interaction with RBPs. Furthermore, many mRNA isoforms differ in its 3'UTR and these isoforms are often expressed in a cell-specific manner (Mayr, 2019).

Translation process in higher eukaryotes

Protein synthesis is a universal process in all living organisms and can be considered the last step of expression of genetic information, together with post-translational modifications. This highly-regulated process involves the mRNA, the ribosome, translation factors and many other regulatory proteins that assemble in a stepwise manner to ensure its fidelity, processivity, efficiency and accuracy. In eukaryotes, translation is commonly divided into four phases: initiation, elongation, termination and ribosome recycling (Jackson, 2010; Dever & Green, 2012). Before focusing on the translation process, a brief description is given with the most relevant facts of the human ribosome.

Human ribosome

The human ribosome comprises the small subunit (40S) and the large subunit (60S) that together – see Figure 2 – forms the 80S ribosomal complex. The 40S subunit is formed by 18S rRNA and 33 ribosomal proteins. The 60S subunit consists of 28S, 5S and 5.8S rRNAs and 47 ribosomal proteins (Khatter et al., 2015). Small and large ribosomal proteins are encoded by *RPS* and *RPL* gene families, respectively. Additionally, one relevant ribosome-associated protein not included in *RPS* gene family is the receptor for activated C-kinase 1 (RACK1).

Ribosome anatomy and functional centers can be simplified with a few terms. In 40S, there are two anatomic elements: the head containing the beak and the body containing the platform, and the left and right feet. The mRNA binding channel/cleft is situated between the head and the body, where the transcript is threaded. In the 60S, there are three visible extremities called L1-stalk, central protuberance (CP) and P-stalk. The ribosome exit tunnel in the large subunit consists in a channel where the nascent polypeptide chain gets out. Finally, the decoding center is situated in the intersubunit interface, where the codon-anticodon interactions occur.

Compared to the prokaryotic ribosome, the eukaryotic one possesses rRNA extensions termed Expansion Segments (ES). These segments are often located in the solvent side of subunits and act as flexible arms of the ribosomal core. Actually, this flexibility impedes the interpretation of their structures resolved by structural biology techniques.

Determining how ES can be stabilized for structural studies remains an open area of research (Yusupova & Yusupov, 2017). For this reason, ES are poorly characterized. It is hypothesized that ESs would increase translation fidelity and participate in other ribosomal functions (Fujii et al., 2018). The 18S rRNA folds in 45 helixes and contains up to 12 ES – see Supplementary Figure 1.

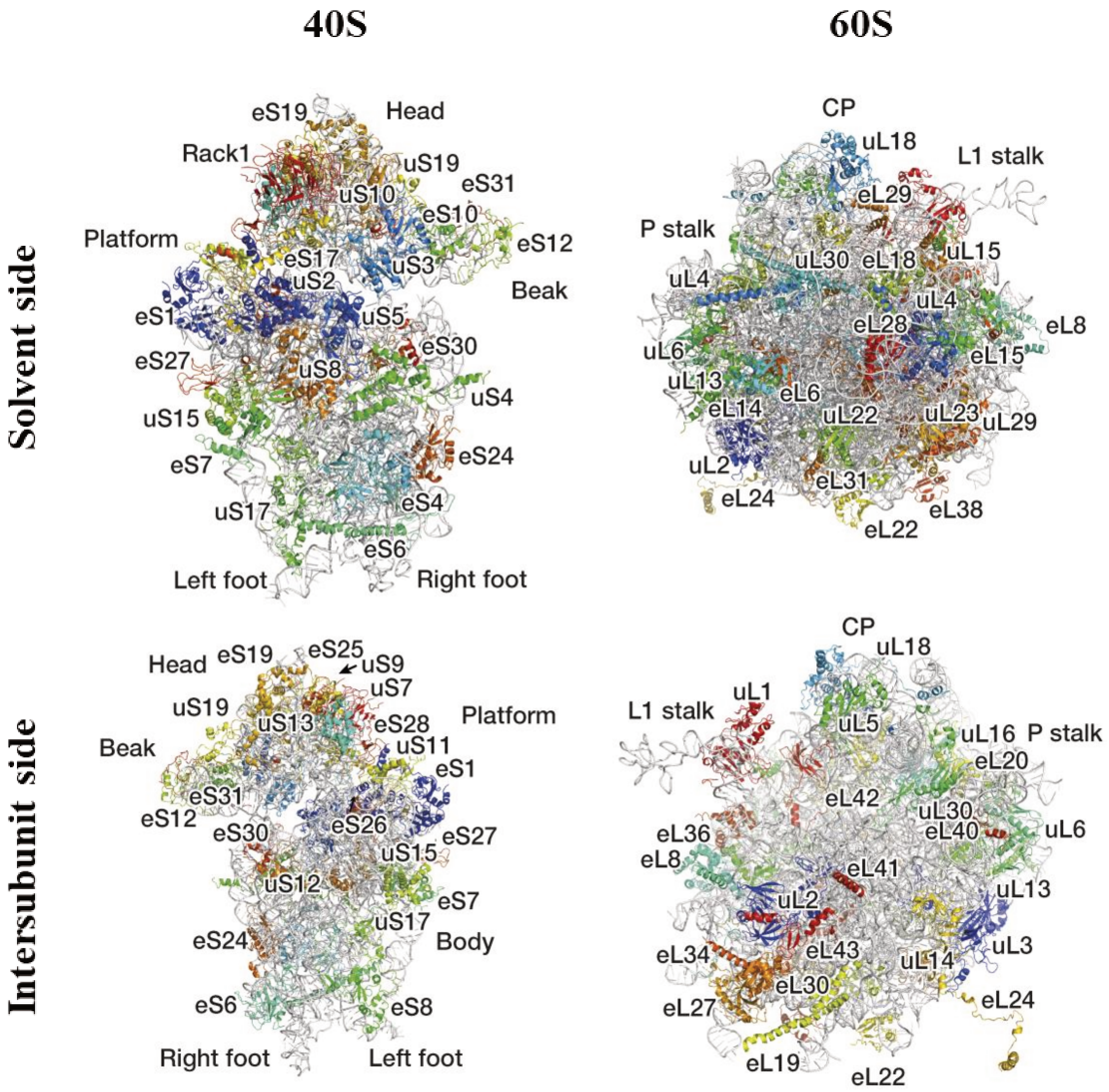

Figure 2. Cryo-electron microscopy structures of the 40S and 60S subunits of the human ribosome from HeLa cells. 40S and 60S subunit are represented in the solvent or intersubunit perspective. Ribosomal proteins are indicated and colored, while rRNAs remain white. Head, beak, platform and left and right feet are indicated in the 40S. L1-stalk, CP or P-stalk are denoted in the 60S subunit. Universal ribosomal proteins or eukaryote-specific proteins have the prefix "u" or "e", respectively. Figure adapted from (Khatter *et al.*, 2015).

Translation initiation in higher eukaryotes

Initiation is the beginning of the translation process, where the mRNA is recruited into the small subunit with the coordinated help of a dozen eukaryotic initiation factors (eIFs) and it mainly consists in the search of the initiation codon to start the protein synthesis (Figure

3). Translation is mainly regulated at the initiation stage to permit a rapid and reversible control of gene expression.

Due to the cyclic nature of translation, separated ribosomal subunits that participate in initiation derives from their recycling in translation post-termination. Recycled 40S subunits are bound to ABCE1, eIF1, eIF1A, the multi-subunit eIF3 complex and eIF5, which all together assist the assembly of the ternary complex (TC) formed by the heterotrimeric factor eIF2 bound to GTP (eIF2αβγ-GTP) and the initiator methionyl tRNA (Met-tRNAi^{Met}; Kapp et al., 2004). The latter translation initiation complex is known as the 43S pre-initiation complex (43S PIC).

The 43S PIC requires the cooperative action of the so-called eIF4F or cap-binding complex for mRNA recruitment. eIF4F comprises the cap-binding protein eIF4E, the DEAD-box RNA helicase eIF4A and the scaffold protein eIF4G, that binds the two first proteins but also eIF3 and the poly-A binding protein (PABP). PABP simultaneous interaction with eIF4G and the poly-A tail permits the approach of both the 5' and 3' mRNA ends – this step is often described as mRNA circularization although it can be confused with circular RNAs where ends are covalently bound. Once the mRNA has been recruited, the formed 48S initiation complex (48S IC) is enabled to scan throughout the 5'UTR in the search of the start codon. The local mRNA structure elements encountered by 48S IC are unwound with energy consumption – ATP – primarily by eIF4A. Nonetheless, other RNA helicases are implicated in the translation initiation process, such as those from the DEAD box family (i.e., DHX29; Pisareva et al., 2008). The RNA helicase activity of eIF4A can be modulated by its binding partners: eIF4B and eIF4H enhance the RNA unwinding of eIF4A whereas Programmed Cell Death 4 (PDCD4) impairs its function (Rozovsky et al., 2008; Suzuki et al., 2008). The function of eIF4B is crucial for certain mRNAs with structured 5′ UTRs and this factor interacts directly with the 40S subunit near the mRNA entry channel, suggesting that it could act independently of eIF4A to promote mRNA translation (Sen et al., 2016).

The 40S can adopt two interconvertible states (open and close conformation) through head movements relative to the body. In open conformation, the mRNA binding cleft is widened, which allows scanning and avoids extensive interaction of mRNA and Met-tRNAi at the P-site. eIF1 is able to recognize a start codon and dissociates from the initiation complex upon codon recognition, which induces the closed conformation in the 40S. In close conformation, the codon-anticodon duplex – formed between the AUG triplet of mRNA and the Met-tRNAi^{Met} – is stabilized and other translation factors are subjected to large conformational arrangements (Hinnebusch, 2017; Guca & Hashem, 2018). In this step, the Kozak sequence is a nucleic acid motif that ensures the efficient recognition of the start codon and the codon-anticodon interaction depends on the Kozak context surrounding the AUG codon. In a "strong" Kozak sequence, A_{-3} binds Arg55 of eIF2α and G_{+4} directly interacts with Trp70 of eIF1A. Furthermore, mRNA in the binding channel has been reported to make contacts with 18S rRNA, ribosomal proteins and eIF3a, d (Pisarev et al., 2008; Hussain et al., 2014; Simonetti et al., 2020). In the late-stage 48S IC, eIF2γ has already hydrolysed GTP, the inorganic phosphate is released and eIF2-GDP leaves the complex together with eIF5. eIF2-GDP is further recycled by eIF2B, a guanine nucleotide exchange factor. The 60S

subunit joins the late-stage 48S IC and forms the 80S IC, triggered by eIF5B GTPase activity that induces at last instance the release of the remaining initiation factors. Finally, 80S is competent for the first elongation cycle. All these sequential assemblies are considered within the canonical translation initiation model, and it is supported by numerous biochemical,

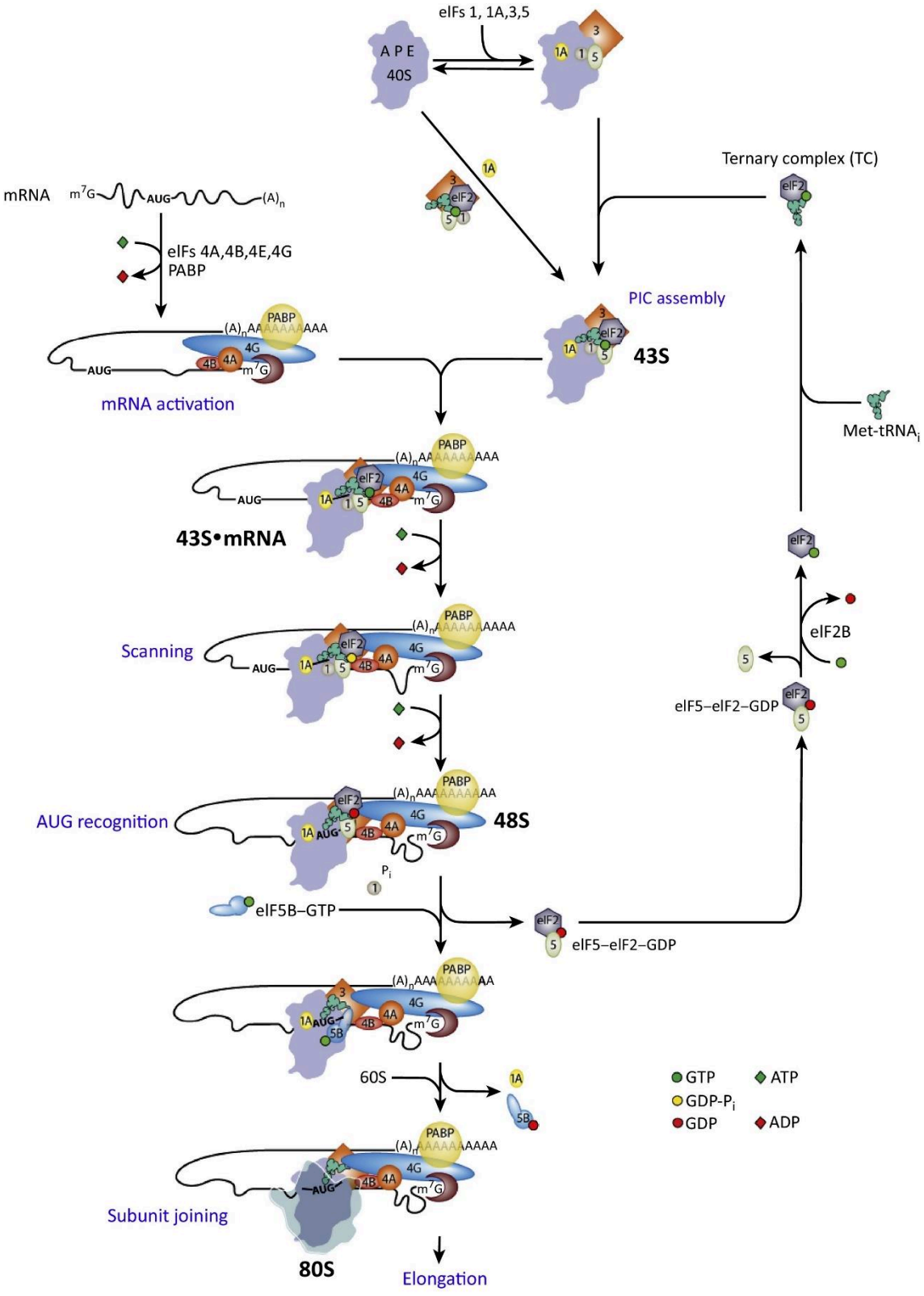

genetic, and structural studies.

Figure 3. Model of the canonical translation initiation mechanism in eukaryotes. Translation initiation pathway is represented as different steps beginning with the assembly of the 43S PIC. Recruitment of mRNA occurs through its interaction of eIF4F, eIF4B and PABP, that further associate to the 43S PIC. Scanning of the 5'UTR is done with the consumption of ATP. GTP hydrolyse on the TC and the release of phosphate is then triggered by recognition of the start codon and eIF1 dissociation. GTP-bound eIF5B promotes joining of the 60S subunit to the 48S IC to form the 80S IC. GTP hydrolysis of eIF5B promotes its dissociation as well as the release of eIF1A, eIF2–GDP in complex with eIF5 and others. TC is formed again when eIF2-GTP is recycled to eIF2–GTP by the guanine exchange factor eIF2B. Figure adapted from Hinnebusch, 2017.

Structural studies of eukaryotic translation initiation complexes

Structural studies of eukaryotic translation complexes have only been possible thanks to the development of X-ray crystallography, cryo-electron microscopy (cryo-EM) and the use of specific translation inhibitors (Jackson, 2010; Hinnebusch, 2014; Brown & Shao, 2018). Moreover, the advancements in cryo-EM sample preparation of ribosomal complexes give an alternative to classical *in vitro* reconstruction, thus translation complexes can be assembled from cell extract components in near-to-native conditions (Simonetti et al., 2016; Martin et al., 2016; Rol-Moreno et al., 2020).

The first yeast 40S complex was solved by cryo-EM at low resolution (~20Å) in V. Ramakrishnan's lab. They showed that eIF1 and eIF1A, positioned at the E-site and A-site respectively, make the mRNA entry channel more accessible and enhance the binding of the TC (Passmore et al., 2006). In N. Ban's lab, a crystal structure at 3,9 Å resolution from the eukaryotic *Tetrahymena thermophila* 40S with eIF1 demonstrated with unprecedent details the folding of the 18S rRNA and all the ribosomal proteins as well as their positioning. Additionally, these authors rather located eIF1 at the top of h44 directly below the P-site and they suggested that eIF1 alone cannot keep the 40S in open conformation (Rabl et al., 2010). Next year, the M. Yusupov's lab published the crystal structure of yeast ribosome at 3.0 Å (Ben-Shem et al., 2011).

In the J. Frank's lab, a cryo-EM structure at 11.6 Å was obtained by *in vitro* assembling the mammalian 43S along with DHX29 – all components being purified from rabbit reticulocyte lysate (RRL). Soon after, the same structure was obtained at ~6 Å (again in the Frank lab). This model revealed the structural disposition of eIF3 core – which is an octamer formed by subunits eIF3a, c, e, f, h, k, l, m and n (Hashem et al., 2013; des Georges et al., 2015). This core resides precisely on the back of the 40S subunit, data that was previously reported by the lab of J. Doudna (Siridechadilok et al., 2005). eIF3d, a peripheral eIF3 subunit, is localized on the 40S head behind RACK1, opposite to the beak and near the mRNA exit. Finally, the RNA helicase DHX29 was positioned under the beak and near h16. The Y. Hashem lab published a cryo-EM structure of rabbit 48S IC at 5.8 Å and showed that eIF3 subunits are rearranged upon mRNA binding and start codon recognition (Simonetti et al., 2016). Particularly, eIF3 core is displaced and moves away from the 40S head. More importantly, peripheral subunits such as eIF3b relocates upon mRNA binding to interact with the TC and eIF3g, eIF3i moves to the 40S intersubunit side after start-codon recognition. However, the densities assigned to eIF3g and eIF3i were not correct and actually corresponded to another unexpected factor: ABCE1. This protein from the ATP-binding

cassette family, at the beginning considered as a ribosome recycling factor, is also present all along translation initiation and dissociates to allow eIF5B binding (Mancera-Martinez et al., 2017).

Yeast 48S IC (*in vitro* reconstituted) at 6.3 Å showed the location of the RNA Recognition Motif (RRM) of eIF4B in the solvent side at the entrance of the mRNA channel and suggest that this position is crucial to maintain the mRNA unwound (Eliseev et al., 2018). Furthermore, the position of eIF5 was described in a yeast translation initiation complex, localized on the platform below the P and E-site. This factor interacts with eIF1 and eIF3 during the 43S PIC and 48S IC assembly (Zeman et al., 2019) and replaces eIF1 upon start codon recognition in the yeast late-stage 48S IC. This step also promotes a conformational change of the 40S head to lock tRNAi in a close conformation (Llácer et al., 2015; 2018). The Hashem lab obtained two cryo-EM structures of rabbit late-stage 48S IC bound to β-globin or H4 mRNA, at 3.0 and 3.5 Å resolution, respectively (Simonetti et al., 2020; see the first late-stage 48S IC in Figure 4A). These structures highlighted the relevance of the Kozak sequence for start codon recognition as well as the numerous mRNA contacts with ribosomal proteins, initiation factors and the 18S rRNA.

Although the composition and arrangement of eIF4F is well studied, its position into the translation initiation complex have always been elusive. The I. Ventoso lab observed that the ES6 of the scanning 48S IC constitutes an extended binding cavity for eIF4A-mediated unwinding of mRNA with structured 5′ UTRs (Diaz-Lopez et al., 2019). Again in Ramakrishnan's lab, a human scanning 48S IC (*in vitro* reconstituted) was resolved by cryo-EM at 3.4 Å resolution, showing for the first time that eIF4F location at the mRNA exit site facilitates scanning at some extent, by pulling mRNA through the channel (Brito Querido et al., 2020; see the human scanning 48S IC in Figure 4B). eIF4A make contacts with eIF3e+k+l and together with eIF4G, they were placed in the solvent side near the ES6 –eIF4A. Unfortunately, eIF4E had no assigned density.

Finally, the labs of J. Puglisi and I. Fernández combined single molecule fluorescence analysis with cryo-EM and obtained a yeast 80S IC structure with ribosome together with eIF5B and Met-tRNAi^{Met}. They showed that at the last step of translation initiation, eIF5B-GTP binds to the 48S and interact with the aminoacylated CCA end of the tRNAi for its correct positioning. 60S joins the complex, inducing conformational changes for eIF5B hydrolysis of GTP and its release to allow the first elongation cycle (Wang et al., 2020).

One can observe how structures obtained by cryo-EM drastically increased in a lapse of 15 years, from low-resolution structures that only permit to discern the global shape of initiation complexes to near-atomic resolution structures. This is mainly due to the commercialization of direct electron detectors and the development of advanced data processing software (Frank, 2017). However, all these structures were focused to solve some of the main questions about canonical translation initiation mechanism, but the structural study of alternative translation initiation complexes remains an unexplored field of research.

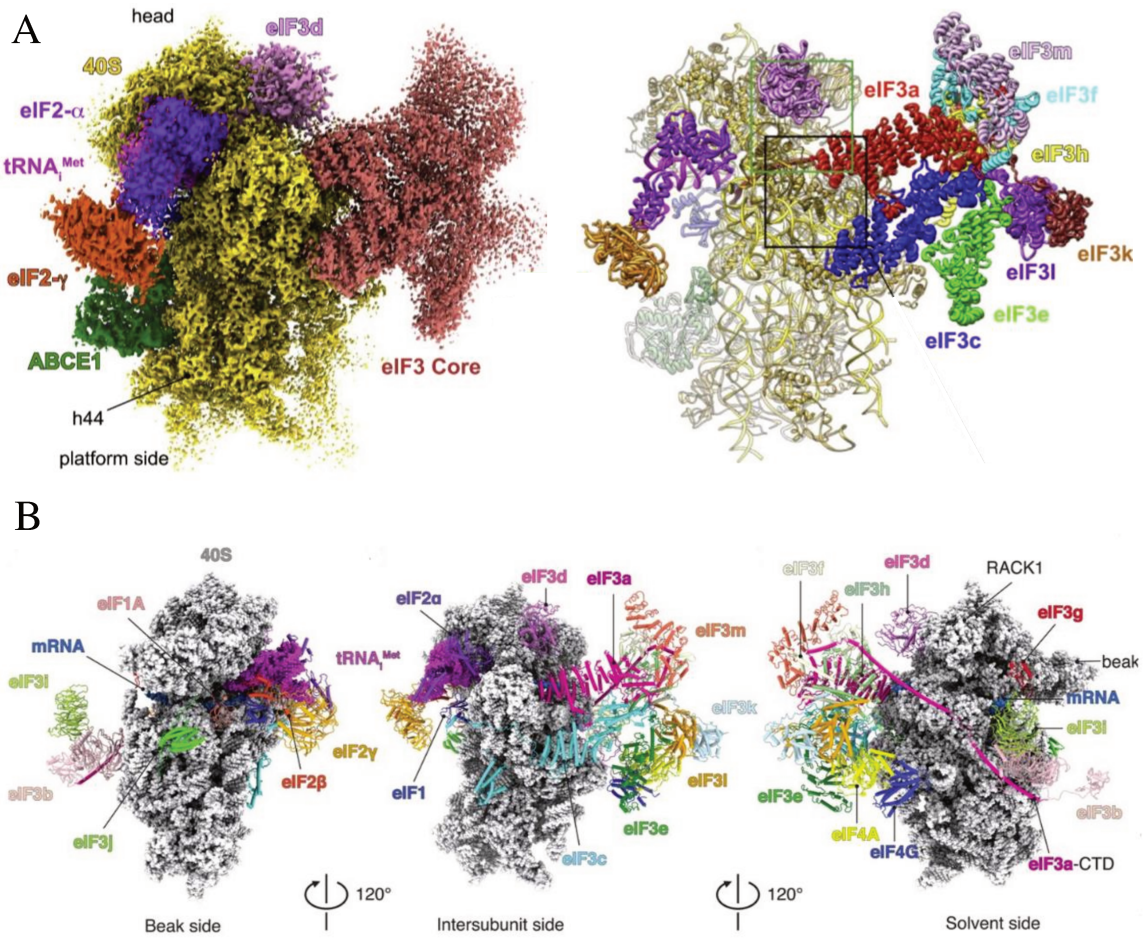

Figure 4. High-resolution structures of mammalian scanning and late-stage 48S IC. (A) Human scanning 48S IC with a synthetic RNA Proteins are indicated in different colours. The same complex is represented in three perspectives. Figure adapted from Querido et al 2020 (PDB 6ZMW) (B) Rabbit late-stage 48S IC bound to *HBB* mRNA. The colour electron density map (left) or the coloured atomic model (right) are represented. Figure adapted from Simonetti et al 2020 (PDB 6YAL).

Alternative mechanisms of translation initiation

Unconventional translation initiation mechanisms evading the canonical model have been reported, showing the ribosome potential to adapt its machinery in response to different stimuli by interpreting mRNA signals for ribosome recruitment (James et al., 2019).

The cap structure recognition is the first requisite of ribosome recruitment, although some mRNAs hijack this classical step in translation. The best-known RNA elements driving cap-independent translation are contained in viral Internal Ribosome Entry Sites (IRESs; Martinez-Salas et al., 2018). Viral IRESs were first described within the 5'UTR of some viruses of the *Picornaviridae* family. These elements allow taking control of the host translation machinery for their own translation, primarily in a cap-independent manner and without scanning step (Pelletier & Sonenberg, 1988; Jang et al., 1988). At present, four types of viral IRESs have been proposed regarding their structure complexity and the requirement

of eIFs, which are inversely correlated (Mailliot & Martin, 2018). IRESs from diverse viral families lack sequence homology and exhibit different structural organization.

IRES activity has also been reported in several eukaryotic mRNAs, whose translation could not be explained in conditions where the translation is globally reduced. Noteworthy, the use of IRES concept for eukaryotic mRNAs can be misleading because viral IRES-driven translation is conceived to succeed in the host infection and alternative translation in cellular mRNAs occurs in other physiological contexts (Jackson, 2013). Therefore, cap-independent translation enhancer (CITE) is often a more appropriate concept because, unlike viral IRESs, these elements can be very simple, located anywhere in the mRNA and interact with translation factors (Shatsky et al., 2018).

Alternative translation initiation comprises IRES-driven mechanisms, but also cap-dependent and/or scanning-dependent mechanisms, which is often unclear in the scientific literature. Increasing evidence has emerged supporting the hypothesis that certain *cis*-acting RNA elements present at the 5'UTR of eukaryotic mRNAs can initiate translation in a non-canonical manner. These elements can be RNA structure elements, RNA sequences, 5' CITE, RNA modifications – like m6A modifications –, upstream ORFs, etc (Lacerda et al., 2017; Leppek et al., 2018). It is important to highlight that the cap structure is a general feature of almost all eukaryotic mRNA and non-canonical translation can easily adjust to a cap-dependent model. To give a few examples:

- H4 mRNA has a peculiar cap-dependent tethering mechanism for ribosome recruitment that increase its translation during the S-phase of cell cycle. RNA structure elements create crucial contacts with h16 of 18S rRNA and eIF3c, d, e, f subunits (Martin et al., 2016; Hayek et al., 2021)
- *RON* mRNA contains two putative RNA G-quadruplexes (rG4s) that modulate its translation through hnRNP A1 binding. This transcript encodes a tyrosine kinase receptor and its expression, together with the one of hnRNP A1, are linked to tumour progression (Cammas et al., 2016).
- Genome-wide analysis revealed that approximately, 20% of mRNAs are translated through eIF4G2 (also known as DAP5) and eIF3d in a cap-dependent but eIF4E-independent manner (de la Parra et al., 2018).
- LARP1 competes with eIF4F in the translation of mRNAs containing 5' terminal oligopyrimidine (5'TOP) motif, to regulate the expression of proteins related to cell growth (Philippe et al., 2020).

Although some of these examples permit to widen the spectra of diverse alternative translation mechanisms, their study remains limited into cells cultured under standard conditions and the use of a small subset of cell lines.

Cellular stress and translation

The occurrence of alternative mechanisms arises in cell stress conditions to keep the translation potential for certain mRNAs, permitting adaptation in response to stress and overcoming the general reduction of protein synthesis. These stresses include DNA damage, hypoxia, nutrient stress, oxidative stress and temperature shock (Figure 5A; Spriggs et al.,

2010). Translation during cellular stresses is strongly reduced due to the modulation of three highly-regulated features at the level of initiation and elongation: the sequestering of eIF4E and the phosphorylation states of eIF2α and eukaryotic elongation factor 2 (eEF2) (Figure 5B; Liu et al., 2014).

The eIF4E-binding protein (4E-BP) shares a similar eIF4E-interaction motif with eIF4G. Thus, 4E-BP competes with eIF4G for eIF4E binding, acting as a negative regulator of translation initiation by repressing the assembly of eIF4F at the 5′ end of transcripts. 4E-BP activity depends on its phosphorylation status; under normal growth conditions, it is heavily phosphorylated and has lower affinity with eIF4E. However, nutrient deprivation reduces the 4E-BP phosphorylation and it binds eIF4E and impairs eIF4E-eIF4G interaction (Romagnoli et al., 2021). 4E-BP phosphorylation is mediated by the mammalian target of rapamycin complex 1 (mTORC1), an evolutionarily conserved serine/threonine kinase that senses extracellular signals as well as the intracellular energy status. Moreover, the phosphorylation status of eIF4E can modulate the efficacy of eIF4F to bind the cap. Phosphorylation of eIF4E in Ser209 by the MAPK interacting protein kinases (MNK) 1 and 2 increase the ability of this factor to bind the cap structure and promotes tumorigenesis (Furic *et al*., 2010).

Another regulated feature under stress conditions is the formation of the TC through eIF2. While the γ subunit of eIF2 possesses the GTPase activity, the β subunit is responsible of contacts with 40S and the α subunit operates as the regulatory subunit (Kimball, 1999). After GTP hydrolysis of the TC, eIF2B catalyses the recycling of GDP to GTP. Nevertheless, eIF2α phosphorylation in Ser51 during different cell stresses impairs the interaction with eIF2B, therefore the guanine exchange cannot take place. Hence, phosphorylation of eIF2α inhibits the TC activity and general translation is importantly reduced. Four kinases are capable of phosphorylating eIF2α depending on the stress:

- General control non-derepressible-2 (GCN2) is activated by the sensing of uncharged tRNAs and it functions as an amino acid sensor. It phosphorylates eIF2α mainly due to nutrient starvation (Anda et al., 2017).

- Heme-regulated inhibitor kinase (HRI) is activated upon oxidative stress caused by different stimuli. It was discovered on cells under oxidative stress derived from arsenite exposure (McEwen et al., 2005). Heme group promotes disulfide bond formation between HRI monomers, forming an inactive dimer that inhibits HRI kinase activity. HRI can also be activated by other stresses including heat shock and osmotic stress, independently from heme inactivation (Pakos-Zebrucka et al., 2016).

- Protein kinase R (PRK) senses dsRNA upon viral infection and activates its kinase activity on eIF2α (Dabo et al., 2012). Apart from the canonical activator of PKR, dsRNA, other stresses induce its activity such as reactive oxygen species (ROS), irradiation, hypoxia, mechanical stress and more (Gal-Ben-Ari et al., 2019).

- PKR-like ER kinase (PERK) is activated under ER-stress and hypoxia and induces the phosphorylation of eIF2α (Koumenis et al., 2002).

These four kinases are integrated in the so-called Integrated Stress Response (ISR) pathway. Importantly, it is suggested that the kinases are not exclusively activated by a single type of cellular stress and together, they cover a wide range of stresses to modulate the translational output of the cell (Pakos-Zebrucka et al., 2016). Their phosphorylation of eIF2α reduces global translation, but it paradoxically increases the translation of the activating transcription factor 4 (ATF4) mRNA, a key effector implicated in stress adaptation. ATF4 mRNA translation is enabled in stress conditions by eIF2D, an unconventional Met-tRNAi^{Met} delivery protein reviewed below and the density-regulated reinitiation and release factor (DENR) that permit reinitiation after its uORF translation (Vasudeman et al., 2020).

The third regulation pathway of translation during stress occurs in the elongation cycle and it consists in the phosphorylation of eEF2. This GTP-dependent factor promotes the translocation of the two tRNAs and the mRNA after peptidyl transferase reaction on the 80S ribosome. Generally, eEF2 kinase (eEF2K) phosphorylates eEF2 at Thr56 and this post-translational modification interferes with its ability to bind to the ribosome. The mTOR pathway, when activated, phosphorylates eEF2K. In this manner, elongation can pursue and when mTORC1 kinase activity is impaired by nutrient starvation, eEF2 is phosphorylated by its kinase and translation elongation is reduced (Leprivier et al., 2013).

Apart from these three translation regulation pathways, other changes may arise during cellular stresses. Recently, ribosome heterogeneity has emerged as a new concept to illustrate the variability of ribosome composition within the cell. The differences in ribosome populations reside in the modification pattern of rRNAs, ribosomal proteins, their stoichiometry and post-translational modifications. Ribosome may change its composition in response to stress and specialize for the translation of a subset of transcripts (Genuth and Barna, 2018). Furthermore, a few studies have shown the role of initiation factors to modify translation in cells submitted to stress as well as the formation of alternative cap-binding complexes. Noteworthy, each of the components of eIF4F have at least three isoforms (eIF4A1-3, eIF4E1-3 and eIF4G1-3, isoform being 1 the most abundant for these initiation factors). Here, we briefly focused on secondary cap-binding proteins apart from eIF4E and alternative tRNA carriers different from eIF2 (Figure 5C):

- Other cap-binding proteins. Gemin5 contains WD repeat domains necessary for the cap binding activity. Moreover, Gemin5 binds L3 and L4 into the 60S ribosomal subunit through its N-terminal domain and it is involved in global mRNA translation (Bradrick and Gromeier., 2009; Francisco-Velilla et al., 2016). The eIF3 subunit eIF3d, located near the mRNA exit at the back of 40S head, can also bind the 5' end cap. It is implicated in the translation of certain mRNAs regulating proliferation (Lee *et al*., 2016). The existence of alternative cap-binding protein supposes the specific control of protein synthesis in cellular environments where eIF4E is inactivated.
- Alternative Met-tRNAi^{Met} carriers. eIF2A (do not confuse with the α subunit of eIF2) can be another initiator tRNA carrier that acts synergistically with eIF5B. The latter has also properties to bind the Met-tRNAi^{Met}. Both factors are reported to enable the translation of Hepatitis C Virus (HCV) genomic RNA, although another study of Luis Carrasco's lab contradicts this theory. (Kim et al. 2018; Gonzalez-Almela et al., 2018;

Komar & Merrick, 2020). Finally, eIF2D is the last initiation factor known to date that can act as an alternative initiator tRNA carrier. These factors are refractory to the phosphorylation of the four kinases integrated in the ISR and thus, may escape this regulation. However, very little is known about the function of these alternative carriers in general translation and during stress response.

In sum, we summarised the three regulated pathways that generally downregulates translation during stress and the existence of alternative pathways to overcome this inhibition. Hence, certain mRNAs are still able to bypass stress-induced downregulation of translation by using non-canonical translation initiation mechanisms to mediate stress response. The best human model for studying the translation under stress conditions are cancer cells. Besides, new therapies in the oncology field are focusing on the translation step.

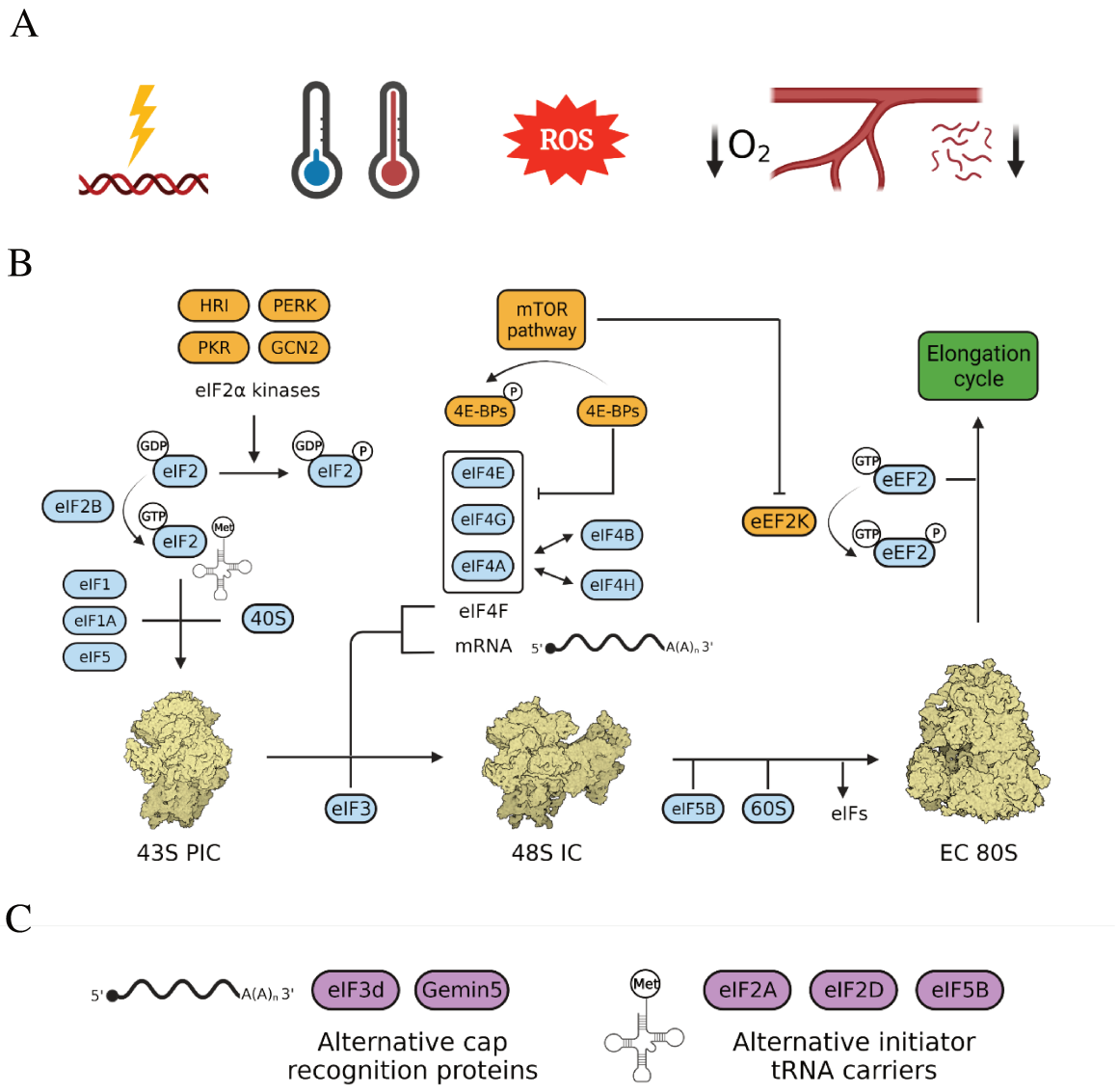

Figure 5. Translation regulation pathways activated during cellular stresses. (A) Representation of the main cellular stresses in mammalian cells. (B) The three translation regulation pathways controlling global translation under cellular stresses: phosphorylation of eIF2α, sequestration of eIF4E by hypophosphorilated 4E-BP controlled through the mTOR pathway and phosphorylation of translocation factor eEF2. The three

translation complexes represented come from PDBs 3J81, 6ZMW and 4UG0 from left to right. Ribosomal subunits and eIFs are represented in blue, whereas regulatory proteins are denoted in orange. (C) Alternative cap-recognition proteins and initiator tRNA carriers are indicated. The whole figure was made with BioRender.com

Cancer, translation in tumour cells and anticancer therapies

Cancer is in essence a genetic disease. The accumulation of molecular alterations in the genome of somatic cells is the basis of cancer progression. This affirmation has been possible thanks to the availability of the human genome, the development of molecular genetics and the advances in Next Generation Sequencing (NGS). The speed and cost reduction to sequence a whole individual genome have given an enormous potential to understand the main genetic features of each type of cancer and the existence of tumour heterogeneity as well. Additionally, the establishment of new biomarkers and the recent use of liquid biopsies have further improved diagnosis in clinical oncology (Nones & Patch, 2020). In the last two decades, novel drugs based on small molecules and monoclonal antibodies have enlarged the therapeutic options of many types of malignancies. Furthermore, precision oncology has emerged as an approach to prevent, diagnose or treat tumours supported by the use of molecular biology tools to evaluate the risks, to characterize the patient tumour and to personalise the patient treatment (de Vita et al., 2020).

However, these advances are still far from removing cancer from the top list of deadly diseases. According to the Global Cancer Statistics of GLOBOCAN, 19.3 million new cases were diagnosed and almost 10 million people died from cancer in 2020 (Figure 6A). These data positioned cancer as the second main cause of death worldwide, after cardiovascular diseases. It becomes the first cause of death in high-income countries. Sorting types of cancers by incidence in 2020 reveals that breast, lung, colorectal and prostate cancer are the most prevalent ones. Regarding the number of deaths worldwide the same year, lung cancer is the first of the list and together with colorectal, liver, stomach and breast cancer, is responsible for half of the total deceases (Sung et al., 2021). In the future, global cancer burden is predicted to increase in magnitude, particularly in developing countries due principally to demographic changes. Therefore, efforts must be made to strengthen cancer prevention measures and anticancer treatments in transitioning countries to reduce the impact of global cancer deaths.

Genetic alterations occur during an individual lifetime and only some of them can lead to tumorigenesis. Specific mutations in cancer driver genes increase net cell growth together with microenvironmental conditions. There are about 300 cancer driver genes that have been described by multidisciplinary approaches (Bailey et al., 2018). These genes can be oncogenes or tumour suppressor genes. Moreover, most of the mutations in cancer driver genes are point mutations, indels (insertions or deletions), chromosomal fusions or DNA methylation events. In terms of functions, gene mutations modulate one or several capabilities acquired to enable tumour cells to establish, to grow and to escape from apoptosis. These biological abilities are integrated in the Hallmarks of cancer (Figure 6B) and are defined as follows: sustain of proliferative signaling, evasion of growth suppressors,

deregulation of cell metabolism, immune destruction avoidance, cell death resistance, enabling replicative immortality, genetic instability and inflammation, phenotypic plasticity, non-mutational epigenetic reprogramming, angiogenesis, presence of senescent cells, microbiome profile, activation of invasion and metastasis (Hanahan, 2022). These acquired capabilities have been observed in most forms of cancer. More importantly, these skills of cancer cells cannot be explained *per se* by regarding individual cancer cells, unless they are described in their physiological context: the tumour microenvironment (Figure 6C).

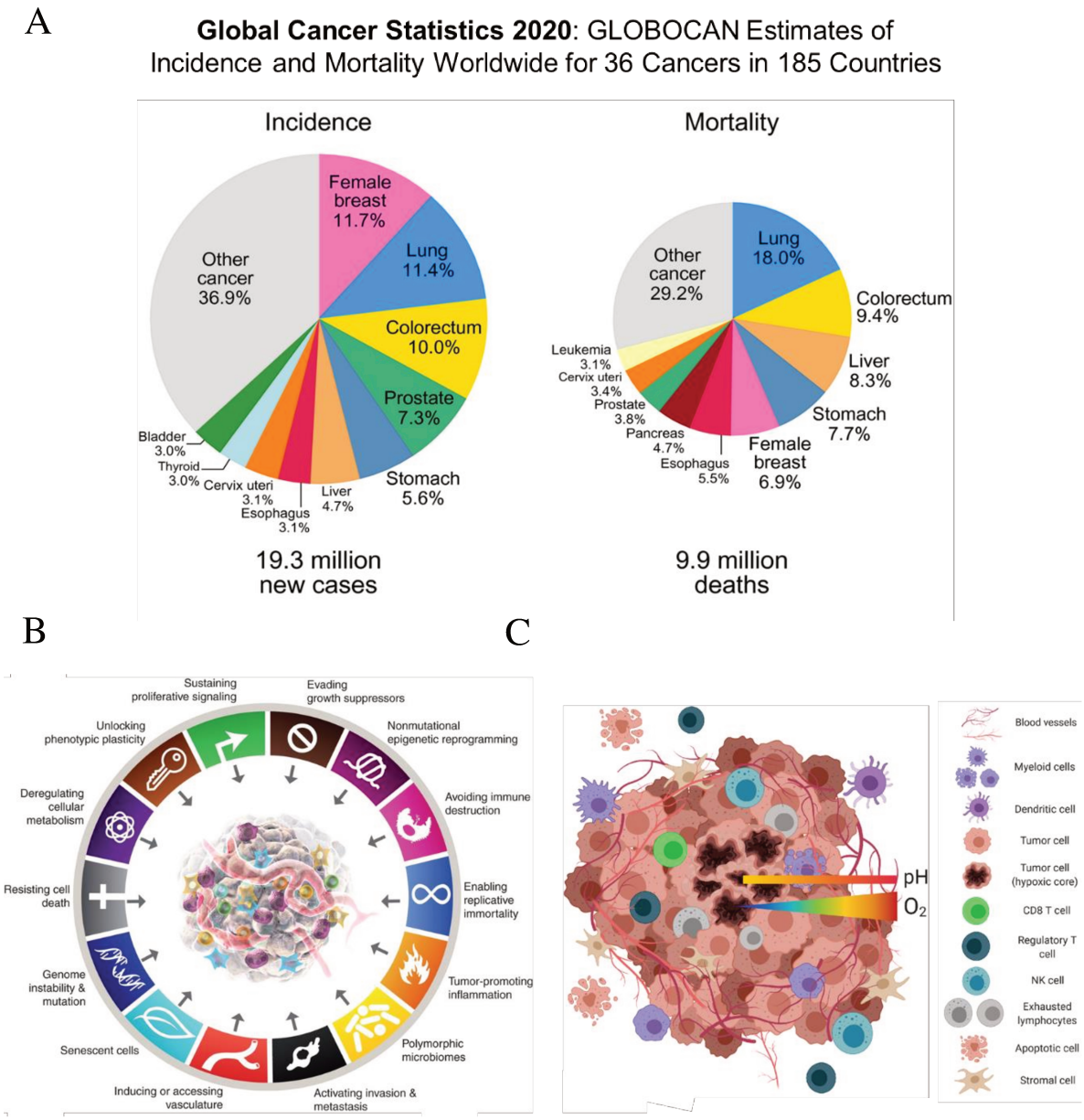

Figure 6. Global cancer incidence and mortality, hallmarks of cancer and tumour microenvironment. (A) GLOBOCAN cancer statistics about incidence and mortality worldwide by type of cancer. Graphics adapted from Sung et al., 2021. (B) Hallmarks of cancer. Figure adapted from Hanahan, 2022. (C) Tumour microenvironment schematized with different cell types and blood vessels surrounding the tumour mass. Oxygen and pH gradients are represented from low (left) to high (right). Darker zones represent necrotic cells. Image modified from Piñeiro-Fernandez et al., 2019.

Tumour microenvironment and hypoxia

Most cancers develop as solid malignant tumours – except leukaemia, that consists in individual blood cancer cells circulating in the bone marrow, the bloodstream, etc. One of the possible tumour classifications depends on the tissue of origin; carcinomas that develop from epithelial cells, sarcomas which derived from connective tissue (muscle, adipocytes, bone or blood vessels), lymphomas that originate from lymphocytes forming solid tumours in lymph nodes, blastomas that arise from precursor cells and tumours of mixed origin. Moreover, other classifications help to describe the tumour in terms of its grade, related to the morphology and cell differentiation and link to prognosis, or to its stage, related to the tumour development and spreading throughout the organism (Carbone, 2020).

Solid tumours consist in a mass of heterogeneous population of cancer cells integrated with a variety of immune and stromal cells, metabolites, extracellular matrix components and exosomes, all together known as the tumour microenvironment (TME). TMEs are evolving entities with different composition among tumour types. In general, they are deficiently perfused, following accumulation of cancer cell metabolites, decrease of oxygen level and nutrient starvation; conditions that the cells in the TME try to overcome by promoting angiogenesis/neovascularization (Anderson & Simon, 2020).

Hypoxia is a cellular condition that is characterized by deficient cell oxygenation compromising biological functions. It is important to consider that oxygen represents the 21% of the atmosphere gases at the sea level, which is equivalent to a partial oxygen pressure oxygen (pO_2) of 160 mmHg at sea-level atmospheric pressure (760 mmHg). Standard cell cultures are subjected to similar oxygen levels, usually defined as normoxia. However, the real oxygen level in human peripheral tissues vary from approximately 3% O_2 (pO_2 = 23 mmHg) to 7,5% O_2 (pO_2 = 57 mmHg) depending on the organ; this oxygen range can be described as the physiological oxygen level or "physoxia". Thus, when blood supply is insufficient, cancer cells become hypoxic. The majority of tumours that are subjected to pathological hypoxia bear oxygen levels <1% O_2 (pO_2 = 7,5 mmHg) although it can vary among tissues (McKeown, 2014; Swartz et al., 2020).

In hypoxia, tumour growth decelerates, and Hypoxia Inducible Factors (HIFs) within the TME promote the secretion of proteins as Vascular Endothelial Growth Factor (VEGF), that induce angiogenesis on the tumour and stromal cells. New vascularization attempts to compensate the oxygen deficiency in the tumour mass. However, the high proliferation rate of cancer cells and the uncontrolled activation of hypoxia signalling often result in an aberrant vascularisation that fails to compensate oxygen deficiency. Therefore, new blood vessels transiently restore oxygenation, and in this manner, the tumour has interchanging areas with acute and chronic hypoxia (Petrova et al., 2018).

TME strongly influences tumour progression and often determines the efficacy of therapeutic response and drug resistance. The current therapeutic strategy targeting the TME is based on the inhibition of the checkpoint system of immune cells (i.e., Cytotoxic T-Lymphocyte Antigen 4 (CTLA-4) or Programmed death-ligand 1 (PD-L1)) with monoclonal antibodies to potentiate the immune response (Marshall & Djamgoz, 2018). Nonetheless,

other aspects of the TME like hypoxia has been poorly exploited to improve therapeutic effectiveness. The behaviour of cancer cells under chronic hypoxia and specially the mRNA translation under this stress are two important features for the search of new anticancer therapies.

Translation reprogramming in cancer

Tumour cells are submitted to several stress conditions (i.e., hypoxia, nutrient deprivation and inflammation) that particularly downregulates canonical translation. The existence of alternative translation initiation mechanisms would explain the expression maintenance of a subset of cellular mRNAs encoding proteins implicated in stress response and adaptation, despite the canonical translation initiation process being compromised.

Although eIF4E is sequestered by 4E-BPs upon mTOR inhibition in starving cells, eIF4E level can increase through its upregulation or phosphorylation by MNK1 and 2. In this manner, eIF4E is activated or overexpressed in a large number of tumours. Moreover, eIF4E is a convergence point for several cancer-related signalling pathways (Siddiqui & Sonenberg, 2015). The formation of eIF4F in tumours correlates to cell proliferation and innate or acquired drug resistance and could be considered the major current target of mRNA translation to improve anticancer treatment response (Boussemart et al., 2014).

In the second pathway of translational control, although the phosphorylation of eIF2α impairs the formation of TC and downregulates global translation, eIF2α-independent ternary complexes can promote translation of specific mRNAs. Enhanced translation of transcripts containing uORF is exemplified by the ATF4 mRNA re-initiation (described above). On the other side, increased translation of mRNAs without uORFs could rely on structural elements in their 5'UTR under conditions of reduced TC availability (Holcik, 2015). Hypoxic cells undergo these translational changes, as well as the selective mRNA translation by the recruitment of mRNAs to the ER. In this manner, ER localization of HIF-targeted transcripts such as VEGF mRNA contributes to hypoxic adaptation (Chee et al., 2019).

Not only the initiation factors but also the deregulation of ribosomal protein expression can lead metastatic potential of cancer cells. Indeed, the overexpression of *RPL15* coordinates the upregulation of ribosomal proteins in circulating tumour cells and consequently increased global translational activity (Ebright et al., 2020). Moreover, *RPL13* is upregulated in gastrointestinal cancers and its expression correlates with clinical stage of tumours and chemoresistance (Kobayashi et al., 2006).

In cancer, the study of RNA post-transcriptional modifications is an expanding field. New evidence sustains that m^6A modification can sustain high levels of translation of pro-oncogenic mRNAs. For example, METTL3 and METTL14 are writers of m^6A modification, upregulated in some types of cancers, acting as oncogenes. Other reported mRNA modifications with an oncogenic effect are m^5C, m^7G, pseudouridine and adenosine-to-inosine editing (Barbieri & Kouzarides, 2020).

Hence, deregulated activity of initiation factors and ribosomal proteins are strongly correlated to tumour growth and metastatic processes of cancer cells. Together with mRNA

localization and mRNA *cis*-acting elements (RNA structural elements and post-transcriptional modifications), they reprogram the translational output of tumour cells and overcome the global reduction of protein synthesis under stress. These features open an interesting area for clinical investigation and drug design against translation of cancer cells.

Drug resistance and anticancer therapies targeting translation

Therapy resistance in cancer arises from multiple factors and it turns into the bottleneck to achieve the cure of oncology patients. In the recent history of anticancer treatment, single-agent chemotherapy has gradually been abandoned by combination therapy in many patients with poor therapeutical response and new strategies including specific small molecules and immuno-oncology have arisen. The biological determinants of resistance are primarily tumour growth kinetics, tumour heterogeneity, biological barriers, the TME, the immune system, the undruggability of cancer drivers and the selective pressure upon anticancer treatment. The actual solutions to diminish drug resistance events comprise early diagnosis, adaptative treatment and therapeutic monitoring (Vasan et al., 2019).

Translational reprogramming is a reversible process that often allows tumour cells to reduce drug efficacy. Indeed, components of the eIF4F complex, some ribosomal proteins, such as *RPL23*, or modifications like m6A in certain mRNAs, drive chemoresistance to several anticancer drugs (i.e., fluorouracil, platinum analogues, paclitaxel). Importantly, chemotherapy itself activates the stress response of tumour cells and it can induce drug persistence in a subset of tumour cells described as persister cells (Fabbri et al., 2021).

Protein synthesis converges with essential signalling pathways in the cell and its machinery is altered in cancer, which makes it a suitable process to target. mTOR inhibitors and eIF4F inhibitors account for the majority of translation-targeting drugs in preclinical and clinical settings (Bhat *et al.*, 2015). Currently, eIF4F inhibitors are based on drugs targeting eIF4E, eIF4E/eIF4G interaction and eIF4A binding to mRNA. For direct inhibition of eIF4E, two strategies are described: cap analogues or antisense oligonucleotides (ASO) against eIF4E mRNA. Moreover, three potent molecules, discovered by high-throughput screening, inhibit eIF4E/eIF4G interaction: 4EGI-1, 4E1RCat and 4E2RCat (Lu et al., 2016). Another indirect strategy to reduce eIF4E activity consists in the inhibition of eIF4E kinase MNK1 with eFT508, a small molecule currently in clinical phase II.

In the case of eIF4A, three main classes of inhibitors are known to date: rocaglates (or flavaglines), hippuristanol, and pateamine A. All of them are obtained from natural compounds and are considered as potent anticancer and antiviral drugs. Rocaglates, purified from plants of the *Aglaia* genus, act by clamping eIF4A into RNA preferentially in polypurine sequences. Hippuristanol, extracted from corals, inhibits the interaction of mRNA with eIF4A. Pateamine A, extracted from marine sponges, impairs eIF4A interaction with eIF4G although it increases RNA helicase activity. However, a simplified version of this molecule, desmethyl, diamino pateamine A was reported to possess antitumoral potential (Malka-Mahieu et al., 2017).

Other inhibitors target the formation of the TC, by increasing the phosphorylation of eIF2α, for example salubrinal, a phosphatase inhibitor that hinders the dephosphorylation of

eIF2α. Nevertheless, phosphorylation state of eIF2α is known to activate apoptosis, although it can also increase the survival of cancer cells through adaptation in response to stress. Thus, eIF2α phosphorylation acts as a switch that controls the balance between the death and survival of cells in response to stress including nutrient deprivation (Muaddi et al., 2010).

In conclusion, the use of translation-targeting inhibitors to treat cancer in combination therapies shows a promising strategy to overcome the issue of tumour heterogeneity and acquired resistance. Also, it will strengthen new investigations to understand cancer processes from the perspective of translation. Below, the introduction focuses on the description of two proteins relevant in cancer progression, β-catenin and HIF-1α, with difficulties to be directly targeted by current drugs.

The catenin family: β-catenin

Catenins – derived from the latin word "catena" (chain) – are a protein family mainly involved in the link of the actin cytoskeleton with cadherins, which are the cell adhesion molecules of animal cells. Cadherins in conjunction with catenins mainly form the so-called adherens junctions between epithelial cells. There are four types of catenins (Figure 7A):

- *CTNNA1* gene encodes for α-catenin and shares common structure features with vinculin. α-Catenin creates a dynamic binding between the cadherin-catenin complex and vinculin associated with filamentous actin. This interaction depends on the monomeric or homodimeric state of α-catenin (Drees et al., 2005).
- *CTNNB1* gene encodes for β-catenin, the vertebrate homologous of the well-known "armadillo" protein that was first discovered in the fruit fly (Peifer et al., 1992). In humans, this protein has 781 amino acids and can be divided into three regions (Figure 7B). The N-terminal (amino acid position 1-141) and C-terminal domain (positions 664-781) are predominantly unstructured, while the central region is folded in twelve repetitions of the same protein domain called armadillo repeat (Arm). This domain consists of two contiguous alpha-helixes forming a hairpin. β-Catenin binds directly to the cytoplasmic tail of classical cadherins and regulates the interaction with the actin cytoskeleton by α-catenin and vinculin (Niessen & Gottardi, 2008)
- *JUP* gene encodes for γ-catenin, also known as plakoglobin. This protein contains twelve Arm repetitions and it shares a very similar structure with β-catenin (70% sequence identity in humans). It contributes to the establishment of adherens junctions, although it principally participates into the binding between cadherins and keratin filaments in desmosomes (Aktary et al., 2017).
- *CTNND1* gene encodes for δ-catenin (also known as p120). It contains Arm repeats similar to β-catenin and binds to the cytoplasmic domain of cadherins as well. This protein stabilizes cadherins and prevents its endocytosis as well as recruiting microtubules for maturation of adherens junctions (Kourtidis et al., 2013).

In summary, the four types of catenins participates in the correct functioning and integrity of the cadherin junctions with the cytoskeleton. β-Catenin, plakoglobin and p120 possess Arm repeats and have some similarities in terms of structure and function. Despite β-catenin

plays the role of an intracellular structural component of cadherin-based adherens junctions, it is actually a multifunctional protein with two independent roles in the cell. In addition to the structural role mentioned above, it is indeed acting as the main effector of the Wnt pathway.

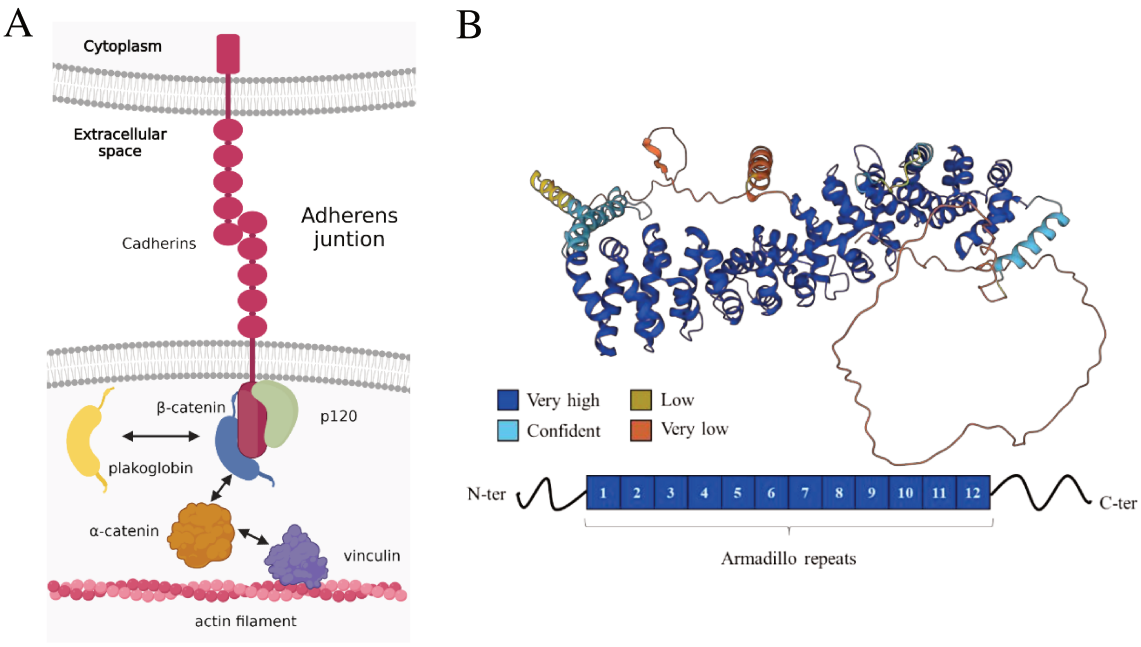

Figure 7. Role of catenins in adherens junctions and β-catenin structure. (A) Representation of adherens junctions between epithelial cells. Cadherins strongly interact in the extracellular space forming the adherens junctions. β-Catenin, plakoglobin and p120 bind the cytoplasmic tail of cadherins for junction stabilization and α-catenin joins the cadherin-catenin complex with actin filaments associated with vinculin. (B) Structure of β-catenin predicted with AlphaFold and deposited in Uniprot as AF-P35222-F1. Residue confidence score is represented with four colors from very high to very low (in order, dark blue, light blue, yellow and orange). The folding of the twelve Arm repetitions in dark blue had already been resolved in the past by several crystallography studies.

Wnt/β-catenin pathway

Wnt signaling pathway (Nusse et al., 1991) is a signal transduction pathway that regulates transcription of genes involved in proliferation via cell-cell communication or autocrine signaling and it is highly conserved in animals. Most of the components of this pathway were discovered in the fruit fly – related to the segment polarity – and were given names according to their knockout phenotype (Wodarz and Nusse, 1998). There are several branches of the Wnt pathway: the canonical Wnt//β-catenin pathway that is involved in proliferation, and non-canonical Wnt/planar cell polarity (PCP) or Wnt/Ca^{2+} pathways that regulate cellular polarization and migration (Komiya & Habas, 2008).

In mammalian Wnt/β-catenin pathway (see Figure 8), specific ligands of the family of WNTs bind to Frizzled receptor, a transmembrane protein that co-localizes with the low-density lipoprotein receptor–related proteins 5 and 6 (LRP5/LRP6) in the plasmatic membrane. These two receptors activate downstream signaling events when they bind the

WNT ligand. This activation primarily consists in the stabilization of β-catenin that plays the key effector role in the canonical Wnt signaling. Proteostasis of β-catenin is highly regulated by the action of the destruction complex and depends on its phosphorylation status. The destruction complex contains, among others, the adenomatous polyposis coli (APC), the scaffold protein axin, casein kinase 1 (CK-1) and glycogen synthase kinase 3 (GSK3) (Valenta et al., 2012). In fact, APC was discovered in patients with an inherited condition where mutated APC contributes to the formation of polyps (benign neoplasm) in the epithelium of large intestine which can become cancerous.

In the absence of WNT ligand, GSK3 phosphorylates β-catenin and target it for further proteasomal degradation. In the presence of WNTs, GSK3 is phosphorylated by Dishevelled (DVL) and consequently inactivated, thus it cannot phosphorylate β-catenin. β-Catenin is then stabilized, it accumulates in the cytoplasm and translocate to the nucleus where it activates the transcription of target genes in complex with T-cell factor (TCF) transcription factor. Among these downstream genes, β-catenin/TCF activates cyclin-D1 and c-myc transcription (Clevers & Nusse, 2012). These genes induce the progression in the cell division cycle.

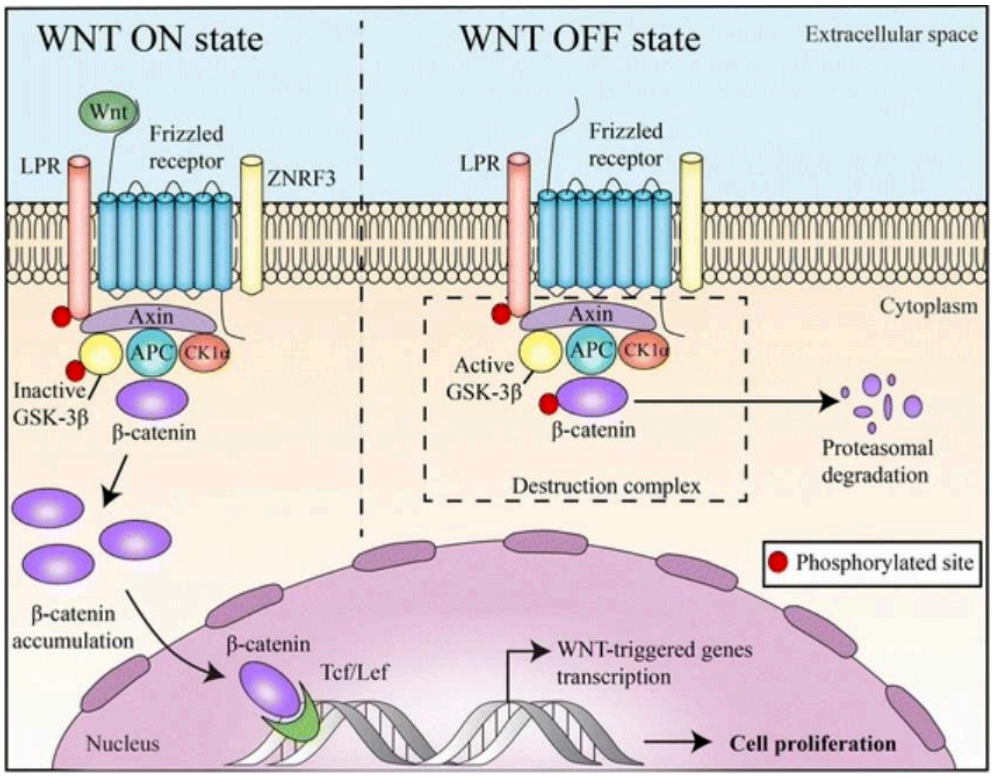

Figure 8. Wnt/ β-catenin pathway. In the WNT ON state**,** WNT ligand binds to Frizzled receptor and the LRP co-receptor. The destruction complex is associated to the Wnt receptors through Axin. GSK-3β is phosphorylated and therefore inactivated. This prevents phosphorylation of β-catenin and the latter is translocated into the nucleus and associates with TCF/LEF to promote the transcription of Wnt-targeted genes, which in last instance increase the cell proliferation rate. In WNT OFF state, the absence of WNT ligand activates the destruction complex of β-catenin, formed by axin, APC, CK-1 and GSK3β. Figure adapted from Pai et al., 2017.

Briefly, the Wnt pathway is activated by extracellular ligands and drives transcriptional changes through β-catenin, regulating relevant processes in the cell: development, proliferation and migration. The proliferation effects of activated Wnt/β-catenin pathway are often deregulated in cancer cells.

β-Catenin in cancer and hypoxia. Therapeutic target

As explained above, colorectal, hepatocellular and gastric carcinomas accounts for a third of the worldwide deaths caused by cancer. In these life-threatening carcinomas of the digestive tract, β-catenin is aberrantly accumulated due to mutations in the components of Wnt signaling pathway; especially, *APC* loss-of-function mutations in colon cancer and *CTNNB1* activating mutations in liver cancer that make β-catenin avoid phosphorylation in the destruction complex and escape degradation. In a non-negligible number of cases, *CTNNB1* mutations in hepatocellular carcinomas are caused during hepatitis B or hepatitis C virus infection, that are well-known oncoviruses (Javanmard et al., 2020). Therefore, the accumulation of unphosphorylated β-catenin allows constitutive translocation of the protein that binds TCF and enhances the expression of proliferative genes (Nusse & Clevers, 2017; Bugter et al., 2021).

Among stresses in the TME, hypoxia is able to inhibit the canonical Wnt/β-catenin signaling pathway. Hypoxia-induced ER stress inhibits normal Wnt protein processing and secretion. However, tumour cells harboring common mutations in Wnt/β-catenin pathway are insensitive to this hypoxic modulation (Verras et al., 2008). β-catenin accumulation has been reported under hypoxic conditions in cancer cells, without any variation of its mRNA level (Hong et al., 2017). Moreover, the crosstalk between the Wnt/β-catenin pathway and HIF-1α signaling under hypoxic microenvironment induces tumour cells to invade other tissues (Zhang et al., 2013; Liu et al., 2015). MYC regulates the activity of eIF4F by increasing the expression of all its components and in return, eIF4F enhances *c-myc* mRNA translation, generating a feedforward loop that support tumorigenesis (Lin et al., 2008).

Due to the notable implication of Wnt pathway in cancer progression, many drugs that target different components of the pathway have been developed and are now in preclinical or phase I trials. These small molecules were identified through high-throughput screenings, and few of them target β-catenin directly. Only two compounds, PFK115-584 and CGP049090 (Novartis Pharma Inc.) can block at some extent β-catenin/TCF interaction (Krishnamurthy & Kurzrock, 2018). Although β-catenin can bind small molecules, these drugs cannot inhibit its function in the Wnt pathway, meaning that β-catenin is rather a yet-to-be-drugged protein (Cui et al., 2018). For these reasons new strategies must be developed to overcome the difficulty to target β-catenin, i.e., focusing on the inhibition of *CTNNB1* mRNA translation.

CTNNB1 mRNA

The complete mRNA sequence of *CTNNB1* gene was already obtained, denoting two splice variants differing in the 3'UTR length and an invariable 5'UTR of 214 nts (Nollet et

al., 1996). The stability of these spliced variants differs on the presence of AU-rich elements in the 3'UTR that control *CTNNB1* mRNA turnover (Thiele et al., 2006). Concerning the translation mechanism of β-catenin mRNA, a putative IRES was reported in its 5'UTR. Apparently, the IRES-dependent translation is activated when cells are treated with paclitaxel, an anticancer drug which specifically binds tubulin and inhibits microtubules disassembly. Paclitaxel then increases the level of nuclear β-catenin that in consequence enhances the transcription of c-MYC to promote cell proliferation (Fu et al., 2015). Nevertheless, the mechanism of β-catenin mRNA translation has been poorly studied in cancer cells.

Hypoxia inducible factors

HIFs are factors that mediate the adaptative transcriptional response to hypoxia and that they are fundamental in embryogenesis and development. In animals, HIFs were originated from the need of providing cells a mechanism to adapt and regulate the oxygen distribution. These factors span to their maximum complexity in vertebrates. HIFs form heterodimer complexes comprising an inducible α subunit acting as an oxygen sensor and a constitutively expressed β subunit. All subunits possess a basic helix-loop-helix-PAS (bHLH-PAS) domain responsible of heterodimerization and DNA binding (Semenza, 2012).

In mammals, there are three genes encoding α subunits: *HIF1A*, *HIF2A*/*EPAS1* and *HIF3A*. HIF-1α and HIF-2α are essential for the oxygen stress response and share 90% of protein identity, while HIF-3α is shorter and its role remains elusive (Wu et al., 2015). The β subunit, HIF-1β (also known as aryl hydrocarbon receptor nuclear translocator, ARNT), is encoded by the *ARNT* gene. There are three isoforms of *ARNT* gene and one of them is ubiquitously expressed (Mandl & Depping, 2014).

Transcriptional regulation exerted by HIF-1 is mediated through the hypoxia response elements (HRE) located near promoter regions and have a consensus sequence RCGTG (where R is a purine). Most of the HIF-1 target genes are involved in angiogenesis (i.e., VEGF), erythropoiesis (i.e., erythropoietin (EPO)), glucose metabolism, survival and proliferation (Slemc & Kunej, 2016).

The regulation of *HIF1A* gene at transcriptional is well established, although HIF-1α mRNA is expressed constitutively in many types of cells. Sequences activating and repressing transcription were identified in the *HIF1A* promoter. Also, HRE were found in the promoter region, indicating a possible self-regulating system for the synthesis of HIF-1α. Finally, the presence of a DNA G-quadruplex was reported on the promoter of *HIF1A* gene and it seemed to modulate the mRNA level (Galbán & Gorospe, 2009; Chen et al., 2014).

HIF-1 and HIF-2 stability and activation is tightly controlled via post-translational regulation of the α-subunit (see Figure 9). HIF-1α is hydroxylated at Pro402 and Pro564 by prolyl hydroxylases (PHD) when cells are in physiological oxygen conditions, while they become dehydroxylated in the lack of oxygen. Hence, the hydroxylation state of HIF-1α renders this protein an oxygen sensor and the stability of the protein is regulated through

these hydroxyl groups. The latter are recognised by the von Hippel-Lindau tumour-suppressor protein (VHL), an E3 ubiquitin-protein ligase that targets HIF-1α for proteasomal degradation. Therefore, in the absence of hydroxyl groups in hypoxia, HIF-1α is stabilised and the protein level increases. Hence, HIF-1α is translocated into the nucleus and together with HIF-1β, they promote the transcription of their targeted genes (Semenza, 2004). Moreover, p300 functions as a transcriptional co-activator binding to the N-terminal domain of HIF-1α.

Certain mutations in VHL impair HIF-1α degradation system in standard oxygen conditions. These mutations, generally exon deletions or missense mutations that generates a truncated protein, cause an inherited pathology known as VHL disease. It is characterized by the occurrence of certain tumours, including central nervous system (CNS) and retinal angiomas, as well as renal cell carcinomas. The prevalence of VHL disease is around 1 in 40000 births and no cure exists for the moment. Nonetheless, early diagnosis and tumour removal improves life expectancy and quality of life for patients (Maher et al., 2011). Apart from inherited diseases, HIFs are involved in the progression of tumour growth and metastasis.

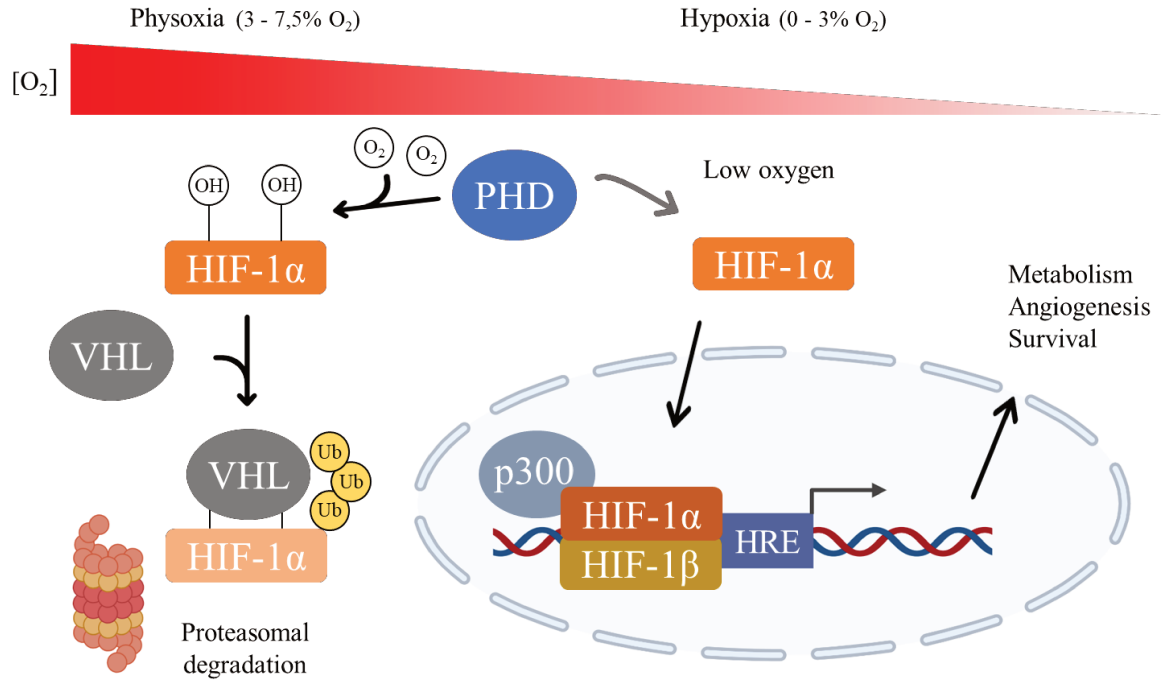

Figure 9. HIF-1 pathway and HIF-1α post-translational regulation. In physiological oxygen conditions (physoxia), HIF-1α is hydroxylated by PDH. VHL recognizes hydroxyl groups in specific prolines and HIF-1α is ubiquitinated for further proteasomal degradation. In hypoxia, mow oxygen impairs PDH hydroxylation of HIF-1α and VHL do not recognise it for degradation. In this manner, HIF-1α can enter the nucleus and form a complex with HIF-1β. In this manner, HIF-1 in cooperation with p300 regulates transcription of target genes by binding HREs. These genes are involved in modulation of anaerobic metabolism, angiogenesis and cell survival among others.

HIF-1α in cancer. Therapeutic target.

Blood supply is reduced in emerging solid tumour cells with poor or defective vascularization. In the TME, low tumour oxygenation generates chronic hypoxia in both cancer and stromal cells. Additionally, nutrient supply may be reduced and consequently the tumour cells have less access to essential nutrients. HIF-1 activity promotes tumour neovascularization and switches the cell metabolism to glycolytic mode and the generation of protons acidifies the medium. More importantly, transcriptional changes derived from HIF-1 activity promotes cancer cell migration and invasion of other tissues to evade the adverse conditions of the TME (Petrova et al., 2018).

In colorectal cancer, *HIF1A* overexpression is associated with poor prognosis and higher mortality, whereas *HIF2A* expression changes are unrelated with clinical outcome (Baba et al., 2010). In pediatric high-grade gliomas, HIF-1α expression sustains tumour adaptation to hypoxia, cancer progression and metastasis. Additionally, it reduces radiotherapy effectivity and location into the brain often hinders surgical intervention for tumour removal (Fuchs et al., 2020).

Considering the impact of HIF-1α on cancer progression, there is a great interest to understand the deregulation of HIF-1α pathway in cancer cells and the development of drugs targeting HIF-1. Although new HIF-1 inhibitors have been described, the complexity of HIF-1α pathway has made the process of drug design very challenging as well as inhibitor's lack of specificity. For the moment, no HIF-1α selective inhibitor has reached clinical approval. However, some drugs commercially available can indirectly modulate HIF-1 activity and could be used in combination therapy together with classical treatment for certain types of cancers. For example, acriflavine inhibits HIF-1α dimerization or echinomycin binds HRE sequences to prevent HIF-1α DNA binding (Masoud & Li, 2015). More research must be done to find drugs that reduce aberrant HIF-1α level specifically in certain tumours and, a novel strategy could aim to inhibit *HIF1A* mRNA translation.

HIF1A mRNA

Human *HIF1A* mRNA have three reviewed isoforms (NCBI Reference sequences: NM_001530.4, NM_181054.3 and NM_001243084.2, for isoform 1, 2 and 3, respectively). The prominent variant is isoform 1 that consists in a 5'UTR of 292 nts, an ORF of 2478 nts and a long 3'UTR of 1175 nts. The untranslated regions of this gene have not been structurally characterized and little is known about their function in translation and mRNA stability. A large region of the 5'UTR was reported to upregulate translation during hypoxia in metastatic cells lines, as the human glioblastoma cell line U87MG, and additionally, AU-rich elements (AREs) in the 3'UTR cis-regulate mRNA decay (Yasuda et al., 2014). Interestingly, the cytoplasmic polyadenylation element binding protein (CPEB2) slows down the translation elongation of *HIF1A* mRNA under normoxia by binding to the 3′UTR and interacting with eEF2. However, when cells are subjected to hypoxia, CPEB2 dissociates from *HIF1A* mRNA, leading to rapid synthesis of HIF-1α for hypoxic adaptation (Chen & Huang, 2012).

The translation of HIF-1α during hypoxia was originally attributed to an IRES within the 5′UTR of its mRNA. Nonetheless, other studies revealed that this region did not possess IRES activity. RNA-binding proteins regulate instead the translation rate of *HIF1A* mRNA through the 3′ UTR (Ivanova et al., 2019). Additionally, a recent report made a correlation between m^6A-methylation of *HIF1A* mRNA and the increase of protein translation and abundance in adipose tissue (Wu et al., 2021). Hence, the translation regulation of *HIF1A* mRNA through its 5'UTR remains elusive.

Thesis objectives

The general interest of our lab is to characterise alternative mechanisms of mRNA translation in human cancer cells using biochemical and structural biology approaches. In this context, the aim of my thesis project comprises the study of translation of two mRNAs involved in tumour growth and adaptation to hypoxic stress by analysing the translational role of the RNA elements of their 5'UTRs. In this way, we are providing essential information of mRNA translation in the tumour context as a starting point for therapies targeting the translation of specific mRNAs, to fill the undruggability gap of their encoded proteins.

The first objective of my project consists in obtaining the secondary structure model of the 5'UTR of human *CTNNB1* and *HIF1A* mRNAs, performing RNA chemical probing *in vitro* combined with RNA structure prediction software. Furthermore, an RNA structure model *in vivo* would give more valuable information of the mRNA folding in cells. The second aim is to set up the preparation of human cancer cell extract for *in vitro* translation assays, as well as transfecting the mRNAs of interest into cells. Besides, cancer cell lines can be subjected to stresses mimicking the TME, such as hypoxia, for a better understanding of protein synthesis in these conditions. Another objective of this general characterization is to validate that *CTNNB1* and *HIF1A* mRNAs are not affected by transcriptional changes under stress conditions.

We prioritise β-catenin mRNA in the analysis of its translation in cancer cells. A relevant objective of this project is to isolate the 48S IC bound to β-catenin mRNA directly from cell extracts cultured in normoxic and hypoxic conditions. The composition of the complex is analysed by mass spectrometry and the structure solved by cryo-electron microscopy. This approach will reveal how β-catenin mRNA is anchored on the translation machinery and will allow to identify initiation factors and other stress-induced factors involved in its translation.

The combination of different techniques to elucidate 5'UTR structures, their function in translation and the human initiation complexes of these mRNAs at high resolution will provide a novel fundamental insight of translation in cancer, in order to develop new anticancer strategies based on mRNA-targeting drugs.

RESULTS

Article 1: The GC-rich element within the 5'UTR of β-catenin mRNA modulates its translation under hypoxia

Abstract

Protein synthesis is a universal process mainly regulated at the initiation stage to permit a fast adaptation and response to environmental changes. Actively growing tumour cells are rapidly submitted to hypoxia, a condition known to downregulate canonical cap-dependent translation by the unavailability of the cap-binding factor eIF4E. In this condition, translation of several oncogenic mRNAs, is nevertheless maintained to promote cancer sustain and progression. However, the understanding of translation process under hypoxia in cancer remains elusive. Increasing evidence of unconventional translation initiation mechanisms evading the canonical model, have indicated the importance of signals in the 5'UTR regions of mRNAs to promote ribosome recruitment. β-Catenin mRNA has a 214-nucleotide-long 5'UTR, which contains a GC-rich element folded into a three-way junction. RNA transfection assay in HeLa and others cancer cell lines highlights its key role in the expression of β-catenin and its translation enhancement under hypoxia. We demonstrated by mass spectrometry, EMSA and footprinting assays that in the absence of eIF4E, the GC-rich element drives the hypoxic β-catenin translation being the anchoring point for eIF4A, eIF4B and eIF4G, and leading the 43S PIC recruitment. We confirmed that β-catenin mRNA translation is inhibited upon treatment with silvestrol, an eIF4A inhibitor. This study uncovers the stress-induced translational regulation of β-catenin mRNA via its 5'UTR and set an innovative approach to explore alternative translation mechanisms of mRNAs related to cancer progression.

Key words

translation initiation, alternative mechanisms, 5'UTR, hypoxia, cancer, β-catenin, eIF4A, eIF4B

IN SUBMISSION

The GC-rich element within the 5'UTR of β-catenin mRNA modulates its translation under hypoxia

Authors: Rol-Moreno J.[1,2], Bec G. [1], Kuhn L. [3], Ennifar E. [1] and Simonetti A. [1]*

[1]Université de Strasbourg, CNRS - Architecture et Réactivité de l'ARN - UPR 9002, 67084 Strasbourg, France.

[2]Sanofi-Aventis R&D, Open Innovation Access Platform, Strasbourg, France.

[3]Plateforme protéomique Strasbourg Esplanade, Université de Strasbourg, CNRS, 67084 Strasbourg, France.

*Corresponding author

Introduction

Protein synthesis is the last stage of the gene expression pathway, and it is accomplished by the ribosome in conjunction with accessory proteins that assemble transiently, assisting the whole process and ensuring its fidelity, processivity, efficiency and accuracy. It is commonly divided into four phases: initiation, elongation, termination and ribosome recycling. Due to the high energy consumption during translation, the initiation step is the most tightly-regulated and rate-limiting process for the fine and rapid regulation of gene expression in response to different stimuli. In eukaryotes, a dozen of eukaryotic initiation factors (eIFs) is required to ensure accurate start codon localization through base-triplet inspection from the mRNA 5' end. A common feature between the multiple pathways for the start codon recognition is the dynamic and chronologically ordered assembly of several ribosomal complexes with numerous eIFs, which associate and relocate on the ribosome at different stages of the initiation process (Guca & Hashem, 2018; Hinnebusch, 2014, 2017; Jackson et al., 2010; Parsyan et al., 2011; Sonenberg & Hinnebusch, 2009). For most of the eukaryotic mRNAs, translation starts with the assembly of the heterotrimeric eukaryotic initiation factor 2 (eIF2), which binds initiator methionyl-tRNA (Met-tRNA$_i^{Met}$) in a GTP-dependent manner, forming the ternary complex (TC; Kapp & Lorsch, 2004). Assisted by eIF1, eIF1A, the multi-subunit complex eIF3 and eIF5 the TC is then recruited onto the 40S ribosomal subunit to form the 43S pre-initiation complex (43S PIC; des Georges et al., 2015; Erzberger et al., 2014; Hashem et al., 2013).

Eukaryotic transcripts generally possess a 7-methylguanylate (m7G-cap) at the 5' end, which confers stability to the mRNA. Eukaryotic initiation factor 4E (eIF4E) is responsible of the m7G cap structure recognition and, together with the DEAD-box RNA helicase eIF4A assembled onto the scaffold protein eIF4G, form the cap-binding complex or eIF4F. In the canonical translation initiation pathway, eIF4G interacting with eIF3 and PABP, helps bringing the 43S PIC at the 5' end of the eIF4E-bound mRNA to form a scanning-competent 48S initiation complex (SC48S IC) (Brito Querido et al., 2020; des Georges et al., 2015; Pelletier & Sonenberg, 2019; Villa et al., 2013). Notably, in the SC48S IC the Met-tRNAi is not fully accommodated in the ribosomal P-site (open /P$_{out}$ state; Hussain et al., 2014).

During the active search of the start codon to establish the reading frame, SC48S IC can encounter different RNA structural elements. Besides, scanning is a more challenging step in higher eukaryotes due the evolutionary increase of 5'UTR length from yeast to mammals (Leppek et al., 2018). The ATP-dependent RNA helicase eIF4A is responsible for the unwinding of local structured elements of the 5'UTR and its activity is enhanced by other initiation factors such as eIF4B, eIF4G and eIF4H (Rogers et al., 2001; Sun et al., 2012). The scanning ends when the codon-anticodon duplex formed between the mRNA and the Met-$tRNA_i$ which is now locked in the P-site (close P_{in} state), stabilizes the SC48S IC on the start codon (Hussain et al., 2014).

The Kozak sequence context interacting with eIF1A and eIF2α, several ribosomal proteins and nucleotides of the 18S rRNA flanking the mRNA channel allows correct start codon recognition and influences the stability of codon-anticodon duplex (Simonetti et al., 2020). The recognition of the start codon is then followed by a chronologically order events comprising the GTP hydrolysis induced by the γ-subunit of eIF2, dissociation of eIF1 and relocation of eIF1A and eIF5 which conducts to the formation of the late-stage 48S IC (LS48S IC; Llácer et al., 2018).

Finally, the large ribosomal subunit 60S joins the LS48S IC inducing the release of eIF5B after GTP-hydroysis. This event renders 80S ribosome competent for the elongation step permiting the first elongator aminoacyl-tRNA (aa-tRNA) to position on the A site (Pestova et al., 2000). This canonical translation initiation model is supported by numerous biochemical, genetic and structural studies (Donahue, 2000; Gingras et al., 1999; Guca & Hashem, 2018; Hinnebusch, 2017; Kozak, 1991).

Nevertheless, alternative mechanisms that elude this classical model and its fine-tuned regulation have been reported showing the capability of the translation machinery to adopt different strategies driven by mRNA signals often located in the 5'UTR region (Jackson, 2013; Jackson et al., 2010; Leppek et al., 2018; Mailliot & Martin, 2018; Shatsky et al., 2018). In the late 80s, Internal Ribosome Entry Site element (IRES) was first described within the 5'UTR of picornavirus RNAs, which allows hijacking host translation machinery for their own translation, primarily in a cap-independent manner and even without scanning step (Jang et al., 1988; Pelletier & Sonenberg, 1988). Since then, four types of viral IRESes have been proposed regarding their secondary structure and the requirement of eIFs (Kieft, 2008; Mailliot & Martin, 2018; Martinez-Salas et al., 2018). Soon after the finding of this novel translation mechanism, IRES activity was also reported in several vertebrate mRNAs, whose translation could not be explained in conditions where the translation is globally reduced. IRES-driven mechanism can be conceived as a virus strategy to ensure its genome translation, where RNA elements can usurp the host translational machinery to use it for their own benefit. Despite the initial controversy on its existence, the cellular IRES-driven mechanism is now considered one of the possible strategies that cells use to synthesize proteins necessary for cell survival and stress adaptation (Gilbert, 2010; Jackson et al., 2010; Shatsky et al., 2018). The presence of a long and highly-structured 5'UTR or the translation persistence under stress conditions in a subset of mRNAs cannot be considered an argument only for IRES, but rather for the search of non-canonical initiation mechanisms (Terenin et al., 2017).

Since last decade, alternative translation mechanisms of cellular mRNAs have received special attention due to its emerging significance in cancer progression, since most of the RNA elements described are held in mRNA coding to proteins involved in the control of cell growth, division and apoptosis (Baird et al., 2006; James & Smyth, 2018). In tumour cells, translation is subjected to reprogram due to aberrant oncogenic signaling and microenvironmental stress, such hypoxia, nutrient starvation and immune response (Fabbri et al., 2021). Among these stresses, hypoxia arises when oxygen availability drops under normal levels – although oxygen level varies in different tissues. Solid tumor cells are often submitted to chronic hypoxia, cycling between hypoxic and normoxic states (Chee et al., 2019). During stress, two main features provoke the decrease of global translation rate: i) the phosphorylation of eIF2α performed by the kinases of the Integrated Stress Response system (ISR) prevents nucleotide recycling of eIF2-GDP by the guanine exchange factor eIF2B (Adomavicius et al., 2019; Jackson et al., 2010), and ii) the sequestering of the cap-binding factor eIF4E upon hypo-phosphorylation of its inhibitory binding partner eIF4E-binding protein (4E-BP) through inactivation of mTOR kinase (Pópulo et al., 2012). Despite a general inhibition of translation due to these events, some mRNAs are still translated via alternative mechanisms, often driven through mRNA *cis*-acting elements located in their 5'UTRs. These elements comprise IRESs, RNA structure elements, cap-independent translation enhancers (CITE), RNA modifications and upstream ORFs. Moreover, several trans-acting factors and canonical initiation factors participates in the regulation of translation in response to different stress stimuli interacting with the above mentioned 5'UTR elements (Lacerda et al., 2017; Leppek et al., 2018; Shatsky et al., 2018). Recently, eIF4B were reported to bind the head of the 40S and, together with eIF4A, they facilitate mRNA loading on the 43S PIC (Walker et al., 2013; Yourik et al., 2017). Noteworthy, despite the stress-induced inhibition of the canonical cap-dependent translation certain oncogenic mRNAs involved in tumour progression – as β-catenin, MYC and HIF-1α – can maintain their translation promoting cancer cell persistence and plasticity (L. J. Lee et al., 2021; Shang et al., 2017).

In humans, *CTNNB1* gene encodes for β-catenin, the vertebrate homologous of the well-known *armadillo* protein in the fruit fly (Peifer et al., 1992). It is a multifunctional protein with two independent roles in the cell. Firstly, β-catenin functions as an intracellular structural component of cadherin-based adherens junctions. Proteostasis of β-catenin is highly regulated by the action of the destruction complex and depends on its phosphorylation status. Indeed, phosphorylation of β-catenin triggers its recruitment for ubiquitination and subsequent proteasomal degradation. In contrast, unphosphorylated β-catenin accumulates in the cytoplasm, and translocate in the nucleus where it plays its second role becoming the key nuclear effector of canonical Wnt signalling (Verheyen & Gottardi, 2009). In addition, in some life-threatening cancers – as colorectal, hepatocellular and gastric carcinomas –, β-catenin is aberrantly accumulated due to mutations in the components of Wnt signaling pathway; especially, APC loss-of-function mutations in colon cancer and *CTNNB1* activating mutations in liver cancer, make β-catenin escape degradation. In the nucleus, β-catenin binds T-cell factor (TCF) and enhances the expression of genes involved in cell proliferation and migration such as c-myc and cyclin-D1 (Bugter et al., 2021; Nusse & Clevers, 2017). β-catenin accumulation has also been reported under hypoxic conditions in cancer cells, without any variation of its

mRNA level (Hong et al., 2017). Moreover, the crosstalk between the Wnt/β-catenin pathway and HIF-1α signaling under hypoxic microenvironment induces tumour cells to invade other tissues (Liu et al., 2015; Zhang et al., 2013). Concerning the regulation of translation of β-catenin mRNA, a putative IRES mechanism was reported in its 5'UTR (Fu et al., 2015). However, the mechanism of β-catenin mRNA translation has been poorly studied. The possibility of an alternative translation mechanism, as well as a translational upregulation under hypoxia is yet to be proved.

To address the unresolved aspects of human β-catenin mRNA translation regulation, we obtained the first secondary structure model of its 5'UTR that reveal two independent structural modules. One of these elements, the GC-rich three-way junction, is involved in the translation efficiency of β-catenin and its translation enhancement under hypoxia in HeLa and SW480 cell lines. Mass spectrometry analysis of normoxic and hypoxic human 48S IC bound to β-catenin mRNA highlights an increase of eIF4B in hypoxia. By footpriting assay we identified the interaction site of eIF4A and eIF4B in a purine tract within the GC-rich three-way junction. Besides, we demonstrate the sensitivity of β-catenin mRNA to silvestrol, a potent eIF4A inhibitor, as a starting point for exploiting the inhibition of β-catenin mRNA translation specifically in cancer cells and overcoming the β-catenin protein druggability issue (Cui et al., 2018).

Results

β-Catenin 5'UTR contains two different RNA elements

Human β-catenin mRNA possesses a 5'UTR of 214 nucleotides and an open reading frame (ORF) of 2346 nucleotides. The 3'UTR varies in length and can hold AU-rich elements that influence mRNA stability(Thiele et al., 2006). The ORF of β-catenin is highly conserved throughout vertebrates, while the sequence of its 5'UTR is only conserved in some mammals (Supplementary Figure 1). The GC-content distribution defines the fate (translatability, stability, and storage) of an mRNA (Courel et al., 2019). The sequence of β-catenin mRNA highlights a singularity (Figure 1, plot): most of the 5'UTR is enriched in GC nucleotides, while at its 3' side, a short tract of AU nucleotides precedes the AUG codon. This evidence suggests that the 5'UTR is probably folded into two independent entities. Downstream the start codon, the GC content in the ORF is stable (48%), while it drops at the 3'UTR (33,5%).

Because mRNA structure plays a key role at every step of gene regulation including ribosome recruitment in translation initiation, knowing the secondary structure of the 5'UTR of β-catenin mRNA is a starting point for investigating its role in translation (Leppek et al., 2018). Here, we show the secondary structure model of β-catenin 5'UTR (Figure 1) obtained by SHAPE and validated by chemical probing data with DMS and CMCT. SHAPE probes create an adduct at the 2'OH of the ribose depending on the nucleotide flexibility. On the other side, dimethyl sulfide (DMS) and N-Cyclohexyl-N′-(2-morpholinoethyl)-carbodiimide (CMCT) are two probes modifying the nitrogenous bases of A/C or U/G, respectively. The modification patterns of benzoyl cyanide (BzCN) and 2-methylnicotinic acid imidazolide

(NAI) – two different SHAPE reagents – are very similar (Supplementary Figure 2), permitting to obtain a reliable *in vitro* model.

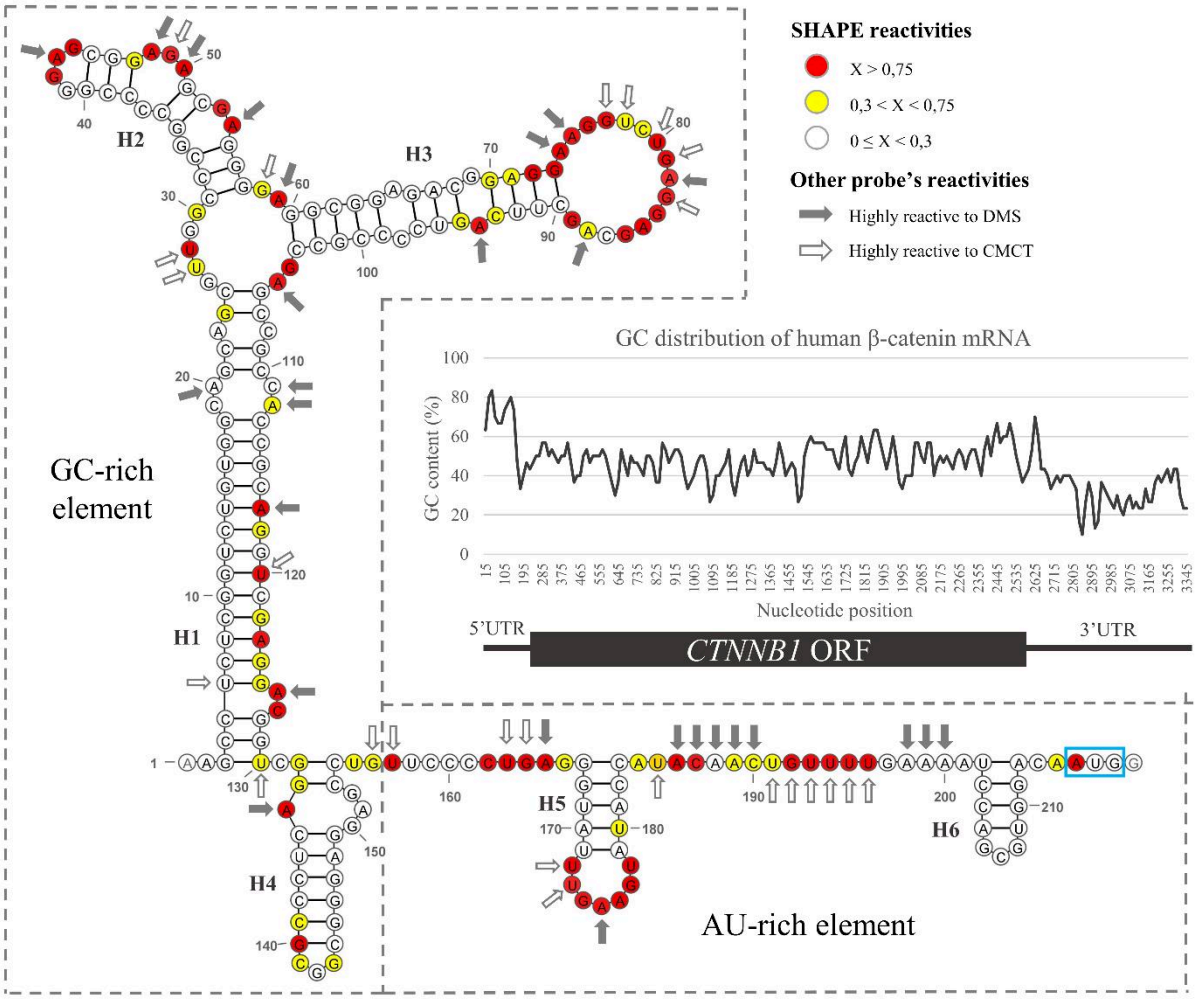

Figure 1. Secondary structure of the 5'UTR of β-catenin mRNA, based on SHAPE, DMS and CMCT probing experiments. High reactivity to each probe detects single-stranded regions of RNA or very flexible nucleotides. Normalized SHAPE reactivity is represented with white, yellow or red circles at reactivity ranges 0-0.3, 0.3-0.75 or >0.75 respectively, in a scale from 0 to 1. Highly reactive nucleotides to 50 mM DMS or 20 mM CMCT are spotted with grey or white arrows, respectively. First and last nucleotides have no probing data. RNA helices are indicated by H1-7. The two RNA domains are delimited by lined grey boxes. GC distribution diagram is represented by plotting the average GC-content value of 30-nucleotide windows each 15 nucleotides. Positions of the untranslated regions (UTR) or the open reading frame (ORF) are in parallel to the diagram. Start codon is highlighted by a cyan blue square.

The 5'UTR of β-catenin mRNA possesses two main structural modules. Named GC-rich element due to its high GC-content, the first element consists in a highly-structured RNA domain shaped in a three-way junction (TWJ) formed by Helix 1-3. This structural module continues with Helix 4, which is tightly connected to the TWJ. Importantly, the TWJ holds a purine rich sequence between the loops of Helix 2 and 3, with the latest holding a very reactive 16-nt stem loop. GC-rich domain is followed by the second structural element called AU-rich domain and formed by a tract enriched in AU nucleotides. AU-rich element is rather unstructured and present two small hairpins (Helices 5 and 6). Additionally, the initial AUG

codon remains in a single-stranded region and is surrounded by an optimum (strong) Kozak sequence (A_{-3} and G_{+4}, being $A_{+1}U_{+2}G_{+3}$), which ensures correct start codon recognition and the fidelity of the translation.

Predicting the RNA folding of the 5'UTR is essential prior to studying its function in translation. Indeed, the model obtained model allows to design a truncated version of the 5'UTR to remove the GC-rich element and analyze its translational role.

The GC-rich element of β-catenin 5'UTR is needed for translation efficiency

5'UTRs are relevant for the recruitment of the ribosomal initiation complex to the mRNA and are involved in the control of translation efficiency (Hinnebusch et al., 2016). According to the obtained secondary structure model, we designed four different transcripts containing or not the GC-rich element, the AU-rich element and the beginning of β-catenin ORF. These constructs were tested by RNA transfection assay to understand their contribution into the translation of the firefly luciferase reporter gene in HeLa cells. Schematic illustrations of *CTNNB1* and control constructs are shown in Figure 2A. The transcripts designated as *CTNNB1_1* and *CTNNB1_2* contained both the full-length 5'UTR (214 nts) upstream the firefly luciferase coding region. *CTNNB1_3* and *CTNNB1_4* constructs hold a short 5'UTR (63 nts) where the GC-rich element has been removed. A small segment of the ORF of *CTNNB1* gene (102 nts) is present only on the first and third construct. These 7-methylguanylate-capped (m7G-capped) monocistronic mRNAs were transfected into HeLa cells and luciferase activity was measured.

In Figure 2B, we observed that the *CTNNB1_1* transcript reached the highest translation rate whereas *CTNNB1_4* had the lowest. These results strongly suggest that GC-rich element is required to efficiently translate the reporter gene, which is two-fold more translated when this structural element is present. Besides, the beginning of β-catenin ORF seems to improve the translation level. Indeed, comparing the translation level of *CTNNB1_1* and *CTNNB1_2* constructs, we could observe that the translation of the reporter gene is slightly increased in presence of the first 102 nucleotides of β-catenin ORF.

The results of the translation assay in HeLa cells evidence that the TWJ has a pivotal role in the expression of β-catenin rendering reporter translation more efficient. Moreover, the beginning of the ORF seems to act synergistically with the TWJ and the cap is necessary for its translation (see Figure S3). We next decided to explore the impact on the translation of β-catenin under stress, particularly hypoxia, being a relevant feature of the microenvironment of many solid tumors.

The GC-rich element drives β-catenin translation enhancement during hypoxia

The lack of oxygen is one of the main stresses that tumor cells are chronically facing, and tumor hypoxia often leads to chemoresistance and metastasis (Muz et al., 2015). During hypoxia, global translation is reduced due to eIF2α phosphorylation and decreased availability of eIF4E to form the cap-binding complex (Connolly et al., 2006; Pakos-Zebrucka et al., 2016).

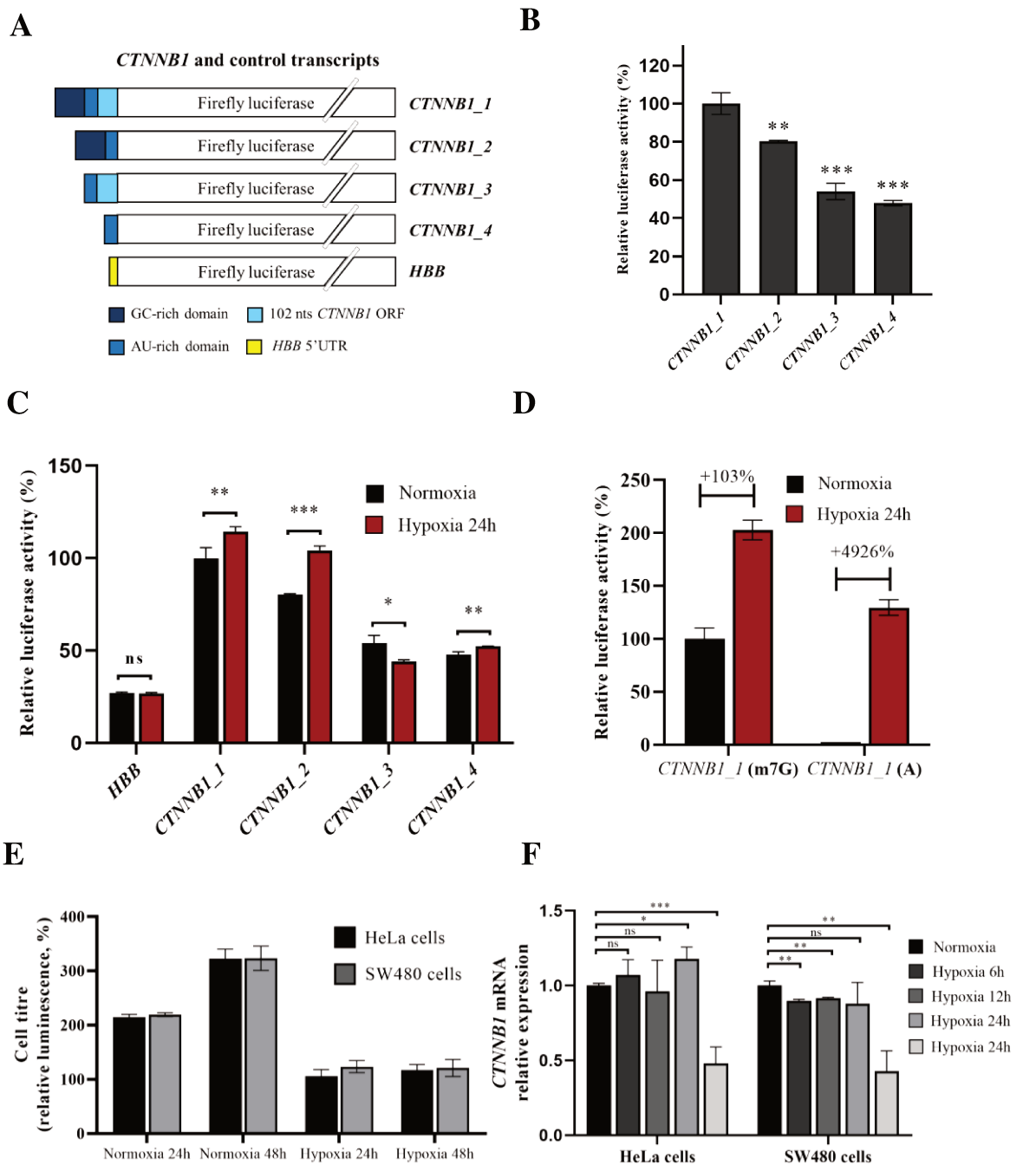

Figure 2. The GC-rich element of *CTNNB1* 5'UTR enhances mRNA translation under hypoxia. (A) The different *CTNNB1* and control transcripts used in this study. (B) mRNA transfection experiment was performed on HeLa cells using Renilla luciferase as co-transfection control. Unpaired t-test was performed comparing to *CTNNB1_1* translation level. Experiments were performed in triplicates. (C) mRNA transfection experiments were performed on HeLa cells in normoxic or hypoxic conditions using Renilla luciferase as co-transfection control. Unpaired t-test comparing translation of one mRNA in normoxia to its level in hypoxia. Experiments were performed in triplicates. (D) *in vitro* mRNA translation on HeLa cell extracts cultured under hypoxia or normoxia conditions. The *CTNNB1_1* transcript was used either m7G-capped (m7G) or A-capped (A). (E) Cell titer in HeLa and SW480 cells under normoxic or hypoxic conditions, normalized to the number of cells at t=0 hours (100%). (F) Fold change of endogenous *CTNNB1* mRNA level in HeLa and SW480 cells subjected to different hypoxia exposures compared to the level in standard oxygen conditions. Ct number was normalized to the mRNA level of the following reference genes: *EEF1A1*, *RPL13* and *HIF1A*. ns (no significant), * $p \leq 0.05$, ** $p \leq 0.01$, *** $p \leq 0.001$ and **** $p \leq 0.0001$.

However, translation still occurs for some mRNAs implicated in adaptation to stress and maintenance of cell physiology (Chee et al., 2019).

To understand the effect of hypoxic stress on β-catenin mRNA translation, the above described m7G-capped transcripts were transfected into HeLa cells cultured in standard oxygen conditions (18% O_2) or under severe hypoxia and the reporter translation was observed. Figure 2C showed that full-length β-catenin 5'UTR (*CTNNB1_1* and *CTNNB1_2* constructs) significatively increase the translation of the reported gene in 24h hypoxic HeLa cells, whereas this translational effect is abolished when the GC-rich element is removed (*CTNNB1_3* and *CTNNB1_4* constructs). These results strongly suggest that the TWJ acts as a translation enhancer during hypoxic stress.

To further analyze the requirement of eIF4E in hypoxic conditions, m7G-capped and A-capped *CTNNB1_1* constructs were tested using *in vitro* translation assay in HeLa cell extract cultured in normoxia or hypoxia. In Figure 2D, the luciferase activity of *CTNNB1_1* transcript showed again an increase of the translation in hypoxia compared to the normoxic condition. Importantly, the A-capped mRNA was barely translated in normal conditions, but its translation boosted 50-fold in HeLa cell extract cultured in hypoxia. These results suggest that under hypoxic stress the translation of β-catenin is maintained by the GC-rich structural element and become independent from eIF4E, which is consistent with its low availability during hypoxia.

Generally, hypoxia significantly reduces global translation and consequently cell growth (Petrova et al., 2018). Nonetheless, we observed an increment of the reporter gene expression in hypoxia which is directly related to the presence of the β-catenin GC-rich structural element. To understand if the regulation of β-catenin translation in hypoxia could indirectly influence cell growth, we first investigated the impact of severe hypoxia on HeLa cell proliferation. Number of cells was measured with a luciferase-based assay dependent on the ATP present in the culture. The greater is the number of cells, the more ATP is available for luciferase reaction to form a luminescent product. Therefore, a correlation can be made between cell number and luciferase activity. In Figure 2E, we observed that the growths of HeLa and SW480 cells were significantly reduced in hypoxia at 24h and 48h compared to the same cells cultured in normoxia. This assay evidence that cell growth under severe hypoxia is sustained although at a low rate.

Furthermore, RT-qPCR experiments were performed to analyze the endogenous β-catenin mRNA expression during a given hypoxia timeline. In Figure 2F, we showed the variation of β-catenin mRNA level in HeLa and SW480 cells cultured from 0 to 48 hours of severe hypoxia. In HeLa cells, there was no significant change in β-catenin mRNA expression, except after 48 hours of hypoxia exposure, where we observed a 2-fold reduction of its mRNA level. In SW480 cells, a slight significant decrease in β-catenin mRNA expression is observed at 6 and 12 hours of hypoxia, while mRNA level clearly diminishes at 48 hours, similarly to HeLa cells. These results suggest a decrease of endogenous β-catenin mRNA after prolonged exposure to hypoxia. Therefore, the hypoxic induction of β-catenin synthesis is probably regulated at the translational level. Previous works have already shown the upregulation of β-catenin at the translational level in lung cancer cells without any changes in its mRNA level (Hong et al., 2017; Varela-Nallar et al., 2014).

Analysis of the hypoxic 48S IC bound to *CTNNB1* mRNA revealed specific translation features

In cellulo study has evidence that β-catenin translation is modulated under hypoxia through the described RNA structural element which is present in its 5'UTR. To reveal the particularities of its hypoxia-driven translation initiation mechanism, we assembled and isolated directly from HeLa cell extract normoxic or hypoxic LS48S IC with bound *CTNNB1_1* construct (lacking firefly ORF). For our purpose, we adapted to HeLa cells a recently published method called Grad-cryo-EM, which involves the purification of mammalian translation initiation intermediates complexes from Rabbit Reticulocyte Lysate (RRL) in the presence of a non-hydrolysable analog of GTP (GMP-PNP) to stall the initiation process at the LS48S IC stage. This innovative strategy allows investigating of structure and composition of intermediate ribosomal complexes by cryo-EM and mass spectrometry analysis (Rol-Moreno et al., 2020; Simonetti et al., 2016, 2020). Purified hypoxic and normoxic *CTNNB1* LS48S ICs were then analyzed by nanoLC-MS/MS to investigate their protein composition.

In Figure 3A, a list with the spectrum number of eukaryotic initiation factors and other translation-related proteins is given. There are few differences between the normoxic and hypoxic *CTNNB1* LS48S IC, although they are crucial to understand the switch from canonical to alternative translation initiation mechanism that occurs during hypoxia. As expected, the initiation factor eIF4E responsible of 5' cap binding is absent in the hypoxic complex. This is probably due to the sequestering of eIF4E by 4E-BPs occurring during this stress condition. PKR, one of the four eIF2α kinases, was only present in hypoxia *CTNNB1* LS48S ICs. The absence of eIF4E and the presence of one eIF2 kinase ensure that hypoxic condition is properly reproduced on the HeLa cells used to assemble *CTNNB1* LS48S IC. Notably, other factors are over-represented in the hypoxic complex: eIF4B, eIF4G2, eIF5, eIF5B (see Figure 3B).

We also analysed by nanoLC-MS/MS the protein composition of the hypoxic 48S IC bound to the *CTNNB1_3* construct (no firefly ORF) in which the GC-rich element is depleted (ΔGC LS48S IC) and compare it to the same complex with bound full-length *CTNNB1* 5'UTR (CTNNB1_1). In Figure 3C, we observed that the three isoforms of eIF4G, eIF4A1 and eIF4B are less abundant in the ΔGC LS48S IC, while it contains a higher number of spectra for some subunits of eIF3, notably eIF3d. As observed for the hypoxic *CTNNB1* LS48S IC, eIF4E is absent. Interestingly, in absence of the GC-rich element, PKR is absent, the level of eIF5B strongly decreases, whereas the abundance of eIF2 notably increases. Taken together, these results suggests that in hypoxia, the absence of eIF4E doesn't impair 48S IC assembly on the β-catenin mRNA which is driven by the GC-rich element of its 5'UTR and relies on the synergic action of eIF4A, eIF4B, eIF4G.

Eukaryotic initiation factor 4A and 4B directly interact with β-catenin 5'UTR

Highly-structured 5'UTRs need RNA helicases to unwind secondary structures thus allowing the SC48S IC to search of the start codon. eIF4A is one of the best-known RNA helicases that participates in the translation initiation process. Its main function is accomplished

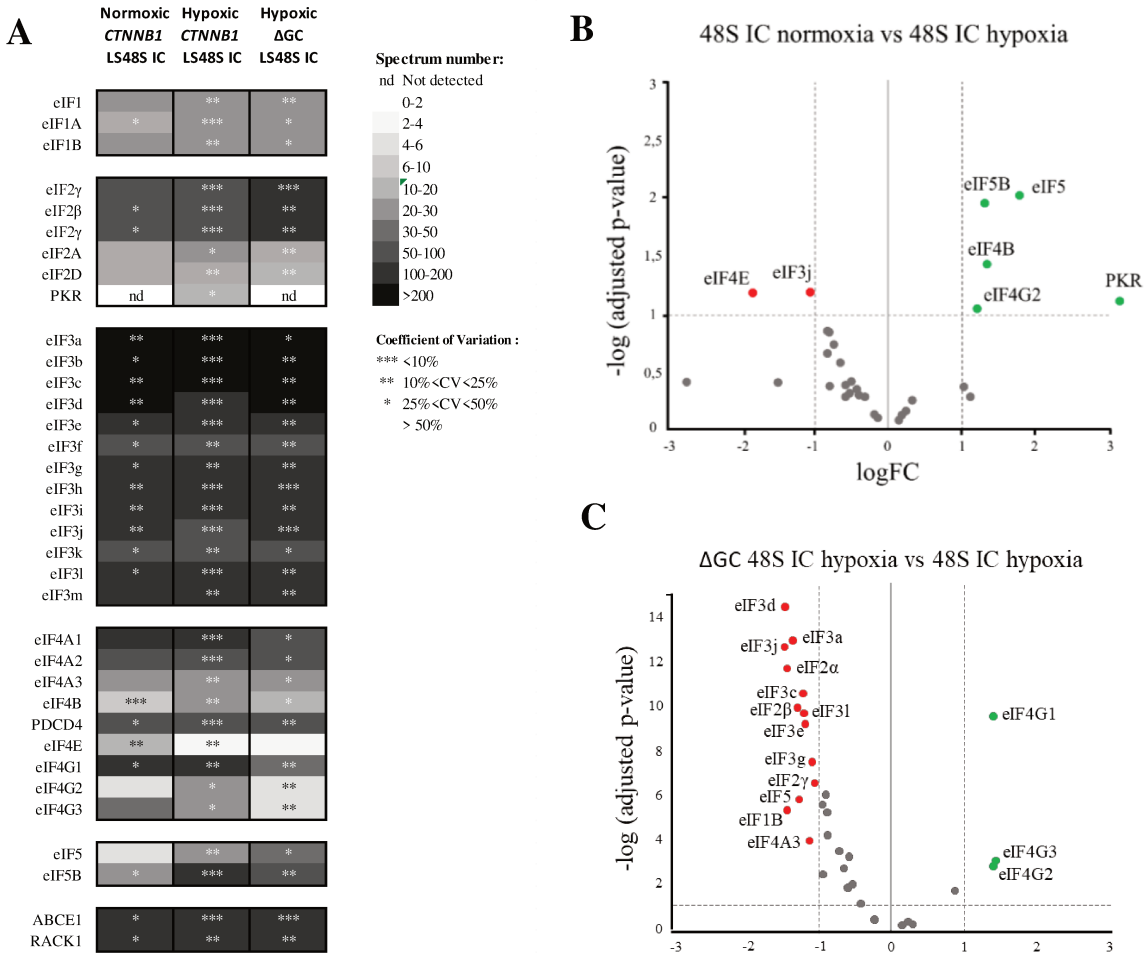

Figure 3. Mass spectrometry analysis of LS48S ICs in normoxia and hypoxia. (A) Semiquantitative mass spectrometry analysis of the initiation factors in normoxic and hypoxic 48S ICs, indicating the abundance of each eIF on the basis of the normalized spectrum counts (NSCs). The NSCs are presented as heatmaps, with a greyscale between white and black, where white indicates low abundance and black denotes high abundance. All eIFs are included on the list as wells as proteins related to the translation initiation process: ABCE1, PDCD4, PKR and RACK1. Stars indicate the values of the coefficients of variation calculated for each NSC. (B) Fold change and adjusted p-value of the comparison between normoxic and hypoxic *CTNNB1* LS48S IC composition is represented in a volcano plot. Red and green dots represent the proteins significantly more abundant in the normoxic or hypoxic complexes, respectively. (C) Volcano plot comparing hypoxic LS48S IC bound to ΔGCRNA with the same complex bound to the mRNA with full-length 5'UTR. Red and green dots represent the proteins significantly more abundant in the hypoxic complex bound to ΔGC *CTNNB1* mRNA or to *CTNNB1* mRNA, respectively.

into the cap-binding complex eIF4F, although some evidence suggests that free eIF4A is also involved in ribosome recruitment independently from its helicase activity (Sokabe & Fraser, 2017; Yourik et al., 2017). Mass spectrometry analysis has revealed high abundance in eIF4A and the increase of eIF4B in the hypoxic LS48S IC when bound to the full-length *CTNNB1* 5'UTR. In line with this result, we suspected that eIF4A, with the help of eIF4B, could have an active role in the 43S PIC recruitment on the GC-rich element of β-catenin 5'UTR. To verify this hypothesis, we purified human eIF4A1 and eIF4B and performed Electrophoretic Mobility Shift Assay (EMSA) to test their direct binding to β-catenin 5'UTR *in vitro*.

EMSA was performed using three different *CTNNB1* constructs: i) RNA 1 contains the full-length 5'UTR and the beginning of the ORF, ii) RNA 2 comprises only the GC-rich element and iii) RNA 3 includes the AU-rich element and the ORF (see Figure 4A). Only the constructs containing the GC-rich element were found to interact with eIF4B. Direct interaction of *CTNNB1* 5'UTR with eIF4A could not be shown by EMSA. This experiment confirmed that eIF4B directly binds the 5'UTR of β-catenin mRNA through the GC-rich element.

To further identify the interaction site of eIF4A and/or eIF4B on the β-catenin 5'UTR, SHAPE-directed footprinting assays were run using benzoyl cyanide. This SHAPE reagent modifies the RNA depending on ribose flexibility and allows to detect which nucleotides are recognized by either eIF4A, eIF4B or both. Indeed, reduction in reactivity can be associated to factor binding regions, while a reactivity increment to a factor-induced conformational change. Figure 4B shows SHAPE reactivity profiles obtained from electropherograms for the following conditions: only RNA, RNA with either eIF4A, eIF4B or both proteins. Two main footprints were noticed. One in the internal loops of H2 and the other in H3 step loop, mainly driven by both proteins. Additionally, some nucleotides become more reactive in the strands of H2 and H3 opposite to the factor's binding sites (see increase of reactivities on nucleotides 18-44 and 86-110), suggesting an RNA conformational change upon factor binding.

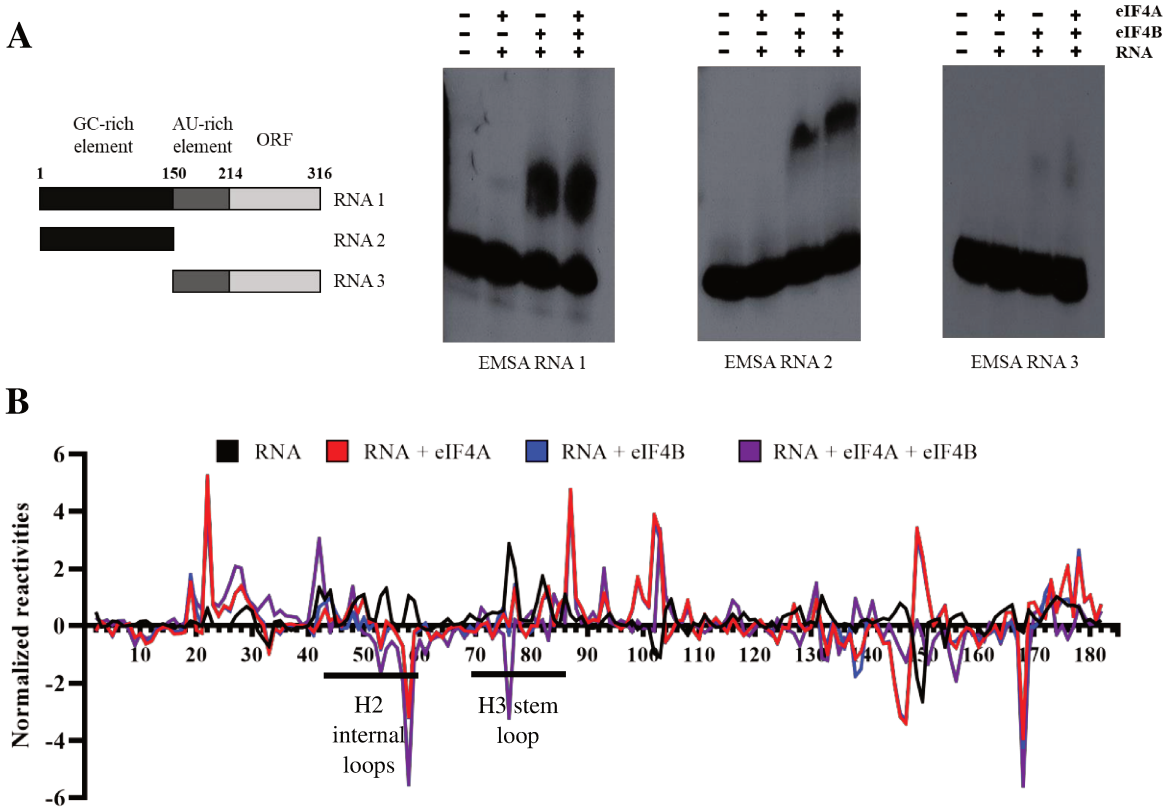

Figure 4. The GC-rich element binds eIF4A and eIF4B *in vitro* through H2 internal loops and H3 stem loop. (A) GC-rich element binding to human eIF4B. EMSAs were performed with a fixed concentration of radiolabeled RNA, ± 0,5 µM eIF4A and ± 0,5 µM eIF4B. RNA used in each experiment are schematized on the right and named EMSA RNA 1, 2 and 3**.** GRE: GC-rich element; ARE (AU-rich element) and ORF (102 nts *CTNNB1* ORF). (B) Footprinting of eIF4A and eIF4B on the purine track of the GC-rich element. In the RNA condition, SHAPE reactivities were calculated comparing the electropherogram of BzCN-modified RNA with the one of unmodified RNA. In the other conditions, the comparison was between an electropherogram containing BzCN-modified RNA

incubated with proteins with the one containing only BzCN-modified RNA. Experiments were done in triplicates and only one replicate of each condition is represented.

We had previously observed that the TWJ has a purine enrichment from the H2 internal loops to the H3 stem loop. Our data confirm that eIF4A and eIF4B interact with the 5'UTR of *CTNNB1* mRNA exactly in this region. Moreover, rather than a specific sequence signature on this element, we suggest that these factors bind single stranded purines. Notably, previous studies have already described the eIF4A preference to bind single stranded purines (Iwasaki et al., 2016).

Silvestrol inhibits the translation of β-catenin mRNA clamping eIF4A on the GC-rich element

Drugs targeting protein synthesis in eukaryotic cells have gained increasing attention during the last years because of their potential in anticancer and antiviral therapy. Several families of eIF4A inhibitors have been described to impair translation at the initiation stage such as rocaglates, hippuristanol and pateamine A (Naineni et al., 2020). Among them, rocaglates (i.e., silvestrol and rocaglamide A) are the more diverse group of compounds that reversibly clamp eIF4A onto RNA and hence block mRNA translation (Taroncher-Oldenburg *et al*., 2020). Once confirmed the interaction of eIF4A1 and eIF4B with the GC-rich element of *CTNNB1* 5'UTR, we decided to explore β-catenin translation inhibition and its eIF4A dependency using available compounds targeting eIF4A. Following this aim, we treated HeLa cells with 25 nM silvestrol or its vehicle (DMSO) prior to RNA transfection. The transfected mRNAs were *HBB* and the four *CTNNB1* constructs. We further extended this analysis to SW480 cells and glioblastoma cell line U87MG to investigate the specificity of this inhibition in other cancer cell lines.

As shown in Figure 5A, silvestrol was able to inhibit solely the translation of the mRNA constructs containing the GC-rich element of *CTNNB1* 5'UTR. The inhibition occurs in HeLa cells cultured in both, standard and hypoxic condition – with 35 and 45% of β-catenin inhibition rate in each condition, respectively. This result confirmed that silvestrol inhibition takes place in presence of the GC-rich element. In addition, Figure 5B shows a higher translation inhibition of *CTNNB1_1* transcript transfected into SW480 cells as well as in U87MG cells in both normoxic and hypoxic conditions (30-50% reduction of translation rate).

In these experiments, we showed the efficacy of silvestrol to block β-catenin reporter translation in three different cancer cell lines at nanomolar concentration. We also observed the translation enhancement of *CTNNB1_1* transcript in SW480 cells but not in U87MG. We have also demonstrated that β-catenin translation inhibition by silvestrol depends on the presence of GC-rich element. Moreover, hypoxic cells remained as sensitive to silvestrol as non-stressed cells. The basis of silvestrol inhibition in β-catenin translation might reside on the purine-rich interacting region of eIF4A and eIF4B that was identified in the 5'UTR by RNA footprinting. Previous crystal structure with another rocaglate, rocaglamide A, showed the specificity of silvestrol rocaglates to restrain eIF4A1 on purines instead of pyrimidines (Iwasaki et al., 2019).

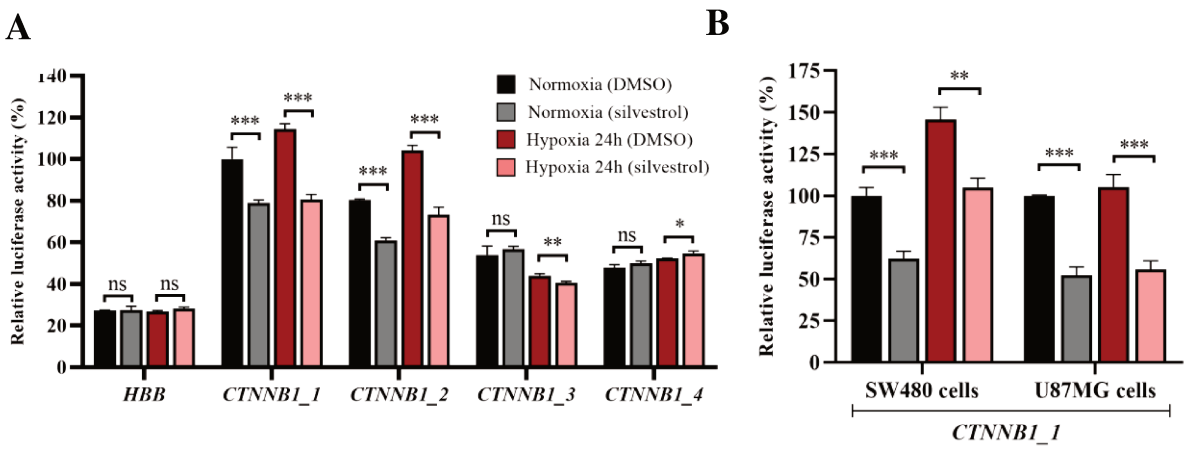

Figure 5. Silvestrol specifically inhibits β-catenin translation through the GC-rich element. (A) mRNA transfection experiments were performed on HeLa cells in normoxic or hypoxic conditions using Renilla luciferase as co-transfection control. Cells were treated either with 0.005% DMSO v/v or 25 nM silvestrol prior to transfection. (B) Same experiment was made in SW480 and U87MG cells for the *CTNNB1_1* construct. Unpaired t-test comparing translation of one mRNA treated with DMSO to its level under silvestrol treatment. Experiments were performed in triplicates. ns (no significant), * $p \leq 0.05$, ** $p \leq 0.01$, *** $p \leq 0.001$ and **** $p \leq 0.0001$.

Discussion

β-catenin protein is an integral structural component of cadherin-based adherent junctions, and the key nuclear effector of canonical Wnt signalling in the nucleus (Valenta et al., 2012). Its intracellular accumulation and nuclear import, caused by specific mutations in the β-catenin protein or in the components of the Wnt/β-catenin pathway, promote cell proliferation and invasion especially in tumors of the gastrointestinal tract. J. Jin and coworkers have shown that β-catenin expression increased in cells under chemotherapy treatment with paclitaxel (PTX) without corresponding changes in transcript abundance (Fu et al., 2015). Notably, they have showed that the 5'UTR of β-catenin mRNA contains an IRES element which regulates its translation initiation when cells are stressed after PTX treatment. Although the proteostasis of β-catenin has been extensively reviewed, its mRNA translation mechanism has been much less studied.

Using RNA chemical probing, we obtained the secondary structure model of β-catenin 5'UTR which is composed of a highly-structured GC-rich element folded into a TWJ at its 5' side, followed by an unstructured AU-rich region just before the start codon. This structural organization of the 5'UTR do not seem to be a unique feature of *CTNNB1* mRNA, but rather an intrinsic property of several cellular mRNAs sharing similar GC content distribution (Waldron et al., 2019). We observed that the 5'UTR sequence of CTNNB1 mRNA in vertebrates is more conserved at the AU-rich region while the TWJ purine tract has probably been acquired late in evolution (Supplementary Figure 1).

We unraveled the functional relevance of the TWJ for the translation efficiency of β-catenin and, observed a synergy between this element with the beginning of β-catenin coding sequence. However, we did not find any long-distance interaction between β-catenin 5'UTR and the beginning of its ORF. Noteworthy, we discovered that β-catenin 5'UTR did increase

the reporter gene translation in HeLa and SW480 cells under severe hypoxia. Our results strongly suggest that β-catenin mRNA translation is enhanced through the TWJ present within its 5'UTR in hypoxic cells.

Hypoxia is a common feature which many solid tumours deal with. In response to hypoxia, cells reduced their global protein synthesis to a minimum, although the translation of a set of mRNAs encoding proteins with adaptive functions is maintained (Thomas & Johannes, 2007). Thus, translation reprogramming is driven in part by mRNA signals often located in the 5'UTR of mRNAs. In hypoxia, eIF4E is sequestered by 4E-BPs, therefore eIF4F formation is impaired (Montoya, 2012). We showed that translation in hypoxic conditions of *CTNNB1* reporter gene mainly occurs in a cap-independent manner. In line with this result, mass spectrometry revealed the absence of eIF4E as well as an increase of the abundance of eIF4B and eIF4G2 in the hypoxic *CTNNB1* LS48S IC. In hypoxia mRNA recruitment to the 43S IC probably undergo a mechanistic switch from cap-recognition by eIF4E to mRNA-direct recognition through eIF4A, eIF4G and eIF4B. Additionally, we hypothesize that PKR is only present in hypoxic *CTNNB1* LS48S IC and it is absent in the hypoxic ΔGC LS48S IC. Although PERK is the well-known eIF2α kinase induced under hypoxia (Koumenis & Wouters, 2006), here we propose that PKR would drive eIF2α phosphorylation in translation initiation of β-catenin mRNA under hypoxia. These data illustrate the balance between the abundance of eIF2 subunits (and hence the TC) and its kinases within translation initiation complexes. We hypothesize that the more abundant eIF5B in hypoxic *CTNNB1* LS48S IC together with eIF2A (do not confuse with eIF2α) act as initiator tRNA carriers, based on previous publications have shown the tRNAi binding capacity of these factors in stress conditions (Kim et al., 2018). In the hypoxic ΔGC LS48S IC, the absence of eIF4E, the strong reduction of the three eIF4G isoforms and the abundance of eIF2 and eIF3, may suggest a mechanism dependent on eIF3d, according to a recent study demonstrating the eIF3d capability to bind the cap structure and to lead eIF4E-indepedendent translation (A. S. Y. Lee et al., 2016). Thus, in the absence of eIF4E, translation of mRNAs lacking highly-structured elements in their 5'UTR could be driven by eIF3d in hypoxia.

The initiation factor eIF4B enables the translation of mRNA with highly-structured 5'UTRs by enhancing eIF4A helicase activity and promoting mRNA recruitment to 43S PIC through its direct association with the 40S subunit near the mRNA binding channel (Sen et al., 2016). In our search of a protein factor responsible of translation enhancement of β-catenin mRNA in hypoxia, we demonstrated the direct interaction of eIF4B with the GC-rich element and the footprints produced by eIF4A and eIF4B in the single stranded purines of the TWJ. For the first time we gave evidence of the β-catenin translation inhibition in cancer cells using silvestrol. Also, we depicted the mechanism of action of silvestrol probably clamping eIF4A in the single stranded purines of the TWJ of β-catenin 5'UTR. In this manner, inhibition upon silvestrol treatment allowed us to confirm that the β-catenin translation strongly depends on eIF4A. It has been demonstrated that the only rocaglate currently used in clinical trials, eFT226 (zotafilin), has a strong effect on MYC translation reduction. We propose that this effect occurs because zotafilin inhibits β-catenin translation and consequently MYC expression is reduced (Thompson et al., 2021). β-catenin mRNA as well as our mRNA transfection approach could be an optimal model to test eFT226 effect. Thus, rocaglates are the best candidates to reduce

the translation of β-catenin in cancer cells. Furthermore, β-catenin mRNA could become a reference model to screen eIF4A inhibitors. Nonetheless these inhibitors are dependent on a protein-RNA interaction and they are not specific for this mRNA. Crystallization of the TWJ could be attempted in the future in order to explore RNA-binding small molecules that interacts specifically to this element. TWJs are considered interesting motifs to hold pockets with complex structures where small molecules could bind (Warner et al., 2018). In the future, validation of the secondary structure of endogenous β-catenin mRNA in living cells would greatly complement the obtained *in vitro* model. However, probing low-abundant RNA, including mRNAs, in cells remains very challenging.

In conclusion, the analysis of the 5'UTR structure of β-catenin mRNA revealed a TWJ that is implicated in the translation enhancement under hypoxia and involves several initiation factors such as eIF4A, eIF4B and eIF4G, in the absence of eIF4E. β-Catenin translation can be targeted through the TWJ using eIF4A inhibitors. Also, we focused on the use of monocistronic mRNA transfection as a robust approach, instead of classical DNA transfection experiments with a bicistronic reporter gene vector that is prone to artifacts (Jackson, 2013). Moreover, this analysis provides new insights into the investigation of mRNA translation under stress conditions and supports the existence of a diversity of translation initiation mechanisms. It also open new perspectives in the search of drugs targeting initiation factors and RNA.

Materials and Methods

Plasmids

Human 5'UTR of *CTNNB1* mRNA (214 nts) +/- the first 102 nts of *CTNNB1* ORF were fused upstream the firefly luciferase ORF in pGL3. Human 5'UTR of *HBB* (50 nts) was cloned upstream the luciferase sequence in both pGL3 and in pRL. Cloning service was done by Proteogenix. Resulting plasmids were used as a template for PCR amplifications. 5'UTR sequences were based on the NCBI Reference Sequences: NM_001904.4 (*CTNNB1* mRNA isoform 1) and NM_000518.5 (*HBB* mRNA).

The human eIF4AI coding sequence was optimized for bacterial expression and inserted in pET15b – that contains a His6-tag and a thrombin cleavage site –, while the optimized coding sequence of human eIF4B was inserted in pnEAvH – that includes a His6-tag and a TEV cleavage site. These plasmids were transformed in BL21(DE3) pLysS *E. coli* for further protein expression.

RNA transcription and m7G-capping

The template for every mRNAs used in this study was generated by PCR amplification from the plasmids detailed above. DNA template consisted in a PCR product containing the T7 promoter and the sequence of interest. PCR product purification and *in vitro* transcription of different constructs were performed as described previously (Simonetti et al., 2020). Purified transcripts were capped using the ScriptCap™ m7G Capping System (CELLSCRIPT). Radioactively labelled transcripts were obtained by substituting GTP from the latter kit with 20

µCi [α-^{32}P] GTP (PerkinElmer). A-capped mRNAs were prepared adding the G(5')ppp(5')A RNA Cap Structure Analog (NEB) co-transcriptionally following manufacturer's instructions.

RNA probing

The 5'UTR of *CTNNB1* mRNA was probed by selective 2'-hydroxyl acylation analyzed by primer extension (SHAPE) and chemical modification of the bases with the chemical dimethyl sulfate (DMS) and CMCT). The sites of chemical modification were subsequently defined by a primer extension-termination assay in which cDNA was synthesized by reverse transcriptase from a fluorescent-complementary oligonucleotide,hybridizing downstream the region of interest. In this study we used two different probes: benzoyl cyanide (BzCN) and 2-methylnicotinic acid imidazolide (NAI). NAI was synthetized as a 1:1 mixture with imidazole in DMSO as described previously (Spitale et al., 2013).

Prior to chemical probing, 2 pmol of RNA were refolded in a final volume of 10 µL using a predetermined program on Thermomixer C (Eppendorf): heating at 95°C for 2 min, decreasing the temperature at 65°C, adding refolding buffer (20 mM sodium cacodylate pH 7.0, 100 mM KOAc and 1 mM $Mg(OAc)_2$) at these temperature, maintaining this temperature 5 min, diminishing at 37°C and keeping the latter temperature for RNA modification. 2 pmol of yeast total RNA were added in addition to the probe. Final concentrations and incubation times are as follows: 50 mM NAI for 15 min, 50 mM BzCN for 1 min, 50 mM DMS (diluted in absolute ethanol) for 2 min and 20 mM CMCT for 20 min. Untreated RNA additionally contains either 5% DMSO or 5% ethanol to be comparative with SHAPE reagents or DMS, respectively. Reactions were stopped adding an excess of water.

Primer extension

For oligonucleotide extension, 2 pmol of unmodified or modified RNA were first annealed to 2 pmol of 5' fluorescently-labelled primers (Thermo Fisher Scientific) at 95°C for 2 min and at 4°C for 2 min. We utilized VIC fluorophore to analyze the probe modifications and in parallel NED fluorophore for ddGTP sequencing to obtain a reference sequence that was aligned to the reactivity data in order to position each nucleotide. Both, VIC and NED primers, hybridize in positions +30 to +49 of *CTNNB1* ORF and have the same following sequence: 5' CTGGTTCCATGGCCATGTCC 3'. Samples were then incubated in RT buffer (25 mM Tris-HCl pH 8.3, 50 mM KCl, 5 mM MgCl2, 2 mM DTT), 0.5 mM dNTPs and 2 U of avian myeloblastosis virus (AMV) reverse transcriptase (Life Sciences Advanced Technologies) at 42°C for 30 min and 50°C for 15 min. Sequencing reactions with NED fluorophore are performed in similar conditions but supplementing with 10 µM ddGTP and 125 µM dGTP instead. Resulting cDNA products were precipitated and dry pellets were resuspended in Hi-Di formamide (Applied Biosystems) and loaded on a PCR-96-AB-C microplate (Axygen) for capillary electrophoresis and data collection on a 3130xl Genetic Analyzer (Applied Biosystems). Reverse transcriptase arrests are considered proportional to the reactivity of each nucleotide.

Reactivity data analysis

Chemical probing electropherograms were analyzed using QuSHAPE software (Karabiber et al., 2013). The reactivity values were obtained subtracting untreated RNA profile to the corresponding modified RNA stops in order to obtain the net reactivities for all nucleotides. Reactivityalues were assigned to each nucleotide by overlapping the parallel ddGTP sequencing to the already known RNA sequence. Reactivities for each dataset were normalized to a scale between 0 to 2, where 0 indicates unreactive nucleotides and relatively reactive nucleotides are set at 1-2. Three independent experiments were performed.

The secondary structure model was obtained using RNA structure software (Reuter & Mathews, 2010) by constraining the RNA prediction with the reactivity values as pseudo-free energy changes that strongly correlate with local nucleotide flexibility (Low & Weeks, 2010). Among different possible predictions, we chose the structure at the lowest minimum free energy to be our model. RNA was represented with all reactivity values using the RNA visualization tool VARNA (Darty et al., 2009).

Cell culture and cell extract preparation

Three cell lines were used for cell-free extract preparation and *in cellulo* studies: HeLa, colon carcinoma cell line SW480 (ATCC) and glioblastoma cell line U87MG. HeLa and U787MG cells were cultured in Dulbecco's modified eagle medium (DMEM) + GlutaMAX and SW480 cells in RPMI-1480 medium, both supplemented with 10% fetal bovine serum (FBS) and 100 U/mL of penicillin/streptomycin. Severe hypoxia (<0.1% O_2) was induced by culturing cells in a Whitley DG250 Anaerobic Workstation (dwscientific) with previously deoxygenated medium.

Cell lysate was prepared with a starting material of several 150mm cell culture dishes with 5 million cells per plate and waited until reaching a confluence higher than 75%. Cell lysis was done by nitrogen cavitation with 4639 Cell Disruption Vessel (Parr Instrument Company) at 500 psi, stirring with a small magnet at 500 rpm in a cold room (4°C). Lysis buffer contained 20 mM HEPES/NaOH pH 7.4, 100 mM KOAc, 1 mM DTT, 0.5 mM $Mg(OAc)_2$, 100U of Recombinant RNasin (Promega) and Halt Protease inhibitor cocktail (ThermoFisher). Lysate was centrifuged at 1000 g for 5 minutes and the supernatant was recovered avoiding the foam (membranes) and the pellet (nuclei). Finally, cell extract was aliquoted, fast-freeze in liquid N_2 and stored at -80°C for further use.

In vitro translation assays

HeLa cell-free extract prepared in the lab and RRL, nuclease-treated (Promega) were utilised for *in vitro* translation. Reaction mixture contained 12,5 mg/mL of cell extract (A_{260nm} = 20, proportional to the ribosome amount), 0,5 µg of Fluc mRNA, 40 µM complete amino acid mixture (Promega), 20 U of RNasin® Ribonuclease Inhibitor (Promega), 30 mM HEPES/NaOH pH 7.4, 100 mM KOAc, 1.5 mM $Mg(OAc)_2$, 1 mM ATP, 0.2 mM GTP. Incubation was carried out at 30°C for 3 hours. Luciferase luminescence was measured with Luciferase Reagent Assay (Promega) in the GloMax® 96 Microplate Luminometer (Promega).

In cellulo translation assays (mRNA transfection)

For silvestrol treatment, cells were treated with 25 nM silvestrol 30 minutes before transfection until harvesting the cells. 0,005% DMSO were added for the control condition.

Cells at 70-80% confluent were transfected in 24-well tissue culture plates using Opti-MEM medium, 0.5 µg of mRNA and Lipofectamine™ MessengerMAX™ Transfection Reagent (Invitrogen). 0.25 µg of Rluc mRNA was co-transfected in each condition as a normalization control. Luciferase activity was measured using the Dual-Glo Luciferase Assay System in the GloMax® 96 Microplate Luminometer (Promega).

Total RNA extraction and RT-qPCR

RNA was extracted from 2×10^6 cells in 6-well tissue culture plates using RNeasy Mini Kit (QIAGEN) following manufacturer's instructions. 1 µg of total RNA was reverse-transcribed using High-Capacity RNA-to-cDNA™ Kit (Applied Biosystems) following manufacturer's mode of use. The resulting cDNAs were quantified by real time qPCR on a CFX96 Touch Real-Time System (Bio-Rad) using GoTaq® Probe qPCR Master Mix (Promega) and PrimePCR™ Probe Assay (Bio-Rad). Probe IDs for human *CTNNB1*, *EEF1A1*, *HIF1A* and *RPL13* genes are qHsaCEP0053779, qHsaCEP0052990, qHsaCEP0050075 and qHsaCEP0052324. No PCR product was detected in the no-template control and minus RT samples for each condtion shown in this publication. *CTNNB1* expression was normalized to the other reference genes and GADPH could not be used as a reference gene as it is transcriptionally upregulated during hypoxia (Higashimura et al., 2011).

eIF4A and eIF4B protein expression

eIF4A and eIF4B plasmids were transformed into BL21(DE3) pLysS *Escherichia coli* (Promega). Bacteria were cultured until $A_{600nm} = 0.6$ and induced with 0.5 mM IPTG for 2 hours at 37°C in LB supplemented with 100µg/mL ampicillin and 34 µg/mL chloramphenicol. After centrifugation, pellet was washed with washing buffer (20mM HEPES/KOH pH 7.5, 20 mM KCl and 10% w/v sucrose). Cells were sonicated in lysis buffer (20 mM HEPES pH 7.5, 500 mM KCl, 5 mM $MgCl_2$ and 10 mM 2-mercaptoethanol), supplemented with 1 mM $CaCl_2$, 1 µg/mL DNase I (RNase-free, Roche) and Halt Protease Inhibitor Cocktail (ThermoFisher). Cellular debris was removed by centrifugation at 100000 g for 40 min at 4 ºC in a 70 Ti fixed-angle rotor (Beckman Coulter). The recovered supernatant was purified on a Ni-NTA agarose resin column (Dynamic Biosensors) following the manufacturer's manual. Binding and washing buffer contained 20 mM Tris pH 8.0, 150 mM KCl, 2 mM imidazole, 5% w/v sucrose and 10 mM 2-mercaptoethanol. Proteins were eluted with the same buffer using an imidazole gradient of 20–500 mM. eIF4A is dialyzed (in a buffer containing 70 mM NaHPO4 pH 7.5, 10 mM 2-mercaptoethanol and 10 % w/v glycerol) and then cleaved with 150 U thrombin at 20°C for 1 hour, while eIF4B is directly incubated with homemade TEV protease at 30°C for 45 minutes.

eIF4A was further purified by HA CHT5-I column, eluting the protein with a NaHPO4 gradient of 5-450 mM. Protein is concentrated and stored in the same dialysis buffer supplemented with 50% w/v glycerol. eIF4B was further purified using an anion exchange

column (DynamicBiosensors), a centricon and a Superdex 200 column following manufacturer's instructions. Protein was stored in a buffer containing 20 mM Tris pH 8.0, 250 mM KCl, 5.0% v/v glycerol and 10 mM 2-mercaptoethanol.

Electrophoretic Mobility Shift Assay

To test 5'UTR-protein interactions, 1 µM eIF4A and/or 0,5 µM eIF4B (as indicated in Figure 5) were added to the 5'-end radiolabelled RNAs (1000 cpm/µL) in a total volume of 10 µl containing EMSA buffer (50 mM HEPES/NaOH pH 7.4, 100 mM KOAc, 1 mM $Mg(OAc)_2$, 3 mM DTT, 0.5 mM spermidine). Prior to assembly, protein was incubated in the presence of EMSA buffer during 10 min at 37 ºC and radiolabelled RNA was denatured heating 2 minutes at 95ºC, cooled 2 minutes on ice and renatured for 10 min at 20 ºC. Complex formation was performed at 37°C during 5 min. After incubation, 10 µl of glycerol blue was added and the samples were loaded on a 6% PAGE under non-denaturing conditions (1h, 300 V, 4°C). Finally, the gel was covered with a plastic film to avoid dehydration and was exposed to a Super RX X-ray film (Fujifilm) overnight at - 80ºC. Apparent dissociation rate (K_D) for each RNA could not be calculated because of eIF4B tendance to aggregate above 1 µM. RNA in complex with these proteins were tested at least three times.

Sucrose gradient analysis and complex purification

HeLa 48S IC/β-catenin mRNA was assembled using 100 mM KOAc, 0.5 mM $Mg(OAc)_2$, 0.5 mM 5 mM GPM-PNP as inhibitor. Later, it was loaded on top of 5-25% sucrose gradients containing 25 mM HEPES/NaOH pH 7.4, 80 mM KOAc, 0.5 $Mg(OAc)_2$ and 2 mM DTT. Gradients were centrifuged for 4h in a SW41Ti rotor (Beckman Coulter) at 37000 rpm (4°C). A control sample contained radioactive m7G-capped mRNA to localized it into the gradient fractions by measuring radioactivity the Multipurpose Scintillator Counter (Beckmann Coulter). Fractions containing the 48S IC were further centrifuged in a S140-AT rotor (ThermoFisher) for 1h30 at 108000 rpm (4°C) and ribosomal pellet was resuspended in a buffer containing 10 mM HEPES-KOH pH 7.4, 50 mM KOAc, 10 mM NH_4Cl, 5 mM $Mg(OAc)_2$ and 2 mM DTT.

Mass spectrometry and spectrum analysis

10 µL of protein extracts at 2.5 OD_{260nm} were diluted and precipitated overnight with glacial 0.1 M ammonium acetate in 100 % methanol (5 volumes, -20°C). After centrifugation at 12.000 g and 4°C during 15 min, the resulting pellets were washed twice with 0.1 M ammonium acetate in 80% methanol and further dried under vacuum (Speed-Vac concentrator). Pellets were resuspended in 100 µL of 50 mM ammonium bicarbonate and submitted to reduction (5 mM DTT, 95°C, 10 min) and alkylation (10 mM iodoacetamide, room temperature, 20 min). Proteins were finally digested overnight with 150 ng of sequencing-grade trypsin (Promega). The proteomic datasets were obtained by the injection of 1/4 of each peptidic mixture on an orbitrap mass spectrometer (Q-Exactive Plus, Thermo-Fisher Scientific, USA) coupled to an EASY-nanoLC-1000 (Thermo-Fisher Scientific, USA).

The obtained raw data was converted to .mgf files with the Proteome Discoverer Daemon software (Thermo-Fisher Scientific, script "Export-to-mgf", version 2.2). MS data

were further searched against the *Homo sapiens* Swissprot sub-database with a decoy strategy (Swissprot release 2021_04 from November 2021, 20376 forward protein sequences). Peptides and proteins were identified with Mascot algorithm (version 2.6.1, Matrix Science, London, UK). The following parameters were used: (i) Trypsin/P was selected as enzyme, (ii) three missed cleavages were allowed, (iii) methionine oxidation, acetylation of protein N-term, carbamidomethylation of cysteine and phosphorylation of serine / threonine / tyrosine were set as variable modifications, (iv) mass tolerance for precursor ions was set at 10 ppm, and at 0.02 Da for fragment ions. Mascot data were further imported into Proline v2.0 software (http://proline.profiproteomics.fr/) (Bouyssié et al., 2020). Proteins were validated on Mascot pretty rank equal to 1, and 1% FDR (False Discovery Rate) on both peptide spectrum matches (PSM score) and protein sets (Protein Set score). The total number of MS/MS fragmentation spectra was used to quantify each protein from at least three independent biological replicates: this "BasicSC" value calculated by Proline includes all PSMs of all peptides, including the modified peptides and the peptides shared by different protein sets. After a normalization of the data matrix with the total number of spectra in one sample, the "BasicSC" spectral count values were submitted to a negative-binomial test using an edgeR GLM regression through R (R v3.2.5) through the IPinquiry4 R package (https://github.com/hzuber67/IPinquiry4). The statistical test was based on the published msmsTests R package available in Bioconductor to process label-free LC-MS/MS data by spectral counts (Gregori J et al., 2019). For each identified protein, an adjusted p-value (adjp) corrected by Benjamini–Hochberg was calculated, as well as a protein fold-change (FC).

Acknowledgements

CrPV pRL plasmid was a generous gift of Eric Jan. We thank Benoit Marteyn for the utilization of the hypoxic workstation at IBMC. This work was supported by Association Nationale de la Recherche et de la Technologie (ANRT) funding *Convention CIFRE* 0898/2018 in association with Sanofi-Aventis R&D.

References

Adomavicius, T., Guaita, M., Zhou, Y., Jennings, M. D., Latif, Z., Roseman, A. M., & Pavitt, G. D. (2019). The structural basis of translational control by eIF2 phosphorylation. *Nature Communications*, *10*(1), 2136. https://doi.org/10.1038/s41467-019-10167-3

Baird, S. D., Turcotte, M., Korneluk, R. G., & Holcik, M. (2006). Searching for IRES. *RNA*, *12*(10), 1755–1785. https://doi.org/10.1261/rna.157806

Bouyssié, D., Hesse, A.-M., Mouton-Barbosa, E., Rompais, M., Macron, C., Carapito, C., Gonzalez de Peredo, A., Couté, Y., Dupierris, V., Burel, A., Menetrey, J.-P., Kalaitzakis, A., Poisat, J., Romdhani, A., Burlet-Schiltz, O., Cianférani, S., Garin, J., & Bruley, C. (2020). Proline: an efficient and user-friendly software suite for large-scale proteomics. *Bioinformatics*, *36*(10), 3148–3155. https://doi.org/10.1093/bioinformatics/btaa118

Brito Querido, J., Sokabe, M., Kraatz, S., Gordiyenko, Y., Skehel, J. M., Fraser, C. S., & Ramakrishnan, V. (2020). Structure of a human 48 *S* translational initiation complex. *Science*, *369*(6508), 1220–1227. https://doi.org/10.1126/science.aba4904

Bugter, J. M., Fenderico, N., & Maurice, M. M. (2021). Mutations and mechanisms of WNT pathway tumour suppressors in cancer. *Nature Reviews Cancer*, *21*(1), 5–21. https://doi.org/10.1038/s41568-020-00307-z

Chee, N. T., Lohse, I., & Brothers, S. P. (2019). mRNA-to-protein translation in hypoxia. *Molecular Cancer*, *18*(1), 49. https://doi.org/10.1186/s12943-019-0968-4

Connolly, E., Braunstein, S., Formenti, S., & Schneider, R. J. (2006). Hypoxia Inhibits Protein Synthesis through a 4E-BP1 and Elongation Factor 2 Kinase Pathway Controlled by mTOR and Uncoupled in Breast Cancer Cells. *Molecular and Cellular Biology*, *26*(10), 3955–3965. https://doi.org/10.1128/MCB.26.10.3955-3965.2006

Courel, M., Clément, Y., Bossevain, C., Foretek, D., Vidal Cruchez, O., Yi, Z., Bénard, M., Benassy, M.-N., Kress, M., Vindry, C., Ernoult-Lange, M., Antoniewski, C., Morillon, A., Brest, P., Hubstenberger, A., Roest Crollius, H., Standart, N., & Weil, D. (2019). GC content shapes mRNA storage and decay in human cells. *ELife*, *8*. https://doi.org/10.7554/eLife.49708

Cui, C., Zhou, X., Zhang, W., Qu, Y., & Ke, X. (2018). Is β-Catenin a Druggable Target for Cancer Therapy? *Trends in Biochemical Sciences*, *43*(8), 623–634. https://doi.org/10.1016/j.tibs.2018.06.003

Darty, K., Denise, A., & Ponty, Y. (2009). VARNA: Interactive drawing and editing of the RNA secondary structure. *Bioinformatics*, *25*(15), 1974–1975. https://doi.org/10.1093/bioinformatics/btp250

des Georges, A., Dhote, V., Kuhn, L., Hellen, C. U. T., Pestova, T. v., Frank, J., & Hashem, Y. (2015). Structure of mammalian eIF3 in the context of the 43S preinitiation complex. *Nature*, *525*(7570), 491–495. https://doi.org/10.1038/nature14891

Donahue, T. F. (2000). Genetic approaches to translation initiation in Saccharomyces cerevisiae. *Cold Spring Harbor Monograph Series*, *39*, 487–502.

Erzberger, J. P., Stengel, F., Pellarin, R., Zhang, S., Schaefer, T., Aylett, C. H. S., Cimermančič, P., Boehringer, D., Sali, A., Aebersold, R., & Ban, N. (2014). Molecular Architecture of the 40S·eIF1·eIF3 Translation Initiation Complex. *Cell*, *159*(5), 1227–1228. https://doi.org/10.1016/j.cell.2014.11.001

Fabbri, L., Chakraborty, A., Robert, C., & Vagner, S. (2021). The plasticity of mRNA translation during cancer progression and therapy resistance. *Nature Reviews Cancer*, *21*(9), 558–577. https://doi.org/10.1038/s41568-021-00380-y

Fu, Q., Chen, Z., Gong, X., Cai, Y., Chen, Y., Ma, X., Zhu, R., & Jin, J. (2015). β-Catenin expression is regulated by an IRES-dependent mechanism and stimulated by paclitaxel in human ovarian cancer cells. *Biochemical and Biophysical Research Communications*, *461*(1), 21–27. https://doi.org/10.1016/j.bbrc.2015.03.161

Gilbert, W. v. (2010). Alternative Ways to Think about Cellular Internal Ribosome Entry. *Journal of Biological Chemistry*, *285*(38), 29033–29038. https://doi.org/10.1074/jbc.R110.150532

Gingras, A.-C., Gygi, S. P., Raught, B., Polakiewicz, R. D., Abraham, R. T., Hoekstra, M. F., Aebersold, R., & Sonenberg, N. (1999). Regulation of 4E-BP1 phosphorylation: a novel two-step mechanism. *Genes & Development*, *13*(11), 1422–1437. https://doi.org/10.1101/gad.13.11.1422

Gregori J, Sanchez A, & Villanueva J. (2019). *msmsTests: LC-MS/MS Differential Expression Tests. R package version 1.22.0.*

Guca, E., & Hashem, Y. (2018). Major structural rearrangements of the canonical eukaryotic translation initiation complex. *Current Opinion in Structural Biology*, *53*, 151–158. https://doi.org/10.1016/j.sbi.2018.08.006

Hashem, Y., des Georges, A., Dhote, V., Langlois, R., Liao, H. Y., Grassucci, R. A., Hellen, C. U. T., Pestova, T. V., & Frank, J. (2013). Structure of the Mammalian Ribosomal 43S Preinitiation Complex Bound to the Scanning Factor DHX29. *Cell*, *153*(5), 1108–1119. https://doi.org/10.1016/j.cell.2013.04.036

Higashimura, Y., Nakajima, Y., Yamaji, R., Harada, N., Shibasaki, F., Nakano, Y., & Inui, H. (2011). Up-regulation of glyceraldehyde-3-phosphate dehydrogenase gene expression by HIF-1 activity depending on Sp1 in hypoxic breast cancer cells. *Archives of Biochemistry and Biophysics*, *509*(1), 1–8. https://doi.org/10.1016/j.abb.2011.02.011

Hinnebusch, A. G. (2014). The Scanning Mechanism of Eukaryotic Translation Initiation. *Annual Review of Biochemistry*, *83*(1), 779–812. https://doi.org/10.1146/annurev-biochem-060713-035802

Hinnebusch, A. G. (2017). Structural Insights into the Mechanism of Scanning and Start Codon Recognition in Eukaryotic Translation Initiation. *Trends in Biochemical Sciences*, *42*(8), 589–611. https://doi.org/10.1016/j.tibs.2017.03.004

Hinnebusch, A. G., Ivanov, I. P., & Sonenberg, N. (2016). Translational control by 5′-untranslated regions of eukaryotic mRNAs. *Science*, *352*(6292), 1413–1416. https://doi.org/10.1126/science.aad9868

Hong, C.-F., Chen, W.-Y., & Wu, C.-W. (2017). Upregulation of Wnt signaling under hypoxia promotes lung cancer progression. *Oncology Reports*, *38*(3), 1706–1714. https://doi.org/10.3892/or.2017.5807

Hussain, T., Llácer, J. L., Fernández, I. S., Munoz, A., Martin-Marcos, P., Savva, C. G., Lorsch, J. R., Hinnebusch, A. G., & Ramakrishnan, V. (2014). Structural Changes Enable Start Codon Recognition by the Eukaryotic Translation Initiation Complex. *Cell*, *159*(3), 597–607. https://doi.org/10.1016/j.cell.2014.10.001

Iwasaki, S., Floor, S. N., & Ingolia, N. T. (2016). Rocaglates convert DEAD-box protein eIF4A into a sequence-selective translational repressor. *Nature*, *534*(7608), 558–561. https://doi.org/10.1038/nature17978

Iwasaki, S., Iwasaki, W., Takahashi, M., Sakamoto, A., Watanabe, C., Shichino, Y., Floor, S. N., Fujiwara, K., Mito, M., Dodo, K., Sodeoka, M., Imataka, H., Honma, T., Fukuzawa, K., Ito, T., & Ingolia, N. T. (2019). The Translation Inhibitor Rocaglamide Targets a Bimolecular Cavity between eIF4A and Polypurine RNA. *Molecular Cell*, *73*(4), 738-748.e9. https://doi.org/10.1016/j.molcel.2018.11.026

Jackson, R. J. (2013). The Current Status of Vertebrate Cellular mRNA IRESs. *Cold Spring Harbor Perspectives in Biology*, *5*(2), a011569–a011569. https://doi.org/10.1101/cshperspect.a011569

Jackson, R. J., Hellen, C. U. T., & Pestova, T. v. (2010). The mechanism of eukaryotic translation initiation and principles of its regulation. *Nature Reviews Molecular Cell Biology*, *11*(2), 113–127. https://doi.org/10.1038/nrm2838

James, C. C., & Smyth, J. W. (2018). Alternative mechanisms of translation initiation: An emerging dynamic regulator of the proteome in health and disease. *Life Sciences*, *212*, 138–144. https://doi.org/10.1016/j.lfs.2018.09.054

Jang, S. K., Kräusslich, H. G., Nicklin, M. J., Duke, G. M., Palmenberg, A. C., & Wimmer, E. (1988). A segment of the 5' nontranslated region of encephalomyocarditis virus RNA directs internal entry of ribosomes during in vitro translation. *Journal of Virology*, *62*(8), 2636–2643. https://doi.org/10.1128/jvi.62.8.2636-2643.1988

Kapp, L. D., & Lorsch, J. R. (2004). GTP-dependent Recognition of the Methionine Moiety on Initiator tRNA by Translation Factor eIF2. *Journal of Molecular Biology*, *335*(4), 923–936. https://doi.org/10.1016/j.jmb.2003.11.025

Karabiber, F., McGinnis, J. L., Favorov, O. v., & Weeks, K. M. (2013). QuShape: Rapid, accurate, and best-practices quantification of nucleic acid probing information, resolved by capillary electrophoresis. *RNA*, *19*(1), 63–73. https://doi.org/10.1261/rna.036327.112

Kieft, J. S. (2008). Viral IRES RNA structures and ribosome interactions. *Trends in Biochemical Sciences*, *33*(6), 274–283. https://doi.org/10.1016/j.tibs.2008.04.007

Kim, E., Kim, J. H., Seo, K., Hong, K. Y., An, S. W. A., Kwon, J., Lee, S.-J. v., & Jang, S. K. (2018). eIF2A, an initiator tRNA carrier refractory to eIF2α kinases, functions synergistically with eIF5B. *Cellular and Molecular Life Sciences*, *75*(23), 4287–4300. https://doi.org/10.1007/s00018-018-2870-4

Koumenis, C., & Wouters, B. G. (2006). "Translating" Tumor Hypoxia: Unfolded Protein Response (UPR)–Dependent and UPR-Independent Pathways. *Molecular Cancer Research*, *4*(7), 423–436. https://doi.org/10.1158/1541-7786.MCR-06-0150

Kozak, M. (1991). Structural features in eukaryotic mRNAs that modulate the initiation of translation. *Journal of Biological Chemistry*, *266*(30), 19867–19870. https://doi.org/10.1016/S0021-9258(18)54860-2

Lacerda, R., Menezes, J., & Romão, L. (2017). More than just scanning: the importance of cap-independent mRNA translation initiation for cellular stress response and cancer. *Cellular and Molecular Life Sciences*, *74*(9), 1659–1680. https://doi.org/10.1007/s00018-016-2428-2

Lee, A. S. Y., Kranzusch, P. J., Doudna, J. A., & Cate, J. H. D. (2016). eIF3d is an mRNA cap-binding protein that is required for specialized translation initiation. *Nature*, *536*(7614), 96–99. https://doi.org/10.1038/nature18954

Lee, L. J., Papadopoli, D., Jewer, M., del Rincon, S., Topisirovic, I., Lawrence, M. G., & Postovit, L.-M. (2021). Cancer Plasticity: The Role of mRNA Translation. *Trends in Cancer*, *7*(2), 134–145. https://doi.org/10.1016/j.trecan.2020.09.005

Leppek, K., Das, R., & Barna, M. (2018). Functional 5′ UTR mRNA structures in eukaryotic translation regulation and how to find them. *Nature Reviews Molecular Cell Biology*, *19*(3), 158–174. https://doi.org/10.1038/nrm.2017.103

Liu, H.-L., LIU, D., DING, G.-R., LIAO, P.-F., & ZHANG, J.-W. (2015). Hypoxia-inducible factor-1α and Wnt/β-catenin signaling pathways promote the invasion of hypoxic gastric cancer cells. *Molecular Medicine Reports*, *12*(3), 3365–3373. https://doi.org/10.3892/mmr.2015.3812

Llácer, J. L., Hussain, T., Saini, A. K., Nanda, J. S., Kaur, S., Gordiyenko, Y., Kumar, R., Hinnebusch, A. G., Lorsch, J. R., & Ramakrishnan, V. (2018). Translational initiation factor eIF5 replaces eIF1 on the 40S ribosomal subunit to promote start-codon recognition. *ELife*, *7*. https://doi.org/10.7554/eLife.39273

Low, J. T., & Weeks, K. M. (2010). SHAPE-directed RNA secondary structure prediction. *Methods*, *52*(2), 150–158. https://doi.org/10.1016/j.ymeth.2010.06.007

Mailliot, J., & Martin, F. (2018). Viral internal ribosomal entry sites: four classes for one goal. *WIREs RNA*, *9*(2). https://doi.org/10.1002/wrna.1458

Martinez-Salas, E., Francisco-Velilla, R., Fernandez-Chamorro, J., & Embarek, A. M. (2018). Insights into Structural and Mechanistic Features of Viral IRES Elements. *Frontiers in Microbiology*, *8*. https://doi.org/10.3389/fmicb.2017.02629

Montoya, M. (2012). Translation under hypoxia. *Nature Structural & Molecular Biology*, *19*(6), 602–602. https://doi.org/10.1038/nsmb.2326

Muz, B., de la Puente, P., Azab, F., & Azab, A. K. (2015). The role of hypoxia in cancer progression, angiogenesis, metastasis, and resistance to therapy. *Hypoxia*, 83. https://doi.org/10.2147/HP.S93413

Naineni, S. K., Itoua Maïga, R., Cencic, R., Putnam, A. A., Amador, L. A., Rodriguez, A. D., Jankowsky, E., & Pelletier, J. (2020). A comparative study of small molecules targeting eIF4A. *RNA*, *26*(5), 541–549. https://doi.org/10.1261/rna.072884.119

Nusse, R., & Clevers, H. (2017). Wnt/β-Catenin Signaling, Disease, and Emerging Therapeutic Modalities. *Cell*, *169*(6), 985–999. https://doi.org/10.1016/j.cell.2017.05.016

Pakos-Zebrucka, K., Koryga, I., Mnich, K., Ljujic, M., Samali, A., & Gorman, A. M. (2016). The integrated stress response. *EMBO Reports*, *17*(10), 1374–1395. https://doi.org/10.15252/embr.201642195

Parsyan, A., Svitkin, Y., Shahbazian, D., Gkogkas, C., Lasko, P., Merrick, W. C., & Sonenberg, N. (2011). mRNA helicases: the tacticians of translational control. *Nature Reviews Molecular Cell Biology*, *12*(4), 235–245. https://doi.org/10.1038/nrm3083

Peifer, M., McCrea, P. D., Green, K. J., Wieschaus, E., & Gumbiner, B. M. (1992). The vertebrate adhesive junction proteins beta-catenin and plakoglobin and the Drosophila segment polarity gene armadillo form a multigene family with similar properties. *Journal of Cell Biology*, *118*(3), 681–691. https://doi.org/10.1083/jcb.118.3.681

Pelletier, J., & Sonenberg, N. (1988). Internal initiation of translation of eukaryotic mRNA directed by a sequence derived from poliovirus RNA. *Nature*, *334*(6180), 320–325. https://doi.org/10.1038/334320a0

Pelletier, J., & Sonenberg, N. (2019). The Organizing Principles of Eukaryotic Ribosome Recruitment. *Annual Review of Biochemistry*, *88*(1), 307–335. https://doi.org/10.1146/annurev-biochem-013118-111042

Pestova, T. v., Lomakin, I. B., Lee, J. H., Choi, S. K., Dever, T. E., & Hellen, C. U. T. (2000). The joining of ribosomal subunits in eukaryotes requires eIF5B. *Nature*, *403*(6767), 332–335. https://doi.org/10.1038/35002118

Petrova, V., Annicchiarico-Petruzzelli, M., Melino, G., & Amelio, I. (2018). The hypoxic tumour microenvironment. *Oncogenesis*, *7*(1), 10. https://doi.org/10.1038/s41389-017-0011-9

Pópulo, H., Lopes, J. M., & Soares, P. (2012). The mTOR Signalling Pathway in Human Cancer. *International Journal of Molecular Sciences*, *13*(2), 1886–1918. https://doi.org/10.3390/ijms13021886

Reuter, J. S., & Mathews, D. H. (2010). RNAstructure: software for RNA secondary structure prediction and analysis. *BMC Bioinformatics*, *11*(1), 129. https://doi.org/10.1186/1471-2105-11-129

Rogers, G. W., Richter, N. J., Lima, W. F., & Merrick, W. C. (2001). Modulation of the Helicase Activity of eIF4A by eIF4B, eIF4H, and eIF4F. *Journal of Biological Chemistry*, *276*(33), 30914–30922. https://doi.org/10.1074/jbc.M100157200

Rol-Moreno, J., Kuhn, L., Marzi, S., & Simonetti, A. (2020). *Grad-cryo-EM: Tool to Isolate Translation Initiation Complexes from Rabbit Reticulocyte Lysate Suitable for Structural Studies* (pp. 329–339). https://doi.org/10.1007/978-1-0716-0278-2_21

Sen, N. D., Zhou, F., Harris, M. S., Ingolia, N. T., & Hinnebusch, A. G. (2016). eIF4B stimulates translation of long mRNAs with structured 5′ UTRs and low closed-loop potential but weak dependence on eIF4G. *Proceedings of the National Academy of Sciences*, *113*(38), 10464–10472. https://doi.org/10.1073/pnas.1612398113

Shang, S., Hua, F., & Hu, Z.-W. (2017). The regulation of β-catenin activity and function in cancer: therapeutic opportunities. *Oncotarget*, *8*(20), 33972–33989. https://doi.org/10.18632/oncotarget.15687

Shatsky, I. N., Terenin, I. M., Smirnova, V. v., & Andreev, D. E. (2018). Cap-Independent Translation: What's in a Name? *Trends in Biochemical Sciences*, *43*(11), 882–895. https://doi.org/10.1016/j.tibs.2018.04.011

Simonetti, A., Brito Querido, J., Myasnikov, A. G., Mancera-Martinez, E., Renaud, A., Kuhn, L., & Hashem, Y. (2016). eIF3 Peripheral Subunits Rearrangement after mRNA Binding and Start-Codon Recognition. *Molecular Cell*, *63*(2), 206–217. https://doi.org/10.1016/j.molcel.2016.05.033

Simonetti, A., Guca, E., Bochler, A., Kuhn, L., & Hashem, Y. (2020). Structural Insights into the Mammalian Late-Stage Initiation Complexes. *Cell Reports*, *31*(1), 107497. https://doi.org/10.1016/j.celrep.2020.03.061

Sokabe, M., & Fraser, C. S. (2017). A helicase-independent activity of eIF4A in promoting mRNA recruitment to the human ribosome. *Proceedings of the National Academy of Sciences*, *114*(24), 6304–6309. https://doi.org/10.1073/pnas.1620426114

Sonenberg, N., & Hinnebusch, A. G. (2009). Regulation of Translation Initiation in Eukaryotes: Mechanisms and Biological Targets. *Cell*, *136*(4), 731–745. https://doi.org/10.1016/j.cell.2009.01.042

Spitale, R. C., Crisalli, P., Flynn, R. A., Torre, E. A., Kool, E. T., & Chang, H. Y. (2013). RNA SHAPE analysis in living cells. *Nature Chemical Biology*, *9*(1), 18–20. https://doi.org/10.1038/nchembio.1131

Sun, Y., Atas, E., Lindqvist, L., Sonenberg, N., Pelletier, J., & Meller, A. (2012). The eukaryotic initiation factor eIF4H facilitates loop-binding, repetitive RNA unwinding by the eIF4A DEAD-box helicase. *Nucleic Acids Research*, *40*(13), 6199–6207. https://doi.org/10.1093/nar/gks278

Terenin, I. M., Smirnova, V. v., Andreev, D. E., Dmitriev, S. E., & Shatsky, I. N. (2017). A researcher's guide to the galaxy of IRESs. *Cellular and Molecular Life Sciences*, *74*(8), 1431–1455. https://doi.org/10.1007/s00018-016-2409-5

Thiele, A., Nagamine, Y., Hauschildt, S., & Clevers, H. (2006). AU-rich elements and alternative splicing in the β-catenin 3′UTR can influence the human β-catenin mRNA stability. *Experimental Cell Research*, *312*(12), 2367–2378. https://doi.org/10.1016/j.yexcr.2006.03.029

Thomas, J. D., & Johannes, G. J. (2007). Identification of mRNAs that continue to associate with polysomes during hypoxia. *RNA*, *13*(7), 1116–1131. https://doi.org/10.1261/rna.534807

Thompson, P. A., Eam, B., Young, N. P., Fish, S., Chen, J., Barrera, M., Howard, H., Sung, E., Parra, A., Staunton, J., Chiang, G. G., Gerson-Gurwitz, A., Wegerski, C. J., Nevarez, A., Clarine, J., Sperry, S., Xiang, A., Nilewski, C., Packard, G. K., … Webster, K. R. (2021). Targeting Oncogene mRNA Translation in B-Cell Malignancies with eFT226, a Potent and Selective Inhibitor of eIF4A. *Molecular Cancer Therapeutics*, *20*(1), 26–36. https://doi.org/10.1158/1535-7163.MCT-19-0973

Valenta, T., Hausmann, G., & Basler, K. (2012). The many faces and functions of β-catenin. *The EMBO Journal*, *31*(12), 2714–2736. https://doi.org/10.1038/emboj.2012.150

Varela-Nallar, L., Rojas-Abalos, M., Abbott, A. C., Moya, E. A., Iturriaga, R., & Inestrosa, N. C. (2014). Chronic hypoxia induces the activation of the Wnt/β-catenin signaling pathway and stimulates hippocampal neurogenesis in wild-type and APPswe-PS1ΔE9 transgenic mice in vivo. *Frontiers in Cellular Neuroscience*, *8*. https://doi.org/10.3389/fncel.2014.00017

Verheyen, E. M., & Gottardi, C. J. (2009). Regulation of Wnt/β-catenin signaling by protein kinases. *Developmental Dynamics*, NA-NA. https://doi.org/10.1002/dvdy.22019

Villa, N., Do, A., Hershey, J. W. B., & Fraser, C. S. (2013). Human Eukaryotic Initiation Factor 4G (eIF4G) Protein Binds to eIF3c, -d, and -e to Promote mRNA Recruitment to the Ribosome. *Journal of Biological Chemistry*, *288*(46), 32932–32940. https://doi.org/10.1074/jbc.M113.517011

Waldron, J. A., Tack, D. C., Ritchey, L. E., Gillen, S. L., Wilczynska, A., Turro, E., Bevilacqua, P. C., Assmann, S. M., Bushell, M., & le Quesne, J. (2019). mRNA structural elements immediately upstream of the start codon dictate dependence upon eIF4A helicase activity. *Genome Biology*, *20*(1), 300. https://doi.org/10.1186/s13059-019-1901-2

Walker, S. E., Zhou, F., Mitchell, S. F., Larson, V. S., Valasek, L., Hinnebusch, A. G., & Lorsch, J. R. (2013). Yeast eIF4B binds to the head of the 40S ribosomal subunit and promotes mRNA recruitment through its N-terminal and internal repeat domains. *RNA*, *19*(2), 191–207. https://doi.org/10.1261/rna.035881.112

Warner, K. D., Hajdin, C. E., & Weeks, K. M. (2018). Principles for targeting RNA with drug-like small molecules. *Nature Reviews Drug Discovery*, *17*(8), 547–558. https://doi.org/10.1038/nrd.2018.93

Yourik, P., Aitken, C. E., Zhou, F., Gupta, N., Hinnebusch, A. G., & Lorsch, J. R. (2017). Yeast eIF4A enhances recruitment of mRNAs regardless of their structural complexity. *ELife*, *6*. https://doi.org/10.7554/eLife.31476

Zhang, Q., Bai, X., Chen, W., Ma, T., Hu, Q., Liang, C., Xie, S., Chen, C., Hu, L., Xu, S., & Liang, T. (2013). Wnt/β-catenin signaling enhances hypoxia-induced epithelial–mesenchymal transition in hepatocellular carcinoma via crosstalk with hif-1α signaling. *Carcinogenesis*, *34*(5), 962–973. https://doi.org/10.1093/carcin/bgt027

Supplementary materials

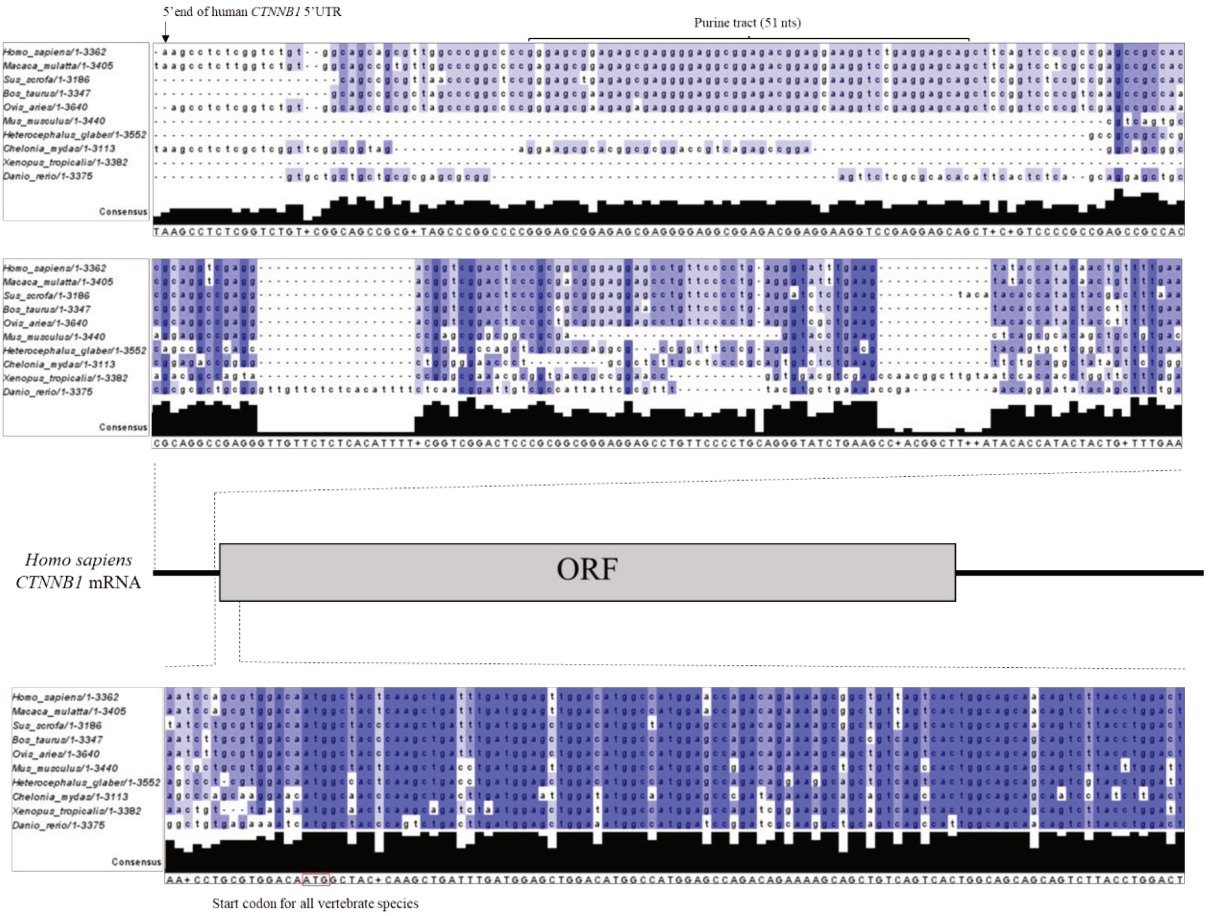

Figure S1. Sequence conservation in regions of the CTNNB1 mRNA in vertebrates. Sequence alignment was performed with Multiple Alignment using Fast Fourier Transform (MAFFT) online server with default parameters and represented with Jalview 2.11. Whole vertebrate mRNA sequences were obtained from the following NCBI Reference Sequences: NM_001904.4 (Homo sapiens), (Macaca mulatta), NM_001165902.1 (Mus musculus), NM_001303303.1 (Heterocephalus glaber), Sus Scrofa (NM_214367.1), NM_001076141.1 (Bos taurus), XM_043540769.1 (Chelonia mydas), NM_001016958.1 (Xenopus tropicalis) and NM_131059.2 (Danio Rerio). Darker blue indicates more sequence conservation.

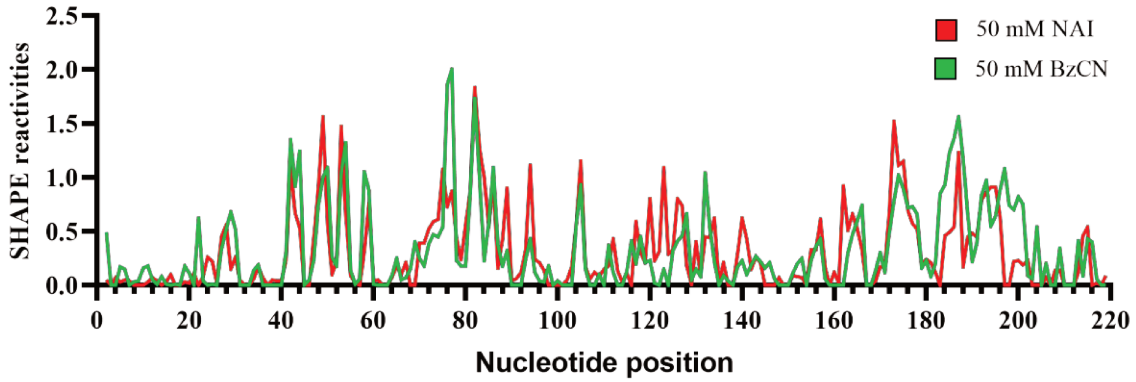

Figure S2. NAI and BzCN reactivity profiles for the 5'UTR of *CTNNB1* mRNA. Electropherograms of BzCN and NAI reactivity data on *CTNNB1* 5'UTR. Normalization is performed with QuSHAPE software and values ranges from 0-2. Negative values were set to 0.

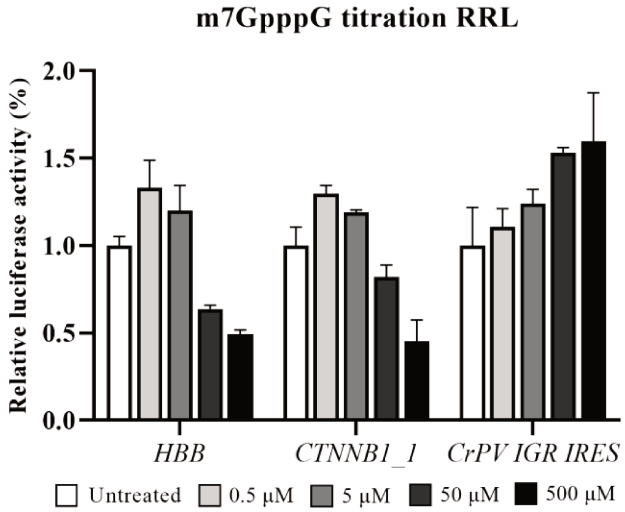

Figure S3. *In vitro* translation assay in RRL using a range of m7GpppG concentration. *In vitro* translation assay on RRL was made using different concentrations of m7GpppG from 0 to 500 µM. *HBB*, *CTNNB1_1* and *CrPV IGR IRES* transcripts used were m7G-capped. Each condition was performed in triplicates.

Structural and functional characterization of the 5'UTR of *CTNNB1* mRNA and its role in translation

Probing the 5'UTR of *CTNNB1* mRNA in HeLa cells by in-cell SHAPE

In vitro RNA probing is the first step to gain insight in the folding of a given RNA. However, obtaining the RNA native folding is important to further understand its function in cells. DMS is a well-known chemical probe with extended application in RNA probing and permeable into cells. During the last decade, new SHAPE reagents have also been designed to improve their solubility and permeability into cells, such as NAI (Lee et al., 2017). For that reason, two SHAPE reagents were used in this study: benzoyl cyanide and NAI. The first one is a classical reagent utilized *in vitro*, whereas NAI was conceived to probe RNA in cells. Secondary structure models obtained *in cellulo* from abundant RNAs, as rRNA or viral RNA are available (Diaz-Toledano et al., 2017). However, the main drawback of probing mRNAs in cells is the lack of sensitivity because they are low-abundant and comprise less than 5% of the total RNA.

We try to set up a workflow to probe the 5'UTR of *CTNNB1* mRNA in HeLa cells, based on the method conceived for low-abundant RNA by Bevilacqua and co-workers (Kwok et al., 2013a). Our method basically consists in the incubation of cells with a SHAPE reagent, followed by total RNA extraction, reverse transcriptase on the mRNA of interest and RNA alkaline hydrolysis. Then, cDNA fragments are ligated to a DNA linker and a PCR step is done to amplify the cDNA fragments. For the amplification, ^{32}P labelled oligonucleotides were utilised, producing radiolabelled dsDNA fragments. Thus, the workflow relies on the amplification step to gain sensitivity for the detection of cDNA.

The radioactive PCR fragments were run on denaturing PAGE, and we could observe bands of different sizes and a full extension band at the top of the gel (data not shown). This gel suggested that reverse transcriptase, DNA ligation and PCR step succeeded for *CTNNB1* 5'UTR. Unfortunately, the interpretation of dsDNA migration profile was difficult because we could not see differences between the unmodified and probe-modified RNA sample. Furthermore, the parallel ddNTP sequencing was missing – because we had only focused on the workflow for RNA samples. Some issues that we encountered during this workflow will be indicated for its optimization in the future:

- Before probing the *CTNNB1* 5'UTR, we should start with an easier approach such as 5S rRNA probing (a short and abundant RNA), in order to validate each of the steps of this workflow (except the PCR amplification), such as RNA modification, RNA extraction and reverse transcription.
- The limiting step of this method was DNA ligation, which is a reaction with low efficiency. Soon after we tried Bevilacqua's protocol, another publication showed the significance of choosing a suitable DNA oligonucleotide, as well as the appropriated experimental conditions using T4 DNA ligase for ssDNA ligation (Kwok et al., 2013b).
- Compared to denaturing urea PAGE, the PCR fragments are separately more efficiently in a sequencer by capillary electrophoresis, as for the case of cDNA fragments (ssDNA) obtained after *in vitro* SHAPE. From our point of view, the dsDNA produced after in-cell SHAPE would migrate differently in the sequencer

compared to ssDNA. For that reason, we had decided to migrate the radioactively-labelled PCR fragments in a denaturing gel.

Further efforts must be done to succeed in probing low-abundant RNA in living cells. For example, an engineered reverse transcriptase that instead of stopping on the probe-modified nucleotides incorporates mutations further identified by the direct sequencing of cDNA, could be used to elude amplification bias (Tomezsko et al., 2020).

To characterize the translation of β-catenin mRNA from the secondary structure model as a starting point, we performed *in vitro* translation with HeLa cell extract and we attempt to improve the conditions of translation by depleting the endogenous mRNAs.

Depletion of endogenous mRNA on HeLa cell extract

Cell-free translation systems (CFTSs) are widely used to produce biologically relevant proteins for clinical application and to investigate the mechanism of protein synthesis. Among them, rabbit reticulocyte lysate (RRL) has been the most utilised mammalian CFTS for decades (Jackson & Hunt, 1983). RRL treated with micrococcal nuclease to deplete the endogenous mRNAs and reduce background translation to a minimum is commercially available. Since our research is focused on human cancer, I have set up a method to produce CFTS from HeLa cells and other human cancer cell lines.

To improve the translational output of HeLa CFTS, a mild treatment with *Staphylococcus aureus* micrococcal nuclease (MNase) was performed to degrade endogenous mRNAs, based on a protocol from Hentze's laboratory (Rakotondrafara et al., 2013). MNase digestion experiments were performed in a buffer containing $CaCl_2$, which is essential for the enzyme catalysis. The enzyme was inactivated by adding EGTA, a chelating agent that as a preference for Ca^{2+} over other divalent cations. The following parameters were considered for the nuclease digestion: enzymatic units, $CaCl_2$ concentration, EGTA concentration, enzyme incubation time and temperature. After nuclease treatment, translation efficiency of HeLa CFTS was measured by *in vitro* translation assays using *CTNNB1_1* construct (see Article 1).

In Figure 10A, translation of the luciferase protein can be observed after nuclease digestion performed in different conditions on HeLa CTFS. Among four tested $CaCl_2$ concentrations (see A-D bars), treatment with 1,5 and 2 mM were the only conditions that significantly improved the translational output compared to translation of untreated HeLa CFTS. Based on the parameters tested, the following results were obtained:

I. Optimal enzymatic units for digestion were set at 5 U (see conditions A-E). The treatment with 10 U of enzyme was discarded as translation was substantially reduced (see condition F).
II. 25°C was the optimal temperature, whereas digestion at 30°C resulted in the total absence of translation (see condition G).
III. Finally, a longer nuclease incubation (> 10 minutes) did not improve mRNA translation rate (data not shown).

IV. Inactivation with 3 mM EGTA is preferred over 6 mM (see condition E). Indeed, lower concentration of chelator may avoid the sequestration of the Mg^{2+} present in the cell extract or added on translation assays. Mg^{2+} is essential for the correct functioning of the translational machinery.

In Figure 10B, the parameters tested in conditions A-G are summarized and the comparison between the indications from MNase's manufacturer (New England Biolabs, NEB), the protocol of Hentze's lab and our current protocol is shown. For our cell extracts, the best condition to deplete mRNA consisted in a digestion of 10 minutes at 25°C with 5 U of MNase in presence of 1,5 mM $CaCl_2$ which is stopped by 3 mM EGTA. These experiments showed the need of redefining the concentration of both the enzyme and $CaCl_2$ to improve the translation rate of the reporter mRNA, and hence, the depletion of endogenous mRNAs.

However, the nuclease treatment was finally skipped for cell extract preparation because the translation was only slightly improved (see condition C). Therefore, *in vitro* translation assays were made in a mRNA competitive environment. Conversely, translation initiation complex assembly and isolation was performed using a large amount of the mRNA of interest to compensate the competition with endogenous mRNAs.

A

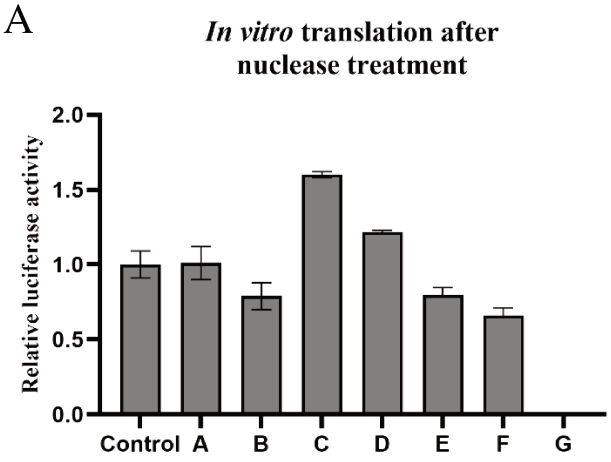

Figure 10. Effect of nuclease digestion on the luciferase reporter translation in HeLa cell extract. (A) Reporter translation using nuclease-treated HeLa CFTS was measured by luciferase activity. Conditions A-G are normalised to the luciferase level of control condition. (B) Digestion parameters performed in conditions A-G are sumarized. Digestion conditions from manufacturer (NEB), Hentze's lab and our optimized protocol are indicated. *NEB considered 1 U of MNase per 1 µg of nucleic acid, Hentze's lab 15 U per 50 µg of protein and we considered 5 U for 500 µg of cell extract protein .

B

	A	B	C	D	E	F	G		NEB	Hentze	Optimization
Nuclease (U)	5	5	5	5	5	10	10		1*	15*	5*
$CaCl_2$ (mM)	0,75	1	1,5	2	1,5	1,5	1,5		5	0,75	1,5
EGTA pH 7,5 (mM)	3	3	3	3	6	3	3		"excess"	3	3
Incubation time (min)	10	10	10	10	10	10	10		15	7	10
Temperature (°C)	25	25	25	25	25	25	30		37	25	25

Rocaglates inhibit cell growth in cells both under normoxia and hypoxia

Rocaglates are comprised in a class of natural compounds isolated from plants of the genus *Aglaia* and act as potent inhibitors of translation initiation (i.e., Rocaglamide A (RocA) and silvestrol). Indeed, these compounds, stabilizing eIF4A-RNA interactions, inhibits the RNA helicase activity of eIF4A and the recruitment of the 43S PIC on the mRNA. Among eIF4A inhibitors known to date, silvestrol is one of the most potent anticancer drugs. It

inhibits cell growth and induces cell death in several cancer cell types (Kogure et al., 2013; Chen et al., 2016).

Here we explored the effect of this molecule on HeLa and SW480 cell growth. Cell growth was measured using a luciferase-based assay dependent on the ATP present in the culture. The greater is the number of cells, the more ATP is available for luciferase reaction to form a luminescent product. Therefore, a correlation can be made between cell number and luciferase activity. The number of cells after incubation with silvestrol was compared to the one right before treatment (100%). Both cell lines were treated with 25 nM or 50 nM of silvestrol or its vehicle (0.01% v/v DMSO) for 24 or 48 hours. Furthermore, cells were cultured either in normoxia or severe hypoxia (<0.1% O_2). Luciferase activity is shown for HeLa and SW480 cells in Figure 11A and 11B, respectively.

Severe hypoxia significantly declined the growth of both HeLa (214% and 322% in normoxia against 105 and 117% in hypoxia, at 24 or 48h, respectively) and SW480 cells (219% and 323% in normoxia against 123 and 121% in hypoxia, at 24 or 48h, respectively). In both oxygen conditions, treatment with silvestrol has strongly reduced the growth of HeLa cells, while this effect was less significant on SW480 cells.

To conclude, our studies showed that cell growth under severe hypoxia was significantly affected in both HeLa and SW480 cells. However, growth arrest upon silvestrol treatment was substantially different between the two cell lines, being HeLa cell growth much more sensible to silvestrol treatment, while SW480 cell growth was slightly reduced. Although the increase of cell death after silvestrol treatment is expected, these experiments were conceived to quantify the relative number of cells but not cell viability. These results confirmed that silvestrol is a potential anticancer candidate to target both normoxic and hypoxic cancer cells. The sensitivity of hypoxic tumour cells to silvestrol treatment is especially relevant, seen that these cells are prone to chemotherapy resistance. Due to the different behaviour of HeLa and SW480 cells to silvestrol treatment, we could hypothesize that the efficacy of cell growth inhibition and/or apoptosis is probably dependent on the tumour cell types and even the stage or grade of the cancer.

Rocaglates inhibit the translation of *CTNNB1* mRNA.

Rocaglates affect cell growth and apoptosis by modulating gene expression at the level of translation. The inhibition role of these molecules is correlated to the eIF4A-dependency of mRNAs to be translated (Iwasaki et al. 2016). We have recently shown *in cellulo* that silvestrol inhibits the translation of *CTNNB1* mRNA when the GC-rich element is present, further confirming its eIF4A-dependency (see Article 1). The inhibitory role of silvestrol has been shown by RNA transfection for different cell types (HeLa and several cancer cells) and it has been more evident when cells were cultured in severe hypoxic condition. Here, the effect of silvestrol and RocA, two rocaglates with high relevance in clinical applications, were comparatively evaluated by *in vitro* translation assays using HeLa cell extract.

In Figure 11C is shown the relative translation of the luciferase reporter mRNA carrying the full-length 5'UTR of *HBB* or *CTNNB1* mRNA in presence of 25 nM or 50 nM of a rocaglate. Additionally, for the *CTNNB1* construct the inhibition due to the rocaglates was tested in normoxic and hypoxic conditions. The translation of *CTNNB1_1* construct was significantly inhibited in all silvestrol and RocA concentrations tested, while the one of *HBB* construct was barely reduced at the highest concentration both rocaglates. Moreover, the rocaglates tested were able to inhibit the translation of *CTNNB1_1* construct in both normoxic and hypoxic HeLa cell extract. RocA exhibited a stronger reduction of luciferase translation at lower concentration (25 nM) compared to silvestrol at the same concentration.

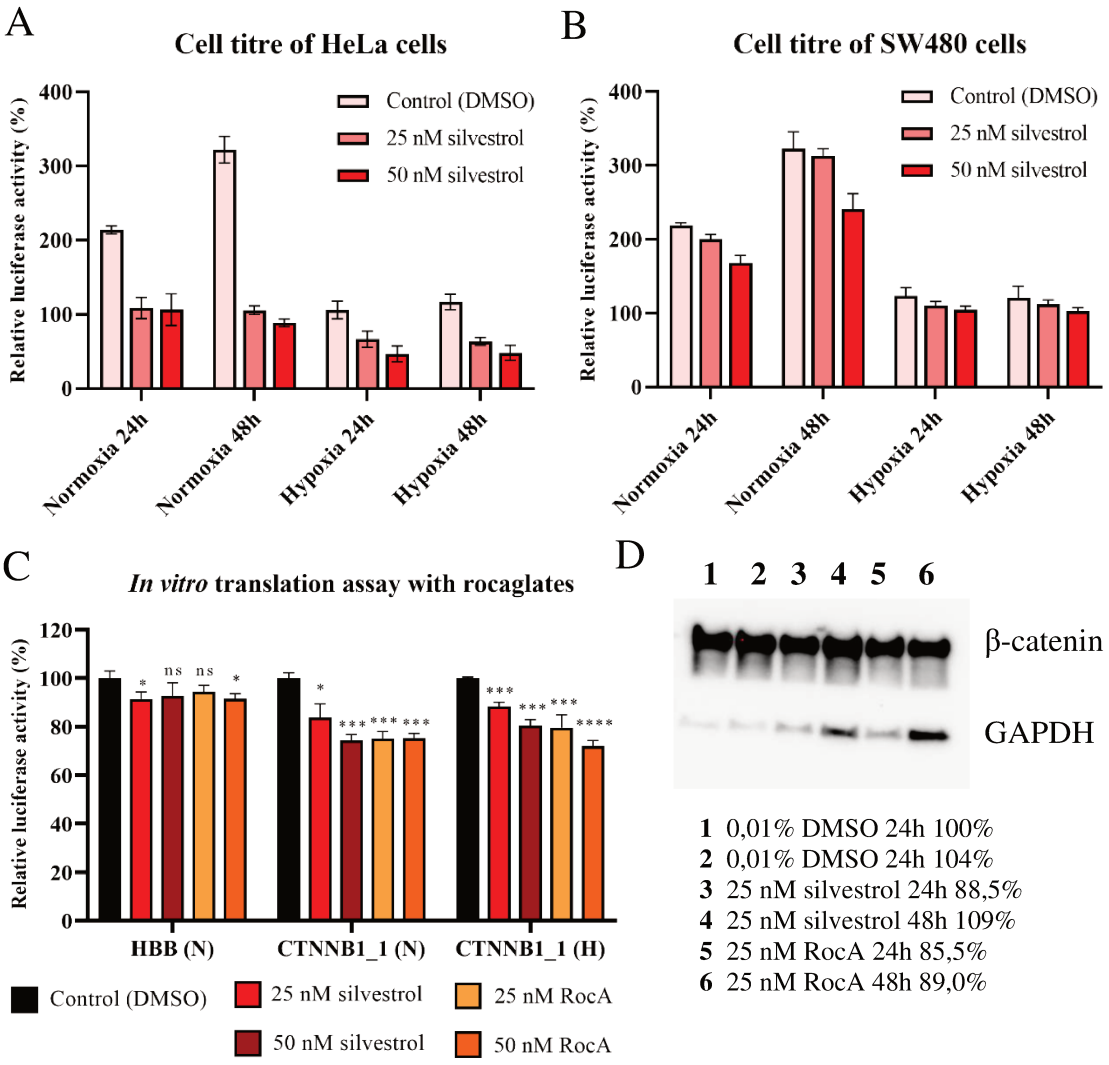

Figure 11. Rocaglate effect in cell growth and in the translation inhibition of β-catenin. Cell titer of HeLa (A) and SW480 cells (B) by a luciferase-based assay. Luciferase activity was normalize to the level of translation at time 0 hours, right before cell treatment with vehicle or rocaglates. Each condition has at least 6 replicates. (C) *In vitro* translation assay under rocaglate treament in HeLa cell extract. Experiments were performed with *HBB* transcript in normoxia, and *CTNNB1_1* construct in normoxia and hypoxia. Unpaired t-test was performed comparing the control condition to every treated condition for each transcript. (D) Western blotting from HeLa total protein samples cultured for 24 or 48 hours in 0,01% v/v DMSO, 25 nM silvestrol and 25 nM RocA.

To evaluate the rocaglate-induced translation inhibition of β-catenin in cells, a Western blot was performed on total protein samples extracted from HeLa cells treated for 24 or 48 hours with silvestrol or RocA (Figure 11D). Bradford assay was performed to ensure loading the same amount of total protein of each sample. The protein level was quantified and a reduction of β-catenin in cells treated with RocA could be noticed. Unfortunately, GAPDH (control protein) level notably increased after 48 hours of silvestrol or RocA treatment probably due to the translational upregulation of some mRNAs independent of eIF4A activity. Therefore, another protein should be used as a loading control.

To conclude, the results of the *in vitro* translation assay indicated that silvestrol and RocA effectively inhibits *CTNNB1* mRNA translation in HeLa cells cultured in normoxic and in hypoxic conditions. Moreover, western blotting results confirms the RocA-induced translation inhibition of *CTNNB1* mRNA at the nanomolar range in cells.

CTNNB1 mRNA/48S IC preparation from RRL or HeLa cell extract

Our research is focused on the investigation of the mechanism that regulates the translation of *CTNNB1* mRNA via its 5'UTR. The mechanism of translation of an mRNA can be analysed by diverse structural and molecular biology methods. To gain mechanistic insight on the translation of β-catenin driven by the GC-rich element within its 5'UTR, we decided to use our published method Grad-cryo-EM to investigate intermediate ribosomal complexes isolated directly from HeLa cell extract (Rol-Moreno et al., 2020). The strategy of this approach resides in the use of a specific inhibitor that can block translation at a step of interest – such as scanning translation initiation, late-stage translation initiation, translation elongation, etc – directly from RRL, and the isolation of the translation complex by sucrose gradient. Then, the complex composition is analysed by mass spectrometry and its high-resolution structure is obtained by cryo-EM. This protocol was first set-up to isolate late-stage 48S IC (LS48S IC) attached to the mRNA of interest directly form nuclease-treated RRL. This is possible thanks to the utilization of guanosine 5'-(β, γ-imido) triphosphate (GDPNP), a non-hydrolysable nucleotide that blocks the GTP hydrolysis of eIF2α subunit and synchronises translation initiation complexes at the star codon.

Two different transcripts were utilised to assemble and to isolate in 48S IC directly from nuclease-treated RRL (Figure 12A). *HBB* mRNA has been chosen as a reference for the 48S formation because it has been previously studied (Simonetti et al., 2020). Then, a short construct based of *CTNNB1* mRNA was prepared with the purpose of studying the full-length 5'UTR as well as conserving the first nucleotides of β-catenin coding sequence. The formation of translation initiation complexes has been monitored following the sucrose gradient profile via the nucleic acid absorbance at 260 nm ($A_{260\ nm}$) and the radioactivity profile of the ^{32}P-labeled *HBB* or *CTNNB1* mRNA (Figure 12B).

According to the radioactivity profile, the peak corresponding to the 48S IC bound to the exogenous mRNA was located between fractions 20 and 32. Noteworthy, *CTNNB1* short transcript yielded more translation initiation complex than *HBB* mRNA. This is consistent

with the higher translation rate of *CTNNB1* mRNA in the HeLa cell compared to *HBB* mRNA that we have shown previously in mRNA transfection experiments (see Article 1).

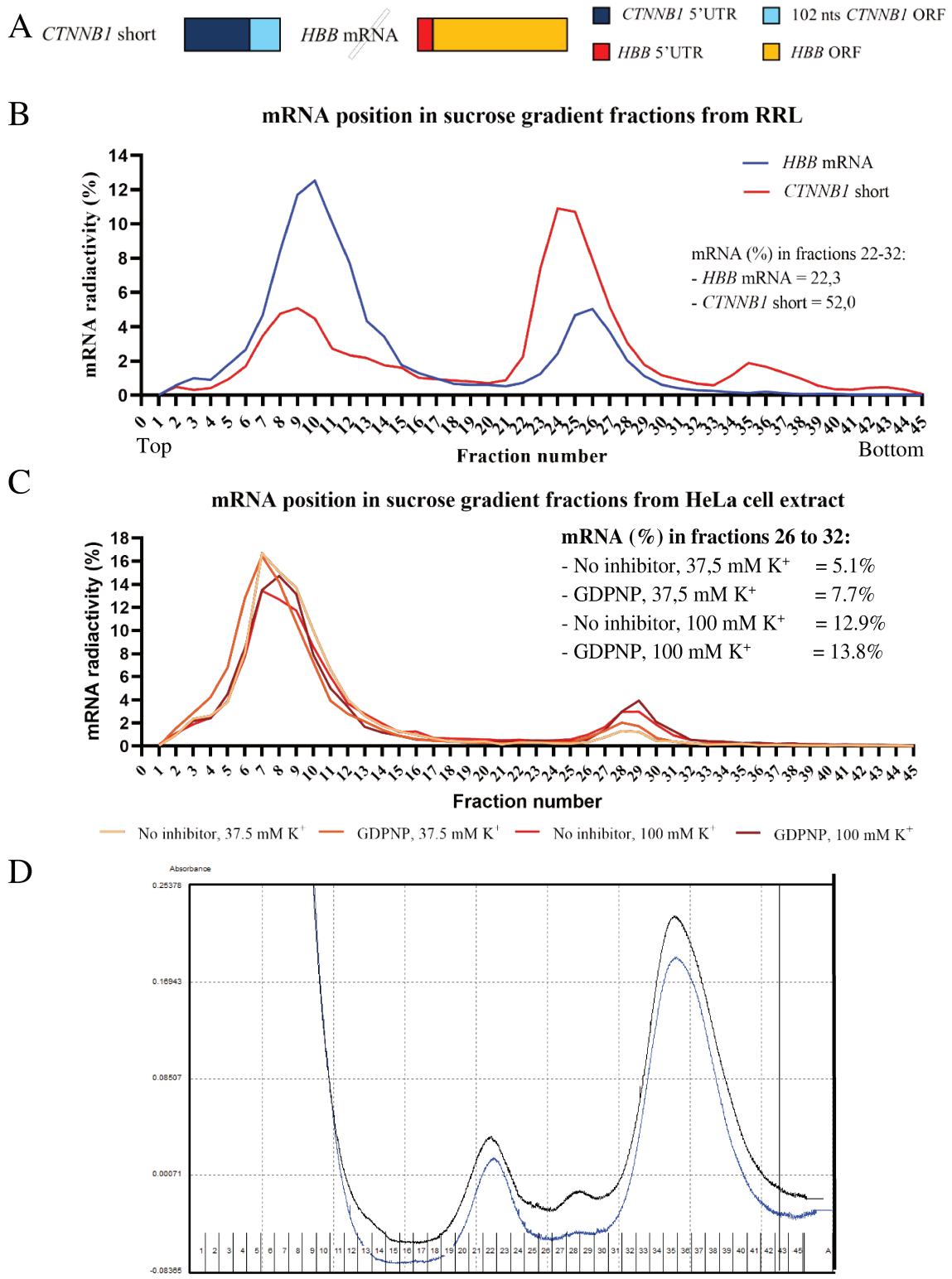

Figure 12. *CTNNB1* mRNA/48S IC isolation from RRL and HeLa cell extract. (A) Schematization of transcripts used to assemble late stage 48S IC in RRL. (B) mRNA radioactivity plot from fractionation of a 5-25% sucrose gradient for isolation of a late stage 48S IC bound to the mRNA of study. Proportion (%) of mRNA present in the 48S fractions from total radioactivity in the gradient are indicated in a text box for each sample. Samples were prepared using RRL (C) mRNA radioactivity plot from fractionation of a 5-25% sucrose gradient for isolation of *CTNNB1* mRNA/48S IC using *CTNNB1* short transcript. Samples were prepared using HeLa

cell extract cultured in standard conditions. (D) Absorbance profile at 260 nm of a sucrose gradient with *CTNNB1* mRNA assembled on 48S IC from HeLa cell extract. Complexes were prepared in 37.5 mM (blue) or 100 mM (black) of potassium.

Once demonstrated that it was possible to isolate directly from RRL the LS48S IC with bound the short *CTNNB1* transcript, the same construct was chosen to adapt the Grad-cryo-EM approach to human cell extracts. In first instance, translational activity of HeLa cell extract was tested by *in vitro* translation assays and then the same preparation was used for the isolation of human 48S IC. The depletion of endogenous mRNA by micrococcal nuclease treatment was skipped, especially to avoid the remaining active nuclease that could cleave rRNA, tRNA and the exogenous transcript. Hence, we used a large amount of *CTNNB1* short transcript to compensate the competition with endogenous mRNAs.

As potassium concentration is crucial for the formation of ribosomal complexes (Nierhaus, 2014), two potassium concentrations were tested. In Figure 12C, the mRNA radioactivity peak corresponding to *CTNNB1* LS48S IC can be observed from fractions 26 to 32. More initiation complex was yielded when incubating with 100 mM K^+ (13.8%) instead of 37.5 mM (7.7%). In Figure 12D, the 48S peak in the A_{260nm} profile of the sucrose gradient can be seen when assembling the 48S at 100 mM potassium but this peak is notably less visible in the low potassium condition. This result highlights the significance of assembling the *CTNNB1* mRNA/48S IC at physiological potassium concentration.

Taken together, *CTNNB1* LS48S IC was isolated from RRL applying the Grad-cryo-EM protocol. Notably, we achieved to adapt this method to HeLa cell extract for isolation of *CTNNB1* LS48S IC without the need of nuclease treatment. A near physiological potassium concentration was essential to obtain a reasonable yield of late-stage translation initiation complex. The strength of the adapted version of Grad-cryo-EM approach relies on the ability to purify 48S and 80S ICs bound on different mRNAs of interest directly from cell extracts of different types of cell lines (HeLa and also other cancer cell lines) even cultured in different cellular stress conditions mimicking the TME.

Cryo-EM dataset analysis of hypoxic *CTNNB1* and ΔGC LS48S IC

We succeeded in optimizing the conditions to isolate *CTNNB1* LS48S IC from HeLa cell extracts cultured in both standard oxygen conditions and severe hypoxia. Then, we proceeded to prepare the sample for Grad-cryo-EM analysis. We assembled and isolated from HeLa cell extract three different complexes: normoxic and hypoxic *CTNNB1* LS48S IC, as well as the hypoxic ΔGC LS48S IC – corresponding to the *CTNNB1* mRNA without the GC-rich element. Protein composition of the isolated complexes were analysed by nanoLC-MS/MS (see Figure 3 in Article 1).

The hypoxic LS48S IC complexes with bound full-length *CTNNB1* 5'UTR or its truncated mutant, were flash-frozen in several grids. These grids were first screened in a Glacios to control the quality of the sample. The grids with well-distributed and oriented particles were chosen to acquire movies in a Titan Krios transmission electron microscope. Data processing was performed using three different workflows: cryoSPARC, software

framework Scipion or a combination of the pre-processing tool Warp and RELION (see Supplementary Figure 3 for the schematized flowchart of the three strategies).

The hypoxic *CTNNB1* LS48S IC dataset was first process using cryoSPARC 3.1, a software based on the stochastic gradient descent (SGD) and branch-and-bound maximum likelihood optimization algorithms. These algorithms permit to speed-up pre-processing steps, particularly the 2D classification – for an overview of cryoSPARC 2D classification, see supplementary Figure 5. We obtained a set of ~540000 particles and performed homologous refinement with an internal reference generated with the ab-initio modelling. In Figure 13A, the electron density map of the refined volume is represented with a fitted atomic model of the human scanning 48S IC which is deposited in PDB as 6ZMW (Querido et al., 2020). The 3D structure is at the overall resolution of 3.2 A, where we can observe densities for the 40S, ABCE1, the TC (without eIF2β), and a partial occupancy for the eIF3 core. However, cryoSPARC 3.1 does not have a 3D classification tool to solve sample heterogeneity. Therefore, we decided to process again the hypoxic *CTNNB1* LS48S IC dataset using Scipion framework software. Using Relion 3D classification algorithm, we obtained the 3D structure of one main class at the overall resolution of 3,64 Å. In Figure 13B is represented the electron density map of the refined main 3D class with the fitted atomic model of the rabbit *HBB* LS48S IC (Simonetti et al., 2020; 6YAL PDB). Comparing the latter structure with the obtained electron density map, we can observe that our translation initiation complex contains overlapping densities for the small ribosomal subunit, the ternary complex (including the Met-tRNAi^{Met} and eIF2α and γ, but no eIF2β), ABCE1, eIF1A, most of the subunits of eIF3 and clear extra density sitting on ribosomal ES6. Nonetheless, we believe this 3D classification is not entirely appropriate because many particles were misaligned during the classification and only one 48S class out of 10 were obtained. For this reason, we reprocess the *CTNNB1* LS48S IC using RELION 4.0. The Warp-RELION strategy is still ongoing – see Supplementary Figure 6 for 2D classification in RELION. Using the two first strategies, we understood that 512 voxels of box size is more appropriate because it considers all ribosomal densities, including that for eIF3, allowing a better alignment and sorting of the particles. Finally, we recently acquired ΔGC LS48S IC dataset on Titan Krios and we have started to analyse it.

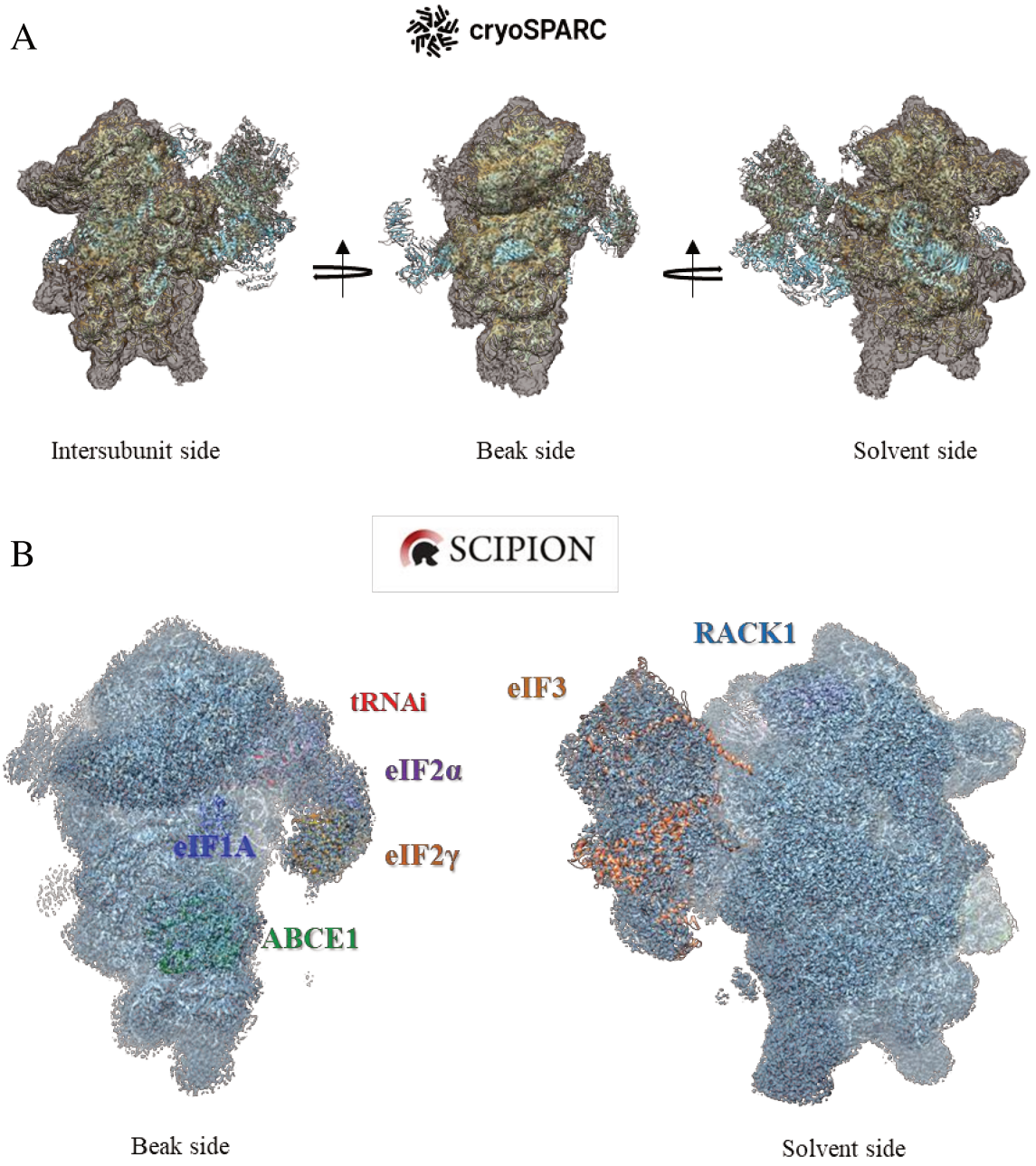

Figure 13. Cryo-EM density maps of hypoxic CTNNB1 LS48S IC obtained with the cryoSPARC and Scipion workflows. Electron density map of hypoxic *CTNNB1* LS48S IC in different perspectives. (A) The 6ZMW PDB structure was fitted in the in the density volume obtained with cryoSPARC. (B) The 6YAL PBD structure was overlapped to visualize the elements present in the minor 3D class from Scipion. Structure is shown in grey blue in two perspectives: solvent and beak side. The following factors are highlighted in the model: ABCE1, eIF2 subunit alpha and gamma, eIF3, RACK1 and tRNAi.

Structural and functional characterization of the 5'UTR of *HIF1A* mRNA and its role in translation

The 5'UTR of HIF1A mRNA is folded in a four-way junction and contains a putative G-quadruplex

The percentage of GC-content in the human *HIF1A* mRNA is high throughout the 5'UTR (68,7%; see Figure 14A), decreases in the ORF (40,8%) and still diminishes at the 3'UTR (29,3%). To confirm whether the 5'UTR of this mRNA is highly-structured due to its high GC-content, the secondary structure model was obtained by combining RNA structure prediction and chemical probing analysis. For this study we used a 254-nt sequence, a shorter version of the 5'UTR of *HIF1A* mRNA isoform 1, lacking exactly the first 38 nts. This 5'UTR length was chosen according to RNA and DNA transfection experiments of dicistronic reporter constructs performed to demonstrate that HIF-1α has an IRES-mediated translation mechanism for its basal translation under hypoxia, when cap-dependent translation is compromised (Lang et al., 2002; Bert et al., 2006; Young et al., 2008).

The secondary structure of the 5'UTR of human *HIF1A* mRNA (*HIF1A* 5'UTR) was determined by SHAPE analysis and validated with other chemical probes: DMS and CMCT. The electropherograms representing BzCN or NAI modifications on the 5'UTR are very similar (Figure 14B), although the NAI coverage was not complete due to saturation of the electropherogram signal at the 5' side of *HIF1A* 5'UTR. We believe that due to the high GC-content, the AMV RT struggles to produce cDNA at the 5' end of this 5'UTR. Furthermore, a bigger adduct created by NAI compared the smaller one formed by BzCN, could impede the full primer extension of the sequence at the 5' side of the mRNA.

The secondary structure of *HIF1A* 5'UTR is presented in Figure 14C. This model shows a unique RNA domain comprising helixes 1-6 and organized in a four-way junction – forming a "tree shape". An extensive base-pairing region defining Helix 1 (H1) is continued by a long helix (H2) with an internal loop and a long stem loop. The model defines another element composed by a small helix (H3) whose nucleotides appear single-stranded in some alternative predictions (data not shown), and a longer helix (H4), all belonging to the four-way junction. H4 is continued by a helix with a small stem loop (H5) and finally, helix 6 (H6) containing a 23-nts stem loop. This highly-compact RNA structural element is followed by a single-stranded region with a relatively small helix (H7) and the start codon. The initial AUG codon is situated within the optimum (strong) Kozak sequence (A_{-3} and G_{+4}, being $A_{+1}U_{+2}G_{+3}$), that ensures the slowing down of scanning 48S complex and thus, correct start codon recognition and efficient translation.

Strikingly, the cDNA profile of *HIF1A* 5'UTR resulted from reverse transcription showed a very strong arrest at positions G_{86} and G_{87} (see Figure 15A, green profile). We hypothesized that G_{86} and G_{87} participate in the formation of a very stable structure at which the AMV RT frequently stops. Because of the 3'-to-5' polymerization sense of the reverse transcriptase, these two guanosines would be located at the 3' side of this RNA structural element. To confirm this hypothesis, guanosines G_{86} and G_{87} were substituted by two adenosines ($G_{86}G_{87}>A_{86}A_{87}$). Reverse transcriptase was performed on the *HIF1A* 5'UTR wildtype and its mutant transcript (from here onwards, *HIF1A_mut*). The cDNA profile from

HIF1A_mut showed the disappearance of the strong AMV RT stop at positions 86 and 87, validating the implication of these two nucleosides in the formation of a very stable structure (Figure 14A, pink profile).

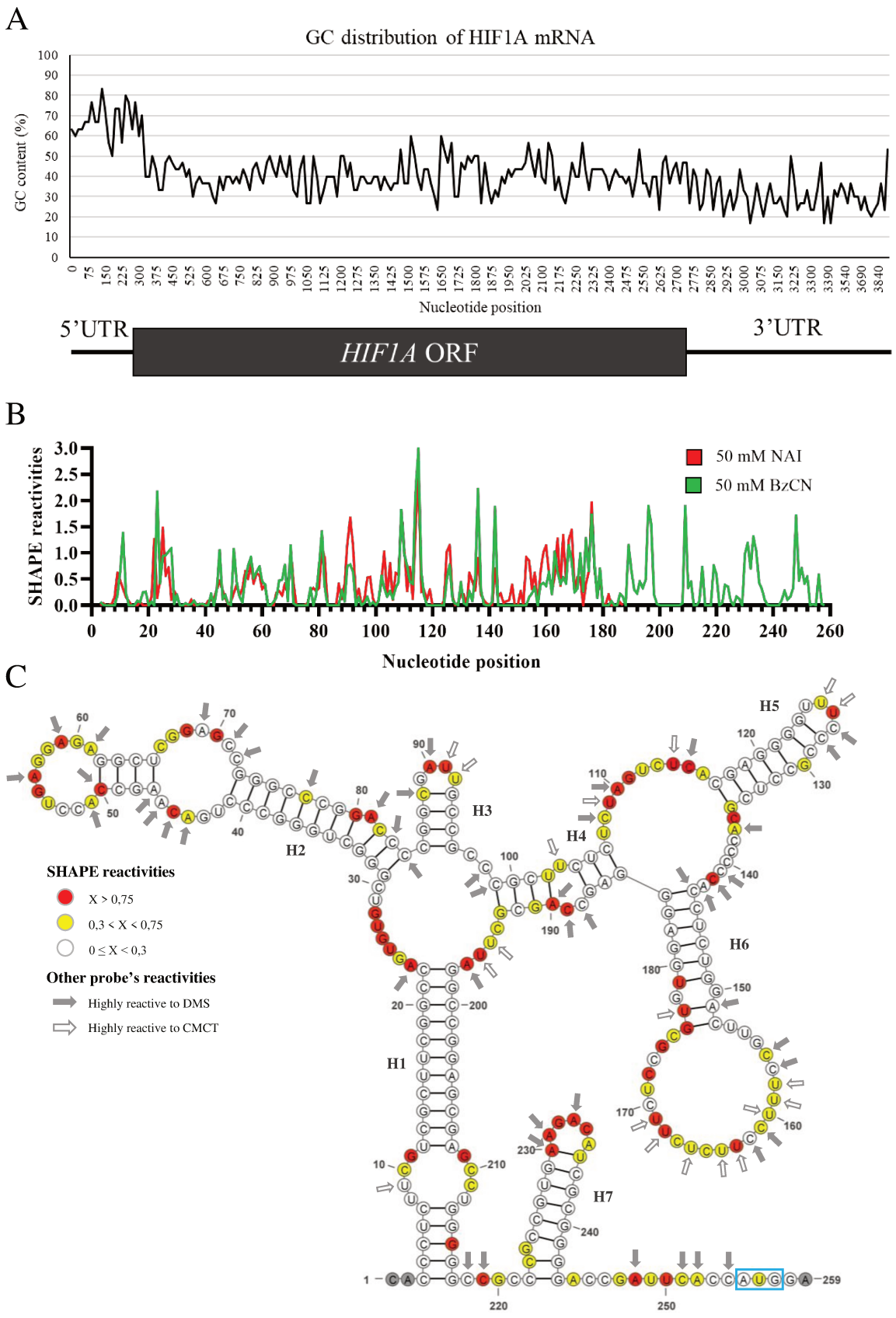

Figure 14. Secondary structure model of the 5'UTR of HIF1A mRNA. (A) GC distribution is represented by plotting the average GC-content value of 30-nucleotide windows each 15 nucleotides. Positions of the 5'UTR, ORF and 3'UTR are schematized in parallel to nucleotide positions. (B) Electropherograms of BzCN and NAI reactivity data on HIF1A 5'UTR. Normalization is performed with QuSHAPE software and values ranges from 0-3. Negative values were set to 0. (C) Normalized SHAPE reactivity is represented by white, yellow or red circles at reactivity ranges 0-0.3, 0.3-0.75 or >0.75 respectively, in a scale from 0 to 1. Grey nucleotides have no SHAPE reactivity data. Highly reactive nucleotides to 50 mM DMS or 20 mM CMCT are indicated with grey or white arrows, respectively. High reactivity to each probe detects single-stranded regions of RNA or very flexible nucleotides. RNA helices are indicated by H1-7. Start codon is highlighted with a cyan blue square.

It exists a particular nucleotide disposition called G-tetrad or G-quartet, where four guanosines are arranged in non-canonical Hoogsteen hydrogen bonding and aligned on the same plane. G-quartets can be then stacked into each other by the coordination of a monovalent ion – the most suitable being potassium (K^+) due to its atomic radium –, to form a G-quadruplex. G-quadruplexes can be found in both DNA and RNA. DNA G-quadruplexes were first found in telomeres (Dipankar et al., 1988; Paeschke et al., 2005). More recently, several RNA G-quadruplexes (rG4) were described *in vitro* and *in vivo*, with the potential of giving RNA new regulatory functionalities at different steps of gene expression, as transcription, splicing, translation and many others. Notably, rG4s positioned within 5'UTRs have been found to activate or repress translation. (Millevoi et al., 2012; Lyu et al., 2021). Hence, the involvement of rG4s in key biological processes make them attractive targets for new therapeutics (Wolfe et al., 2014)

A search for rG4s in *HIF1A* mRNA sequence was performed using QGRS Mapper web server, whose algorithm predicts composition and distribution of putative quadruplex forming G-rich sequences (QGRS). QGRS Mapper is a user-friendly application that provides an output list of possible rG4 sequences classified according to the G-scores (Kikin et al., 2006). Higher G-scores indicates a better candidate for G-quadruplex formation. The software predicted the presence of putative rG4s predominantly at the 5'UTR of *HIF1A* mRNA (see Figure 15B), consistent with the high guanosine content of this region. Among the predicted rG4s, the one with the highest G-score contained the above cited G_{86} and G_{87}. A model of rG4 containing these nucleotides is represented in Figure 15C. However, there are other possible G-quadruplex topologies (Popenda et al., 2020).

Taken together, the results of the reverse transcriptase of *HIF1A_mut* and the rG4 prediction suggests the presence of putative G-quadruplex in the 5'UTR of *HIF1A* mRNA. In the foreseeable future, further analysis will be made to confirm the presence of a G-quadruplex and more importantly, its existence *in vivo*. To validate its existence, rG4 mutational analysis will be coupled to primer extension assay performed in presence of lithium (Li^+) that, differently from K^+, destabilized the G-quadruplex motif. Pilot experiments shown that using Li^+ in reverse transcription with the AMV RT, the arrest at G_{86} and G_{87} was reduced (data not shown) suggesting that these two nucleotides actively participate in the formation of a stable RNA structure.

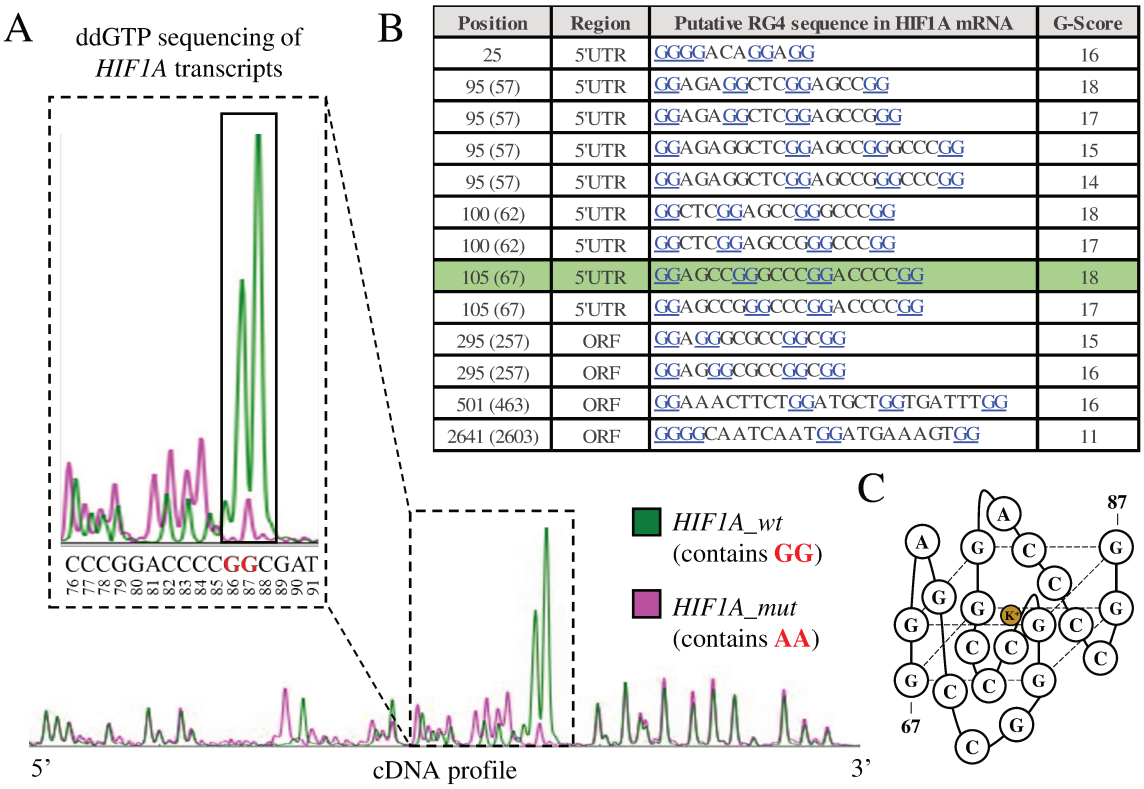

Position	Region	Putative RG4 sequence in HIF1A mRNA	G-Score
25	5'UTR	GGGGACAGGAGG	16
95 (57)	5'UTR	GGAGAGGCTCGGAGCCGG	18
95 (57)	5'UTR	GGAGAGGCTCGGAGCCGGG	17
95 (57)	5'UTR	GGAGAGGCTCGGAGCCGGGCCCGG	15
95 (57)	5'UTR	GGAGAGGCTCGGAGCCGGGCCCGG	14
100 (62)	5'UTR	GGCTCGGAGCCGGGCCCGG	18
100 (62)	5'UTR	GGCTCGGAGCCGGGCCCGG	17
105 (67)	5'UTR	GGAGCCGGGCCCGGACCCCGG	18
105 (67)	5'UTR	GGAGCCGGGCCCGGACCCCGG	17
295 (257)	ORF	GGAGGGCGCCGGCGG	15
295 (257)	ORF	GGAGGGCGCCGGCGG	16
501 (463)	ORF	GGAAACTTCTGGATGCTGGTGATTTGG	16
2641 (2603)	ORF	GGGGCAATCAATGGATGAAAGTGG	11

Figure 15. Validation of the putative RNA G-quadruplex and prediction model. (A) ddGTP sequencing profile of part of HIF1A 5'UTR. Within the black box, the strong arrest can be appreciated in the wildtype sequence (green), but it is removed in the AA mutant (pink). (B) QRGS output table including the putative rG4 sequences of *HIF1A* mRNA. Each sequence indicates the position of the first nucleotide of the rG4 within the mRNA and a G-score. Blue underlined nucleotides represent guanines forming the rG4. Position in brackets is considered from our 254-nt 5'UTR. (C) Schematized representation of the putative G-quadruplex between positions 67 to 87. The two stacked G-quartets are denoted with a lined four-sided shape. Coordinated potassium atom is symbolized by a gold circle.

The putative rG4 located within the 5'UTR of *HIF1A* mRNA influences the translation of the reporter gene

RT analysis and rG4 prediction suggested the implication of G_{86} and G_{87} in the formation of a stable RNA structure located at the 5'UTR of *HIF1A* mRNA. To investigate its functional significance, *in vitro* translation assay and luciferase-based mRNA transfection were performed using Hela cells. Since HIF-1α is involved in the cell hypoxic response, HeLa cell were cultured in different oxygen conditions. Two RNA constructs were prepared in which the wildtype 5'UTR of *HIF1A* mRNA (*HIF1A*) or its mutant (*HIF1A_mut*), comprising the beginning of its ORF, were cloned upstream the *Fluc* ORF (Figure 16A).

To analyse in cells the impact of the putative rG4 on the translation of the reporter gene, *HIF1A* and *HIF1A_mut* transcripts were transfected into HeLa cells cultured in standard oxygen conditions (18% O_2) or under severe hypoxia (<0,1% O_2). In Figure 16B, the luciferase activity of *HIF1A* transcript was reproducibly higher than *HIF1A_mut* construct (two-fold difference). Noteworthy, while the luciferase activity of *HIF1A_mut* construct was similar in the two conditions, *HIF1A* construct had a higher luciferase activity

in hypoxic condition (two-fold increment over normoxic condition). Our results suggests that the putative rG4 has a pivotal role in the expression of the reporter gene acting as a translation enhancer element in hypoxic conditions.

To validate its role in the translation regulation, *HIF1A* and *HIF1A_mut* constructs were tested by *in vitro* translation assay using normoxic and hypoxic HeLa cell extract (Figure 16C). Similar to the *in vivo* study, in hypoxic conditions we observed an rG4-dependent expression highlighting its relevant role on the translation of the reporter gene. Indeed, *HIF1A* was translated twice more in hypoxia compared to normoxia, while the translation of *HIF1A_mut* is remarkably reduced compared to the normoxic level. Altogether, these results demonstrate that the rG4 has a significant effect on the expression of *HIF1A* mRNA.

In conclusion, our results strongly suggest that the translation of *HIF1A* mRNA during hypoxia is driven by the putative rG4 within its 5'UTR. To understand whether trans-acting elements recognizing the rG4 participate in the translation regulation of *HIF1A* mRNA, additional investigations are necessary (i.e., CLIP and Grad-Cryo-EM).

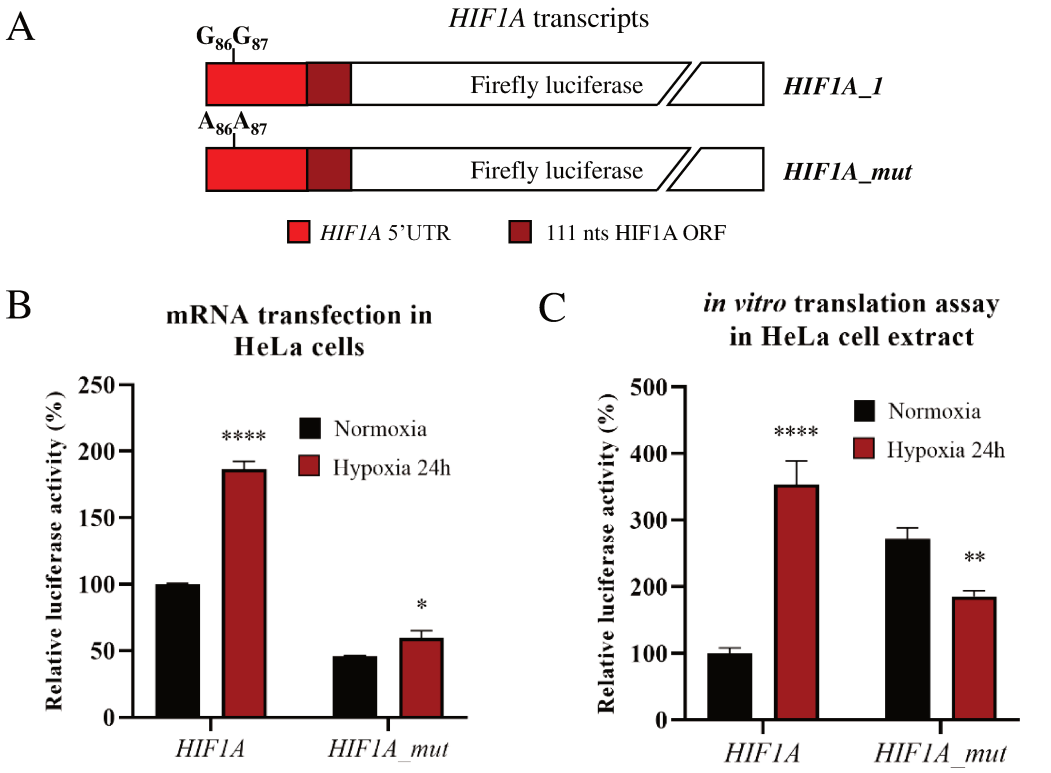

Figure 16. Cap independency and translation efficiency of HIF1A mRNA is driven by a 5'UTR structural element. (A) HIF1A transcripts used in this analysis are schematised. The mutation of HIF1A is represented by highlighting the position of the substitutions. (B) mRNA transfection of *HIF1A* and *HIF1A_mut* constructs on HeLa cells cultured in normoxia or hypoxia 24h. Renilla luciferase was co-transfected and used as a normalization control. (C) *in vitro* translation assay of *HIF1A* and *HIF1A_mut* constructs in HeLa cell extract cultured in normoxia or 24h of hypoxia. Unpaired T-test was performed in hypoxia condition of each mRNA comparing with its level in normoxia. *$p \leq 0.05$, **$p \leq 0.01$ and ****$p \leq 0.0001$.

The RNA structural element at the 5'UTR of HIF1A mRNA drive its cap-independent translation

The results of the *in vitro* and *in cellulo* translation assay suggest that the putative rG4, on which formation G_{86} and G_{87} participates, is an important cis-acting regulatory element for the translation of *HIF1A* mRNA. To get insight into the rG4-driven mechanism, we analysed the requirement of the 5'cap performing competitive inhibition of *HIF1A* and *HIF1A_mut* translation by m7GpppG (cap analog) titration. Being exclusively translated in a cap-dependent manner, the 5'UTR of *HBB* mRNA fused to the luciferase coding sequence was chosen as a control. The cap analog m7GpppG is a modified dinucleotide linked by a 5' to 5' phosphodiester bond, that mimicking the cap structure competes with the m7G-capped mRNAs to bind eIF4E, thereby inhibiting 48S IC formation. Hence, the translation of m7G-capped mRNAs will be reduced in case the 5' cap is required for its translation.

In Figure 17A, the results of the in vitro translation assay are represented. They were performed to test the translation of three constructs (*HIF1A*, *HIF1A_mut* and *HBB*) in presence of increasing amount of the cap analog and obtained using RRL. As it was expected, the translation of *HBB* transcript was clearly reduced. On the other hand, the translation of m7G-capped *HIF1A* construct remained unaffected for all concentration tested of m7GpppG, suggesting that eIF4E is not required for efficient translation of the reporter gene holding this 5'UTR. Surprisingly, *HIF1A_mut* recovered the cap dependency, behaving very similar to *HBB* construct. These results support the hypothesis that the rG4 is the regulatory element for the translation initiation of *HIF1A* mRNA in a cap-independent manner.

To further analyse the requirement of eIF4E in hypoxic conditions, m7G-capped or A-capped *HIF1A* and *HIF1A*_mut constructs have been tested by *in vitro* translation assay using normoxic and hypoxic HeLa cell extracts. The non-functional A-cap (ApppG) cannot be recognised by eIF4E due to the presence of an adenosine (A) instead of a 7-methylguanosine at the 5' end. As expected, in normoxic condition the A-capped mRNAs construct were translated less efficiently than the ones m7G-capped (Figure 17B). Notably, in hypoxic condition all the m7G capped mRNAs tested were translated at least 2-fold more than in normoxic conditions. This is particularly the case for the m7G capped *HIF1A* construct whose translation was four-fold higher in hypoxia. Noteworthy, among the three tested A-capped constructs, the translation of *HIF1A* in hypoxia was the solely that was two-fold higher compared to his expression in cells cultured in standard oxygen conditions. Moreover, the m7G/A cap translation ratio, related to the cap dependency, diminished differently depending on the 5'UTR of the mRNA:

- m7G/A cap translation ratio in *HBB*: 3.5 in normoxia and in 2.8 hypoxia.

- m7G/A cap translation ratio in *HIF1A*: 6.3 in normoxia and 2.3 in hypoxia.

While the cap dependency was barely altered in *HBB* transcript, the translation of *HIF1A* construct was remarkably less dependent of eIF4E when translated in hypoxia.

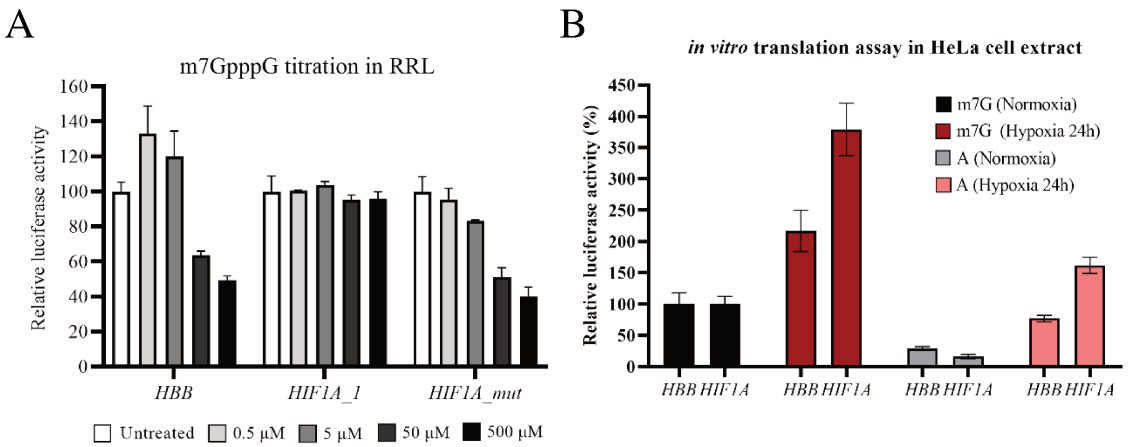

Figure 17. Cap-independency of *HIF1A* transcript in RRL and HeLa cell extract. (A) in vitro translation assay on RRL using different concentrations of m7GpppG from 0 to 500 µM. Each condition was performed in triplicates. (B) in vitro translation assay in HeLa cell extract cultured in normoxia (N) or 24h of hypoxia (H). Experiments were performed in triplicates.

To conclude, these experiments confirm that *HIF1A* mRNA translation is regulated via its 5'UTR. The rG4 located in the 5'UTR is the regulatory element responsible of the translation initiation mechanism switch occurring in hypoxia. The existence of an eIF4E-independent initiation mechanism represents for *HIF1A* mRNA a translation advantage because of the described unavailability of eIF4E during hypoxic stress.

Endogenous *HIF1A* mRNA expression is not affected in severe hypoxia

The regulation of *HIF1A* gene at transcriptional and post-translational level are well known. However, little is known about *HIF1A* mRNA level during cell stress related to deficient blood supply as hypoxia and glucose starvation. Apart from HeLa cells, U87MG, a cancer cell line derived from glioblastoma (Monteiro et al., 2017) – one of the most lethal malignant tumours known– was chosen to study the effects of hypoxia on *HIF1A* expression.

Reverse transcriptase coupled to quantitative PCR (RT-qPCR) enables precise quantification of mRNA level in cells. RT-qPCR was performed to investigate the expression of the HIF1A mRNA in response to different cell oxygen conditions and/or to glucose starvation. In Figure 18A, the expression changes of *HIF1A* mRNA in HeLa cells can be observed. Cells were exposed to different times of severe hypoxia (<0.1% O_2). No difference in mRNA level was seen at all hypoxia exposure times from 0 to 48h. However, there were difficulties to find good reference genes whose expression level remain unchanged under hypoxia. Although GAPDH is one of the gold standards for normalization, it is transcriptionally upregulated in hypoxia (Yamaji et al., 2003). For all the qPCRs done, EEF1A1 is the best choice because of the stable Ct throughout the hypoxia timeline.

Additionally, RT-qPCR was performed on total RNA samples isolated from HeLa or U87MG cells exposed to two different stresses glucose starvation or severe hypoxia (<0.1% O2). Cells were incubated under standard conditions (normoxia, 25 mM α-D-glucose),

hypoxia, glucose starvation (0.5 mM α-D-glucose) or combining both stresses. In Figure 18B and 5C, it can be observed *HIF1A* mRNA level in HeLa cells and U87MG cells, respectively. None of the stress conditions resulted in a change in *HIF1A* mRNA expression. However, mRNA level decreased under hypoxia or glucose starvation, and the combination of both reduced the mRNA level more than 2-fold.

These data suggest that *HIF1A* mRNA is not upregulated during hypoxia and its level even diminished when combined to glucose starvation in HeLa cells. However, no effect was seen in U87MG cells. At last instance, a transcriptional up-regulation of *HIF1A* due to hypoxic stress can be discarded in these conditions.

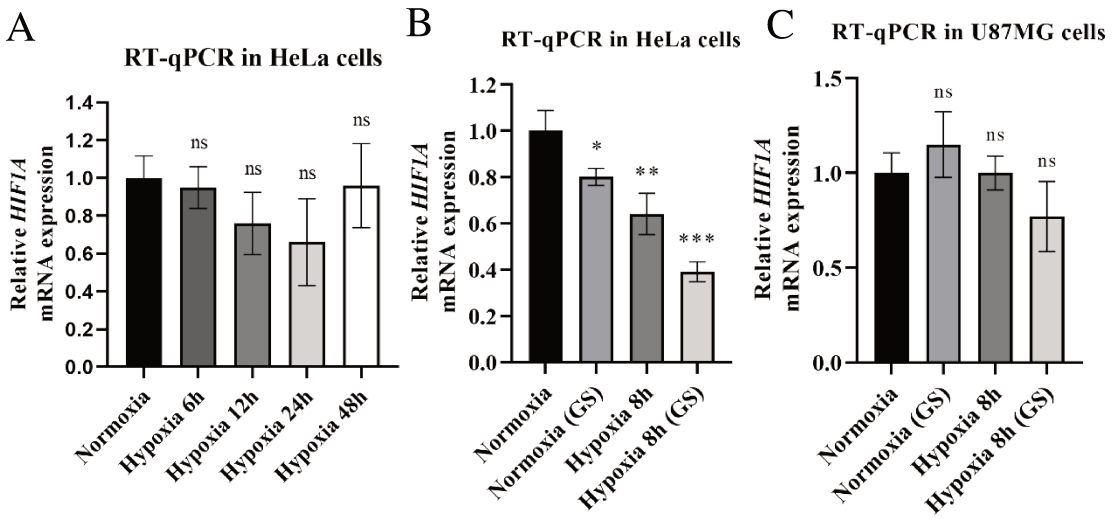

Figure 18. Endogenous *HIF1A* mRNA level at different stress conditions. (A) RT-qPCR from total RNA of HeLa cells under different times of hypoxia exposure, from 0 to 48h. (B) and (C) RT-qPCR from total RNA of HeLa or U87MG cells in different stress conditions. *EEF1A1* and *RPL13A* were used as reference genes. Unpaired t-test was performed between the standard and the stress condition. GS (glucose starvation), ns (non-significant), * ($p \leq 0.05$), ** ($p \leq 0.01$) and *** ($p \leq 0.001$).

HIF1A LS48S IC isolation from U87MG cell extract.

The translation initiation mechanism of *HIF1A* mRNA is poorly studied. The role of the 5'UTR in translation, particularly the putative rG4, should be revealed by an integrative structural approach. For this reason, the translation initiation mechanism of HIF-1α was analysed through Grad-cryo-EM approach. For our studies, translationally active cell extracts were prepared from U87MG cells cultured in normoxia or after 24 hours in hypoxia. These cell extracts were treated with GDPNP to stall 48S ICs bound to *HIF1A* or *CTNNB1* mRNA. Finally, a 5%–25% sucrose density gradient fractionation was used to isolate mRNA-bound 48S ICs. The formation of translation initiation complexes was monitored following the ribosome profile via the nucleic acid absorbance at 260 nm and in parallel, an additional sucrose gradient using a radioactive m7G-capped mRNA.

In Figure 19A, the radioactive mRNA profile can be observed for normoxia and hypoxia U87MG cell extract. *HIF1A* mRNA or *CTNNB1* mRNA were loaded more efficiently in the normoxic 48S from U87MG cells According to the radioactivity and the A_{260nm} profile, the 48S IC was situated in fractions 25-28. On the other side, mRNA assembled on hypoxic 48S were fractioned on positions 27-30.

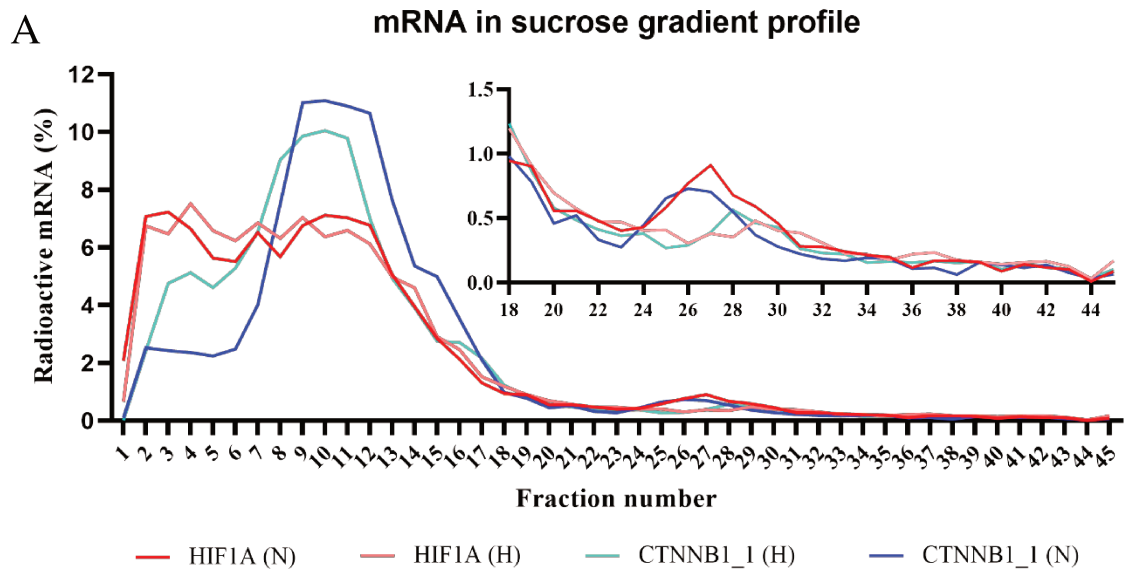

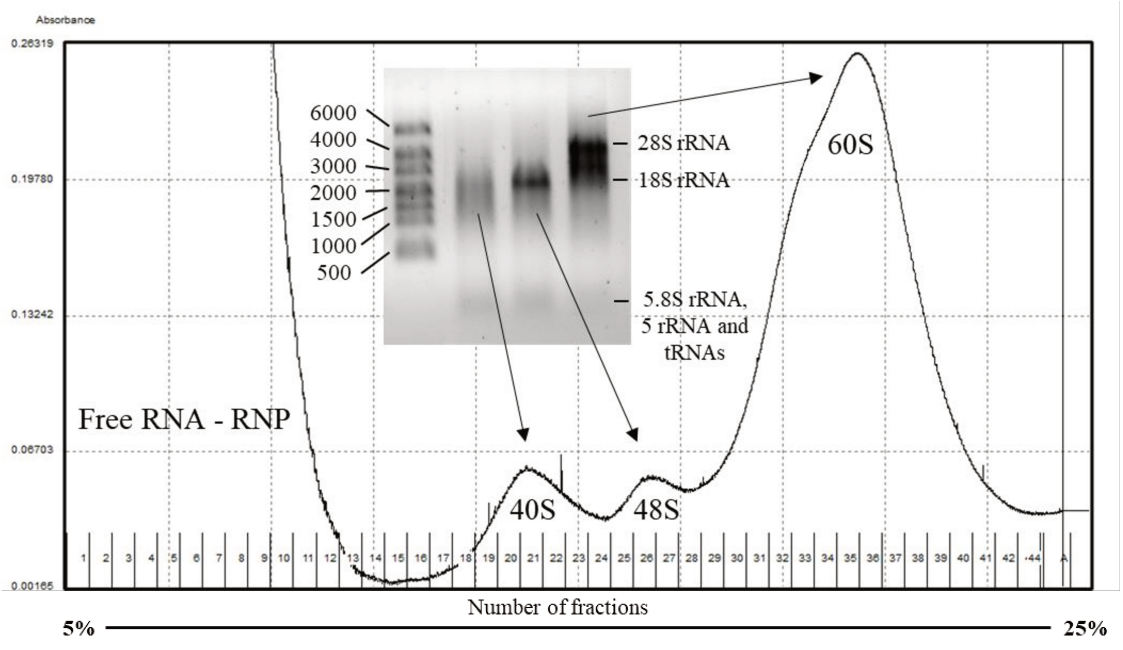

Figure 19. Isolation of HIF1A LS48S IC from U87MG cell extract. (A) mRNA quantification in the 5-25% sucrose gradient. Radiolabelled m7G-capped *HIF1A* mRNA was measured in each collected fraction and the percentage was calculated dividing the radioactivity value of the fraction to the total radioactivity of the gradient. The fractions 18 to 45 are zoomed to better see the mRNA peak overlapping the 48S position. N (normoxia) and H (hypoxia). (B) Absorbance profile at 260 nm of a sucrose gradient with HIF1A mRNA assembled on 48S IC from U87MG cell extract. 1% w/v agarose gel is shown with the isolated pooled particles: 40S, 48S, and 60S pool contained fractions 20-23, 25-28, and 34-37, respectively. Human 28S rRNA, 18S rRNA, 5.8S rRNA and 5S rRNA have 5070, 1869, 157 and 121 nts. RNP (ribonucleoparticles).

In Figure 19B, the A_{260nm} profile to detect RNA on the sucrose gradient fractions is shown. Four peaks can be distinguished: the large peak corresponding to "Free RNA – RNP" and the 40S, 48S and 60S peaks, collected in this order from top to the bottom of the sucrose gradient. Fractions of interest were pooled, centrifuged, and loaded on an agarose gel, where rRNA can be observed. It can be seen in the gel that the 48S fraction is not contaminated by the 60S subunit (visualised by the 28S rRNA) because there is only a band corresponding to the 18S rRNA.

This proof-of-concept experiment will lead to the analysis of *HIF1A* LS48S IC from human cell lines other than HeLa. The study of initiation complexes coming from different cancer cell lines opens a new field in the search of alternative translation initiation mechanisms that allows the reprogramming of the translation machinery in hypoxic cancer cells.

DISCUSSION AND PERSPECTIVES

The present work illustrates the first 5'UTR structure models of *CTNNB1* and *HIF1A* mRNAs and their implication on the translation in human cancer cells. From a methodological point of view, this project combines molecular biology and structural techniques to answer diverse biological questions related to the translation of these mRNAs. Furthermore, it is a pioneer study for the translational analysis of a single species of mRNA under hypoxic conditions and it supposes probably the first human translation initiation complex structure issued from cells cultured in this stress.

5'UTR of β-catenin mRNA

This study reveals the first complete analysis of the structure model of the 5'UTR of β-catenin mRNA and its role in translation. We obtained the secondary structure model of β-catenin 5'UTR, showing a highly-structured GC-rich element folded into a three-way junction (TWJ) at the 5' side and a more unstructured region when approaching the start codon. This TWJ folding is unique – see Supplementary Figure 7 for the tertiary structure prediction –, although other example of a similar TWJ have been reported in the 5'UTR of HIV-1 viral RNA (Song et al., 2021). Still, obtaining the native structure of β-catenin 5'UTR – or the whole mRNA – in cells remains one of the challenging aspects of this project. In the foreseeable future, the implementation of new approaches permitting the probing of endogenous mRNAs in living cells will complement the structural information already obtained *in vitro* (Tomezsko et al., 2020).

We have not observed a consistent conservation in length and sequence of the *CTNNB1* 5'UTR in vertebrates – particularly the TWJ that was acquired late in evolution–, compared to its highly-conserved coding sequence. Evolution of species complexity in eukaryotes is clearly accompanied by an increase of UTR length, augmentation of the GC content in 5′ UTRs, and insertion and expansion of repetitive sequences in these regions (Liu et al., 2012). Nonetheless, the lack of strong conservation in 5'UTRs might give a higher plasticity for mRNAs to adapt their translation depending on the physiological needs among species.

We described the importance of the TWJ for β-catenin translation efficiency in cells, and the synergy of this element with the beginning of the coding sequence. However, we did not find any long-distance interaction between the TWJ into the β-catenin 5'UTR and the beginning of its ORF. Severe hypoxia is supposed to reduce global translation to a minimum, although some mRNAs still associate with polysomes and maintain or enhance its translation (Thomas & Johannes, 2007). Surprisingly, we discovered that β-catenin 5'UTR did increase the reporter translation under this stress. We strongly suggest that in hypoxic cells β-catenin mRNA translation is enhanced through the TWJ present within its 5'UTR. Also, we emphasized in using the transfection of monocistronic mRNAs as a robust approach, instead of classical DNA transfection experiments with a bicistronic reporter gene vector that is prone to artifacts (Jackson, 2013; Shatsky et al., 2018).

Mass spectrometry analysis of the hypoxic LS48S IC bound to β-catenin mRNA exhibited an increase of the abundance of PKR as well as the absence of eIF4E – validating

the fact that the complex components come from cells cultured in hypoxic conditions. Focusing on the cap-binding complex, protein composition of the hypoxic *CTNNB1* LS48S IC suggests that mRNA recruitment to the 43S PIC probably switches from cap-recognition by eIF4E to mRNA-direct recognition driven by the TWJ through eIF4A, eIF4G2 and eIF4B. To validate the hypothesis that eIF4A and eIF4B are responsible of the 43S PIC recruitment on the TWJ of β-catenin 5'UTR, we have proven the direct interaction of eIF4B with the GC-rich element. In addition, the eIF4A and eIF4B let footprints in the tract of purines on the TWJ. The distribution of these purines along helixes 2 and 3 probably ensures the correct unwinding of the TWJ during the scanning step of translation initiation. We have also demonstrated that the abundance of the three isoforms of eIF4G relies on the TWJ because the removal of this element in the *CTNNB1* 5'UTR strongly reduce the level of this initiation factor. To complement the evidence uncovered by the mass spectrometry analysis, the role of eIF4G in the TWJ interaction must be clarified.

The presence of PKR exclusively in hypoxic *CTNNB1* LS48S IC make us hypothesised a relative level of phosphorylated eIF2α. PKR is absent in hypoxic ΔGC *CTNNB1* LS48S IC, whereas eIF2 increase its abundance. These data illustrate the balance between the abundance of eIF2 subunits (and so the TC) and eIF2α kinases within translation initiation complexes. Although PERK is the well-known eIF2α kinase induced under hypoxia (Koumenis & Wouters, 2006), here we suggest that PKR could drive eIF2α phosphorylation in translation initiation of β-catenin mRNA under hypoxia. Noteworthy, the reduction of eIF2 activity does not seem to affect mRNA translation. For this reason, we suspect that eIF5B together with eIF2A (not eIF2α), which are more abundant in hypoxic *CTNNB1* LS48S IC, could act as initiator tRNA carriers. This hypothesis is supported by previous studies that have shown the capacity of these factors to binds the tRNAi in stress conditions (Kim et al., 2018). Mass spectrometry analysis of the 43S PIC also highlights that eIF2A is already present and abundant before the mRNA binding – see Supplementary Figure 2. Concerning the translation of the ΔGC *CTNNB1* mRNA in hypoxia, we noticed a higher abundance of eIF3 subunits – especially eIF3d – compared with the full-length mRNA. In line with this result, we suggest a mechanism more dependent on eIF3d than the cap-binding complex, according to a recent study demonstrating the eIF3d capability to bind the cap structure and to lead eIF4E-indepedendent translation (Lee et al., 2016). Thus, translation of mRNAs lacking highly-structured elements in their 5'UTR could be driven by eIF3d in hypoxia.

We also depicted the eIF4A-dependency of β-catenin mRNA through its 5'UTR. For the first time we gave evidence of the β-catenin translation inhibition using silvestrol and RocA. Importantly, this inhibition was also noticed in all tested cancer cell lines under hypoxia. We obtained an illustrative explanation of the mechanism of action of rocaglates probably clamping eIF4A in the single stranded purines of the TWJ of β-catenin 5'UTR. In this manner, inhibition upon silvestrol treatment allowed us to confirm that the β-catenin translation strongly depends on eIF4A. We also suggest that the only rocaglate currently used in clinical trials, eFT226 (Zotafilin), probably has strong effect on MYC reduction because, at some extent, it inhibits β-catenin translation and consequently MYC expression is reduced (Thompson et al., 2021). Thus, rocaglates are the best candidates to reduce the translation of β-catenin in cancer cells and good choice for hypoxic cells prone to therapeutic resistance.

Furthermore, β-catenin mRNA could become a reference model to screen eIF4A inhibitors. The limitation of this discovery is that these inhibitors rely on a protein-RNA interaction and they are not totally specific for β-catenin mRNA. Therefore, the crystallization of the TWJ could be attempted in the future in order to obtain its tertiary structure at high-resolution. This structure will be essential to explore RNA-binding small molecules that binds specifically to this element. Previous studies have shown the potential of targeting TWJ with small molecules (Warner et al., 2018).

Finally, we started the structural analysis of both hypoxic *CTNNB1* and ΔGC LS48S ICs by cryo-EM. The main aim to complete this project will be to obtain 3D classes of the hypoxic complexes and perform the molecular modelling to obtain their atomic structures. This work will allow us to describe the particularities of the translation initiation mechanism of β-catenin mRNA under low oxygen stress conditions. Importantly, it will be the first human 48S IC structure assembled in stress conditions.

5'UTR of HIF-1α mRNA

We obtained the first human HIF-1α 5'UTR secondary structure model revealing that this 5'UTR comprises a highly compact, tree-shaped four-way junction followed by a single-stranded region near the start codon. In addition, a very strong arrest at positions G_{86} and G_{87} during reverse transcription as well as predictions and further experiments, permit us to hypothesize the presence of a possible G-quadruplex in the 5'UTR of *HIF1A* mRNA.

We focused on the effect of the possible G-quadruplex on translation by using a mutant with only two substitutions in the RT arrest positions. We performed *in vitro* translation assays using the m7GpppG inhibitor and we observed that the translation of the *HIF1A* transcript is not affected, suggesting that eIF4E is not required for efficient translation of the reporter gene containing this 5'UTR. In addition, the mutant transcript at positions G_{86} and G_{87} recovers dependence on eIF4E. These results support the hypothesis that G-quadruplex is the regulatory element for the initiation of translation of *HIF1A* mRNA in a cap-independent manner. In translation experiments on cell extracts grown in hypoxia, the translation of HIF1A in hypoxia was twice as high as its expression in cells grown under standard oxygen conditions. The G-quadruplex located in the 5′UTR is responsible of switching the translation initiation mechanism during hypoxia. The existence of an eIF4E-independent initiation mechanism represents a translational advantage for *HIF1A* mRNA due to the reported unavailability of this initiation factor during hypoxic stress. We propose that apart from the post-translational regulation of HIF-1α in hypoxia, another regulation step occurs in the translation initiation of its mRNA.

The ultimate objective of the characterization of *HIF1A* 5'UTR will be to validate the putative rG4 *in vivo* as well as obtaining the atomic model of the normoxic and hypoxic 48S ICs bound to *HIF1A* mRNA and their protein composition by Grad-cryo-EM. The obtention of a tridimensional structure of the G-quadruplex will allow to perform a high-throughput screening to discover small molecules targeting and inhibiting the translation of *HIF1A* mRNA. These inhibitors would contribute to establish a new anticancer strategy for

combination therapy in all tumours were HIF-1α expression is deregulated as well as a new hope to find the cure of von Hippel-Lindau disease.

Final conclusion

In conclusion, this study highlights the relevance of studying 5'UTR structures from a structural and functional point of view, in order to unravel possible regulatory mechanisms relying on the structure elements of the mRNA in interaction with translation-related proteins. This work writes a new page in the analysis of mRNA translation under hypoxia and support the existence of a hidden diversity of translation initiation mechanisms that will surely re-shape the principles of translation in the future. From a technical perspective, it opens the possibility to explore in detail the structure of translation initiation complexes in different cellular contexts and assemble with native components. It also set a precedent to stimulate the investigation of drugs targeting initiation factors and mRNA.

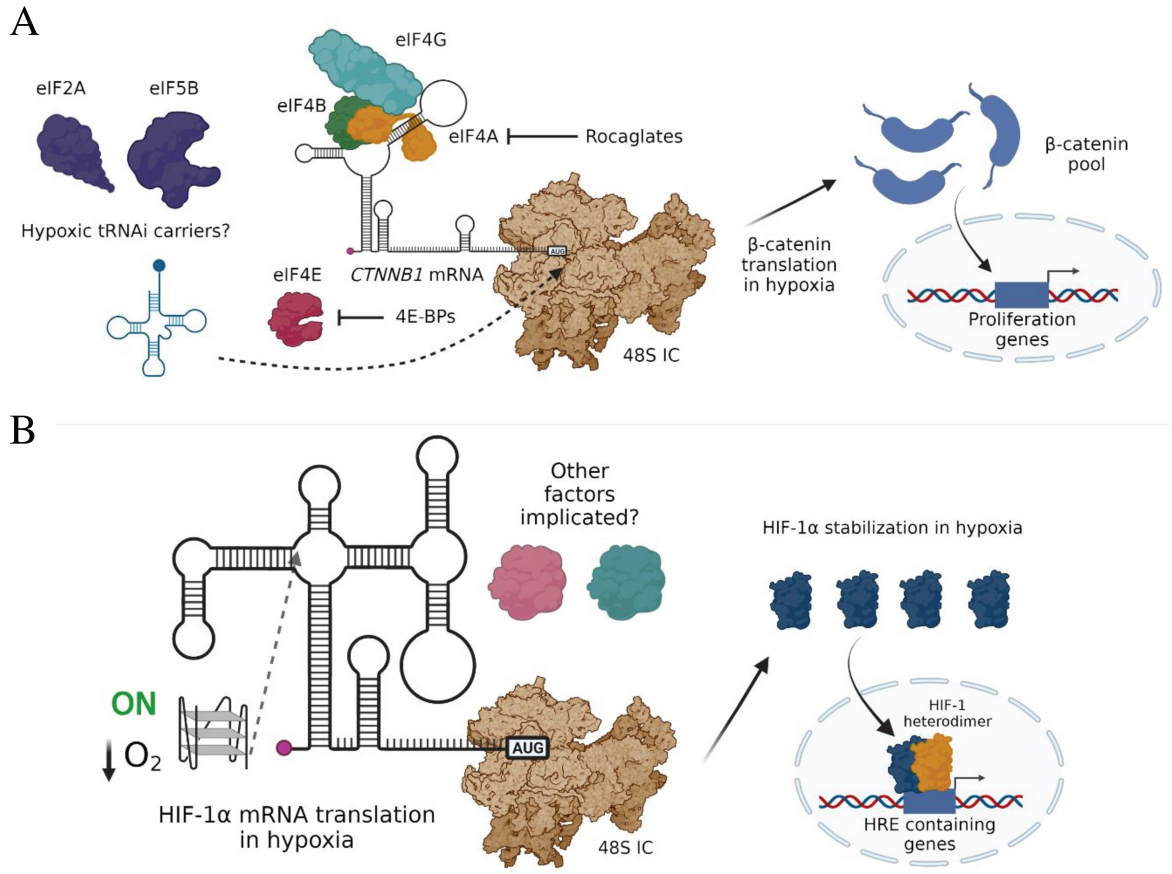

Figure 20. Mechanisms of translation initiation under hypoxia for β-catenin and HIF-1α mRNAs. (A) Translation initiation of β-catenin would occur through the direct recruitment of the 43S PIC by eIF4A, eIF4B and eIF4G interacting with the TWJ. This translation would produce a pool of β-catenin that translocated into the nucleus, activates its target genes. (B) HIF-1α translation would be enhanced via the rG4 located in its 5'UTR, and together with the stabilization of the protein that occurs during hypoxia, promotes the translation of HRE target genes. Figure design has been made with BioRender.com

MATERIALS AND METHODS

Bacterial strains and culture conditions

DH5α competent *Escherichia coli* (Thermo Fisher Scientific) is a suitable strain for plasmid transformation upon heat shock and it was used for this purpose. These bacteria were cultured in Luria-Bertani (LB) medium supplemented with 100 µg/mL ampicillin to select bacteria containing the plasmid.

BL21(DE3) pLysS *Escherichia coli* (Promega) was used for protein expression. They were cultured in LB medium and supplemented with 100 µg/mL ampicillin and 34 µg/mL chloramphenicol for selection of bacteria containing the protein expression plasmids.

Cancer cell lines and culture conditions: standard, hypoxia and glucose starvation

HeLa cell line (ATCC®) is derived from a cervix adenocarcinoma. They were cultured in DMEM, high glucose, GlutaMAX (Gibco) supplemented with 10% v/v of Fetal Bovine Serum (PAN-Biotech) and 1% v/v of 10,000 U/mL Penicillin-Streptomycin (Gibco). They were placed in a CO_2 incubator with saturating humidity at 37°C (considered as the standard conditions).

SW480 cell line (ATCC®) derives from colorectal cancer cells of a male patient. They were cultured with RPMI 1640, GlutaMAX (Gibco) supplemented with 10% v/v of Fetal Bovine Serum (PAN-Biotech) and 1% v/v of 10,000 U/mL Penicillin-Streptomycin (Gibco), in standard conditions.

U87MG cell line (ATCC®) cells were obtained and immortalised from a glioblastoma (Allen et al., 2016). They were cultured in the same conditions of HeLa cells.

These cells were used for *in cellulo* translation assays and /or to prepare translationally active cell extracts. Cells were subjected to severe hypoxia (< 0,1% O_2) in the Whitley DG250 Anaerobic Workstation (dwscientific) with previously deoxygenated medium. Oxygen level was measured with an oxygen sensor inside the chamber. Hypoxic atmosphere consisted in a mixture of gases comprising: 90% N_2, 5% H_2 and 5 % CO_2. Glucose starvation was performed with DMEM - glutamine - no glucose (Gibco) and it was supplement with FBS and antibiotics. We estimated α-D-glucose level at ~0,5 mM considering the blood glucose naturally contained in the FBS at 5 mM.

Plasmids, 5'UTR and gBlocks® sequences, and DNA oligonucleotides

pGL3 contained a 5'UTR sequence of interest, inserted upstream the firefly luciferase coding sequence (cloning service done by ProteoGenix). It encodes an ampicillin resistance cassette. It was utilised for PCR amplification to obtain a DNA template that was used later for *in vitro* transcription. All sequences cloned in pGL3 are indicated in Table 1 and were based on the NCBI Reference Sequences: NM_001904.4 (*CTNNB1* mRNA isoform 1), NM_000518.5 (*HBB* mRNA) and NM_001530.4 (*HIF1A* mRNA).

HBB 5'UTR sequence (Table 1) was inserted in pRL-CMV vector, upstream the Renilla luciferase coding sequence. It possesses an ampicillin resistance cassette. It was utilised for PCR amplification to obtain the DNA template that was further used for *in vitro* transcription.

The human eIF4AI coding sequence was optimized for bacterial expression and inserted in pET15b – containing a His6-tag and a thrombin cleavage site. The optimized coding sequence of human eIF4B was inserted in pnEAvH – which contains a His6-tag and a TEV cleavage site and. These plasmids were transformed in BL21(DE3) pLysS *E. coli* for further protein expression. Both plasmids confer resistance to ampicillin. Sequences of gene blocks (Integrated DNA Technologies) used for plasmid cloning are included in Table 3. Coding sequences were obtained from NCBI Reference Sequences: NM_001416.4 (*EIF4AI* mRNA variant 1) and NM_001300821.3 (*EIF4B* mRNA variant 1).

Plasmid	Insert sequence
pGL3-*CTNNB1* 5'UTR	5'AAGCCTCTCGGTCTGTGGCAGCAGCGTTGGCCCGGCCCCGGGAGCGGAGAGCGAGGGG AGGCGGAGACGGAGGAAGGTCTGAGGAGCAGCTTCAGTCCCCGCCGAGCCGCCACCGCAG GTCGAGGACGGTCGGACTCCCGCGGCGGGAGGAGCCTGTTCCCCTGAGGGTATTTGAAGT ATACCATACAACTGTTTTGAAAATCCAGCGTGGACA 3'
pGL3-*CTNNB1* 5'UTR + ORF	5'AAGCCTCTCGGTCTGTGGCAGCAGCGTTGGCCCGGCCCCGGGAGCGGAGAGCGAGGGG AGGCGGAGACGGAGGAAGGTCTGAGGAGCAGCTTCAGTCCCCGCCGAGCCGCCACCGCAG GTCGAGGACGGTCGGACTCCCGCGGCGGGAGGAGCCTGTTCCCCTGAGGGTATTTGAAGT ATACCATACAACTGTTTTGAAAATCCAGCGTGGACAATGGCTACTCAAGCTGATTTGATG GAGTTGGACATGGCCATGGAACCAGACAGAAAAGCGGCTGTTAGTCACTGGCAGCAACAG TCTTACCTGGACTCTGGA 3'
pGL3- *HBB* 5'UTR or pRL-*HBB* 5'UTR	5'ACATTTGCTTCTGACACAACTGTGTTCACTAGCAACCTCAAACAGACACC 3'
pGL3-*HIF1A* 5'UTR + ORF	5'CACCCTCTTCGTCGCTTCGGCCAGTGTGTCGGGCTGGGCCCTGACAAGCCACCTGAGG AGAGGCTCGGAGCCGGGCCCGGACCCCGGCGATTGCCGCCCGCTTCTCTCTAGTCTCACG AGGGGTTTCCCGCCTCGCACCCCCACCTCTGGACTTGCCTTTCCTTCTCTTCTCCGCGTG TGGAGGGAGCCAGCGCTTAGGCCGGAGCGAGCCTGGGGGCCGCCCGCCGTGAAGACATCG CGGGGACCGATTCACCATGGAGGGCGCCGGCGGCGCGAACGACAAGAAAAAGATAAGTTC TGAACGTCGAAAAGAAAAGTCTCGAGATGCAGCCAGATCTCGGCGAAGTAAAGAATCTGA AGTTTTT 3'
pGL3-*HIF1A_mut* 5'UTR + ORF	5'CACCCTCTTCGTCGCTTCGGCCAGTGTGTCGGGCTGGGCCCTGACAAGCCACCTGAGG AGAGGCTCGGAGCCGGGCCCGGACCCCAACGATTGCCGCCCGCTTCTCTCTAGTCTCACG AGGGGTTTCCCGCCTCGCACCCCCACCTCTGGACTTGCCTTTCCTTCTCTTCTCCGCGTG TGGAGGGAGCCAGCGCTTAGGCCGGAGCGAGCCTGGGGGCCGCCCGCCGTGAAGACATCG CGGGGACCGATTCACCATGGAGGGCGCCGGCGGCGCGAACGACAAGAAAAAGATAAGTTC TGAACGTCGAAAAGAAAAGTCTCGAGATGCAGCCAGATCTCGGCGAAGTAAAGAATCTGA AGTTTTT 3'

Table 1. Inserted sequences in luciferase-containing plasmids pGL3 and pRL. Start codon is underlined. Mutation within the 5'UTR of *HIF1A* is denoted in red.

DNA oligonucleotide	Sequence
T7-*CTNNB1* 5'UTR	5' **TAATACGACTCACTATA**GGAAGCCTCTCGGTCTGTGGCAG 3'
T7-ΔGC *CTNNB1* 5'UTR	5' **TAATACGACTCACTATA**GGCCTGTTCCCCTGAGGGT 3'
T7-*HBB* 5'UTR	5' ATATGCTAGG**TAATACGACTCACTATA**GACATTTGC 3'
T7-*HIF1A* 5'UTR	5' GCGTGCTAGCATAT**TAATACGACTCACTATA**GG 3'
RV-Fluc ORF (pGL3)	5' AGCGGCCGGCCGCCCCGACTCTAG 3'
RV-Rluc ORF (pRL)	5' GTCTGCTCGAAGCGGCCGCTCTAG 3'

RV-*CTNNB1* 102nts ORF	5' TCCAGAGTCCAGGTAAGACTGTTGC 3'
RV-*HBB* mRNA	5' TGCAATGAAAATAAATGTTTTTTATTAGG 3'
RV-*HIF1A* 111nts ORF	5' ATATAAGCTTGGTGAATCGGTCCCCGCGATGTC 3'

Table 2. Primers used to create DNA templates by PCR for in vitro transcription. Forward primers contain the T7 promoter sequence indicated in bold. RV is an abbreviation for reverse primers.

Human eIF4B gBlocks Gene Fragment
5'CAGCCTTCATATGTCGGCTAGCCAAGATTCACGCTCTCGTGACAATGGACCGGATGGCATGGAACCAGAGGGTGTGATTGAG TCTAATTGGAACGAAATTGTCGATTCCTTTGACGACATGAACCTGAGCGAGAGTCTTCTTCGCGGAATTTATGCCTATGGTTTT GAGAAGCCATCTGCTATCCAGCAGCGCGCCATCTTGCCGTGCATTAAGGGATATGACGTGATTGCACAGGCACAGAGTGGAACC GGTAAAACTGCCACTTTTGCTATTTCGATCCTTCAACAAATCGAGTTAGACCTGAAGGCGACTCAAGCACTGGTTTTAGCGCCG ACGCGCGAGCTGGCCCAGCAAATTCAAAAAGTGGTCATGGCTTTAGGAGATTATATGGGCGCAAGCTGCCACGCTTGCATTGGA GGTACGAACGTTCGCGCTGAGGTGCAGAAGTTACAGATGGAGGCACCGCATATTATCGTCGGTACCCCCGGTCGTGTATTTGAT ATGTTGAACCGTCGTTATCTTTCACCTAAGTATATTAAAATGTTTGTCTTGGACGAAGCTGACGAGATGTTGTCACGTGGCTTT AAGGACCAGATTTATGATATTTTCCAGAAATTGAATTCCAACACACAGGTGGTTTTATTATCTGCGACTATGCCAAGTGACGTT TTGGAGGTTACCAAAAAGTTCATGCGCGACCCCATTCGTATCTTAGTTAAAAAAGAGGAACTTACATTGGAAGGTATCCGCCAG TTTTATATCAATGTTGAGCGTGAGGAGTGGAAGCTGGATACGTTGTGCGATCTGTATGAGACATTAACGATTACACAAGCCGTA ATTTTTATCAACACGCGCCGCAAAGTAGATTGGCTTACAGAGAAAATGCACGCACGCGACTTTACCGTCTCGGCCATGCACGGG GACATGGATCAAAAGGAACGCGATGTAATTATGCGTGAATTCCGCTCGGGTAGTAGCCGCGTATTAATCACCACTGACTTGCTG GCTCGCGGCATCGACGTTCAGCAAGTGAGCTTAGTAATTAATTATGACTTGCCGACGAATCGTGAAAATTACATTCATCGCATC GGGCGTGGTGGGCGCTTTGGACGCAAGGGGGTAGCTATCAATATGGTTACCGAAGAGGACAAACGTACGTTACGCGATATTGAG ACGTTTTACAATACCAGTATCGAAGAGATGCCTCTGAACGTCGCTGACTTAATCTAAGGATCCGCG 3'
Human eIF4B gBlocks Gene Fragment
5'CAGCCTTCATATGGCGGCATCAGCGAAAAAAAAGAACAAGAAAGGCAAGACTATCTCCTTAACAGACTTTTTGGCCGAGGAT GGTGGCACTGGTGGTGGCTCGACCTACGTATCTAAGCCTGTGTCATGGGCTGACGAAACAGACGACTTGGAGGGCGACGTGAGC ACAACATGGCATAGTAACGATGACGACGTCTATCGCGCGCCGCCTATCGACCGCTCCATTTTACCGACGGCTCCGCGTGCAGCT CGCGAACCGAATATCGATCGCAGTCGCTTACCGAAGAGCCCTCCTTATACTGCCTTCTTAGGTAATCTTCCGTACGACGTAACA GAGGAGTCAATCAAGGAATTTTTCCGCGGTCTGAACATTTCTGCAGTTCGTTTACCTCGCGAACCGTCGAATCCGGAACGTTTA AAAGGGTTTGGCTATGCGGAATTTGAAGATCTTGACTCATTACTTAGCGCGTTGAGCTTGAACGAGGAATCATTAGGTAATCGT CGTATCCGTGTTGACGTGGCCGATCAGGCGCAAGATAAGGATCGCGATGACCGCAGCTTCGGTCGCGACCGCAACCGTGATAGT GACAAGACTGATACCGATTGGCGCGCACGCCCGGCCACAGATAGTTTTGACGACTACCCACCTCGTCGTGGCGATGATTCGTTT GGCGATAAATACCGTGACCGTTACGATAGTGATCGCTACCGTGACGGCTATCGTGACGGCTACCGCGACGGCCCGCGTCGCGAC ATGGACCGTTATGGTGGCCGCGATCGCTATGACGACCGCGGTTCTCGCGACTACGACCGCGGGTACGACAGTCGCATTGGGTCT GGGCGCCGTGCTTTCGGGAGCGGTTACCGTCGTGACGACGACTATCGTGGCGGCGGTGACCGTTATGAAGACCGCTACGATCGC CGCGATGACCGCTCGTGGTCGTCCCGTGACGATTATTCTCGCGATGACTACCGTCGTGATGACCGTGGTCCGCCTCAACGCCCA AAGCTTAATCTTAAGCCTCGTAGTACCCCAAAGGAAGACGATAGCTCAGCTAGCACCTCACAATCGACACGCGCGGCTTCAATT TTCGGGGGTGCCAAACCAGTAGACACCGCCGCACGTGAGCGTGAGGTAGAAGAGCGCTTGCAAAAAGAACAGGAGAAGCTTCAA CGTCAGCTTGACGAGCCTAAGTTAGAACGCCGTCCGCGCGAACGCCATCCATCATGGCGTTCAGAAGAAACGCAAGAGCGTGAG CGTTCGCGTACAGGGTCGGAGTCCAGTCAAACCGGCACCAGTACTACATCCTCACGCTCGAAGTCCGACCAGGACGCTCGCCGT CGTGAATCAGAGAAATCCCTTGAGAATGAGACCCTTAACAAGGAGGAAGATTGTCACTCCCCTACGAGTAAACCTCCAAAACCA GACCAGCCTCTTAAGGTGATGCCTGCGCCACCACCGAAGGAGAACGCGTGGGTCAAGCGCAGCTCTAACCCTCCGGCACGCTCA CAATCGTCGGACACAGAACAGCAGAGTCCTACCTCGGGTGGTGGGAAGGTGGCACCGGCCCAGCCTTCCGAGGAGGGCCCTGGG CGCAAAGACGAAAATAAAGTCGACGGTATGAACGCCCCAAAGGGTCAAACGGGTAATTCTTCTCGCGGGCCTGGTGACGGCGGT AACCGCGATCACTGGAAAGAAAGCGACCGTAAGGATGGTAAAAAAGATCAGGACTCTCGTTCTGCGCCTGAGCCAAAGAAACCA GAGGAAAATCCTGCCTCGAAATTTAGTTCTGCATCAAAATACGCCGCACTGTCAGTGGACGGTGAAGATGAGAACGAGGGTGAA GACTATGCGGAATAAGGATCCGCG 3'

Table 3. *EIF4AI* and *EIF4B* optimized coding sequence inserts. Sequences were adapted to codon usage in BL21(DE3) pLysS *E. coli*. Star codons and stop codons are highlighted in yellow and cyan blue, respectively. In both gBlocks, the coding sequences are flanked by restriction sites for NdeI in 5' and BamHI in 3'. The restriction sites are underlined.

Plasmid cloning and site-directed mutagenesis

To clone *EIF4AI* and *EIF4B* gBlocks Gene Fragments (see Table 3) into their respective plasmids, we performed NdeI/BamHI double digestion of the plasmid and the

insert separately, for one hour at 37°C. DNA ligation was performed overnight at 16°C using T4 DNA ligase (ThermoFisher) in its buffer with the insert and plasmid in proportion 2:1. Plasmids were transformed in DH5α *E. coli* cells and positive clones were grown and the purified plasmids sequenced. The resulting plasmids were named pET15b - eIF4AI and pnEAvH - eIF4B.

For site-directed mutagenesis of the pGL3-*HIF1A*_5'UTR+ORF, the two Gs in position 86 and 87 at the 5'UTR sequence were substituted with two As, using the QuikChange Site-Directed Mutagenesis Kit following manufacturer's instructions. The resulting plasmid was named pGL3-*HIF1A_mut* 5'UTR + ORF.

Bacterial transformation and plasmid purification

100 ng of plasmid was added to 50 µL of BL21(DE3) pLysS or DH5α competent *E. coli* that was incubated in ice for 30 minutes. After a heat shock for 1 minute at 42°C, the bacteria remained on ice for 5 minutes before adding 300 µL of LB and letting them grow without antibiotic for 1 hour at 37°C. with 300 rpm for one hour. 150 µL of transformed bacteria were seeded in LB-agar plates supplemented with antibiotics and the plate was incubated overnight at 37°C.

Additionally, for plasmid purification on DH5α strains, we set a 4 mL LB-ampicillin culture overnight. Plasmid was extracted using the Plasmid Isolation kit (Macherey-Nagel) following manufacturer's instructions. Finally, clones were checked by DNA sequencing.

Polymerase Chain reaction (PCR)

DNA templates for *in vitro* transcription were obtained by PCR. The plasmids utilized in these reactions are cited above and the DNA oligonucleotides described in Table 2. The PCR was carried out using 1 ng/µL of plasmid with a mixture containing 1x High-Fidelity buffer, 0,2 mM of the four deoxyribonucleoside triphosphates (dNTPs, N= A, C, G and T), 10 pmoles of forward and reverse oligonucleotides, 2 U of Phusion™ High-Fidelity DNA Polymerase (Thermo Scientific) in a final volume of 100 µL. The PCR program was run in a T100 Thermal cycler (Bio-Rad) and consisted in:

- An initial denaturation of 3 min at 95°C
- 35 cycles of amplification comprising:
    - The denaturation at 95°C for 30 seconds.
    - The annealing step was performed at a temperature depending on the oligonucleotides (the temperature was normally 5°C lower than the oligo with the smallest melting temperature) for 30 seconds.
    - The primer extension at 72°C for a time depending on the PCR product length (approximately 1 min per 1000 bps).
- A final extension at 72°C for 5 min.

PCR products were controlled in a 1% w/v agarose gel and visualized after incubation with a water solution with 200 ng/mL ethidium bromide. The amplified DNA is finally precipitated by adding a tenth volume of 3M LiOAc (pH 5) and three volumes of absolute ethanol at -80°C. Then, the sample was centrifuged 15 min at > 12000 g for 15 min, washed with 75 % v/v ethanol, centrifuged again at the same speed for 5 min and dried in a vacuum centrifuge for 5 min. RNA pellet is resuspended in ultrapure water ("Milli-Q H2O") and stored at -20°C.

In vitro transcription, RNA purification and 5' capping

All transcripts were synthetised with recombinant T7 RNA polymerase from DNA templates obtained by PCR. The DNA templates comprise the T7 promoter and the transcript sequence. *In vitro* transcription of different constructs was performed with a mixture containing 1x T7 buffer (40 mM Tris/HCl pH 8, 50 mM NaCl and 15 mM $MgCl_2$), 4 mM of the four ribonucleoside triphosphates (NTPs, N= A, C, G and U), 20 µg/mL Bovine Serum Albumin (BSA), 1 mM dithiothreitol (DTT), 1 mM spermidine, 40 U RNasin® Ribonuclease Inhibitor (Promega), 10-30 µg DNA template and 250 µg/mL T7 RNA polymerase. The reaction was made in 400 µL of final volume and it was incubated 3 hours at 37°C and 300 rpm.

DNase treatment was done by adding 5 U of RQ1 RNase-free DNase (Promega) for 30 minutes at 37°C and 300 rpm. Reaction was stopped by adding 1 volume of ROTI®Aqua-Phenol/Chloroform/Isoamyl alcohol, for RNA extraction (ROTH) and mixture was subsequently vortexed. Sample was centrifuged >12000 g for 5 min at 4°C. Aqueous phase was recovered and precipitated by adding a tenth volume of 3 M LiOAc (pH 5) and three volumes of absolute ethanol at -80°C. Then, the sample was centrifuged 15 min at > 12000 g for 15 min, washed with 75 % v/v ethanol, centrifuged again at the same speed for 5 min, dried in a vacuum centrifuge for 5 min and resuspended in ultrapure water. Importantly, centrifugations were done at 4°C.

Short transcripts (≤ 800 nts) were purified in a denaturing urea PAGE (6-10% acrylamide, 8 M urea) after RNA incubation for 3 min at 95°C in urea blue buffer (8M urea, 0,025% w/v bromophenol blue and 0,025% w/v xylene cyanol). RNA was visualised after gel migration by UV shadowing, irradiating the gel with a UV lamp at 254 nm and over a silica-coated thin-layer chromatography plate (Sigma-Aldrich). The gel band containing the RNA was cut and RNA was eluted overnight at 4°C with elution buffer (0,5 M ammonium acetate and 1 mM EDTA). Finally, RNA was ethanol precipitated as indicated previously in this section and resuspended in ultrapure water.

Long transcripts (> 1000 nts) were further purified using Micro Bio-Spin™ P-6 Gel Columns in Tris Buffer (Bio-Rad) following manufacturer's instructions, to remove the excess of NTPs.

RNA concentration was determined at 260 nm wavelength with Nanodrop ND-1000 Spectophotometer. Purified transcripts were capped using the ScriptCap™ m7G Capping

System (CELLSCRIPT) following manufacturer's manual. Radioactively labelled transcripts were obtained by substituting GTP from the capping kit with 20 µCi [α-^{32}P] GTP (PerkinElmer). A-capped mRNAs were prepared adding the G(5')ppp(5')A RNA Cap Structure Analog (NEB) co-transcriptionally following manufacturer's instructions.

In vitro SHAPE and RNA probing with DMS/CMCT

To obtain the secondary structure of *CTNNB1* and *HIF1A* 5'UTRs, RNAs were refolded and then modified using four different probes, separately (Figure 1A): i) two different SHAPE reagents that specifically modify the 2'OH of nucleosides depending on their flexibility: benzoyl cyanide (BzCN) and NAI (2-methylnicotinic acid imidazolide) and ii) two different probes that create an adduct in the nitrogenous base of nucleosides in the absence of base pairing dimethyl sulfate (DMS) has a selectivity for A and C, and CMCT for U and G. The modifications were detected by primer extension with fluorescently-labelled oligonucleotides and the resulting cDNA profile was migrated in capillary electrophoresis. Finally, data analysis was carried out and reactivity profile was combined with RNAstructure (Reuter & Matthews, 2010) prediction software to obtain a secondary structure model.

- **RNA refolding**

RNA was refolded in a ThermoMixer® C (Eppendorf) with lid. 200 nM RNA, in presence of a buffer including 50 mM sodium cacodylate pH 7 and 100 mM KOAc, were refolded following a program with controlled decrease of temperature. The program was set as follows: 2 min at 95°C, ~10 min to get to 65°C, 5 min at 65°C where we add $Mg(OAc)_2$ to a final concentration of 1 mM, 20 min to get to 37°C, 10 min at 37°C. RNA was then ready for probe modifications (Figure 1B). Refolding was made in a final volume of 10 µL. Conformation of RNA was controlled by native PAGE.

- **Preparation of probes. SHAPE, DMS and CMCT reactions**

NAI was produced as 1:1 mixture with imidazole in DMSO as described (Spitale et al., 2013). Briefly, 137 mg (1 mmol) of 2-methylnicotinic acid was dissolved in 0,5 mL anhydrous DMSO. Then, a solution of 162 mg (1 mmol) 1,1´-carbonyl diimidazole in 0,5 ml anhydrous DMSO, was added drop wise under the chemical hood. The resulting solution was stirred at room temperature until gas evolution was complete and powder was totally dissolved. The stock solution (1 M) is stable for not more than two months stored at −80°C and must be protected from light.

DMS, CMCT and BzCN solutions for RNA modification were freshly prepared the same day of the experiment. BzCN was melted and diluted in anhydrous DMSO. On the other side, DMS was diluted in absolute ethanol and CMCT powder was dissolved in ultrapure water. After refolding, RNA was supplemented with 1 pmol of yeast tRNA (Thermo Fisher Scientific) to sponge the excess of modifications created by probes. Probe reaction was

performed at 37°C. Final concentration and incubation times for each probe are indicated in Figure 1C. Reactions were stopped by adding an excess of water and RNA was precipitated as described above. Control RNAs were not modified with probes (unmodified RNA) and were incubated in either 5% DMSO, 5% ethanol or in water.

- **Primer extension**

The reverse transcription or primer extension reaction produces reverse transcriptase arrests in positions where nucleosides have been modified by probes, to identify nucleosides in single-stranded regions and exposed to the solvent. Reverse transcriptase arrests are considered proportional to the reactivity of each nucleotide.

2 pmols of unmodified or modified RNA were annealed to 2 pmol of 5' fluorescently-labelled primer (Thermo Fisher Scientific) at 95°C for 2 min and then on ice for 2 min. We utilized oligonucleotide with VIC fluorophore to analyse the probe modifications and in parallel, primer with NED fluorophore to obtain a reference sequence that was later aligned to the reactivity values to determine the position of each nucleotide.

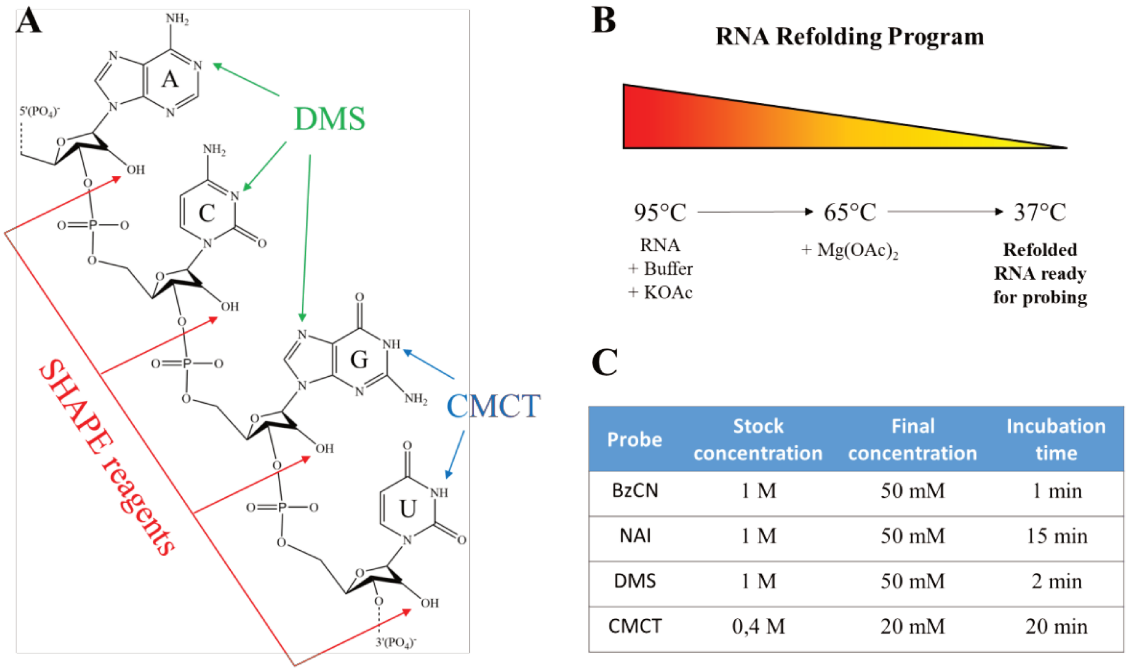

Probe	Stock concentration	Final concentration	Incubation time
BzCN	1 M	50 mM	1 min
NAI	1 M	50 mM	15 min
DMS	1 M	50 mM	2 min
CMCT	0,4 M	20 mM	20 min

Figure 20. RNA probes and refolding program. (A) Modification position of SHAPE reagents, DMS and CMCT in ribonucleosides. (B) RNA folding program is schematized. (C) Stock and final concentration, as well as incubation times are denoted for each probe used in this study.

Primer sequence and annealing position are indicated in Table 4. Samples were then incubated in RT buffer (25 mM Tris-HCl pH 8.3, 50 mM KCl, 5 mM MgCl2, 2 mM DTT), 0.5 mM dNTPs and 2 U of AMV reverse transcriptase (Life Sciences Advanced Technologies) at 42°C for 30 min and 50°C for 15 min. Sequencing reactions are performed in separated tubes and in similar conditions but supplementing with 10 µM ddGTP and 125

µM dGTP instead. Resulting cDNA products were precipitated and dry pellets were resuspended in Hi-Di formamide (Applied Biosystems). VIC and NED resulting cDNA were pooled in the same tube. Finally, samples were loaded on a PCR-96-AB-C microplate (Axygen) for capillary electrophoresis and data collection on a 3130xl Genetic Analyzer (Applied Biosystems). Data rely on fluorescence detection of cDNA fragment of different sizes by the sequencer.

Name	Sequence	Fluorophore	Annealing position
Fluo-CTNNB1	5' CTGGTTCCATGGCCATGTCC 3'	VIC or NED	+30 after AUG codon
Fluo-HIF1A	5' CTTTTCGACGTTCAGAAC 3'	VIC or NED	+41 after AUG codon

Table 4. Fluorescently-labelled oligonucleotides for primer extension step. Fluorophores VIC and NED had the same sequence when targeting the same RNA. Position of primer annealing at its 3' is indicated.

- **Reactivity data analysis**

Chemical probing electropherograms were analyzed using QuSHAPE software (Karabiber et al., 2013). The reactivity values were obtained subtracting the cDNA fluorescence profile from untreated RNA to the one corresponding to modified RNA in order to obtain the net reactivities (RT arrests) for all nucleotides. Reactivity values were assigned to each nucleotide by overlapping the parallel ddGTP sequencing and at the same time using the known RNA sequence. Reactivities for each dataset were internally normalized during QuSHAPE protocol to a scale between 0 to a positive number (2-3), where 0 indicates unreactive nucleotides. Three independent experiments were performed for each probe.

The secondary structure model was obtained using RNAstructure software version 6.0.1 (Reuter et al., 2010) by constraining the RNA prediction with the reactivity values as pseudo-free energy changes that strongly correlate with local nucleotide flexibility (Low et al., 2010). Among different possible predictions, we chose the structure at the lowest minimum free energy to be our model. RNA was represented with all reactivity values using the RNA visualization tool VARNA v3-93 (Darty et al., 2009).

In-cell SHAPE

Confluent HeLa cells were scratched and centrifuged at 300 g for 5 min and the cell pellet was resuspended with a DPBS containing either 5% v/v DMSO or 50 mM NAI for 10 min. Then, total RNA was extracted as explained below, and a specific primer extension was done using Fluo-CTNNB1 oligo (Table 4) without fluorophore. RNA was hydrolysed in alkaline conditions to keep only cDNA. A ssDNA linker was added in 3' by T4 RNA ligase incubating overnight at 16°C. Finally, a PCR was done with a ^{32}P-labelled oligo and the DNA profile was resolved by denaturing urea PAGE.

Cell extract preparation

Cytoplasmic cell lysate from HeLa or U87MG were prepared in ten 150-mm cell culture dishes with 5 million cells per plate. Cells were harvested with a cell scraper when they reached a confluence higher than 75%. For hypoxic cell extracts, cells were placed in the anoxic chamber when they get to the latter confluence due to the slow growth of cells in severe hypoxia (see Results).

Cell lysis was done by nitrogen cavitation with 4639 Cell Disruption Vessel (Parr Instrument Company) injecting nitrogen at final pressure of 500 psi for 20 minutes, stirring with a small magnet at 500 rpm in a cold room (4°C). Lysis buffer contained 20 mM HEPES/NaOH pH 7.4, 100 mM KOAc, 1 mM DTT, 0.5 mM $Mg(OAc)_2$, 100 U of Recombinant RNasin (Promega) and Halt Protease inhibitor cocktail (ThermoFisher). Lysate was centrifuged at 1000 g for 5 minutes and the supernatant was recovered avoiding the foam (membranes and organelles) and the pellet (nuclei). Finally, cell extract was aliquoted, fast-freeze in liquid N_2 and stored at -80°C for further use.

Concentration of cytoplasmic cell extract was approximately ~25 mg/mL of total protein ($A_{280nm} = 25$ and $A_{260nm} = 40$). It is important that all prepared extracts are normalized based on their protein concentration, to minimize unspecific variations in translation activity.

Depletion of endogenous mRNAs by micrococcal nuclease treatment

Staphylococcus aureus micrococcal nuclease (MNase) digestion experiments were performed in different conditions to optimize previous existing protocols. Nuclease treatment was performed on 25 mg/mL of HeLa cell extract by adding 0,5-2 mM $CaCl_2$ and 5-10 U of MNase enzyme (New England Biolabs). Incubation was performed in Thermomixer C (Eppendorf) at 25-30°C for 10 minutes or more. Enzyme was inactivated by adding 3-6 mM ultra-pure grade EGTA (Euromedex) pH 7,5. After nuclease treatment, translation efficiency of HeLa CFTS was measured by *in vitro* translation assay using *CTNNB1_1* construct (see Article 1).

Cell growth upon rocaglate treatment

Relative number of cells were measured using CellTiter-Glo® Luminescent Cell Viability Assay (Promega) following manufacturer's instructions. The reagent was thawed directly at room temperature the same day of the experiment and it was stored at 4°C for further utilization. Cells were incubated in standard oxygen conditions or under severe hypoxia for 24 or 48 hours. Additionally, cells were treated with 25-50 nM of RocA, silvestrol or its vehicle (0,01% v/v DMSO). Cell titre of reference was measured right before incubating cells in the hypoxic workstation and before treating them with rocaglates or DMSO.

In vitro translation assay

HeLa cell-free extract prepared in the lab and RRL, nuclease-treated (Promega) were utilised for *in vitro* translation assays. Reaction mixture contained 12,5 mg/mL of cell extract (A_{280nm} = 10 or A_{260nm} = 20, proportional to the ribosome amount), 0,5 µg of firefly luciferase transcript, 40 µM complete amino acid mixture (Promega), 20 U of RNasin® Ribonuclease Inhibitor (Promega), 30 mM HEPES/NaOH pH 7.4, 100 mM KOAc, 1.5 mM $Mg(OAc)_2$, 1 mM ATP, 0.2 mM GTP. Incubation was carried out at 30°C for 3 hours. Luciferase luminescence was measured with Luciferase Reagent Assay (Promega) in the GloMax® 96 Microplate Luminometer (Promega).

m7G(5')ppp(5')G RNA Cap Structure Analog (New England Biolabs) was dissolved in ultrapure water and stored -20°C. Increasing amount of m7GpppG cap structure was added to the in vitro translation mixture and incubated at RT for 5 minutes before adding the mRNA.

Silvestrol and Rocaglamide A (Clinisciences) powder were dissolved in anhydrous DMSO at a final concentration of 5 mM and stored at -80°C. 25-50 nM silvestrol or RocA, or 0,005% v/v DMSO (vehicle) were added to the *in vitro* translation mixture together with the rest of components.

In cellulo translation assay (mRNA transfection into cells)

~80000 cells were seeded per well in a 24-well plate, one day prior to transfection experiment. Cells at 70-80% confluency were transfected using Opti-MEM medium, 0,5 µg of firefly luciferase transcript of interest, 0,25 µg of Renilla luciferase mRNA for co-transfection control and Lipofectamine™ MessengerMAX™ Transfection Reagent (Invitrogen). Luciferase activity was measured using the Dual-Glo Luciferase Assay System in the GloMax® 96 Microplate Luminometer (Promega).

For silvestrol treatment, cells were treated with 25 nM silvestrol or 0,005% v/v DMSO (vehicle), 30 minutes prior to transfection until lysing the cells for luminescence measurements.

Total RNA extraction, reverse transcriptase and quantitative PCR

RNA was extracted from 2 × 10^6 cells in 6-well tissue culture plates using RNeasy Mini Kit (QIAGEN) following manufacturer's instructions. 1 µg of total RNA was reverse-transcribed using High-Capacity RNA-to-cDNA™ Kit (Applied Biosystems) following manufacturer's mode of use. The resulting cDNA fragments were quantified by real time qPCR on a CFX96 Touch Real-Time System (Bio-Rad) using GoTaq® Probe qPCR Master Mix (Promega) and PrimePCR™ Probe Assay (Bio-Rad). Probe IDs for human *CTNNB1*, *EEF1A1*, *HIF1A* and *RPL13* genes are qHsaCEP0053779, qHsaCEP0052990, qHsaCEP0050075 and qHsaCEP0052324. No PCR product was detected in the no-template control (NTC) and minus RT samples for each condition shown in this publication. *CTNNB1* expression was normalized to the other reference genes.

Western Blotting

Total protein concentration of HeLa cell lysates was determined by a Bradford colorimetric assay using QuantiPro TM BCA Assay Kit following manufacturer's manual. Briefly, in a 384-well plate, each protein sample was diluted to a final volume of 80 µL. In parallel, we performed a BCA concentration range from 0 to 30 µg/mL of BSA in 80 µL of final volume. 20 µL of reagent mixture were added and incubated for 1 hour at 37°C. The absorbance was measured at 540 nm and protein concentration was obtained with the help of the BCA standard curve.

Around 50 µg of total protein from the cellular lysate were migrated on a 4-20% Mini Protean Stain-free Gel (BioRad) in 1x TGS (25 mM Tris, 200 mM Glycine, 1% w/v SDS) for 1 hour at 120 V. Proteins into the gel were transferred onto a nitrocellulose membrane using a Trans-blot Turbo Transfer Pack (BioRad) at 25 V for 10 minutes in a Trans-Blot Turbo device (BioRad). Membranes were cut with the help of the molecular weight protein ladder to separate it in two pieces; one containing β-catenin and the other GAPDH. These membranes were incubated separately in blocking solution comprising TBST and milk (50 mM Tris-HCl pH 7.5, 150 mM NaCl, 0,1% w/v Tween® 20 detergent, 5% w/v skimmed milk) for one hour at room temperature.

Primary monoclonal antibodies were added and incubated overnight at 4°C. Total β-catenin antibody (β-Catenin (D10A8) XP® Rabbit mAb, Cell Signalling Technology) and GAPDH antibody (GAPDH (D16H11) XP® Rabbit mAb, Cell Signalling Technology) were utilised at 1:1000 dilution. After the primary antibody incubation, the membrane was washed three times with TBST. The secondary antibody (Anti-rabbit IgG, HRP-linked Antibody, Cell Signalling Technology) in 1:5000 dilution was incubated in TBST and milk for one hour at room temperature. Later the membrane was washed three times with TBST. To reveal the signal of the secondary antibody – that contains an enzyme converting a substrate in a chemoluminescent product –, we used Amersham ECL Prime Western Blotting Detection Reagent (GE Healthcare) following manufacturer's guidelines. Chemoluminescent signal was revealed using ChemiDoc™ Touch Imaging System (BioRad). The detected bands were quantified using integrated density measurement with the ImageJ software (Schneider et al., 2012).

Mass spectrometry and spectrum analysis

10 µL of protein extracts – containing the 48S IC – at 2.5 OD_{260nm} were diluted and precipitated overnight with glacial 0.1 M ammonium acetate in 100 % methanol (5 volumes, -20°C). After centrifugation at 12.000 g and 4°C during 15 min, the resulting pellets were washed twice with 0.1 M ammonium acetate in 80% methanol and further dried under vacuum (Speed-Vac concentrator). Pellets were resuspended in 100 µL of 50 mM ammonium bicarbonate and submitted to reduction (5 mM DTT, 95°C, 10 min) and alkylation (10 mM iodoacetamide, room temperature, 20 min). Proteins were finally digested overnight with 150 ng of sequencing-grade trypsin (Promega). The proteomic datasets were obtained by the injection of 1/4 of each peptidic mixture on an orbitrap mass spectrometer (Q-Exactive Plus,

Thermo-Fisher Scientific, USA) coupled to an EASY-nanoLC-1000 (Thermo-Fisher Scientific, USA).

The obtained raw data was converted to .mgf files with the Proteome Discoverer Daemon software (Thermo-Fisher Scientific, script "Export-to-mgf", version 2.2). MS data were further searched against the *Homo sapiens* Swissprot sub-database with a decoy strategy (Swissprot release 2021_04 from November 2021, 20376 forward protein sequences). Peptides and proteins were identified with Mascot algorithm (version 2.6.1, Matrix Science, London, UK). The following parameters were used: (i) Trypsin/P was selected as enzyme, (ii) three missed cleavages were allowed, (iii) methionine oxidation, acetylation of protein N-term, carbamidomethylation of cysteine and phosphorylation of serine / threonine / tyrosine were set as variable modifications, (iv) mass tolerance for precursor ions was set at 10 ppm, and at 0.02 Da for fragment ions. Mascot data were further imported into Proline v2.0 software (http://proline.profiproteomics.fr/) (Bouyssié *et al.*, 2020). Proteins were validated on Mascot pretty rank equal to 1, and 1% FDR (False Discovery Rate) on both peptide spectrum matches (PSM score) and protein sets (Protein Set score). The total number of MS/MS fragmentation spectra was used to quantify each protein from at least three independent biological replicates: this "BasicSC" value calculated by Proline includes all PSMs of all peptides, including the modified peptides and the peptides shared by different protein sets. After a normalization of the data matrix with the total number of spectra in one sample, the "BasicSC" spectral count values were submitted to a negative-binomial test using an edgeR GLM regression through R (R v3.2.5) through the IPinquiry4 R package (https://github.com/hzuber67/IPinquiry4). The statistical test was based on the published msmsTests R package available in Bioconductor to process label-free LC-MS/MS data by spectral counts (Gregori *et al.*, 2019). For each identified protein, an adjusted p-value (adjp) corrected by Benjamini–Hochberg was calculated, as well as a protein fold-change (FC).

Sucrose gradient analysis and complex purification

LS48S IC from RRL, HeLa or U87MG cell extracts were assembled using 100 pmols of m7G-capped mRNA, 100 mM KOAc and 5 mM GPM-PNP at 30°C. Later, sample was loaded on top of 5-25% sucrose gradients containing 25 mM HEPES/NaOH pH 7.4, 80 mM KOAc, 0.5 $Mg(OAc)_2$ and 2 mM DTT – sucrose density gradients were produced with Gradient Master 107 (BioComp). Gradients were centrifuged for 4 hours in a SW41Ti rotor (Beckman Coulter) at 37000 rpm (4°C). A control sample contained radioactive m7G-capped mRNA to localized it into the gradient fractions by measuring radioactivity the Multipurpose Scintillator Counter (Beckmann Coulter). Gradient fractions were collected using Piston Gradient Fractionator (BioComp). Fractions containing the LS48S IC were further centrifuged in a S140-AT rotor (ThermoFisher) for 1h30 at 108000 rpm (4°C) and pellet was resuspended in a buffer containing 10 mM HEPES-KOH pH 7.4, 50 mM KOAc, 10 mM NH_4Cl, 5 mM $Mg(OAc)_2$ and 2 mM DTT.

The quality of the LS48S IC was checked in a 1% w/v agarose gel, to visualise the presence of the 18S rRNA by fluorescence detection of SYBR™ Green II RNA Gel Stain (Thermo Fisher Scientific).

Sample preparation for cryo-EM and data acquisition

Hypoxic *CTNNB1* LS48S IC and ΔGC LS48S IC were isolated from HeLa cell extract and utilized for cryo-EM analysis. 2,5 µl of 180-200 nM IC was applied onto glow-discharged copper grids R 2/2 (Quantifoil Micro Tools GmbH), previously covered with a thin layer of carbon (~20Å) – made in-house. Cryo-EM grids were prepared using a FEI Vitrobot Mark IV at 6°C and 100% humidity, blot force 5 and waiting time of 2 seconds. The grids were plunged into liquid ethane at 93 K in a precision cryostat system. Grids were screened in a Glacios microscope (Thermofisher) to analyse sample quality (particle distribution, vitreous ice thickness, presence of aggregation, contrast, etc). Data acquisitions were made for the grids presenting the best characteristics and the data set was collected on Titan Krios microscope (ThermoFisher) equipped with K3 direct electron detector (Gatan, Inc).

In the case of the hypoxic *CTNNB1* LS48S IC, 10256 micrographs were obtained from a single grid at a magnification of 81,000x and at pixel size of 0.862 Å. 20 frames were collected per second in counting mode with target defocus ranging from -0,4 µm to -1.0 µm, and fluxes of 23,5 e/Å^2 /s. C2 aperture was set at 100 µm and beam size at 980 nm.

For the hypoxic ΔGC LS48S IC, 10465 micrographs were obtained from two grids at a magnification of 81,000x and at pixel size of 0.862 Å. 20 frames were collected per second in counting mode with target defocus ranging from -0,5 µm to -2.5 µm, and fluxes of 24,75 e/Å^2 /s. C2 aperture was set at 50 µm and beam size at 980 nm.

Cryo-EM data processing

Data processing was performed in a GPU workstation (LinuxVixion) with 4 GPUs RTX 3090. We mainly performed three strategies for data processing with different open-source computer programs for the refinement of our macromolecular complex by single-particle analysis of cryo-EM data:

- cryoSPARC (Punjani et al., 2017) version v.3.1.
- The software framework Scipion v 3.0.8 (de la Rosa-Trevin et al., 2016) that contains RELION, cistem, Xmipp, EMAN, etc.
- Warp + RELION. Pre-processing of movies was performed with Warp (Tegunov & Cramer, 2019) and the rest of the steps with REgularized LIkelihood OptimizatioN (RELION version 4.0 Beta; Scheres et al., 2012).

Briefly, in the three strategies, the imported movies (containing 40 frames) were motion corrected. In the resulting micrographs, CTF was estimated and ~200 micrographs were discarded due to very evident optical aberrations or the presence of abundant ice crystals noticed in the power spectra – see Supplementary Figure 3 for a micrograph example in cryoSPARC. Manual and automated picking was performed with Warp, cryoSPARC or Xmipp within Scipion. Particles were extracted with a box size of 512 volume pixels (voxels). Importantly, we tried different box sizes and we realised that 360 or 440 voxels of box size was too tight to select the 48S IC.

2D classification was done in cryoSPARC (see Supplementary Figure 4) and in Scipion using cryoSPARC binaries. However, this step was skipped in Scipion to lauch directly a 3D classification with RELION binaries. Either the 6ZMW PDB structure of human scanning 48S IC (Brito Querido et al., 2020) or the 5VYC PDB structure of the human 40S (Lomakin et al., 2017) were used as references for the initial cryoSPARC auto-refine or RELION 3D classification. The rest of the steps are still ongoing.

ANNEXES

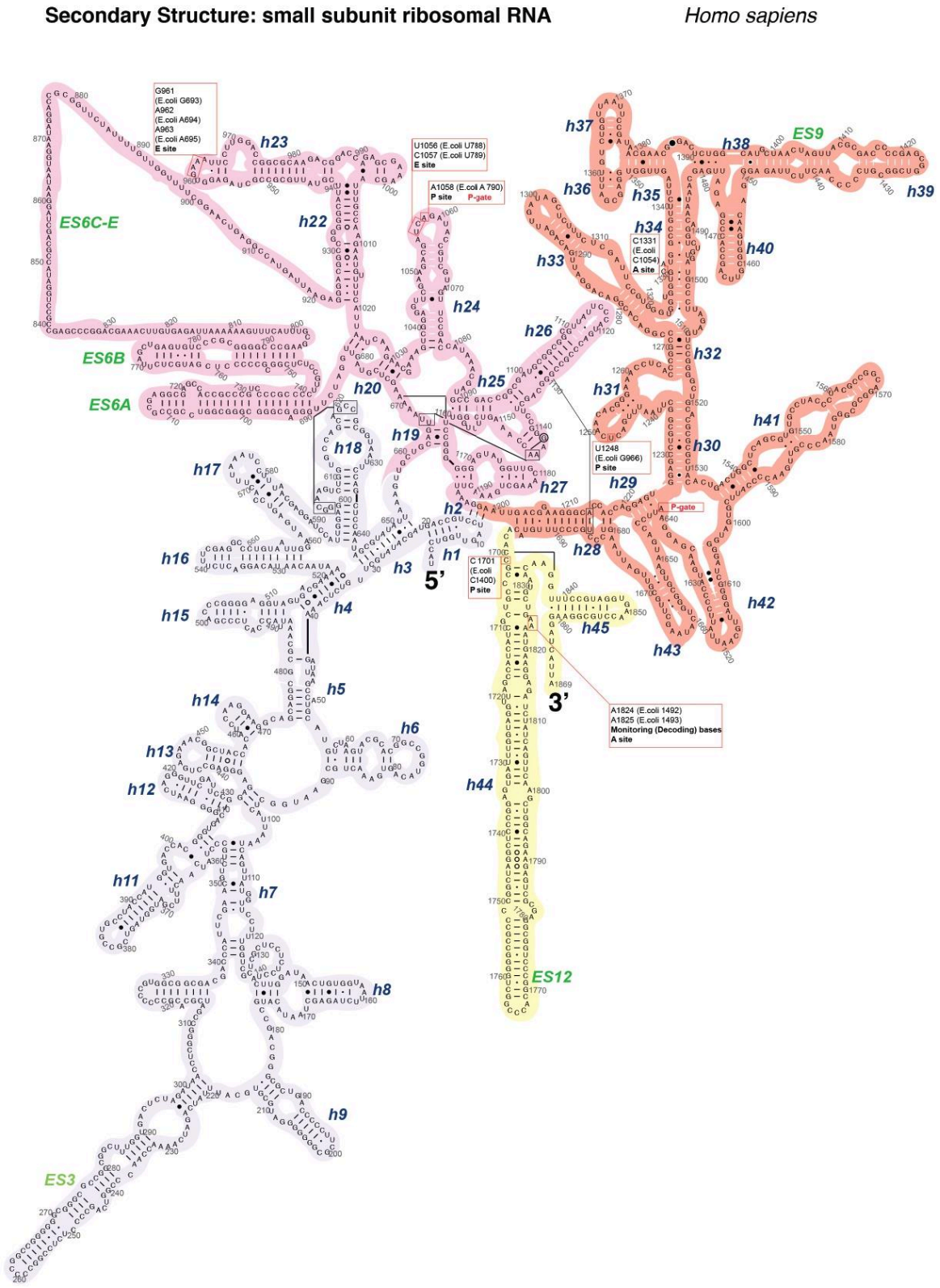

Supplementary Figure 1. Secondary structure of the human 18S rRNA. Helixes (h1-45) and expansion segments (ES1-12) are indicated in the sequence. Universally conserved positions in ribosome functional centres are denoted in text boxes. Downloaded from http://jufali.userpage.fu-berlin.de/rRNA-maps. No citation available. Zones of 18S rRNA forming the E, P and A site are highlighted in pink, salmon red and yellow, respectively.

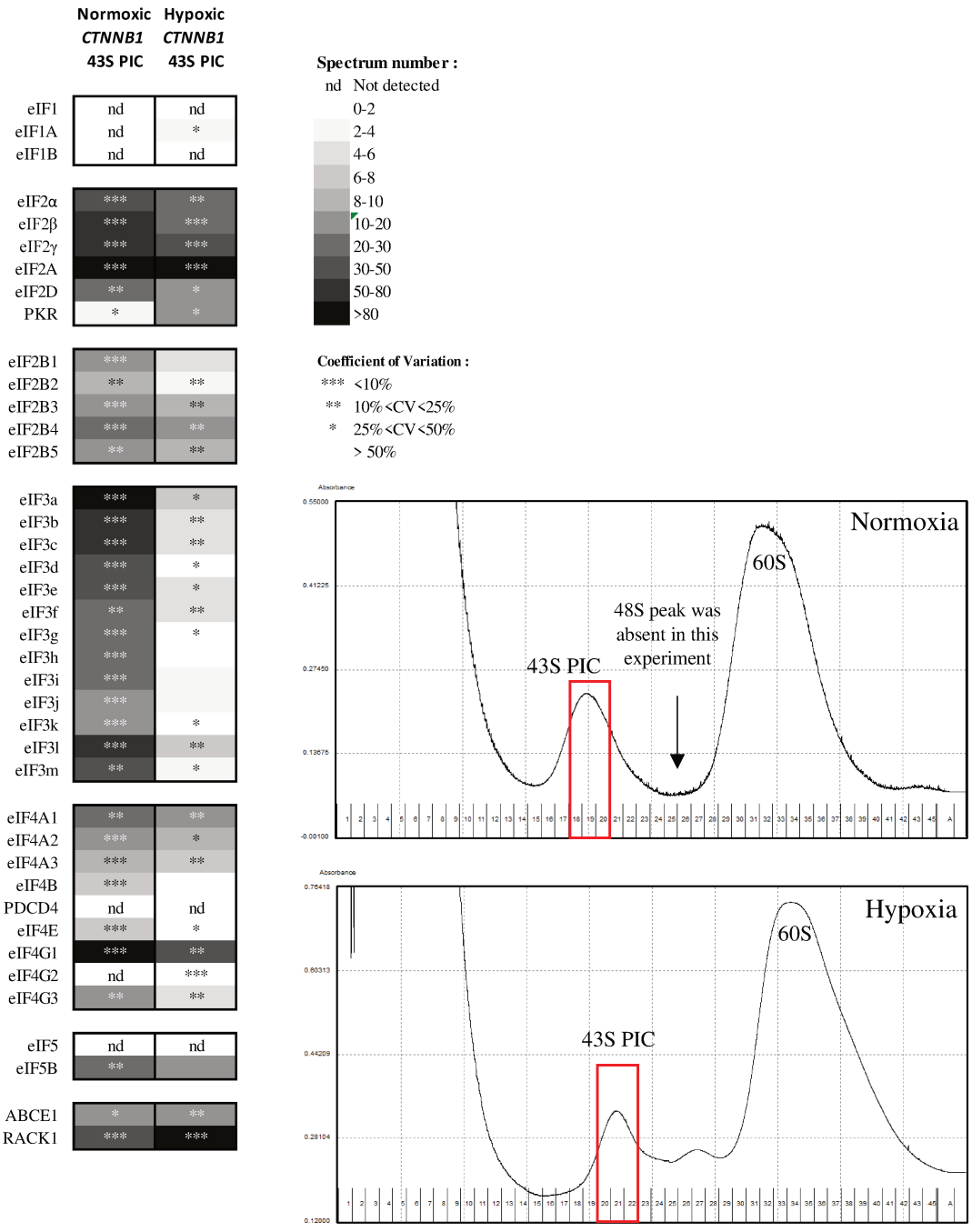

Supplementary Figure 2. Initiation factor composition of the 43S PIC fraction in normoxia and hypoxia. Semiquantitative mass spectrometry analysis of the initiation factors in normoxic and hypoxic 43S PICs, indicating the abundance of each eIF on the basis of the absolut spectrum counts. These counts are presented as heatmaps, with a greyscale between white and black, where white indicates low abundance and black denotes high abundance. All eIFs are included on the list as wells as proteins related to the translation initiation process: ABCE1, PDCD4, PKR and RACK1. Stars indicate the values of the coefficients of variation calculated for each protein. Additionally, sucrose gradient profiles are shown and the fractions analysed by mass spectrometry are denoted in red

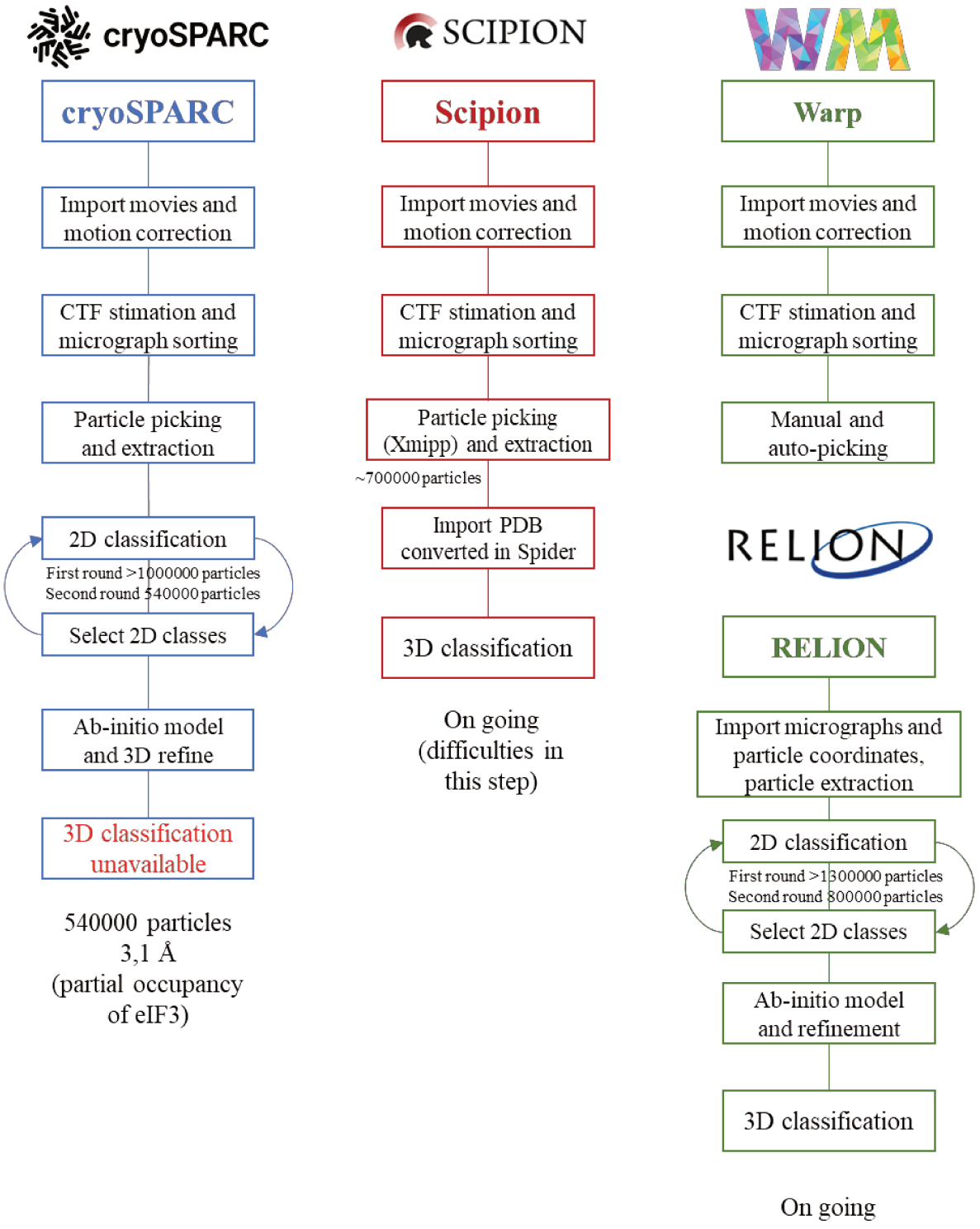

Supplementary Figure 3. Flowchart of single particle cryo-EM data processing for *CTNNB1* LS48S IC. This representation schematized the three different strategies performed for cryo-EM dataset analysis: cryoSPARC, Scipion and Warp-RELION.

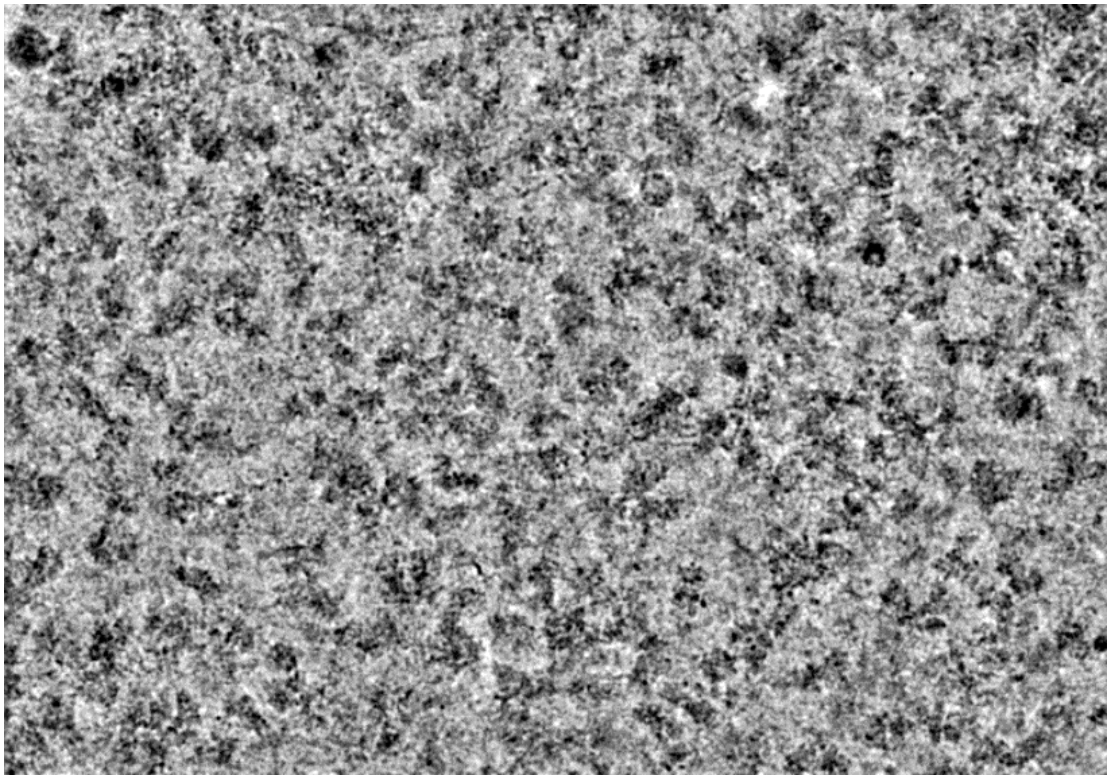

Supplementary Figure 4. Titan Krios TEM micrograph of hypoxic *CTNNB1* LS48S IC. In this image, ribosomal particles can be observed as well as some contaminant particles – probably microtubules found in the mass spectrometry analysis as well. Image was obtained during particle selection in cryoSPARC.

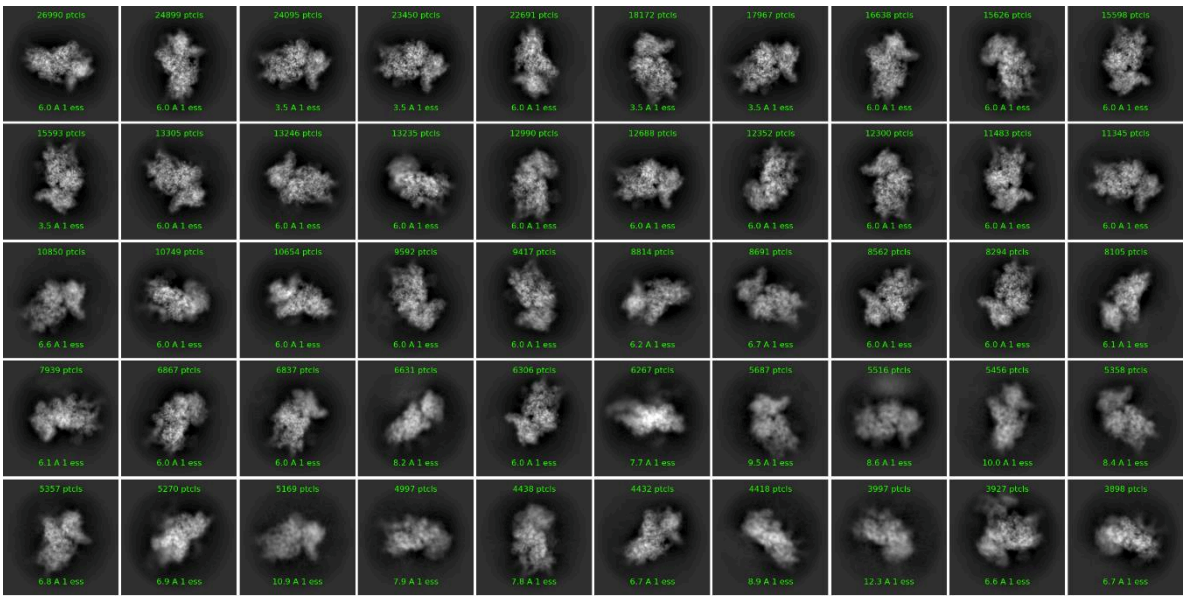

Supplementary Figure 5. 2D classification of hypoxic *CTNNB1* LS48IC in cryoSPARC. 50 classes with approximately 540000 particles. Number of particles and average resolution (Å) per class is indicated.

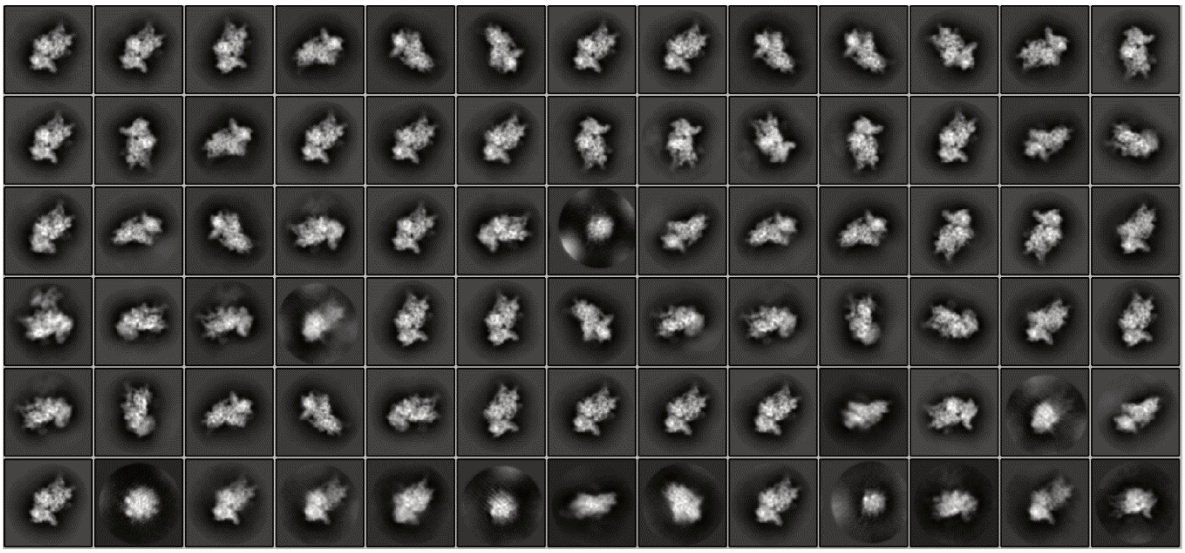

Supplementary Figure 6. 2D classification of hypoxic *CTNNB1* LS48IC in RELION. 70 classes with approximately 800000 particles. Pixel size in this image is 3.448 Å per pixel and 128 px of box size – down sampling 4 times.

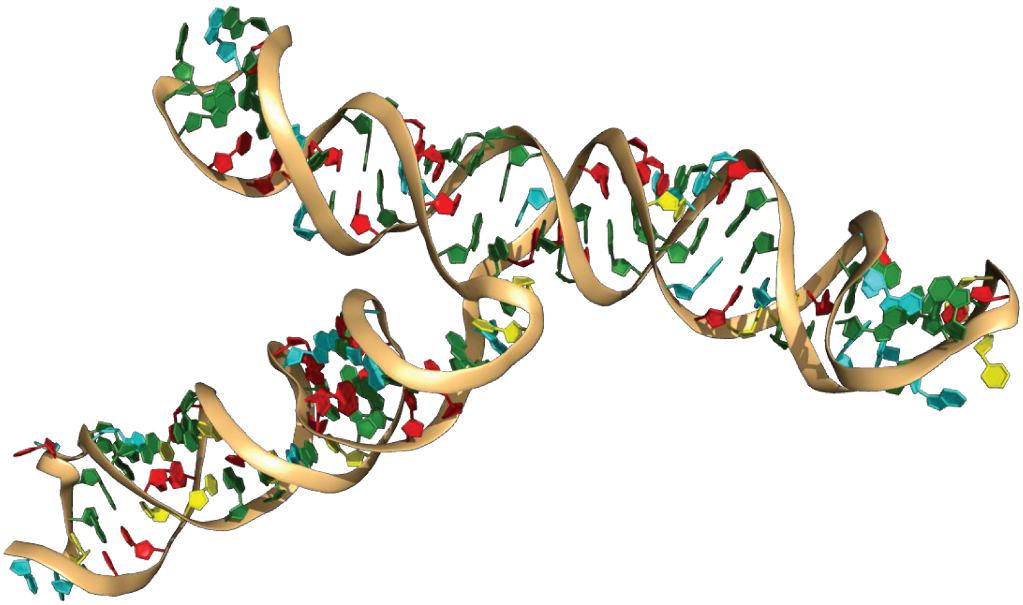

Supplementary Figure 7. TWJ tertiary structure model prediction. The 3D representation of the TWJ of *CTNNB1* 5'UTR was obtained using the secondary structure in dot-backet format as input in RNAComposer software (Popenda et al., 2012). Output PDB file was edited in PymolRNA ribonucleosides A, C, G and U are represented in cyan, red, green and yellow, respectively.

Book chapter

RNA Spectroscopy: Methods and Protocols, Methods in Molecular Biology

Grad-cryo-EM: Tool to Isolate Translation Initiation Complexes from Rabbit Reticulocyte Lysate Suitable for Structural Studies

Javier Rol-Moreno, Lauriane Kuhn, Stefano Marzi, Angelita Simonetti

Chapter 21

Grad-cryo-EM: Tool to Isolate Translation Initiation Complexes from Rabbit Reticulocyte Lysate Suitable for Structural Studies

Javier Rol-Moreno, Lauriane Kuhn, Stefano Marzi, and Angelita Simonetti

Abstract

Since its development, single-particle cryogenic electron microscopy (cryo-EM) has played a central role in the study at medium resolution of both bacterial and eukaryotic ribosomal complexes. With the advent of the direct electron detectors and new processing software which allow obtaining structures at atomic resolution, formerly obtained only by X-ray crystallography, cryo-EM has become the method of choice for the structural analysis of the translation machinery. In most of the cases, the ribosomal complexes at different stages of the translation process are assembled in vitro from purified components, which limit the analysis to previously well-characterized complexes with known factors composition. The initiation phase of the protein synthesis is a very dynamic process during which several proteins interact with the translation apparatus leading to the formation of a chronological series of initiation complexes (ICs). Here we describe a method to isolate ICs assembled on natural in vitro transcribed mRNA directly from rabbit reticulocyte lysate (RRL) by sucrose density gradient centrifugation. The Grad-cryo-EM approach allows investigating structures and composition of intermediate ribosomal complexes prepared in near-native condition by cryo-EM and mass spectrometry analyses. This is a powerful approach, which could be used to study translation initiation of any mRNAs, including IRES containing ones, and which could be adapted to different cell extracts.

Key words Translation initiation, Native ribosome complexes, Cryo-electron microscopy, Mass spectrometry

1 Introduction

The ribosome (80S particle in eukaryotes) is a dynamic molecular machine at the heart of the translation process, which is composed of a large and a small subunit (40S and 60S) made of ribosomal rRNA and proteins. Accompanied by several conformational changes and guided by a multitude of protein factors, the ribosome incorporates amino acids into proteins selecting aminoacylated tRNAs as specified by the mRNA codons. The active protein synthesis phase (translation elongation) is fast and accurate, and its mechanism is conserved though all organisms. In this phase, the

Véronique Arluison and Frank Wien (eds.), *RNA Spectroscopy: Methods and Protocols*, Methods in Molecular Biology, vol. 2113, https://doi.org/10.1007/978-1-0716-0278-2_21,

ribosome incorporates up to 20 amino acids per second with a very low error rate [1–5]. The initiation phase is a much more sophisticated and slow process; the ribosome assembles on the mRNA in the order of seconds [6, 7]. This long time is the result of a highly regulated process to carefully search the start site, usually an AUG codon, along the mRNA molecule. For bulk protein synthesis, the mRNA start codon is found by a base-by-base inspection starting from the 5′ end (usually an m^7G "cap" nucleotide), which positions the proximal AUG in the 40S subunit, a process that has been termed scanning. At least 13 initiation factors (eIFs) are required to ensure accurate AUG localization [8–11]. The first ribosomal initiation complex 43SIC, which is competent for mRNA 5′ → 3′ scanning, is recruited on the cap and is composed of 40S ribosomal subunit and several "core" factors: eIF2/Met-tRNAi^{Met}, eIF1, eIF1A, and eIF3. The scanning ends when the codon–anticodon interaction stabilizes a second ribosomal initiation complex, the 48SIC on the start codon. The third complex is the 80SIC, formed upon subunit joining and release of the initiation factors.

Several molecular aspects of the translation initiation process have been clarified by structural studies on in vitro-reconstituted complexes with a limited set of purified factors and short nonbiologically relevant mRNA mimicking fragments. Nevertheless, several "accessory" factors might be required depending on the structural and sequence features of the mRNAs [12], and their identity, roles, and mechanisms still need to be discovered. Moreover, alternative mechanisms relying on specific mRNA structural features can escape this classical model. Two examples are provided by the translation initiation of IRES containing mRNAs and the tethering mechanism of histone H4 mRNA. Internal ribosomal entry sites (IRES) characterize a heterogeneous class of mechanisms used by some viral and cellular mRNAs to improve translation efficiency and escape global control. mRNA structures located at their 5′ untranslated regions (5′ UTRs) directly guide the ribosome on the start codon without scanning and with the involvement of only a partial set of eIFs, but sometimes requiring IRES transacting factors (ITAFs) [9, 13–15]. Similarly to the IRES, also in the "ribosome tethering", the AUG is found directly without scanning, thanks to two structural RNA elements which are located in the coding region of H4 mRNA [16, 17].

These examples indicate how the eukaryotic translation initiation process is often mRNA-specific, depending on the presence of different signals. Furthermore, new initiation factors are continuously discovered which are involved in specific assembly processes. Therefore, the development of strategies allowing the structural analysis of complexes formed on natural mRNAs and isolated directly from cell extracts, without any a priori prejudice on the eIF composition, would represent a remarkable advance to understand their specific translation initiation mechanisms.

The investigation of labile multifactor translation initiation complexes represents a major challenge for a structural biologist. Single-particle cryo-electron microscopy (cryo-EM) technique had played a fundamental role in the structural study of the ribosome and of the process of translation initiation in both bacteria and eukaryotes. On the other hand, as ribosomes are bulky, electron dense, and distributing nicely on cryo-EM grids, they are producing perfect images and have assisted the development of several image processing methods. Despite this happy *connubium* since the dawn of cryo-EM in the early 1980s [18], the first reconstructions of eukaryotic translation initiation complexes appeared only a little more than 10 years ago [19, 20]. More recently, several studies have clarified the action of factors involved in ribosome scanning and tRNA accommodation [21–23] and the localization of the huge factor platform eIF3 important for mRNA binding [24, 25]. These studies, focused mainly on the canonical cap-dependent mechanism, represent partial or pre-initiation in vitro-assembled complexes. To obviate the need of studying native complexes by cryo-EM, we have recently set up two specific protocols to isolate from rabbit reticulocyte lysates (RRLs) ribosomal particles at different stages during initiation.

The first method [26, 27] allows purification of stable complexes, as the 80SICs, where no factors are bound. This method is based on mRNA ligation to a biotinylated DNA oligo that is immobilized on streptavidin-coated magnetic beads and involves extensive salt washes. In this way, using a combination of cycloheximide–hygromycin to prevent the first translocation step, 80SIC formed on H4 mRNA was purified and its structure solved at 9.3 Å [16], revealing how proper start codon positioning is achieved by a direct mRNA–rRNA interaction.

In this chapter, we provide a detailed protocol of the second method (Grad-cryo-EM) developed to isolate stalled 48SICs assembled on natural in vitro-transcribed mRNAs by sucrose density gradient centrifugation. Sucrose gradients are commonly used to profile ribosomes distribution on mRNA (polysomes), and the presence of specific inhibitors results in the accumulation of translation initiation intermediates, which sediment at the corresponding sucrose densities. Figure 1 shows the different radioactivity profiles on a 7–47% sucrose gradient obtained by incubating radiolabeled β-globin mRNA with nuclease-treated RRL in the absence of any inhibitor (blue line) or in the presence of cycloheximide (green line) or GMP-PNP (red line). While polysomes are detectable without any inhibitor, the addition of cycloheximide, inhibiting the eEF2-mediated translocation, blocks the progression of the translation to the elongation phase with the consequent accumulation of 80S monomer ribosomes [28, 29]. To block translation initiation before 60S association, non-hydrolysable nucleotides can be used. When nuclease-treated RRLs are supplemented with a non-hydrolysable analog of GTP

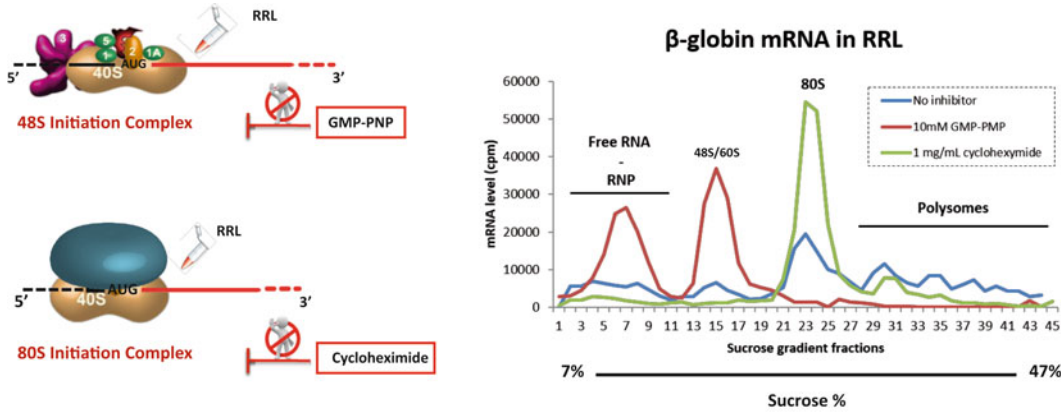

Fig. 1 Grad-cryo-EM strategy to isolate 48S and 80S initiation complexes. The initiation complexes are stalled on the start codon of β-globin mRNA from rabbit reticulocyte lysate (RRL), in the presence of different translation initiation inhibitors, GMP-PNP for the 48SIC, and cycloheximide for the 80SIC. 7–47% sucrose gradient analysis of the initiation complexes is used to monitor the formation of initiation complexes using P^{32} radiolabeled-capped β-globin mRNA. In the absence of any inhibitor (blue line), polysomes are detectable, while in the presence of cycloheximide (green line) or GMP-PNP (red line) could be observed a consequent accumulation of 80S monomer ribosomes and 48SIC, respectively

(GMP-PNP), the assembling of the 48SIC on the mRNA of interest arrests after start codon recognition, prior to eIF2 dissociation and large ribosomal subunit joining [30, 31]. These complexes can be easily isolated by centrifugation on appropriate sucrose gradients, which are both resolutive (even a 48SIC could be separated from 60S large ribosomal subunit) and gentle, preserving factor association. Composition of the isolated complexes will be then determined by mass spectrometry analysis, while their structure is analyzed by cryo-EM using a state-of-the-art framework, allowing to sort out the structures of different complexes present in a single sample. This strategy is adaptable to study translation initiation on any mRNA of interest, including IRES containing ones, with any cell extract that can be made from different cell lines, tissues, plants, insects, etc.

2 Materials

2.1 Cell Extracts, Buffers, Solutions, and Reagents

1. Rabbit reticulocyte lysate system, nuclease treated (L4960—Promega).
2. TMSDT buffer: 40 mM Tris–HCl pH 8.1, 22 mM $MgCl_2$, 5 mM DTT (dithiothreitol), 0.01% Triton-X100, 1 mM spermidine. This buffer is used for in vitro transcription.
3. RNA elution buffer: 0.5 M NH_4OAc pH 6.5, 0,1% sodium dodecyl sulfate (SDS), 1 mM ethylenediaminetetraacetic acid (EDTA).
4. Buffer A: 25 mM HEPES-KOH pH 7.6, 79 mM KOAc, 0.5 mM $Mg(OAc)_2$, 2 mM DTT. This buffer is prepared as

5× stock solution and used to obtain sucrose solutions at different concentrations to make the gradients.

5. 60% sucrose stock solution: Dissolve 60 g of D(+)-saccharose (VWR International) in a total volume of 100 mL of ultrapure water. A 60% sucrose stock solution is used to prepare in Buffer A 1×: (1) 7–47% linear sucrose gradient for analytical polysome profiling and (2) 5–25% linear sucrose gradient for the IC isolation.
6. Buffer B: 10 mM HEPES-KOH pH 7.6, 50 mM K OAc, 10 mM NH_4Cl, 5 mM $Mg(OAc)_2$, 2 mM DTT. This buffer is used to resuspend pelleted isolated complexes for cryo-EM studies.
7. [α-^{32}P]-GTP (6000 Ci/mmol).

Prepare all the solutions using ultrapure RNase-free water (Milli-Q deionized water attaining a sensitivity of 18 MΩ cm at 25 °C). Filter them with 0.22 μm membrane sterile syringe filter (SARSTED) and a 10 mL syringe (*see* **Note 1**).

2.2 Antibiotics and Translation Inhibitors

1. Cycloheximide (Sigma-Aldrich) powder is dissolved in water. Stock solution of 10 mg/mL can be stored at −80 °C for 1 month.
2. GMP-PNP (Sigma-Aldrich) powder is dissolved in water. Stock solution of 50 mM is stored at −80 °C.

2.3 Instrument and Accessories

1. Gradient Master™ device (BioComp Instruments, Fredericton, Canada) is used to generate linear sucrose gradients.
2. Piston Gradient Fractionator™ implemented with Triax™ Flow Cell is used for precise fractionation of sucrose gradients from the top down.
3. Beckman SW41 Ti Swinging-Bucket Rotor and Optima XE-90 ultracentrifuge.
4. Open-Top Polyclear™ centrifuge tubes (Seton Scientific).
5. Sorvall-Hitachi S140AT fixed angle rotor and M150 SE ultracentrifuge.
6. NanoDrop ND-1000 Spectrophotometer (Thermo Fisher Scientific, Waltham, MA, USA) or equivalent.
7. Micro Bio-Spin™ 6 Columns (Bio-Rad).
8. Refrigerated centrifuge.
9. High-precision balance.

3 Methods

3.1 mRNA Transcription and Capping

The template for human β-globin mRNA transcription (494 nt; accession number BC007075) was generated by PCR amplification from a plasmid containing the gene, essentially as described in [27].

The PCR product was phenol-extracted and precipitated with ethanol. The purified PCR product (5–8 μg) was directly used as template for the in vitro transcription of β-globin mRNA using 0.2 mg/mL of T7 RNA polymerase in a 100 μL volume of TMSDT buffer containing 5 mM of each NTP and 40 units of human placenta RNase inhibitor (RNasin, Promega). The reaction was incubated at 37 °C for 2 h followed by a further 1 h in the presence of RNase-free DNase I (4 units, New England Biolabs) to degrade the PCR template. Transcription products were purified to homogeneity from abortive transcription or degradation products using denaturing polyacrylamide-urea gel electrophoresis (urea-PAGE) on 8% polyacrylamide/8 M urea slab gels. After migration, the gel is removed from glass plates, RNA is visualized by UV shadowing on UV fluorescent TLC plate, and the band is cut from the acrylamide gel using a clean scalpel. The RNA is passively eluted at 4 °C overnight by gently mixing in RNA elution buffer and then extracted by phenol–chloroform treatment, precipitated in ethanol, washed with 85% ethanol, and vacuum-dried. The pure transcript was resuspended in ultrapure water, capped using the ScriptCap m^7G Capping System (Epicenter), and stocked at −20 °C. Radiolabeled transcripts were obtained by substituting the GTP from the capping kit with [α^{32}P]GTP. Micro Bio-Spin™ 6 Column is used to remove unincorporated GTP or [α^{32}P]GTP in case of a radiolabeled mRNA.

3.2 Linear Sucrose Gradient Preparation

About 5–25% linear sucrose density gradient centrifugation is used to isolate pure β-globin/48SIC directly from RRL incubated with 10 mM (final concentration) GMP-PNP. To obtain a linear sucrose density gradient, the Gradient Master™ device (BioComp) is used with the "SW41 Short Gradient" program and the corresponding range of sucrose percentage following the manufacturer's manual. The use of the Gradient Master™ device offers the great advantage of preparing six reproducible and identical linear gradients of 12.5 mL (final volume) in one run. Tubes are cupped (short cups) and placed in a magnetic tube holder that adheres to the rotary steel plate on the instrument (*see* **Notes 2–4**). The percentage of sucrose used for linear gradients can be adjusted to optimize the separation of polysomal fractions according to the biological sample or experiment.

3.3 β-Globin/48SIC Formation and Isolation from Sucrose Gradient

In order to stall functional intermediate initiation complexes, compounds that inhibits specific steps of the translation machinery assembly need to be used. As mentioned above, in the presence of GMP-PNP, the GTPase eIF2 remains bound to the ribosome impairing subunits joining and thus blocking the ribosome assembly at the 48S late stage. To identify on the gradient the peak corresponding to the 48SIC, radiolabeled β-globin mRNA (250,000 cpm per gradient) is incubated with nuclease-treated

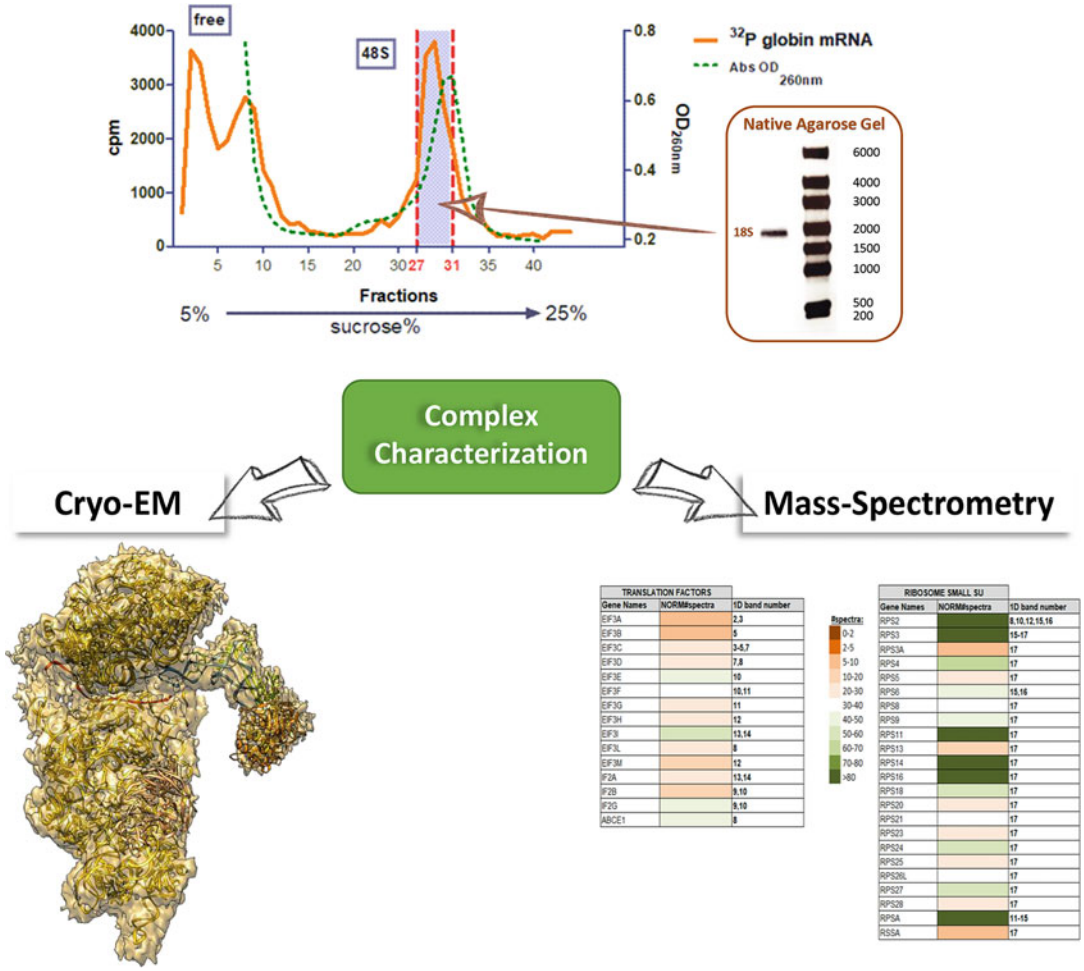

Fig. 2 48SIC isolation, factor composition, and structure determination. β-Globin mRNA is incubated with RRL in the presence of GMP-PNP to accumulate 48SIC. The RRL is fractionated on a 5–25% sucrose gradient to isolate stalled 48SIC, monitored using radioactive-capped β-globin mRNA (orange line). Ribosome localization is confirmed by optical density at 260 nm (green dashed line). After isolation, native agarose gel electrophoresis analysis is performed to assess the purity of the complex. The isolated β-globin-48SIC is then analyzed by nano-LC-MS/MS to get insights into its composition and by cryo-EM to determine its structure [31].

RRL in the presence of 10 mM GMP-PNP as described in [31]. The reaction is fractionated on 5–25% linear sucrose density gradient by centrifugation using SW41 Ti rotor, yielding optimal separation of the 48SIC late-stage particles from the 60S ribosomal subunits, as detected on native agarose gel electrophoresis (Fig. 2). Sample buffer components such as glycerol, sucrose, and detergent can reduce specimen contrast in cryo-EM. To completely remove sucrose, β-globin/48SIC containing fractions are pooled and the ribosomal complexes pelleted by centrifugation. The pellet is resuspended in Buffer B, which is suitable for both cryo-EM and mass spectrometry analysis (Fig. 2). The composition of the isolated

β-globin/48SIC is determined by nano-liquid chromatography (LC) tandem mass spectrometry (MS/MS), helping the interpretation of the 3D density map obtained using cryo-EM.

Grad-cryo-EM approach can be adapted to also isolate the 80SICs by incubating RRL with the β-globin mRNA in the presence of cycloheximide, instead of GMP-PNP.

3.3.1 The Experiment

1. 5–25% linear sucrose gradient should be prepared and stored at 4 °C at least 2 h before loading of the sample.
2. Prior to stall late-stage 48SIC, ribosomes need to be reactivated. Thus, nuclease-treated RRL (Promega) should be incubated for 5 min at 30 °C in presence of a mixture of amino acids and then chilled on ice for 10 min. Amino acid mixture is provided with the Rabbit Reticulocyte Lysate System Kit to optimize translation.
3. Cycloheximide and hygromycin are thawed slowly on ice during ribosome activation step.
4. 60 μL of nuclease-treated RRL is incubated at 30 °C in the presence of 10 mM of GMP-PNP. After 2 min of incubation, 13 μg of β-globin mRNA is added, and the reaction mix is furthered incubated 5 min at 30 °C and chilled on ice for 10 min.
5. The reaction mix is layered (157 μL volume) onto 12.5 mL of 5–25% linear sucrose gradient and centrifugated at 37,000 rpm for 4 h and 37 min in a Beckman SW41 Ti Swinging-Bucket Rotor (average RCF 200,000 *g*; *see* **Note 4**).
6. The gradient is fractionated from the top down using Bio-Comp Piston Gradient Fractionator™ devise implemented with Triax™ Flow Cell. This system allows monitoring the A_{260} absorbance throughout the fractionation process (*see* **Notes 5** and **6**).
7. An identical experiment is performed using 5′-labeled capped β-globin mRNA to identify fractions containing β-globin/48SIC.
8. Once identified, the fractions are centrifugated at 108,000 rpm for 2 h at 4 °C in a Sorvall-Hitachi S140AT fixed angle rotor (average RCF 600,000 *g*) . Ribosome pellet is dissolved in Buffer B, which is compatible for both mass spectrometry and cryo-EM analysis (*see* **Note 7**).
9. Composition of the obtained cryo-EM 3D reconstruction of the purified β-globin/48SIC is confirmed by nanoLC MS/MS analysis.

Grad-cryo-EM method yielded 2106 pmol of pure β-globin/48SIC from the incubation of 60 μL of RRL with 13 μg (108 pmol) of β-globin mRNA in the presence of 10 mM of GMP-PNP. 4 μL of

β-globin/48SIC concentrated 70 nM was applied on 400 mesh holey carbon Quantifoil 2/2 grids (Quantifoil Micro Tools) to perform cryo-EM analysis. The cryo-EM structure of the β-globin/48SIC at 5.86 Å resolution [31] has shown the molecular details of the first decoding event on the start codon occurring at the end of the scanning process. eIF2/Met-tRNAi^{Met} is present, while no density for eIF1 could be observed, thus suggesting its dissociation from the complex upon start codon recognition, as confirmed by mass spectrometry analysis. Surprisingly, the 3D reconstruction has also shown an extra density located on the 40S intersubunit face. Both shape of the density and mass spectrometry data allowed assigning this density to ABCE1, an ATP-binding protein implicated in subunits disjoining after termination of translation [32]. This unexpected result demonstrates the importance of adopting methods for native complexes purification, but at the same time also indicates its limits. In fact, to unambiguously identify new factors when the obtained resolution of the structure is not enough to distinguish amino acid side chains, a deep characterization of the complex should be obtained by combining other techniques. A successful strategy has been attained by using immunolabeled cryo-EM in combination with Grad-cryo-EM [33].

4 Notes

1. All buffers used here are filtered using a 0.22 μm membrane sterile syringe filter (SARSTED) to ensure buffer sterilization and stored at 4 °C. The buffer solutions are made fresh every week.
2. BioComb Gradient Master™ device is provided with two types of tube cup. For our propose, we have used a short tube cup which leaves a 4 mm gap above the finished gradient.
3. Once prepared, the gradients should be handled with care to avoid disturbance and stored at 4 °C for at least 2 h before the layering of the sample.
4. Pay attention not to form air bubbles when the tube cap is removed and during sample layering on the sucrose gradient, since it causes gradient perturbation throughout the centrifugation step.
5. Fractionate the gradient top down using Piston Gradient Fractionator™ connected to a fraction collector. Fast flow rates can reduce resolution and make it more difficult to collect precise fractions. For the isolation of β-globin/48SIC, approximately 250 μL per Eppendorf tube were collected using piston speed of 0.12 mm/s.

6. In case several gradients should be fractionated, a washing step of the Piston Gradient Fractionator system is strongly suggested to avoid contamination of 60S ribosomal subunit.
7. During the ultracentrifugation step, the ribosome complex precipitates, forming an unstable pellet that should be handled carefully. Thus, the supernatant containing sucrose should be quickly and completely removed, avoiding the perturbation of the pellet.

References

1. Sorensen MA, Kurland CG, Pedersen S (1989) Codon usage determines translation rate in Escherichia coli. J Mol Biol 207:365–377
2. Wintermeyer W, Peske F, Beringer M, Gromadski KB, Savelsbergh A, Rodnina MV (2004) Mechanisms of elongation on the ribosome: dynamics of a macromolecular machine. Biochem Soc Trans 32:733–737
3. Lovmar M, Ehrenberg M (2006) Rate, accuracy and cost of ribosomes in bacterial cells. Biochimie 88:951–961
4. Rodnina MV, Beringer M, Wintermeyer W (2007) How ribosomes make peptide bonds. Trends Biochem Sci 32:20–26
5. Zaher HS, Green R (2009) Fidelity at the molecular level: lessons from protein synthesis. Cell 136:746–762
6. Kennell D, Riezman H (1977) Transcription and translation initiation frequencies of the Escherichia coli lac operon. J Mol Biol 114:1–21
7. Gold L (1988) Posttranscriptional regulatory mechanisms in Escherichia coli. Annu Rev Biochem 57:199–233
8. Hinnebusch AG (2011) Molecular mechanism of scanning and start codon selection in eukaryotes. Microbiol Mol Biol Rev 75:434–467, first page of table of contents
9. Jackson RJ, Hellen CU, Pestova TV (2010) The mechanism of eukaryotic translation initiation and principles of its regulation. Nat Rev Mol Cell Biol 11:113–127
10. Parsyan A, Svitkin Y, Shahbazian D, Gkogkas C, Lasko P, Merrick WC, Sonenberg N (2011) mRNA helicases: the tacticians of translational control. Nat Rev Mol Cell Biol 12:235–245
11. Sonenberg N, Hinnebusch AG (2009) Regulation of translation initiation in eukaryotes: mechanisms and biological targets. Cell 136:731–745
12. Aylett CH, Ban N (2017) Eukaryotic aspects of translation initiation brought into focus. Philos Trans R Soc Lond Ser B Biol Sci 372:20160186
13. Spahn CM, Kieft JS, Grassucci RA, Penczek PA, Zhou K, Doudna JA, Frank J (2001) Hepatitis C virus IRES RNA-induced changes in the conformation of the 40s ribosomal subunit. Science 291:1959–1962
14. Spahn CM, Jan E, Mulder A, Grassucci RA, Sarnow P, Frank J (2004) Cryo-EM visualization of a viral internal ribosome entry site bound to human ribosomes: the IRES functions as an RNA-based translation factor. Cell 118:465–475
15. Hashem Y, des Georges A, Dhote V, Langlois R, Liao HY, Grassucci RA, Pestova TV, Hellen CU, Frank J (2013) Hepatitis-C-virus-like internal ribosome entry sites displace eIF3 to gain access to the 40S subunit. Nature 503:539–543
16. Martin F, Menetret JF, Simonetti A, Myasnikov AG, Vicens Q, Prongidi-Fix L, Natchiar SK, Klaholz BP, Eriani G (2016) Ribosomal 18S rRNA base pairs with mRNA during eukaryotic translation initiation. Nat Commun 7:12622
17. Martin F, Barends S, Jaeger S, Schaeffer L, Prongidi-Fix L, Eriani G (2011) Cap-assisted internal initiation of translation of histone H4. Mol Cell 41:197–209
18. Dubochet J, Lepault J, Freeman R, Berriman JA, Homo J-C (1982) Electron microscopy of frozen water and aqueous solutions. J Microsc 128:219–237
19. Gilbert RJ, Gordiyenko Y, von der Haar T, Sonnen AF, Hofmann G, Nardelli M, Stuart DI, McCarthy JE (2007) Reconfiguration of yeast 40S ribosomal subunit domains by the translation initiation multifactor complex. Proc Natl Acad Sci U S A 104:5788–5793
20. Passmore LA, Schmeing TM, Maag D, Applefield DJ, Acker MG, Algire MA, Lorsch JR, Ramakrishnan V (2007) The eukaryotic translation initiation factors eIF1 and eIF1A induce

an open conformation of the 40S ribosome. Mol Cell 26:41–50

21. Llacer JL, Hussain T, Marler L, Aitken CE, Thakur A, Lorsch JR, Hinnebusch AG, Ramakrishnan V (2015) Conformational differences between open and closed states of the eukaryotic translation initiation complex. Mol Cell 59:399–412
22. Hashem Y, Georges A d, Dhote V, Langlois R, Liao HY, Grassucci RA, Hellen CU, Pestova TV, Frank J (2013) Structure of the mammalian ribosomal 43S preinitiation complex bound to the scanning factor DHX29. Cell 153:1108–1119
23. Hussain T, Llacer JL, Fernandez IS, Munoz A, Martin-Marcos P, Savva CG, Lorsch JR, Hinnebusch AG, Ramakrishnan V (2014) Structural changes enable start codon recognition by the eukaryotic translation initiation complex. Cell 159:597–607
24. des Georges A, Dhote V, Kuhn L, Hellen CU, Pestova TV, Frank J, Hashem Y (2015) Structure of mammalian eIF3 in the context of the 43S preinitiation complex. Nature 525:491–495
25. Aylett CH, Boehringer D, Erzberger JP, Schaefer T, Ban N (2015) Structure of a yeast 40S-eIF1-eIF1A-eIF3-eIF3j initiation complex. Nat Struct Mol Biol 22:269–271
26. Prongidi-Fix L, Schaeffer L, Simonetti A, Barends S, Menetret JF, Klaholz BP, Eriani G, Martin F (2013) Rapid purification of ribosomal particles assembled on histone H4 mRNA: a new method based on mRNA-DNA chimaeras. Biochem J 449:719–728
27. Chicher J, Simonetti A, Kuhn L, Schaeffer L, Hammann P, Eriani G, Martin F (2015) Purification of mRNA-programmed translation initiation complexes suitable for mass spectrometry analysis. Proteomics 15:2417–2425
28. Garreau de Loubresse N, Prokhorova I, Holtkamp W, Rodnina MV, Yusupova G, Yusupov M (2014) Structural basis for the inhibition of the eukaryotic ribosome. Nature 513:517–522
29. Schneider-Poetsch T, Ju J, Eyler DE, Dang Y, Bhat S, Merrick WC, Green R, Shen B, Liu JO (2010) Inhibition of eukaryotic translation elongation by cycloheximide and lactimidomycin. Nat Chem Biol 6:209–217
30. Anthony DD, Merrick WC (1992) Analysis of 40 S and 80 S complexes with mRNA as measured by sucrose density gradients and primer extension inhibition. J Biol Chem 267:1554–1562
31. Simonetti A, Brito Querido J, Myasnikov AG, Mancera-Martinez E, Renaud A, Kuhn L, Hashem Y (2016) eIF3 peripheral subunits rearrangement after mRNA binding and start-codon recognition. Mol Cell 63:206–217
32. Mancera-Martinez E, Brito Querido J, Valasek LS, Simonetti A, Hashem Y (2017) ABCE1: a special factor that orchestrates translation at the crossroad between recycling and initiation. RNA Biol 14:1279–1285
33. Brito Querido J, Mancera-Martinez E, Vicens Q, Bochler A, Chicher J, Simonetti A, Hashem Y (2017) The cryo-EM structure of a novel 40S kinetoplastid-specific ribosomal protein. Structure 25:1785–1794 e3

References

A

AbouHaidar, M.G. and Ivanov, I.G. (1999) "Non-Enzymatic RNA Hydrolysis Promoted by the Combined Catalytic Activity of Buffers and Magnesium Ions," *Zeitschrift für Naturforschung C*, 54(7–8), pp. 542–548. doi:10.1515/znc-1999-7-813.

Adomavicius, T. *et al.* (2019) "The structural basis of translational control by eIF2 phosphorylation," *Nature Communications*, 10(1), p. 2136. doi:10.1038/s41467-019-10167-3.

Aktary, Z., Alaee, M. and Pasdar, M. (2017) "Beyond cell-cell adhesion: Plakoglobin and the regulation of tumorigenesis and metastasis," *Oncotarget*, 8(19), pp. 32270–32291. doi:10.18632/oncotarget.15650.

Allen, M. *et al.* (2016) "Origin of the U87MG glioma cell line: Good news and bad news," *Science Translational Medicine*, 8(354). doi:10.1126/scitranslmed.aaf6853.

Allmang, C. *et al.* (1999) "Functions of the exosome in rRNA, snoRNA and snRNA synthesis," *The EMBO Journal*, 18(19), pp. 5399–5410. doi:10.1093/emboj/18.19.5399.

Anda, S., Zach, R. and Grallert, B. (2017) "Activation of Gcn2 in response to different stresses," *PLOS ONE*, 12(8), p. e0182143. doi:10.1371/journal.pone.0182143.

Anderson, N.M. and Simon, M.C. (2020) "The tumor microenvironment," *Current Biology*, 30(16), pp. R921–R925. doi:10.1016/j.cub.2020.06.081.

Anosova, I. *et al.* (2016) "The structural diversity of artificial genetic polymers," *Nucleic Acids Research*, 44(3), pp. 1007–1021. doi:10.1093/nar/gkv1472.

Arias-Gonzalez, J.R. (2014) "Single-molecule portrait of DNA and RNA double helices," *Integr. Biol.*, 6(10), pp. 904–925. doi:10.1039/C4IB00163J.

B

Baba, Y. *et al.* (2010) "HIF1A Overexpression Is Associated with Poor Prognosis in a Cohort of 731 Colorectal Cancers," *The American Journal of Pathology*, 176(5), pp. 2292–2301. doi:10.2353/ajpath.2010.090972.

Bailey, M.H. *et al.* (2018) "Comprehensive Characterization of Cancer Driver Genes and Mutations," *Cell*, 173(2), pp. 371-385.e18. doi:10.1016/j.cell.2018.02.060.

Baird, S.D. *et al.* (2006) "Searching for IRES," *RNA*, 12(10), pp. 1755–1785. doi:10.1261/rna.157806.

Barbieri, I. and Kouzarides, T. (2020) "Role of RNA modifications in cancer," *Nature Reviews Cancer*, 20(6), pp. 303–322. doi:10.1038/s41568-020-0253-2.

Ben-Shem, A. *et al.* (2011) "The Structure of the Eukaryotic Ribosome at 3.0 Å Resolution," *Science*, 334(6062), pp. 1524–1529. doi:10.1126/science.1212642.

Bert, A.G. *et al.* (2006) "Assessing IRES activity in the HIF-1α and other cellular 5′ UTRs," *RNA*, 12(6), pp. 1074–1083. doi:10.1261/rna.2320506.

Bhat, M. *et al.* (2015) "Targeting the translation machinery in cancer," *Nature Reviews Drug Discovery*, 14(4), pp. 261–278. doi:10.1038/nrd4505.

Boussemart, L. *et al.* (2014) "eIF4F is a nexus of resistance to anti-BRAF and anti-MEK cancer therapies," *Nature*, 513(7516), pp. 105–109. doi:10.1038/nature13572.

Bouyssié, D. *et al.* (2020) "Proline: an efficient and user-friendly software suite for large-scale proteomics," *Bioinformatics*, 36(10), pp. 3148–3155. doi:10.1093/bioinformatics/btaa118.

Bradrick, S.S. and Gromeier, M. (2009) "Identification of Gemin5 as a Novel 7-Methylguanosine Cap-Binding Protein," *PLoS ONE*, 4(9), p. e7030. doi:10.1371/journal.pone.0007030.

Brito Querido, J. *et al.* (2020) "Structure of a human 48 *S* translational initiation complex," *Science*, 369(6508), pp. 1220–1227. doi:10.1126/science.aba4904.

Brown, A. and Shao, S. (2018) "Ribosomes and cryo-EM: a duet," *Current Opinion in Structural Biology*, 52, pp. 1–7. doi:10.1016/j.sbi.2018.07.001.

Bugter, J.M., Fenderico, N. and Maurice, M.M. (2021) "Mutations and mechanisms of WNT pathway tumour suppressors in cancer," *Nature Reviews Cancer*, 21(1), pp. 5–21. doi:10.1038/s41568-020-00307-z.

Butcher, S.E. and Pyle, A.M. (2011) "The Molecular Interactions That Stabilize RNA Tertiary Structure: RNA Motifs, Patterns, and Networks," *Accounts of Chemical Research*, 44(12), pp. 1302–1311. doi:10.1021/ar200098t.

C

Calvo, S.E., Pagliarini, D.J. and Mootha, V.K. (2009) "Upstream open reading frames cause widespread reduction of protein expression and are polymorphic among humans," *Proceedings of the National Academy of Sciences*, 106(18), pp. 7507–7512. doi:10.1073/pnas.0810916106.

Cammas, A. *et al.* (2016) "hnRNP A1-mediated translational regulation of the G quadruplex-containing RON receptor tyrosine kinase mRNA linked to tumor progression," *Oncotarget*, 7(13), pp. 16793–16805. doi:10.18632/oncotarget.7589.

Carbone, A. (2020) "Cancer Classification at the Crossroads," *Cancers*, 12(4), p. 980. doi:10.3390/cancers12040980.

Cech, T.R. (2000) "The Ribosome Is a Ribozyme," *Science*, 289(5481), pp. 878–879. doi:10.1126/science.289.5481.878.

Chee, N.T., Lohse, I. and Brothers, S.P. (2019) "mRNA-to-protein translation in hypoxia," *Molecular Cancer*, 18(1), p. 49. doi:10.1186/s12943-019-0968-4.

Chen, C.-H. *et al.* (2011) "The genomic features that affect the lengths of 5' untranslated regions in multicellular eukaryotes," *BMC Bioinformatics*, 12(S9), p. S3. doi:10.1186/1471-2105-12-S9-S3.

Chen, H. *et al.* (2014) "Exploring the Formation and Recognition of an Important G-Quadruplex in a HIF1α Promoter and Its Transcriptional Inhibition by a Benzo[*c*]phenanthridine Derivative," *Journal of the American Chemical Society*, 136(6), pp. 2583–2591. doi:10.1021/ja412128w.

Chen, P.-J. and Huang, Y.-S. (2012) "CPEB2-eEF2 interaction impedes HIF-1α RNA translation," *The EMBO Journal*, 31(4), pp. 959–971. doi:10.1038/emboj.2011.448.

Chen, W.-L. *et al.* (2016) "Silvestrol induces early autophagy and apoptosis in human melanoma cells," *BMC Cancer*, 16(1), p. 17. doi:10.1186/s12885-015-1988-0.

Clevers, H. and Nusse, R. (2012) "Wnt/β-Catenin Signaling and Disease," *Cell*, 149(6), pp. 1192–1205. doi:10.1016/j.cell.2012.05.012.

Connolly, E. *et al.* (2006) "Hypoxia Inhibits Protein Synthesis through a 4E-BP1 and Elongation Factor 2 Kinase Pathway Controlled by mTOR and Uncoupled in Breast Cancer Cells," *Molecular and Cellular Biology*, 26(10), pp. 3955–3965. doi:10.1128/MCB.26.10.3955-3965.2006.

Courel, M. *et al.* (2019) "GC content shapes mRNA storage and decay in human cells," *eLife*, 8. doi:10.7554/eLife.49708.

Cui, C. *et al.* (2018) "Is β-Catenin a Druggable Target for Cancer Therapy?," *Trends in Biochemical Sciences*, 43(8), pp. 623–634. doi:10.1016/j.tibs.2018.06.003.

D

Dabo, S. and Meurs, E. (2012) "dsRNA-Dependent Protein Kinase PKR and its Role in Stress, Signaling and HCV Infection," *Viruses*, 4(11), pp. 2598–2635. doi:10.3390/v4112598.

Darty, K., Denise, A. and Ponty, Y. (2009) "VARNA: Interactive drawing and editing of the RNA secondary structure," *Bioinformatics*, 25(15), pp. 1974–1975. doi:10.1093/bioinformatics/btp250.

Dever, T.E. and Green, R. (2012) "The Elongation, Termination, and Recycling Phases of Translation in Eukaryotes," *Cold Spring Harbor Perspectives in Biology*, 4(7), pp. a013706–a013706. doi:10.1101/cshperspect.a013706.

Díaz-López, I. *et al.* (2019) "An mRNA-binding channel in the ES6S region of the translation 48S-PIC promotes RNA unwinding and scanning," *eLife*, 8. doi:10.7554/eLife.48246.

Diaz-Toledano, R., Lozano, G. and Martinez-Salas, E. (2016) "In-cell SHAPE uncovers dynamic interactions between the untranslated regions of the foot-and-mouth disease virus RNA," *Nucleic Acids Research*, p. gkw795. doi:10.1093/nar/gkw795.

Donahue, T.F. (2000) "Genetic approaches to translation initiation in Saccharomyces cerevisiae," *Cold Spring Harbor Monograph Series*, 39, pp. 487–502.

Drees, F. *et al.* (2005) "α-Catenin Is a Molecular Switch that Binds E-Cadherin-β-Catenin and Regulates Actin-Filament Assembly," *Cell*, 123(5), pp. 903–915. doi:10.1016/j.cell.2005.09.021.

E

Ebright, R.Y. *et al.* (2020) "Deregulation of ribosomal protein expression and translation promotes breast cancer metastasis," *Science*, 367(6485), pp. 1468–1473. doi:10.1126/science.aay0939.

Eliseev, B. *et al.* (2018) "Structure of a human cap-dependent 48S translation pre-initiation complex," *Nucleic Acids Research*, 46(5), pp. 2678–2689. doi:10.1093/nar/gky054.

Erzberger, J.P. *et al.* (2014) "Molecular Architecture of the 40S·eIF1·eIF3 Translation Initiation Complex," *Cell*, 159(5), pp. 1227–1228. doi:10.1016/j.cell.2014.11.001.

F

Fabbri, L. *et al.* (2021) "The plasticity of mRNA translation during cancer progression and therapy resistance," *Nature Reviews Cancer*, 21(9), pp. 558–577. doi:10.1038/s41568-021-00380-y.

Fohrer, J., Hennig, M. and Carlomagno, T. (2006) "Influence of the 2′-Hydroxyl Group Conformation on the Stability of A-form Helices in RNA," *Journal of Molecular Biology*, 356(2), pp. 280–287. doi:10.1016/j.jmb.2005.11.043.

Francisco-Velilla, R. *et al.* (2016) "The RNA-binding protein Gemin5 binds directly to the ribosome and regulates global translation," *Nucleic Acids Research*, 44(17), pp. 8335–8351. doi:10.1093/nar/gkw702.

Frank, J. *et al.* (2007) "The process of mRNA-tRNA translocation," *Proceedings of the National Academy of Sciences*, 104(50), pp. 19671–19678. doi:10.1073/pnas.0708517104.

Frank, J. (2017) "Advances in the field of single-particle cryo-electron microscopy over the last decade," *Nature Protocols*, 12(2), pp. 209–212. doi:10.1038/nprot.2017.004.

Fu, Q. *et al.* (2015) "β-Catenin expression is regulated by an IRES-dependent mechanism and stimulated by paclitaxel in human ovarian cancer cells," *Biochemical and Biophysical Research Communications*, 461(1), pp. 21–27. doi:10.1016/j.bbrc.2015.03.161.

Fuchs, Q. *et al.* (2020) "Hypoxia Inducible Factors' Signaling in Pediatric High-Grade Gliomas: Role, Modelization and Innovative Targeted Approaches," *Cancers*, 12(4), p. 979. doi:10.3390/cancers12040979.

Fujii, K. *et al.* (2018) "Decoding the Function of Expansion Segments in Ribosomes," *Molecular Cell*, 72(6), pp. 1013-1020.e6. doi:10.1016/j.molcel.2018.11.023.

Furic, L. *et al.* (2010) "eIF4E phosphorylation promotes tumorigenesis and is associated with prostate cancer progression," *Proceedings of the National Academy of Sciences*, 107(32), pp. 14134–14139. doi:10.1073/pnas.1005320107.

G

Galban, S. and Gorospe, M. (2009) "Factors Interacting with HIF-1α mRNA: Novel Therapeutic Targets," *Current Pharmaceutical Design*, 15(33), pp. 3853–3860. doi:10.2174/138161209789649376.

Gal-Ben-Ari, S. *et al.* (2019) "PKR: A Kinase to Remember," *Frontiers in Molecular Neuroscience*, 11. doi:10.3389/fnmol.2018.00480.

Genuth, N.R. and Barna, M. (2018) "The Discovery of Ribosome Heterogeneity and Its Implications for Gene Regulation and Organismal Life," *Molecular Cell*, 71(3), pp. 364–374. doi:10.1016/j.molcel.2018.07.018.

des Georges, A. *et al.* (2015) "Structure of mammalian eIF3 in the context of the 43S preinitiation complex," *Nature*, 525(7570), pp. 491–495. doi:10.1038/nature14891.

Gilbert, W. v. (2010) "Alternative Ways to Think about Cellular Internal Ribosome Entry," *Journal of Biological Chemistry*, 285(38), pp. 29033–29038. doi:10.1074/jbc.R110.150532.

Gingras, A.-C. *et al.* (1999) "Regulation of 4E-BP1 phosphorylation: a novel two-step mechanism," *Genes & Development*, 13(11), pp. 1422–1437. doi:10.1101/gad.13.11.1422.

González-Almela, E. *et al.* (2018) "The Initiation Factors eIF2, eIF2A, eIF2D, eIF4A, and eIF4G Are Not Involved in Translation Driven by Hepatitis C Virus IRES in Human Cells," *Frontiers in Microbiology*, 9. doi:10.3389/fmicb.2018.00207.

Gregori J, Sanchez A and Villanueva J (2019) *msmsTests: LC-MS/MS Differential Expression Tests. R package version 1.22.0.*

Guca, E. and Hashem, Y. (2018) "Major structural rearrangements of the canonical eukaryotic translation initiation complex," *Current Opinion in Structural Biology*, 53, pp. 151–158. doi:10.1016/j.sbi.2018.08.006.

H

Hanahan, D. (2022) "Hallmarks of Cancer: New Dimensions," *Cancer Discovery*, 12(1), pp. 31–46. doi:10.1158/2159-8290.CD-21-1059.

Hashem, Y. *et al.* (2013) "Structure of the Mammalian Ribosomal 43S Preinitiation Complex Bound to the Scanning Factor DHX29," *Cell*, 153(5), pp. 1108–1119. doi:10.1016/j.cell.2013.04.036.

Hayek, H. *et al.* (2021) "eIF3 interacts with histone H4 messenger RNA to regulate its translation," *Journal of Biological Chemistry*, 296, p. 100578. doi:10.1016/j.jbc.2021.100578.

Henras, A.K. *et al.* (2015) "An overview of pre-ribosomal RNA processing in eukaryotes," *Wiley Interdisciplinary Reviews: RNA*, 6(2), pp. 225–242. doi:10.1002/wrna.1269.

Higashimura, Y. *et al.* (2011) "Up-regulation of glyceraldehyde-3-phosphate dehydrogenase gene expression by HIF-1 activity depending on Sp1 in hypoxic breast cancer cells," *Archives of Biochemistry and Biophysics*, 509(1), pp. 1–8. doi:10.1016/j.abb.2011.02.011.

Hinnebusch, A.G. (2014) "The Scanning Mechanism of Eukaryotic Translation Initiation," *Annual Review of Biochemistry*, 83(1), pp. 779–812. doi:10.1146/annurev-biochem-060713-035802.

Hinnebusch, A.G. (2017) "Structural Insights into the Mechanism of Scanning and Start Codon Recognition in Eukaryotic Translation Initiation," *Trends in Biochemical Sciences*, 42(8), pp. 589–611. doi:10.1016/j.tibs.2017.03.004.

Hinnebusch, A.G., Ivanov, I.P. and Sonenberg, N. (2016) "Translational control by 5′-untranslated regions of eukaryotic mRNAs," *Science*, 352(6292), pp. 1413–1416. doi:10.1126/science.aad9868.

Holcik, M. (2015) "Could the eIF2α-Independent Translation Be the Achilles Heel of Cancer?," *Frontiers in Oncology*, 5. doi:10.3389/fonc.2015.00264.

Hong, C.-F., Chen, W.-Y. and Wu, C.-W. (2017) "Upregulation of Wnt signaling under hypoxia promotes lung cancer progression," *Oncology Reports*, 38(3), pp. 1706–1714. doi:10.3892/or.2017.5807.

Houseley, J. and Tollervey, D. (2009) "The Many Pathways of RNA Degradation," *Cell*, 136(4), pp. 763–776. doi:10.1016/j.cell.2009.01.019.

Hussain, T. *et al.* (2014) "Structural Changes Enable Start Codon Recognition by the Eukaryotic Translation Initiation Complex," *Cell*, 159(3), pp. 597–607. doi:10.1016/j.cell.2014.10.001.

Hyun, D.-H. (2020) "Insights into the New Cancer Therapy through Redox Homeostasis and Metabolic Shifts," *Cancers*, 12(7), p. 1822. doi:10.3390/cancers12071822.

I

Ivanova, I.G., Park, C. v. and Kenneth, N.S. (2019) "Translating the Hypoxic Response—the Role of HIF Protein Translation in the Cellular Response to Low Oxygen," *Cells*, 8(2), p. 114. doi:10.3390/cells8020114.

Iwasaki, S. *et al.* (2019) "The Translation Inhibitor Rocaglamide Targets a Bimolecular Cavity between eIF4A and Polypurine RNA," *Molecular Cell*, 73(4), pp. 738-748.e9. doi:10.1016/j.molcel.2018.11.026.

Iwasaki, S., Floor, S.N. and Ingolia, N.T. (2016) "Rocaglates convert DEAD-box protein eIF4A into a sequence-selective translational repressor," *Nature*, 534(7608), pp. 558–561. doi:10.1038/nature17978.

J

Jackson, R.J. (2013) "The Current Status of Vertebrate Cellular mRNA IRESs," *Cold Spring Harbor Perspectives in Biology*, 5(2), pp. a011569–a011569. doi:10.1101/cshperspect.a011569.

Jackson, R.J., Hellen, C.U.T. and Pestova, T. v. (2010) "The mechanism of eukaryotic translation initiation and principles of its regulation," *Nature Reviews Molecular Cell Biology*, 11(2), pp. 113–127. doi:10.1038/nrm2838.

Jackson, R.J. and Hunt, T. (1983) "Preparation and use of nuclease-treated rabbit reticulocyte lysates for the translation of eukaryotic messenger RNA," in, pp. 50–74. doi:10.1016/S0076-6879(83)96008-1.

Jacob, F. and Monod, J. (1961) "Genetic regulatory mechanisms in the synthesis of proteins," *Journal of Molecular Biology*, 3(3), pp. 318–356. doi:10.1016/S0022-2836(61)80072-7.

James, C.C. and Smyth, J.W. (2018) "Alternative mechanisms of translation initiation: An emerging dynamic regulator of the proteome in health and disease," *Life Sciences*, 212, pp. 138–144. doi:10.1016/j.lfs.2018.09.054.

Jang, S.K. *et al.* (1988) "A segment of the 5' nontranslated region of encephalomyocarditis virus RNA directs internal entry of ribosomes during in vitro translation," *Journal of Virology*, 62(8), pp. 2636–2643. doi:10.1128/jvi.62.8.2636-2643.1988.

Javanmard, D. *et al.* (2020) "Investigation of CTNNB1 gene mutations and expression in hepatocellular carcinoma and cirrhosis in association with hepatitis B virus infection," *Infectious Agents and Cancer*, 15(1), p. 37. doi:10.1186/s13027-020-00297-5.

K

Kapp, L.D. and Lorsch, J.R. (2004) "GTP-dependent Recognition of the Methionine Moiety on Initiator tRNA by Translation Factor eIF2," *Journal of Molecular Biology*, 335(4), pp. 923–936. doi:10.1016/j.jmb.2003.11.025.

Karabiber, F. *et al.* (2013) "QuShape: Rapid, accurate, and best-practices quantification of nucleic acid probing information, resolved by capillary electrophoresis," *RNA*, 19(1), pp. 63–73. doi:10.1261/rna.036327.112.

Khatter, H. *et al.* (2015) "Structure of the human 80S ribosome," *Nature*, 520(7549), pp. 640–645. doi:10.1038/nature14427.

Kieft, J.S. (2008) "Viral IRES RNA structures and ribosome interactions," *Trends in Biochemical Sciences*, 33(6), pp. 274–283. doi:10.1016/j.tibs.2008.04.007.

Kikin, O., D'Antonio, L. and Bagga, P.S. (2006) "QGRS Mapper: a web-based server for predicting G-quadruplexes in nucleotide sequences," *Nucleic Acids Research*, 34(Web Server), pp. W676–W682. doi:10.1093/nar/gkl253.

Kim, E. *et al.* (2018) "eIF2A, an initiator tRNA carrier refractory to eIF2α kinases, functions synergistically with eIF5B," *Cellular and Molecular Life Sciences*, 75(23), pp. 4287–4300. doi:10.1007/s00018-018-2870-4.

Kimball, S.R. (1999) "Eukaryotic initiation factor eIF2," *The International Journal of Biochemistry & Cell Biology*, 31(1), pp. 25–29. doi:10.1016/S1357-2725(98)00128-9.

Kobayashi, T. *et al.* (2006) "Activation of the ribosomal protein L13 gene in human gastrointestinal cancer," *International Journal of Molecular Medicine* [Preprint]. doi:10.3892/ijmm.18.1.161.

Kogure, T. *et al.* (2013) "Therapeutic Potential of the Translation Inhibitor Silvestrol in Hepatocellular Cancer," *PLoS ONE*, 8(9), p. e76136. doi:10.1371/journal.pone.0076136.

Komar, A.A. and Merrick, W.C. (2020) "A Retrospective on eIF2A—and Not the Alpha Subunit of eIF2," *International Journal of Molecular Sciences*, 21(6), p. 2054. doi:10.3390/ijms21062054.

Komiya, Y. and Habas, R. (2008) "Wnt signal transduction pathways," *Organogenesis*, 4(2), pp. 68–75. doi:10.4161/org.4.2.5851.

Koumenis, C. *et al.* (2002) "Regulation of Protein Synthesis by Hypoxia via Activation of the Endoplasmic Reticulum Kinase PERK and Phosphorylation of the Translation Initiation Factor eIF2α," *Molecular and Cellular Biology*, 22(21), pp. 7405–7416. doi:10.1128/MCB.22.21.7405-7416.2002.

Koumenis, C. and Wouters, B.G. (2006) "'Translating' Tumor Hypoxia: Unfolded Protein Response (UPR)–Dependent and UPR-Independent Pathways," *Molecular Cancer Research*, 4(7), pp. 423–436. doi:10.1158/1541-7786.MCR-06-0150.

Kourtidis, A., Ngok, S.P. and Anastasiadis, P.Z. (2013) "p120 Catenin," in, pp. 409–432. doi:10.1016/B978-0-12-394311-8.00018-2.

Kozak, M. (1991) "Structural features in eukaryotic mRNAs that modulate the initiation of translation.," *Journal of Biological Chemistry*, 266(30), pp. 19867–19870. doi:10.1016/S0021-9258(18)54860-2.

Krishnamurthy, N. and Kurzrock, R. (2018) "Targeting the Wnt/beta-catenin pathway in cancer: Update on effectors and inhibitors," *Cancer Treatment Reviews*, 62, pp. 50–60. doi:10.1016/j.ctrv.2017.11.002.

Kumar, P., Hellen, C.U.T. and Pestova, T. v. (2016) "Toward the mechanism of eIF4F-mediated ribosomal attachment to mammalian capped mRNAs," *Genes & Development*, 30(13), pp. 1573–1588. doi:10.1101/gad.282418.116.

Kwok, C.K., Ding, Y., Sherlock, M.E., *et al.* (2013) "A hybridization-based approach for quantitative and low-bias single-stranded DNA ligation," *Analytical Biochemistry*, 435(2), pp. 181–186. doi:10.1016/j.ab.2013.01.008.

Kwok, C.K., Ding, Y., Tang, Y., *et al.* (2013) "Determination of in vivo RNA structure in low-abundance transcripts," *Nature Communications*, 4(1), p. 2971. doi:10.1038/ncomms3971.

L

de la Parra, C. *et al.* (2018) "A widespread alternate form of cap-dependent mRNA translation initiation," *Nature Communications*, 9(1), p. 3068. doi:10.1038/s41467-018-05539-0.

de la Rosa-Trevín, J.M. *et al.* (2016) "Scipion: A software framework toward integration, reproducibility and validation in 3D electron microscopy," *Journal of Structural Biology*, 195(1), pp. 93–99. doi:10.1016/j.jsb.2016.04.010.

Lacerda, R., Menezes, J. and Romão, L. (2017) "More than just scanning: the importance of cap-independent mRNA translation initiation for cellular stress response and cancer," *Cellular and Molecular Life Sciences*, 74(9), pp. 1659–1680. doi:10.1007/s00018-016-2428-2.

Lang, K.J.D., Kappel, A. and Goodall, G.J. (2002) "Hypoxia-inducible Factor-1α mRNA Contains an Internal Ribosome Entry Site That Allows Efficient Translation during Normoxia and Hypoxia," *Molecular Biology of the Cell*, 13(5), pp. 1792–1801. doi:10.1091/mbc.02-02-0017.

Lee, A.S.Y. *et al.* (2016) "eIF3d is an mRNA cap-binding protein that is required for specialized translation initiation," *Nature*, 536(7614), pp. 96–99. doi:10.1038/nature18954.

Lee, B. *et al.* (2017) "Comparison of SHAPE reagents for mapping RNA structures inside living cells," *RNA*, 23(2), pp. 169–174. doi:10.1261/rna.058784.116.

Lee, L.J. *et al.* (2021) "Cancer Plasticity: The Role of mRNA Translation," *Trends in Cancer*, 7(2), pp. 134–145. doi:10.1016/j.trecan.2020.09.005.

LEONTIS, N.B. and WESTHOF, E. (2001) "Geometric nomenclature and classification of RNA base pairs," *RNA*, 7(4), p. S1355838201002515. doi:10.1017/S1355838201002515.

Leppek, K., Das, R. and Barna, M. (2018) "Functional 5′ UTR mRNA structures in eukaryotic translation regulation and how to find them," *Nature Reviews Molecular Cell Biology*, 19(3), pp. 158–174. doi:10.1038/nrm.2017.103.

Leprivier, G. *et al.* (2013) "The eEF2 Kinase Confers Resistance to Nutrient Deprivation by Blocking Translation Elongation," *Cell*, 153(5), pp. 1064–1079. doi:10.1016/j.cell.2013.04.055.

Li, Y., Syed, J. and Sugiyama, H. (2016) "RNA-DNA Triplex Formation by Long Noncoding RNAs," *Cell Chemical Biology*, 23(11), pp. 1325–1333. doi:10.1016/j.chembiol.2016.09.011.

Lin, C.-J. *et al.* (2008) "c-Myc and eIF4F Are Components of a Feedforward Loop that Links Transcription and Translation," *Cancer Research*, 68(13), pp. 5326–5334. doi:10.1158/0008-5472.CAN-07-5876.

Liu, B. and Qian, S.-B. (2014) "Translational reprogramming in cellular stress response," *Wiley Interdisciplinary Reviews: RNA*, 5(3), pp. 301–305. doi:10.1002/wrna.1212.

Liu, H. *et al.* (2012) "Characterization and evolution of 5′ and 3′ untranslated regions in eukaryotes," *Gene*, 507(2), pp. 106–111. doi:10.1016/j.gene.2012.07.034.

LIU, H.-L. *et al.* (2015) "Hypoxia-inducible factor-1α and Wnt/β-catenin signaling pathways promote the invasion of hypoxic gastric cancer cells," *Molecular Medicine Reports*, 12(3), pp. 3365–3373. doi:10.3892/mmr.2015.3812.

Llácer, J.L. *et al.* (2015) "Conformational Differences between Open and Closed States of the Eukaryotic Translation Initiation Complex," *Molecular Cell*, 59(3), pp. 399–412. doi:10.1016/j.molcel.2015.06.033.

Llácer, J.L. *et al.* (2018) "Translational initiation factor eIF5 replaces eIF1 on the 40S ribosomal subunit to promote start-codon recognition," *eLife*, 7. doi:10.7554/eLife.39273.

Low, J.T. and Weeks, K.M. (2010) "SHAPE-directed RNA secondary structure prediction," *Methods*, 52(2), pp. 150–158. doi:10.1016/j.ymeth.2010.06.007.

Lu, C. *et al.* (2016) "Targeting translation: eIF4E as an emerging anticancer drug target," *Expert Reviews in Molecular Medicine*, 18, p. e2. doi:10.1017/erm.2015.20.

Lyu, K. *et al.* (2021) "RNA G-quadruplexes (rG4s): genomics and biological functions," *Nucleic Acids Research*, 49(10), pp. 5426–5450. doi:10.1093/nar/gkab187.

M

Maher, E.R., Neumann, H.P. and Richard, S. (2011) "von Hippel–Lindau disease: A clinical and scientific review," *European Journal of Human Genetics*, 19(6), pp. 617–623. doi:10.1038/ejhg.2010.175.

Mailliot, J. and Martin, F. (2018) "Viral internal ribosomal entry sites: four classes for one goal," *WIREs RNA*, 9(2). doi:10.1002/wrna.1458.

Malka-Mahieu, H. *et al.* (2017) "Molecular Pathways: The eIF4F Translation Initiation Complex—New Opportunities for Cancer Treatment," *Clinical Cancer Research*, 23(1), pp. 21–25. doi:10.1158/1078-0432.CCR-14-2362.

Mancera-Martínez, E. *et al.* (2017) "ABCE1: A special factor that orchestrates translation at the crossroad between recycling and initiation," *RNA Biology*, 14(10), pp. 1279–1285. doi:10.1080/15476286.2016.1269993.

Mandl, M. and Depping, R. (2014) "Hypoxia-Inducible Aryl Hydrocarbon Receptor Nuclear Translocator (ARNT) (HIF-1β): Is It a Rare Exception?," *Molecular Medicine*, 20(1), pp. 215–220. doi:10.2119/molmed.2014.00032.

Marshall, H.T. and Djamgoz, M.B.A. (2018) "Immuno-Oncology: Emerging Targets and Combination Therapies," *Frontiers in Oncology*, 8. doi:10.3389/fonc.2018.00315.

Martin, F. *et al.* (2016) "Ribosomal 18S rRNA base pairs with mRNA during eukaryotic translation initiation," *Nature Communications*, 7(1), p. 12622. doi:10.1038/ncomms12622.

Martinez-Salas, E. *et al.* (2018) "Insights into Structural and Mechanistic Features of Viral IRES Elements," *Frontiers in Microbiology*, 8. doi:10.3389/fmicb.2017.02629.

Masoud, G.N. and Li, W. (2015) "HIF-1α pathway: role, regulation and intervention for cancer therapy," *Acta Pharmaceutica Sinica B*, 5(5), pp. 378–389. doi:10.1016/j.apsb.2015.05.007.

Mauger, D.M. *et al.* (2019) "mRNA structure regulates protein expression through changes in functional half-life," *Proceedings of the National Academy of Sciences*, 116(48), pp. 24075–24083. doi:10.1073/pnas.1908052116.

Mayr, C. (2019) "What Are 3′ UTRs Doing?," *Cold Spring Harbor Perspectives in Biology*, 11(10), p. a034728. doi:10.1101/cshperspect.a034728.

McEwen, E. *et al.* (2005) "Heme-regulated Inhibitor Kinase-mediated Phosphorylation of Eukaryotic Translation Initiation Factor 2 Inhibits Translation, Induces Stress Granule Formation, and Mediates Survival upon Arsenite Exposure," *Journal of Biological Chemistry*, 280(17), pp. 16925–16933. doi:10.1074/jbc.M412882200.

McKeown, S.R. (2014) "Defining normoxia, physoxia and hypoxia in tumours—implications for treatment response," *The British Journal of Radiology*, 87(1035), p. 20130676. doi:10.1259/bjr.20130676.

Mcnulty, S.E. and Toscano, W.A. (1995) "Transcriptional Regulation of Glyceraldehyde-3-Phosphate Dehydrogenase by 2,3,7,8-Tetrachlorodibenzo-p-Dioxin," *Biochemical and Biophysical Research Communications*, 212(1), pp. 165–171. doi:10.1006/bbrc.1995.1951.

Millevoi, S., Moine, H. and Vagner, S. (2012) "G-quadruplexes in RNA biology," *Wiley Interdisciplinary Reviews: RNA*, 3(4), pp. 495–507. doi:10.1002/wrna.1113.

Monteiro, A. *et al.* (2017) "The Role of Hypoxia in Glioblastoma Invasion," *Cells*, 6(4), p. 45. doi:10.3390/cells6040045.

Montoya, M. (2012) "Translation under hypoxia," *Nature Structural & Molecular Biology*, 19(6), pp. 602–602. doi:10.1038/nsmb.2326.

Muaddi, H. *et al.* (2010) "Phosphorylation of eIF2α at Serine 51 Is an Important Determinant of Cell Survival and Adaptation to Glucose Deficiency," *Molecular Biology of the Cell*, 21(18), pp. 3220–3231. doi:10.1091/mbc.e10-01-0023.

Muz, B. *et al.* (2015) "The role of hypoxia in cancer progression, angiogenesis, metastasis, and resistance to therapy," *Hypoxia*, p. 83. doi:10.2147/HP.S93413.

N

Naineni, S.K. *et al.* (2020) "A comparative study of small molecules targeting eIF4A," *RNA*, 26(5), pp. 541–549. doi:10.1261/rna.072884.119.

Nierhaus, K.H. (2014) “Mg2+, K+, and the Ribosome,” *Journal of Bacteriology*, 196(22), pp. 3817–3819. doi:10.1128/JB.02297-14.

Niessen, C.M. and Gottardi, C.J. (2008) “Molecular components of the adherens junction,” *Biochimica et Biophysica Acta (BBA) - Biomembranes*, 1778(3), pp. 562–571. doi:10.1016/j.bbamem.2007.12.015.

Nollet, F. *et al.* (1996) “Genomic Organization of the Human β-Catenin Gene (CTNNB1),” *Genomics*, 32(3), pp. 413–424. doi:10.1006/geno.1996.0136.

Nones, K. and Patch, A.-M. (2020) “The Impact of Next Generation Sequencing in Cancer Research,” *Cancers*, 12(10), p. 2928. doi:10.3390/cancers12102928.

Nusse, R. *et al.* (1991) “A new nomenclature for int-1 and related genes: The Wnt gene family,” *Cell*, 64(2), p. 231. doi:10.1016/0092-8674(91)90633-A.

Nusse, R. and Clevers, H. (2017) “Wnt/β-Catenin Signaling, Disease, and Emerging Therapeutic Modalities,” *Cell*, 169(6), pp. 985–999. doi:10.1016/j.cell.2017.05.016.

P

Paeschke, K. *et al.* (2005) “Telomere end-binding proteins control the formation of G-quadruplex DNA structures in vivo,” *Nature Structural & Molecular Biology*, 12(10), pp. 847–854. doi:10.1038/nsmb982.

Pai, S.G. *et al.* (2017) “Wnt/beta-catenin pathway: modulating anticancer immune response,” *Journal of Hematology & Oncology*, 10(1), p. 101. doi:10.1186/s13045-017-0471-6.

Pakos-Zebrucka, K. *et al.* (2016) “The integrated stress response,” *EMBO reports*, 17(10), pp. 1374–1395. doi:10.15252/embr.201642195.

Parsyan, A. *et al.* (2011) “mRNA helicases: the tacticians of translational control,” *Nature Reviews Molecular Cell Biology*, 12(4), pp. 235–245. doi:10.1038/nrm3083.

Passmore, L.A. *et al.* (2007) “The Eukaryotic Translation Initiation Factors eIF1 and eIF1A Induce an Open Conformation of the 40S Ribosome,” *Molecular Cell*, 26(1), pp. 41–50. doi:10.1016/j.molcel.2007.03.018.

Peifer, M. *et al.* (1992) “The vertebrate adhesive junction proteins beta-catenin and plakoglobin and the Drosophila segment polarity gene armadillo form a multigene family with similar properties.,” *Journal of Cell Biology*, 118(3), pp. 681–691. doi:10.1083/jcb.118.3.681.

Pelletier, J. and Sonenberg, N. (1988) “Internal initiation of translation of eukaryotic mRNA directed by a sequence derived from poliovirus RNA,” *Nature*, 334(6180), pp. 320–325. doi:10.1038/334320a0.

Pelletier, J. and Sonenberg, N. (2019) “The Organizing Principles of Eukaryotic Ribosome Recruitment,” *Annual Review of Biochemistry*, 88(1), pp. 307–335. doi:10.1146/annurev-biochem-013118-111042.

Pestova, T. v. *et al.* (2000) “The joining of ribosomal subunits in eukaryotes requires eIF5B,” *Nature*, 403(6767), pp. 332–335. doi:10.1038/35002118.

Petrova, V. *et al.* (2018) “The hypoxic tumour microenvironment,” *Oncogenesis*, 7(1), p. 10. doi:10.1038/s41389-017-0011-9.

Philippe, L. *et al.* (2020) “Global analysis of LARP1 translation targets reveals tunable and dynamic features of 5′ TOP motifs,” *Proceedings of the National Academy of Sciences*, 117(10), pp. 5319–5328. doi:10.1073/pnas.1912864117.

Piñeiro Fernández, J. *et al.* (2019) “Hepatic Tumor Microenvironments and Effects on NK Cell Phenotype and Function,” *International Journal of Molecular Sciences*, 20(17), p. 4131. doi:10.3390/ijms20174131.

Pisarev, A. v *et al.* (2008) "Ribosomal position and contacts of mRNA in eukaryotic translation initiation complexes," *The EMBO Journal*, 27(11), pp. 1609–1621. doi:10.1038/emboj.2008.90.

Pisareva, V.P. *et al.* (2008) "Translation Initiation on Mammalian mRNAs with Structured 5′UTRs Requires DExH-Box Protein DHX29," *Cell*, 135(7), pp. 1237–1250. doi:10.1016/j.cell.2008.10.037.

Popenda, M. *et al.* (2012) "Automated 3D structure composition for large RNAs," *Nucleic Acids Research*, 40(14), pp. e112–e112. doi:10.1093/nar/gks339.

Popenda, M. *et al.* (2020) "Topology-based classification of tetrads and quadruplex structures," *Bioinformatics*, 36(4), pp. 1129–1134. doi:10.1093/bioinformatics/btz738.

Pópulo, H., Lopes, J.M. and Soares, P. (2012) "The mTOR Signalling Pathway in Human Cancer," *International Journal of Molecular Sciences*, 13(2), pp. 1886–1918. doi:10.3390/ijms13021886.

Punjani, A. *et al.* (2017) "cryoSPARC: algorithms for rapid unsupervised cryo-EM structure determination," *Nature Methods*, 14(3), pp. 290–296. doi:10.1038/nmeth.4169.

R

Rabl, J. *et al.* (2011) "Crystal Structure of the Eukaryotic 40 *S* Ribosomal Subunit in Complex with Initiation Factor 1," *Science*, 331(6018), pp. 730–736. doi:10.1126/science.1198308.

Rakotondrafara, A.M. and Hentze, M.W. (2011) "An efficient factor-depleted mammalian in vitro translation system," *Nature Protocols*, 6(5), pp. 563–571. doi:10.1038/nprot.2011.314.

Reuter, J.S. and Mathews, D.H. (2010) "RNAstructure: software for RNA secondary structure prediction and analysis," *BMC Bioinformatics*, 11(1), p. 129. doi:10.1186/1471-2105-11-129.

Rogers, G.W. *et al.* (2001) "Modulation of the Helicase Activity of eIF4A by eIF4B, eIF4H, and eIF4F," *Journal of Biological Chemistry*, 276(33), pp. 30914–30922. doi:10.1074/jbc.M100157200.

Rol-Moreno, J. *et al.* (2020) "Grad-cryo-EM: Tool to Isolate Translation Initiation Complexes from Rabbit Reticulocyte Lysate Suitable for Structural Studies," in, pp. 329–339. doi:10.1007/978-1-0716-0278-2_21.

Romagnoli, A. *et al.* (2021) "Control of the eIF4E activity: structural insights and pharmacological implications," *Cellular and Molecular Life Sciences*, 78(21–22), pp. 6869–6885. doi:10.1007/s00018-021-03938-z.

Rozovsky, N., Butterworth, A.C. and Moore, M.J. (2008) "Interactions between eIF4AI and its accessory factors eIF4B and eIF4H," *RNA*, 14(10), pp. 2136–2148. doi:10.1261/rna.1049608.

S

Schaefer, M., Kapoor, U. and Jantsch, M.F. (2017) "Understanding RNA modifications: the promises and technological bottlenecks of the 'epitranscriptome,'" *Open Biology*, 7(5), p. 170077. doi:10.1098/rsob.170077.

Scheres, S.H.W. (2012) "RELION: Implementation of a Bayesian approach to cryo-EM structure determination," *Journal of Structural Biology*, 180(3), pp. 519–530. doi:10.1016/j.jsb.2012.09.006.

Schneider, C.A., Rasband, W.S. and Eliceiri, K.W. (2012) "NIH Image to ImageJ: 25 years of image analysis," *Nature Methods*, 9(7), pp. 671–675. doi:10.1038/nmeth.2089.

Semenza, G.L. (2004) "Hydroxylation of HIF-1: Oxygen Sensing at the Molecular Level," *Physiology*, 19(4), pp. 176–182. doi:10.1152/physiol.00001.2004.

Semenza, G.L. (2012) “Hypoxia-Inducible Factors in Physiology and Medicine,” *Cell*, 148(3), pp. 399–408. doi:10.1016/j.cell.2012.01.021.

Sen, D. and Gilbert, W. (1988a) “Formation of parallel four-stranded complexes by guanine-rich motifs in DNA and its implications for meiosis,” *Nature*, 334(6180), pp. 364–366. doi:10.1038/334364a0.

Sen, D. and Gilbert, W. (1988b) “Formation of parallel four-stranded complexes by guanine-rich motifs in DNA and its implications for meiosis,” *Nature*, 334(6180), pp. 364–366. doi:10.1038/334364a0.

Sen, N.D. *et al.* (2016) “eIF4B stimulates translation of long mRNAs with structured 5′ UTRs and low closed-loop potential but weak dependence on eIF4G,” *Proceedings of the National Academy of Sciences*, 113(38), pp. 10464–10472. doi:10.1073/pnas.1612398113.

Shang, S., Hua, F. and Hu, Z.-W. (2017) “The regulation of β-catenin activity and function in cancer: therapeutic opportunities,” *Oncotarget*, 8(20), pp. 33972–33989. doi:10.18632/oncotarget.15687.

Shatsky, I.N. *et al.* (2018) “Cap-Independent Translation: What’s in a Name?,” *Trends in Biochemical Sciences*, 43(11), pp. 882–895. doi:10.1016/j.tibs.2018.04.011.

Siddiqui, N. and Sonenberg, N. (2015) “Signalling to eIF4E in cancer,” *Biochemical Society Transactions*, 43(5), pp. 763–772. doi:10.1042/BST20150126.

Simonetti, A. *et al.* (2016) “eIF3 Peripheral Subunits Rearrangement after mRNA Binding and Start-Codon Recognition,” *Molecular Cell*, 63(2), pp. 206–217. doi:10.1016/j.molcel.2016.05.033.

Simonetti, A. *et al.* (2020) “Structural Insights into the Mammalian Late-Stage Initiation Complexes,” *Cell Reports*, 31(1), p. 107497. doi:10.1016/j.celrep.2020.03.061.

Siridechadilok, B. *et al.* (2005) “Structural Roles for Human Translation Factor eIF3 in Initiation of Protein Synthesis,” *Science*, 310(5753), pp. 1513–1515. doi:10.1126/science.1118977.

Slemc, L. and Kunej, T. (2016) “Transcription factor HIF1A: downstream targets, associated pathways, polymorphic hypoxia response element (HRE) sites, and initiative for standardization of reporting in scientific literature,” *Tumor Biology*, 37(11), pp. 14851–14861. doi:10.1007/s13277-016-5331-4.

Sokabe, M. and Fraser, C.S. (2017) “A helicase-independent activity of eIF4A in promoting mRNA recruitment to the human ribosome,” *Proceedings of the National Academy of Sciences*, 114(24), pp. 6304–6309. doi:10.1073/pnas.1620426114.

Sonenberg, N. and Hinnebusch, A.G. (2009) “Regulation of Translation Initiation in Eukaryotes: Mechanisms and Biological Targets,” *Cell*, 136(4), pp. 731–745. doi:10.1016/j.cell.2009.01.042.

Song, Z. *et al.* (2021) “The three-way junction structure of the HIV-1 PBS-segment binds host enzyme important for viral infectivity,” *Nucleic Acids Research*, 49(10), pp. 5925–5942. doi:10.1093/nar/gkab342.

Spitale, R.C. *et al.* (2013) “RNA SHAPE analysis in living cells,” *Nature Chemical Biology*, 9(1), pp. 18–20. doi:10.1038/nchembio.1131.

Spriggs, K.A., Bushell, M. and Willis, A.E. (2010) “Translational Regulation of Gene Expression during Conditions of Cell Stress,” *Molecular Cell*, 40(2), pp. 228–237. doi:10.1016/j.molcel.2010.09.028.

Sun, Y. *et al.* (2012) “The eukaryotic initiation factor eIF4H facilitates loop-binding, repetitive RNA unwinding by the eIF4A DEAD-box helicase,” *Nucleic Acids Research*, 40(13), pp. 6199–6207. doi:10.1093/nar/gks278.

Sung, H. *et al.* (2021) "Global Cancer Statistics 2020: GLOBOCAN Estimates of Incidence and Mortality Worldwide for 36 Cancers in 185 Countries," *CA: A Cancer Journal for Clinicians*, 71(3), pp. 209–249. doi:10.3322/caac.21660.

Suzuki, C. *et al.* (2008) "PDCD4 inhibits translation initiation by binding to eIF4A using both its MA3 domains," *Proceedings of the National Academy of Sciences*, 105(9), pp. 3274–3279. doi:10.1073/pnas.0712235105.

Swartz, H.M. *et al.* (2020) "How best to interpret measures of levels of oxygen in tissues to make them effective clinical tools for care of patients with cancer and other oxygen-dependent pathologies," *Physiological Reports*, 8(15). doi:10.14814/phy2.14541.

T

Taroncher-Oldenburg, G. *et al.* (2021) "Targeting the DEAD-Box RNA Helicase eIF4A with Rocaglates—A Pan-Antiviral Strategy for Minimizing the Impact of Future RNA Virus Pandemics," *Microorganisms*, 9(3), p. 540. doi:10.3390/microorganisms9030540.

Tegunov, D. and Cramer, P. (2019) "Real-time cryo-electron microscopy data preprocessing with Warp," *Nature Methods*, 16(11), pp. 1146–1152. doi:10.1038/s41592-019-0580-y.

Terenin, I.M. *et al.* (2017) "A researcher's guide to the galaxy of IRESs," *Cellular and Molecular Life Sciences*, 74(8), pp. 1431–1455. doi:10.1007/s00018-016-2409-5.

Thiele, A. *et al.* (2006) "AU-rich elements and alternative splicing in the β-catenin 3′UTR can influence the human β-catenin mRNA stability," *Experimental Cell Research*, 312(12), pp. 2367–2378. doi:10.1016/j.yexcr.2006.03.029.

Thomas, J.D. and Johannes, G.J. (2007) "Identification of mRNAs that continue to associate with polysomes during hypoxia," *RNA*, 13(7), pp. 1116–1131. doi:10.1261/rna.534807.

Thompson, P.A. *et al.* (2021) "Targeting Oncogene mRNA Translation in B-Cell Malignancies with eFT226, a Potent and Selective Inhibitor of eIF4A," *Molecular Cancer Therapeutics*, 20(1), pp. 26–36. doi:10.1158/1535-7163.MCT-19-0973.

Tomezsko, P.J. *et al.* (2020) "Determination of RNA structural diversity and its role in HIV-1 RNA splicing," *Nature*, 582(7812), pp. 438–442. doi:10.1038/s41586-020-2253-5.

V

Valenta, T., Hausmann, G. and Basler, K. (2012) "The many faces and functions of β-catenin," *The EMBO Journal*, 31(12), pp. 2714–2736. doi:10.1038/emboj.2012.150.

Varani, G. and McClain, W.H. (2000) "The G·U wobble base pair," *EMBO reports*, 1(1), pp. 18–23. doi:10.1093/embo-reports/kvd001.

Varela-Nallar, L. *et al.* (2014) "Chronic hypoxia induces the activation of the Wnt/β-catenin signaling pathway and stimulates hippocampal neurogenesis in wild-type and APPswe-PS1ΔE9 transgenic mice in vivo," *Frontiers in Cellular Neuroscience*, 8. doi:10.3389/fncel.2014.00017.

Vasan, N., Baselga, J. and Hyman, D.M. (2019) "A view on drug resistance in cancer," *Nature*, 575(7782), pp. 299–309. doi:10.1038/s41586-019-1730-1.

Vasudevan, D. *et al.* (2020) "Translational induction of ATF4 during integrated stress response requires noncanonical initiation factors eIF2D and DENR," *Nature Communications*, 11(1), p. 4677. doi:10.1038/s41467-020-18453-1.

Verheyen, E.M. and Gottardi, C.J. (2009) "Regulation of Wnt/β-catenin signaling by protein kinases," *Developmental Dynamics*, p. NA-NA. doi:10.1002/dvdy.22019.

Verras, M. *et al.* (2008) "Tumor Hypoxia Blocks Wnt Processing and Secretion through the Induction of Endoplasmic Reticulum Stress," *Molecular and Cellular Biology*, 28(23), pp. 7212–7224. doi:10.1128/MCB.00947-08.

Villa, N. *et al.* (2013) "Human Eukaryotic Initiation Factor 4G (eIF4G) Protein Binds to eIF3c, -d, and -e to Promote mRNA Recruitment to the Ribosome," *Journal of Biological Chemistry*, 288(46), pp. 32932–32940. doi:10.1074/jbc.M113.517011.

de Vita, V.T., Hellman, S. and Rosenberg, S.A. (2020) *Cancer: Principles & Practice of Oncology: Primer of the Molecular Biology of Cancer*. Third. Lippincott, Williams & Wilkins.

W

Waldron, J.A. *et al.* (2019) "mRNA structural elements immediately upstream of the start codon dictate dependence upon eIF4A helicase activity," *Genome Biology*, 20(1), p. 300. doi:10.1186/s13059-019-1901-2.

Walker, S.E. *et al.* (2013) "Yeast eIF4B binds to the head of the 40S ribosomal subunit and promotes mRNA recruitment through its N-terminal and internal repeat domains," *RNA*, 19(2), pp. 191–207. doi:10.1261/rna.035881.112.

Wang, Jinfan *et al.* (2020) "Structural basis for the transition from translation initiation to elongation by an 80S-eIF5B complex," *Nature Communications*, 11(1), p. 5003. doi:10.1038/s41467-020-18829-3.

Warner, K.D., Hajdin, C.E. and Weeks, K.M. (2018) "Principles for targeting RNA with drug-like small molecules," *Nature Reviews Drug Discovery*, 17(8), pp. 547–558. doi:10.1038/nrd.2018.93.

Weingarten-Gabbay, S. *et al.* (2016) "Systematic discovery of cap-independent translation sequences in human and viral genomes," *Science*, 351(6270). doi:10.1126/science.aad4939.

Westhof, E. and Auffinger, P. (2012) "Transfer <scp>RNA</scp> Structure," in *eLS*. Wiley. doi:10.1002/9780470015902.a0000527.pub2.

Wodarz, A. and Nusse, R. (1998) "MECHANISMS OF WNT SIGNALING IN DEVELOPMENT," *Annual Review of Cell and Developmental Biology*, 14(1), pp. 59–88. doi:10.1146/annurev.cellbio.14.1.59.

Wolfe, A.L. *et al.* (2014) "RNA G-quadruplexes cause eIF4A-dependent oncogene translation in cancer," *Nature*, 513(7516), pp. 65–70. doi:10.1038/nature13485.

Wu, D. *et al.* (2015) "Structural integration in hypoxia-inducible factors," *Nature*, 524(7565), pp. 303–308. doi:10.1038/nature14883.

Wu, R. *et al.* (2021) "m6A methylation promotes white-to-beige fat transition by facilitating Hif1a translation," *EMBO reports*, 22(11). doi:10.15252/embr.202052348.

Y

Yamaji, R. *et al.* (2003) "Hypoxia up-regulates glyceraldehyde-3-phosphate dehydrogenase in mouse brain capillary endothelial cells: involvement of Na+/Ca2+ exchanger," *Biochimica et Biophysica Acta (BBA) - Molecular Cell Research*, 1593(2–3), pp. 269–276. doi:10.1016/S0167-4889(02)00397-X.

Yasuda, M. *et al.* (2014) "Cell type-specific reciprocal regulation of HIF1A gene expression is dependent on 5′- and 3′-UTRs," *Biochemical and Biophysical Research Communications*, 447(4), pp. 638–643. doi:10.1016/j.bbrc.2014.04.058.

Young, R.M. *et al.* (2008) "Hypoxia-mediated Selective mRNA Translation by an Internal Ribosome Entry Site-independent Mechanism," *Journal of Biological Chemistry*, 283(24), pp. 16309–16319. doi:10.1074/jbc.M710079200.

Yourik, P. *et al.* (2017) "Yeast eIF4A enhances recruitment of mRNAs regardless of their structural complexity," *eLife*, 6. doi:10.7554/eLife.31476.

Yusupova, G. and Yusupov, M. (2017) "Crystal structure of eukaryotic ribosome and its complexes with inhibitors," *Philosophical Transactions of the Royal Society B: Biological Sciences*, 372(1716), p. 20160184. doi:10.1098/rstb.2016.0184.

Z

Zeman, J. *et al.* (2019) "Binding of eIF3 in complex with eIF5 and eIF1 to the 40S ribosomal subunit is accompanied by dramatic structural changes," *Nucleic Acids Research*, 47(15), pp. 8282–8300. doi:10.1093/nar/gkz570.

Zhang, Q. *et al.* (2013) "Wnt/β-catenin signaling enhances hypoxia-induced epithelial–mesenchymal transition in hepatocellular carcinoma via crosstalk with hif-1α signaling," *Carcinogenesis*, 34(5), pp. 962–973. doi:10.1093/carcin/bgt027.

Javier ROL MORENO

Structural and functional characterization of the 5’ untranslated regions of β-catenin and HIF-1α mRNAs and their translational role in cancer cells under hypoxia

RÉSUMÉ

La synthèse des protéines est un processus universel chez toutes les espèces et considérée comme la dernière étape de l'expression de l'information génétique. La traduction est principalement régulée au stade de l'initiation pour permettre un contrôle rapide et réversible des changements cellulaires et environnementaux. Des mécanismes non conventionnels d'initiation de la traduction échappant au modèle canonique ont été rapportés, montrant le potentiel du ribosome à adapter sa machinerie en réponse aux différents stimuli en interprétant les signaux dans les ARN messagers, souvent dans leur 5'UTR, pour le recrutement des ribosomes.
Le cancer est une maladie génétique qui se produit par l'accumulation d'altérations moléculaires dans le génome des cellules somatiques. Chez l'Homme, il devient actuellement la deuxième cause de décès dans le monde. Les cellules tumorales sont soumises à plusieurs stress comme l'hypoxie, qui réduit la traduction canonique dépendante de la coiffe. Dans ce contexte, le maintien de la traduction de certains ARNm codant pour des protéines impliquées dans la prolifération et l'adaptation en réponse au stress, comme la β-caténine et HIF-1α, favorise la progression du cancer. Cependant, ce processus est très peu étudié.
Ce projet vise à étudier le mécanisme d'initiation de la traduction des ARN messagers de la β-caténine et du HIF-1α à travers la caractérisation de la structure secondaire de leurs 5'UTRs et le rôle traductionnel des éléments au 5'UTR dans des cellules cancéreuses sous hypoxie. La combinaison de techniques de biologie biochimique et structurale sera une approche innovante pour explorer de nouvelles stratégies anticancéreuses basées sur le ciblage de la traduction des ARN messagers.

Mots clés : ARN, initiation de la traduction, mécanismes alternatifs, 5'UTR, hypoxie, cancer, β-caténine, HIF-1α

SUMMARY

Protein synthesis is a universal process in all species and can be considered the last step of expression of genetic information. Translation is mainly regulated at the initiation stage to permit a rapid and reversible control of cellular and environmental changes. Unconventional translation initiation mechanisms evading the canonical model have been reported, showing the ribosome potential to adapt its machinery in response to different stimuli by interpreting mRNA signals, often in their 5’UTR, for ribosome recruitment.
Cancer is a genetic disease that occurs through the accumulation of molecular alterations in the genome of somatic cells. In humans, it currently becomes the second cause of death worldwide. Tumour cells are submitted to several stresses such as hypoxia, that notably downregulates canonical cap-dependent translation. In this context, translation maintenance of certain mRNAs encoding proteins implicated in proliferation and adaptation in response to stress, as β-catenin and HIF-1α, promotes cancer progression. However, this process is poorly studied.
This project intends to study the translation initiation mechanism of β-catenin and HIF-1α mRNAs through the characterization of the secondary structure of their 5’UTRs and the translational role of the 5’UTR elements, particularly in cancer cells under hypoxia. The combination of biochemical and structural biology techniques will be an innovative approach to explore new anticancer strategies based in the targeting of mRNA translation.

Key words: RNA, translation initiation, alternative mechanisms, 5’UTR, hypoxia, cancer, β-catenin, HIF-1α

Université de Strasbourg
institut de biologie moléculaire et cellulaire ibmc
cnrs
SANOFI
Cifre